Universidad Politécnica de València

Escuela de Doctorado

Programa de Doctorado en Biotecnología

Study of plant-to-plant communication in response to proximity shade

Dissertation submitted by Mikel Urdin Bravo in partial fulfillment of the requirements for the degree of Doctor in Biotechnology at the Doctoral School of the Polytechnic University of Valencia. This research was carried out at the Institute for Plant Molecular and Cellular Biology (IBMCP-CSIC-UPV).

Directors	Tutor	PhD Candidate
Dr. Manuel Rodríguez Concepción	**Dr. Ismael Rodrigo Bravo**	**Mikel Urdin Bravo**
Dr. Jaume Martínez García		

Valencia, Noviembre 2025

Agradecimientos

Este trabajo de tesis ha sido posible gracias a la financiación proporcionada por una beca predoctoral FPU (FPU20/05486) del Ministerio de Ciencia, Educación y Universidades y del Consejo Superior de Investigaciones Científicas, así como por los proyectos de investigación financiados por la Generalitat Valenciana (PROMETEU/2021/065), el MCEU (PID2020-115762GB-I00 / PID2023-149584NB-I00) y la Unión Europea (PCI2021-121941), en el marco de los cuales se ha desarrollado parte de este trabajo. A todos ellos deseo expresar mi más sincero agradecimiento. Asimismo, quiero expresar mi reconocimiento al Instituto de Biología Molecular y Celular de Plantas (IBMCP, CSIC-UPV) por haberme brindado un entorno científico estimulante y todos los recursos necesarios para desarrollar mi investigación.

A mis directores de tesis, Jaume Martínez García y Manuel Rodríguez Concepción, les agradezco su guía constante, su confianza y su dedicación. Su experiencia, entusiasmo y apoyo han sido esenciales en mi formación como investigador y en la realización de este trabajo.

Extiendo mi gratitud a todo el personal investigador, técnico y administrativo del IBMCP por su ayuda, amabilidad y por contribuir a crear un ambiente de trabajo colaborativo y enriquecedor. A mis compañeros y compañeras de laboratorio, gracias por su apoyo diario, por las conversaciones científicas y por los momentos compartidos dentro y fuera del laboratorio.

A mis amigos y amigas, dentro y fuera del ámbito académico, gracias por su paciencia, ánimo y compañía a lo largo de estos años. Su apoyo ha sido fundamental para mantener el equilibrio en esta etapa tan exigente.

Por último, deseo agradecer a mi familia por su amor incondicional, comprensión y apoyo constante. Esta tesis es también el resultado de todo lo que me han enseñado y del ejemplo que me han dado cada día.

Resumen

Las plantas dependen de su capacidad para percibir y responder a señales ambientales en comunidades de alta densidad vegetal. Entre estas señales, la luz actúa como un regulador central: la disminución en la relación rojo/rojo lejano (R:FR) constituye un indicador confiable de proximidad vegetal, desencadenando una serie de respuestas fotomorfogénicas comúnmente conocidas como síndrome de evitación de sombra (SAS). Estudios recientes sugieren que estas respuestas también implican modificaciones específicas a nivel metabólico, en particular la emisión de compuestos orgánicos volátiles (VOCs). Sin embargo, a pesar de la creciente evidencia sobre perfiles volatilómicos alterados bajo condiciones de sombra, aún no existe consenso respecto al posible significado biológico de estas emisiones diferenciales.

El objetivo de esta tesis fue determinar si el “volatiloma de sombra” constituye una señal activa de comunicación entre plantas, esclareciendo posteriormente el papel de VOCs específicos como el etileno y los apocarotenoides β-ciclocitral y β-ionona en este proceso. Para ello, se desarrollaron sistemas experimentales de co-cultivo en condiciones controladas permitiendo exposición a volátiles, utilizando plantas de tomate como emisoras y plántulas de *Arabidopsis thaliana* como receptoras en nuestro modelo. El enfoque combinó análisis fisiológicos y de desarrollo con estudios transcriptómicos y químicos, complementados con ensayos de exposición a volátiles individuales, a fin de evaluar su contribución en el contexto del volatiloma de sombra y de identificar los mecanismos moleculares subyacentes.

Nuestros resultados demuestran que los volátiles liberados por plantas de tomate expuestas a sombra reprimen consistentemente la elongación de hipocotilo en plantas cercanas. Además, desencadenan reajustes transcriptómicos que afectan a genes asociados a respuestas a hipoxia, estrés oxidativo y defensa, con un solapamiento parcial respecto a programas directamente inducidos por bajo R:FR. La caracterización de volátiles individuales reveló que β-ciclocitral y β-ionona, cuya producción

aumenta en condiciones de sombra de proximidad, reproducen ampliamente los efectos del volatiloma de sombra a nivel fenotípico y también molecular. La exposición aérea a estos compuestos reprime el crecimiento vía señalización por brassinosteroides, y promueve la activación de un estado transcripcional de preparación a estrés en plántulas de *A. thaliana.* Adicionalmente, los compuestos mostraron especificidad funcional: β-ciclocitral retrasa germinación, y consolida las respuestas transcriptómicas de resiliencia frente a estrés, mientras que β-ionona incrementa la eficiencia fotosintética y activa redes transcripcionales asociadas con defensa, actuando paralelamente como inhibidores aéreos de SAS.

En conjunto, la tesis establece que el volatiloma de sombra constituye una señal activa de comunicación planta-planta, con β-ciclocitral y β-ionona como componentes centrales. Su acción combinada revela un doble rol ecológico: contrarrestando la elongación excesiva promovida por la sombra de proximidad frente a la promoción de defensa y fotosíntesis. Estos hallazgos expanden el marco conceptual de la respuesta a sombra, añadiendo una nueva capa de regulación frente a la misma, abriendo nuevas perspectivas para comprender la ecología química y las aplicaciones biotecnológicas en la mejora de cultivos en condiciones de alta densidad vegetal.

Resum

Les plantes depenen de la seua capacitat per a percebre i respondre a senyals ambientals en comunitats amb una elevada densitat vegetal. Entre estes senyals, la llum actua com a regulador central: la disminució en la relació roig/roig llunyà (R:FR) constitueix un indicador fiable de proximitat vegetal i desencadena un conjunt de respostes fotomorfogèniques comunament conegudes com a síndrome de fugida de l'ombra (SAS). Estudis recents suggereixen que estes respostes també impliquen modificacions específiques a nivell metabòlic, en particular l'emissió de compostos orgànics volàtils (VOCs). Tanmateix, malgrat l'evidència creixent sobre perfils volatilòmics alterats sota condicions d'ombra, encara no hi ha consens quant al possible significat biològic d'estes emissions diferencials.

L'objectiu d'esta tesi va ser determinar si el *volatiloma d'ombra* constitueix un senyal actiu de comunicació entre plantes, i aclarir posteriorment el paper de VOCs específics com l'etilè i els apocarotenoides β-ciclocitral i β-ionona en este procés. Per a això, es van desenvolupar sistemes experimentals de co-cultiu en condicions controlades que permetien l'exposició a volàtils, emprant plantes de tomaca com a emissores i plàntules d'*Arabidopsis thaliana* com a receptores en el nostre model. L'enfocament va combinar anàlisis fisiològiques i de desenvolupament amb estudis transcriptòmics i químics, complementats amb assajos d'exposició a volàtils individuals, amb la finalitat d'avaluar la seua contribució en el context del volatiloma d'ombra i d'identificar els mecanismes moleculars subjacents.

Els nostres resultats demostren que els volàtils alliberats per plantes de tomaca exposades a ombra reprimeixen de manera consistent l'elongació de l'hipocòtil en plantes pròximes. A més, desencadenen reajustaments transcriptòmics que afecten gens associats a respostes a hipòxia, estrès oxidatiu i defensa, amb un solapament parcial respecte als programes directament induïts per una relació baixa de R:FR. La caracterització de volàtils individuals va revelar que el β-ciclocitral i la β-ionona, la producció

dels quals augmenta en condicions d'ombra de proximitat, reprodueixen àmpliament els efectes del volatiloma d'ombra tant a nivell fenotípic com molecular. L'exposició aèria a estos compostos reprimeix el creixement mitjançant la senyalització per brasinoesteroides, i promou l'activació d'un estat transcripcional de preparació a l'estrès en plàntules d'*Arabidopsis thaliana*. Addicionalment, els compostos van mostrar especificitat funcional: el β-ciclocitral retarda la germinació i consolida les respostes transcriptòmiques de resiliència davant l'estrès, mentre que la β-ionona incrementa l'eficiència fotosintètica i activa xarxes transcriptòmiques associades a la defensa, actuant alhora com a inhibidors aeris del SAS.

En conjunt, la tesi estableix que el volatiloma d'ombra constitueix un senyal actiu de comunicació planta-planta, amb el β-ciclocitral i la β-ionona com a components centrals. La seua acció combinada revela un doble paper ecològic: contrarestant l'elongació excessiva promoguda per l'ombra de proximitat i, al mateix temps, afavorint la defensa i la fotosíntesi. Estes troballes amplien el marc conceptual de la resposta a l'ombra, afegint-hi una nova capa de regulació i obrint noves perspectives per a la comprensió de l'ecologia química i per a les aplicacions biotecnològiques en la millora de cultius en condicions de gran densitat vegetal.

Abstract

Plants rely on their ability to perceive and respond to environmental cues within dense communities. Among these, light is a major regulator: reductions in the red-to-far-red ratio (R:FR) provide reliable information on vegetation proximity, triggering a series of photomorphogenic responses commonly known as the shade avoidance syndrome (SAS). Recent evidence suggests that shade responses also encompass specific metabolic outputs, particularly the emission of volatile organic compounds (VOCs). Yet, despite mounting reports of altered VOC profiles under shade conditions, there is no clear consensus on the biological significance of these differential emissions.

The aim of this thesis was to determine whether the “shade volatilome” could as an active signal in plant-to-plant communication, capable of modulating the development of neighboring plants, while later clarifying the role of specific VOCs such as ethylene and the apocarotenoids β-cyclocitral and β-ionone, in this process. To address this, controlled airborne co-cultivation systems were established, using tomato plants as VOC-emitters and *Arabidopsis thaliana* seedlings as receivers in our model. The approach combined physiological and developmental analysis with transcriptomic and chemical profiling, complemented by exposure experiments to individual VOCs, in order to assign them a role within the context of the shade volatilome and to identify the underlying molecular mechanisms.

Our results demonstrate that VOCs released by shade-exposed tomato plants consistently suppress hypocotyl elongation in neighboring seedlings. Moreover, they induce transcriptomic reprogramming involving genes linked to hypoxia, oxidative stress and defense, partially overlapping with low R:FR driven programs. Targeted experiments revealed that β-cyclocitral and β-ionone, whose production is increased under proximity shade conditions, largely recapitulate the phenotypic and molecular effects of the shade volatilome. Airborne exposure to these compounds represses growth via BRs signaling and elicits a stress-like

transcriptional state in *A. thaliana* seedlings. Additionally, these compounds also showed functional specificity: β-cyclocitral delayed germination and consolidated stress responses, whereas β-ionone enhanced photosynthetic performance and triggered defense-associated transcriptional networks, altogether acting as airborne inhibitors of SAS.

Collectively, this work identifies the shade volatilome as an active channel of plant-to-plant communication, with β-cyclocitral and β-ionone as central components. Their combined action reveals a dual ecological role: antagonizing excessive elongation triggered by proximity shade while priming seedlings for stress resilience, promoting defense and photosynthesis. These findings expand the conceptual framework of shade responses by adding a new regulation layer, providing new insights into chemical ecology with potential applications for optimizing crop adaptation and performance in dense agricultural systems.

Sections Index

Figures Index

Tables Index

Abbreviations

ABA	**Abscisic Acid**
ACC	1-aminocyclopropane -1-carboxylic acid
β-cc	β-cyclocitral
β-ion	β-ionone
BRs	Brassinosteroids
BES1	BRI1-EMS Suppressor 1
BZR1	Brassinazole-resistant 1
CCDs	Carotenoid Cleavage Deoxygenases
D	Darkness
d	Day
DEGs	Differential Expressed Genes
DMSO	Dimethyl Sulfoxide
DW	Dry Weight
EBL	Epibrassinolide, synthetic brassinosteroid
EIC	Extracted Ion Current
E-plants	VOC-emitter plants
FC	Fold Change
FID	Flame-injection detector
FR	Far-red light
Fv/Fm	Maximum quantum efficiency of PSII
FW	Fresh Weight
GA_3	Gibberelic Acid
GC-MS	Gas Chromatography – Mass Spectrometry
GFP	Green Fluorescence Protein
GLVs	Green Leaf Volatiles
GO-BP	Gene Ontology – Biological Process
GS	Glucosinolates
GUS	β-Glucuronidase
h	Hours
HPLC	High Performance Liquid Chromatography
HS	Headspace
JA	Jasmonic Acid
KEGG	Kyoto Encyclopedia of Genes and Genomes
L	Liter
LD	Long-day
low W	Low-intensity White light
M	Molar
m	Meter
MAPK	Mitogen-Activated Protein Kinase
min	Minute
MP	Micropore
MS	Murashige and Skoog medium
PBs	Photobodies
PC1/2	Principal Component 1/2
PCA	Principal Component Analysis
PCR	Polymerase Chain Reaction
PFA	Paraformaldehyde
Pfr	Active Phytochrome
PHY-A/E	Phytochrome A/E
PIC	Picloram, auxin analogue
PIFs	Phytochrome Interacting Factors
PPFD	Photosynthetic Photon Flux Density
Pr	Inactive Phytochrome

qPCR	Quantitative Polymerase Chain Reaction
R	Red light
R:FR	Red-to-Far-Red ratio
RACK1A	Receptor for Activated C Kinase 1A
RNA	Ribonucleic Acid
RNA-seq	RNA sequencing
ROS	Reactive Oxygen Species
R-seedlings	VOC-receiver plants
s	Second
SA	Salicylic Acid
SAS	Shade Avoidance Syndrome
SAUR	Small Auxin Upregulated genes
SD	Standard Deviation
SEM	Standard Error of the Mean
SLs	Strigolactones
SPME	Solid Phase Microextraction fiber
TPMs	Transcripts per Million reads
VOCs	Volatile Organic Compounds
W	White light
W+FR	White light supplemented with Far-Red / simulated shade
WC	Working Concentration
WT	Wild-Type
ZT	Zeitgeber Time
φPSII	Effective quantum yield of PSII

Introduction

Introduction

I.1 Plants as perceptive and communicative organisms

Often regarded as passive and *unconscious* beings, plants are in fact highly perceptive organisms capable of sensing, integrating, and responding to a broad range of environmental cues. Despite lacking a nervous system or conventional sensory organs, their sessile nature has driven the evolution and development of sophisticated mechanisms that allow them to detect and process diverse signals—including light (Gyula *et al.*, 2003), gravity (Björkman, 1988), mechanical forces (Braam, 2005), water and nutrient availability (Amtmann *et al.*, 2005; Lambers & Oliveira, 2019), a wide spectrum of biotic stimuli (Mitchell *et al.*, 2006; Van Dam, 2009), and even sounds (Khait *et al.*, 2019). These sensory capacities are not only essential for their development but also shape how plants interact with their surroundings and neighboring organisms in complex ecological communities, providing plants a great level of developmental plasticity.

Aside from detecting signals, plants, as immobile organisms, must constantly acclimate to changing environments through finely tuned molecular, physiological, and developmental responses. This versatility enables them to withstand many abiotic stressors—such as drought (Basu *et al.*, 2016), salinity (Zhao *et al.*, 2020), flooding (Blom & Voesenek, 1996), extreme temperatures (Zheng *et al.*, 2011), or suboptimal soil pH (Ramírez-Rodríguez *et al.*, 2005), among others. These challenges are not only central to plant ecology but have also become increasingly relevant in agriculture, where global climate change is exacerbating environmental stress and reinforcing the need for more resilient crop systems (Fawzy *et al.*, 2020).

Ultimately, the ability of plants to thrive in diverse natural (and sometimes adverse) environments relies not only on their capacity to sense and respond to abiotic and biotic stressors, but mostly on the continuous processing of information they receive from their ecosystems. Molecularly,

this ability relies on the integration of this information with the endogenous mechanisms that control plant growth and development.

From the ecological standpoint, plants usually live surrounded by other plants (weaving communities of individuals of the same or different species) and by varied non-plant organisms, forming highly intricate ecological networks. Within these communities, plants engage in various types of biotic interactions that influence their physiology, behavior, and survival (Mitchell *et al.*, 2006). These interactions can be broadly categorized as: competition, where individuals contend for limited resources such as light, water, or nutrients (Bengtsson *et al.*, 1994); facilitation, wherein one plant improves environmental conditions to the benefit of its neighbors (Brooker *et al.*, 2008); and mutualism, a reciprocal association in which both organisms derive advantage (Martin *et al.*, 2017). Another particularly relevant form of interaction is allelopathy: the release of bioactive compounds by one plant that directly influence the growth, development, or behavior of neighboring organisms (Rice, 2012). Although often underappreciated, allelopathy represents a clear example of chemically mediated plant communication, revealing how plants can actively shape their surroundings and modulate ecological relationships through the emission of specific molecules (Chou, 1999).

Communication can be defined as the transfer of information between individuals through a signaling process that involves emission, perception, and interpretation of the signal transmitted. As in any communicative system, this process requires an emitter—capable of releasing an encoded signal or message—, a medium or channel through which the signal travels, and a receiver—equipped to perceive, decode, and ultimately respond to that message, if needed. Plants can be both emitters and receivers. Any kind of communication in which a plant is involved either as an emitter or a receiver can hence be considered plant communication. Within plant communities, such interactions may involve the emission of physical or chemical cues that are perceived by other plants or non-plant organisms in the environment, including animals (Bleeker *et al.*, 2009; Cortés *et al.*, 2016), fungi (Bedini *et al.*, 2018; Rozpądek *et al.*, 2018; E. Wang *et al.*, 2012), or bacteria (Jamil *et al.*, 2022; D. L. Smith *et al.*, 2015; Tadrosova *et al.*, 2025). Conversely, these organisms can also act as emitters, engaging in reciprocal information exchange with plants (García-Gómez *et al.*, 2019; Ho-Plágaro & García-

Garrido, 2022; Schikora *et al.*, 2016). This inter-organismal communication underpins many ecological processes and reinforces the idea that plants do not operate in isolation but are integrated into complex signaling networks.

I.2 Plant-to-plant communication signals

Among the many forms of information exchange in which plants are involved, one of the most intriguing and increasingly studied is plant-to-plant communication—the ability of one plant to send signals that are perceived and processed by neighboring plants, ultimately influencing their physiology or behavior. Although historically regarded with skepticism, early evidence from the 1980s (Baldwin & Schultz, 1983; Rhoades, 1983) began to demonstrate that plants could respond to cues emitted by damaged or stressed conspecifics. Since then, growing experimental support has validated this concept, highlighting its ecological importance across diverse natural and agricultural systems (Heil & Karban, 2010; Yoneya & Takabayashi, 2014). Plant-to-plant communication enables individuals to “warn” others of herbivore attack, resource scarcity or environmental stress, thereby enhancing preparedness and resilience at the community level (Coppola *et al.*, 2017; Elhakeem *et al.*, 2018; Midzi *et al.*, 2022).

I.2.1 Belowground signals: root exudates

Root exudates have been regarded as a key mode of belowground plant-to-plant communication among the various chemical mechanisms mediating interplant signaling (Vives-Peris *et al.*, 2020) (Fig. I.1). These exudates, composed of a chemically diverse blend of sugars, amino acids, organic acids, flavonoids, phytohormones and other allelochemicals, are continuously secreted into the rhizosphere and act as powerful modulators of soil chemistry and biology (Broeckling *et al.*, 2008; Canarini *et al.*, 2019; Hu *et al.*, 2018; Kong *et al.*, 2018). While traditionally associated with nutrient mobilization or microbial recruitment, root exudates also play a critical role in mediating plant–plant interactions (Delory *et al.*, 2016; Khashi U Rahman *et al.*, 2019). Through this biochemical exchange, plants can influence the growth, physiology, and even defense responses

of neighboring individuals, whether conspecific or heterospecific (Semchenko *et al.*, 2014). In doing so, they modulate not only individual performance but also the spatial organization and functional dynamics of plant communities from below the surface.

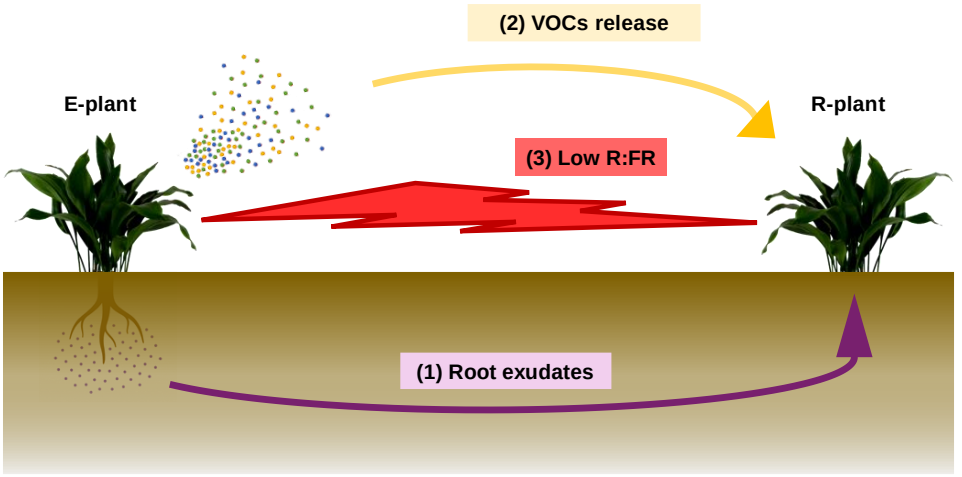

Figure I.1 — Proposed mechanisms of plant-to-plant communication. *Belowground, rood exudates (1) represent one of the most studied plant-to-plant communication signals. Aboveground, volatile organic compounds (VOCs) (2) and reductions in the red to far red light (R:FR) ratio (3), generated by the preferential absorption of R by photosynthetic tissues of nearby plants, represent plant-to-plant communication signals.*

I.2.2 Aboveground signals: Volatile Organic Compounds (VOCs) and light cues

Aboveground, a major class of chemical signals involved in plant-to-plant communication is volatile organic compounds (VOCs) (Fig. I.1). VOCs constitute a chemically diverse group of low-molecular-weight organic compounds with high vapor pressure, allowing them to diffuse rapidly through the atmosphere. Due to their highly complex secondary metabolism, plants constitutively release a wide array of these molecules, collectively referred to as the plant volatilome (Loreto *et al.*, 2014).

Plant VOCs are commonly classified into three major biosynthetic groups: terpenoids (also called isoprenoids), green leaf volatiles (GLVs), and aromatic compounds. Terpenoids (including monoterpenes and

sesquiterpenes), the largest and most structurally diverse group, are involved in a wide range of ecological interactions (Boncan *et al.*, 2020; Büchel *et al.*, 2011; Kos *et al.*, 2013; Rosenkranz *et al.*, 2021). GLVs are six-carbon compounds primarily derived from fatty acid oxidation, rapidly released upon tissue damage and strongly associated with herbivory signaling (Matsui & Engelberth, 2022; Shiojiri *et al.*, 2006). Aromatic compounds, often derived from the shikimate pathway, include benzenoids and phenylpropanoids, and play roles in pollinator attraction and defense (Christaki *et al.*, 2012; Herrmann, 1995). In addition to these main groups, numerous other volatiles with diverse chemical backbones are also produced and released by plants, contributing to the broad and specific spectrum of each species volatilome. Some of the emitted VOCs are usually plant-specific (Huang & Dudareva, 2023; Z. Liu *et al.*, 2023): in fact, many plant species emit characteristic VOCs that act as unique chemical fingerprints, enabling species-level identification (Lo *et al.*, 2021; Lukić *et al.*, 2023). All in all, plant VOCs are a key element in the complex chemical language plants use to mediate biotic interactions not only above but also below ground.

Although sometimes considered just byproducts of their physiological processes, these emissions appear to serve diverse ecological roles: attracting pollinators (Lo *et al.*, 2024), preventing herbivore attacks (Engelberth *et al.*, 2004; Kost & Heil, 2006), modulating interactions with beneficial microbes (D. Guo *et al.*, 2025; Junker & Tholl, 2013) or even transmit ecological information to neighboring plants, which constitutes plant-to-plant communication (Kessler *et al.*, 2023). These low-molecular-weight molecules are released into the atmosphere and can travel across relatively long distances, enabling signaling even beyond immediate neighbors, contributing to the dynamic structuring of ecosystems and, in specific, plant communities (Braasch & Kaplan, 2012; D. Guo *et al.*, 2025). The perception of VOCs by neighboring plants is not passive: it usually involves highly specific receptor-mediated mechanisms, leading to tailored responses depending on the identity and concentration of the volatiles received (Loreto & D'Auria, 2022; Stirling *et al.*, 2024). This complexity underscores the role of VOCs not just as metabolic byproducts, but as finely tuned informational molecules within the plant's communicative repertoire.

What makes VOC-based communication especially remarkable is its versatility and ecological reach, which enables plant acclimation to very

specific environments. In that sense, plants can also modulate their volatile emissions in response to diverse developmental cues or environmental challenges, aiming to warn or inform other individuals about different environmental inputs they would detect (Catola *et al.*, 2018; Nagesh & Piovene, 2011; Ponzio *et al.*, 2013). As an example, during biotic stress events such as herbivore attack or pathogen infection, it has been demonstrated how plants emit a series of stress-induced VOCs serving as airborne signals alerting nearby plants, priming their defense systems before direct damage occurs (Morrell & Kessler, 2014; Paudel Timilsena *et al.*, 2020). VOC-mediated signaling can trigger transcriptomic and metabolic reprogramming in receiver plants, enhancing their resistance capacity and alter their interactions with other organisms (Baldwin *et al.*, 2006). Altogether, VOC-based communication represents a dynamic and increasingly explored mechanism through which plants convey ecologically relevant information, highlighting a growing frontier in plant biology.

VOCs are not the only channel through which plants exchange information aboveground (Figs. I.1 / I.2). Non-chemical cues, particularly those of physical nature, can also serve communicative functions. Among these, light signaling stands out as a powerful input by which plants sense and respond to the presence of neighbors. Often overlooked in this context, light-driven signaling should also be considered a relevant form of plant-to-plant communication, capable of conveying spatial and competitive information in specific vegetative environments (Huber *et al.*, 2021). Due to the central relevance of light signaling for this thesis work, it will be extensively covered in the next section.

I.3 Light in dense vegetative environments

Beyond its fundamental role as an energy source driving photosynthesis, light also acts as a crucial informational cue through which plants monitor their surroundings (Attridge, 1990; Galvão & Fankhauser, 2015). As sessile organisms, plants rely heavily on light cues to detect changes in their environment and to optimize their development accordingly. Plants are sensitive not only to the amount of light they receive, but also to other key parameters such as its direction, duration, and critically, its spectral composition (quality) (Batschauer, 1999). These qualitative features of

light can provide plants with reliable indicators of the proximity and density of neighboring vegetation in diverse ecosystems (Ballaré, 1999). As a result, light serves not only to fuel growth and development but also as a medium through which plants perceive and interpret the structure and dynamics of their communities.

In natural environments, the spectral composition of sunlight reaching a plant is not static but is continuously modulated by many factors (Franklin & Whitelam, 2007; Hughes *et al.*, 1984), including the surrounding vegetation (Durand *et al.*, 2021). Solar radiation comprises a broad spectrum of wavelengths, including red (R, 600-700 nm) and far-red light (FR, 700-750 nm). When sunlight impinges on plant green tissues— especially leaves— R wavelengths are preferentially absorbed for photosynthesis, whereas FR wavelengths are mostly reflected (Martínez-García *et al.*, 2010; Schmitt & Wulff, 1993). This differential reflection alters the light quality environment at the plant community level. In particular, the R to FR ratio (R:FR) acts as the most reliable indicator of vegetation proximity across diverse natural scenarios, enabling plants to adjust their behavior and development in accordance (Ballaré *et al.*, 1990; Martinez-Garcia & Rodriguez-Concepcion, 2023).

In open habitats or low-density plant communities, plants receive unfiltered sunlight with a high R:FR, indicative of unimpeded access to light (Fig. I.2). In contrast, in densely populated plant environments, FR reflection by green tissues of nearby vegetation reduces the R:FR, informing to the plant the close proximity of potential competitors for light (Fig. I.2). This last situation is hereinafter referred to as *proximity shade*, a natural scenario characterized by a particular shift in the R:FR with no impact on the light intensity (Casal, 2013; Roig-Villanova & Martínez-García, 2016).

I.3.1 Molecular mechanisms sustaining the responses to proximity shade

Plants perceive the broad light spectrum through a suite of specialized photoreceptors that convert light cues into developmental and physiological responses. Among them, *phytochromes* are central to the detection of R and FR, existing in two interconvertible forms – active (P_{fr}) and inactive (P_r) that function as molecular switches to regulate light-

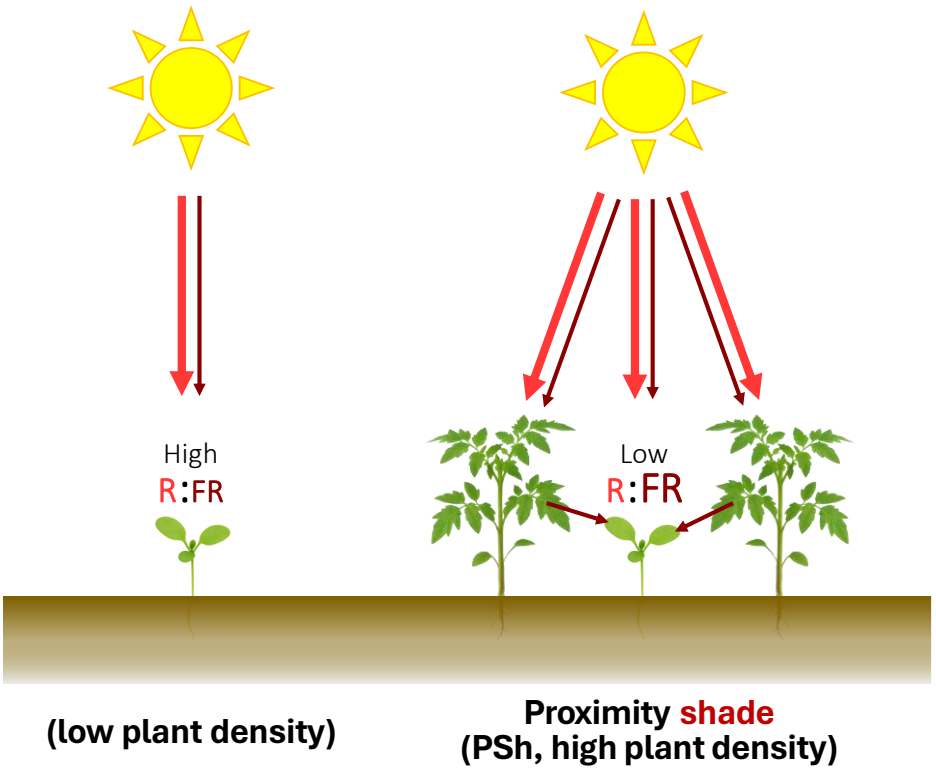

Figure I.2 — Schematic diagram portraying proximity shade.

responsive pathways (Franklin & Quail, 2010; Rockwell *et al.*, 2006). In *Arabidopsis thaliana*, phytochromes are encoded by a small family of five genes (*PHYA* – *PHYE*), with phytochrome B (phyB) playing a pivotal role in detecting changes in the R:FR (Burgie *et al.*, 2014; Franklin & Quail, 2010). This ratio is, again, the key parameter which will modulate and determine the proportion of the active form that defines the dynamic equilibrium of phyB at the protein level, thereby shaping its signaling state (M. Chen *et al.*, 2004; Bae & Choi, 2008; Rockwell *et al.*, 2006). This way, phyB acts as an inducible switch, able to control standard photomorphogenesis as well as initiating downstream responses to proximity shade (Bae & Choi, 2008).

Under high R:FR conditions (i.e., when there is no vegetation nearby), phyB is mostly photoconverted into its active form, preventing shade-associated responses by blocking downstream signaling (Fig. I.3) (Mancinelli, 1994). In contrast, upon detection of low R:FR (i.e., under

proximity shade), phyB becomes inactivated, thereby triggering a cascade of transcriptional and hormonal changes that underlie the molecular shade responses (Sheerin & Hiltbrunner, 2017). This signal is integrated by multiple molecular components, including PHYTOCHROME INTERACTING FACTORS (PIFs), a family of basic helix-loop-helix (bHLH) transcription factors that can physically interact with active phyB (Leivar & Monte, 2014). The function of PIF proteins is directly regulated by phyB. In its active state, phyB physically interacts with PIFs (Fig. I.3), leading to phosphorylation and eventual inactivation by different mechanisms (Leivar & Quail, 2011; Lorrain *et al.*, 2008). When phyB is inactivated by low R:FR, it can no longer bind and inactivate PIFs (Fig. I.3), leading to the activation of target gene expression that orchestrates the shade response (Leivar & Monte, 2014). Among these targets, PIFs rapidly upregulate *PHYTOCHROME RAPIDLY REGULATED* (*PAR)* genes (e.g., *HFR1*), transcriptional regulators that either promote or repress hypocotyl elongation (Roig-Villanova & Martínez-García, 2016). Additionally, besides transcriptional regulators, PIFs activate genes that encode enzymes associated with cellular expansion (EXPANSINs, *EXP)*, cell-wall modification (XYLOGLUCAN ENDOTRANSGLUCOSYLASE / HYDROLASE, *XTH*) and hormone biosynthesis (YUCCAs, *YUCs*) (Hornitschek *et al.*, 2009; Rose *et al.*, 2002). Notably, PIFs play a key role in regulating auxin production and signaling (Fig. I.3) through the induction of genes involved in the *SAV3*-*YUC* biosynthetic pathway (Yang & Li, 2017) or affecting the expression of *SAUR* and *AUX/IAA* genes repressors (Roig-Villanova *et al.*, 2007), respectively. PIFs also repress the expression of photosynthetic pigment genes, including those required for the production of carotenoid pigments (Toledo-Ortiz *et al.*, 2010). All in all, PIFs act as master regulators of shade adaptation at the molecular level, initiating extensive transcriptional reprogramming once alleviated from phyB-mediated repression.

In addition to phyB, several other regulatory components contribute to the fine-tuning of the molecular shade response, either by directly blocking or by modulating transcriptional networks in parallel pathways. Among the phytochromes, phyD and phyE have been shown to act redundantly with phyB in repressing shade-induced responses (Devlin *et al.*, 1998, 1999). In contrast, phyA exerts its influence through a distinct mechanism. PhyA is photolabile and thus typically degraded under high R:FR conditions, via photoconversion to its P_{fr} active form and subsequent 26S proteasome-

mediated degradation (Seo *et al.*, 2004). However, under very low R:FR environments (Fig. I.3), even though the protein equilibrium is favored towards its inactive state, a residual pool of active PhyA remains stable and functional, allowing it to effectively suppress shade signaling (Martínez-García *et al.*, 2014; Molina-Contreras *et al.*, 2019; Pastor-Andreu *et al.*, 2024). This repression is mediated, at least in part, through the activation of *ELONGATED HYPOCOTYL 5* (*HY5*) (Fig. I.3), a basic leucine zipper (bZIP) transcription factor that antagonizes PIF-driven transcriptional programs (Gangappa & Botto, 2016).

Another key repressor is *LONG HYPOCOTYL IN FAR-RED 1* (*HFR1)*, that encodes a bHLH transcriptional cofactor structurally related with PIFs but lacking both DNA-binding and phyB-interacting abilities (Galstyan *et al.*, 2011; Hornitschek *et al.*, 2009). HFR1 heterodimerizes with PIF proteins, thereby sequestering them and preventing of the expression of PIF target genes (Galstyan *et al.*, 2011). Collectively, these components delineate two antagonistic molecular branches that act in different moments and affect the cell elongation of different parts of the hypocotyl: the phyB-PIF-HFR1 axis, which promotes shade-associated gene expression under low R:FR, and the phyA-HY5 axis, which aims to control shade adaptation through an attenuation of these responses (Pastor-Andreu *et al.*, 2024). This dual-channel regulation operates as a molecular "*gas and break*" system, governed by the R:FR, allowing plants to integrate light quality signals and finely adjust their developmental programs to vegetation-driven light cues.

I.3.2 Shade Avoidance Syndrome

The molecular events described above ultimately translate into the activation of several morphological and physiological responses collectively referred to as the shade avoidance syndrome (SAS) (H. Smith & Whitelam, 1997). The SAS is a dynamic adaptative strategy that enables plants to adjust their growth, physiology and development in response to the vegetation-driven changes in light availability. It is important to note, however, that not all plant species exhibit the same responsiveness to proximity shade. The SAS has been extensively characterized in the model species *A. thaliana*, which is considered a *shade-avoider* due to its pronounced morphological and physiological responses to low R:FR

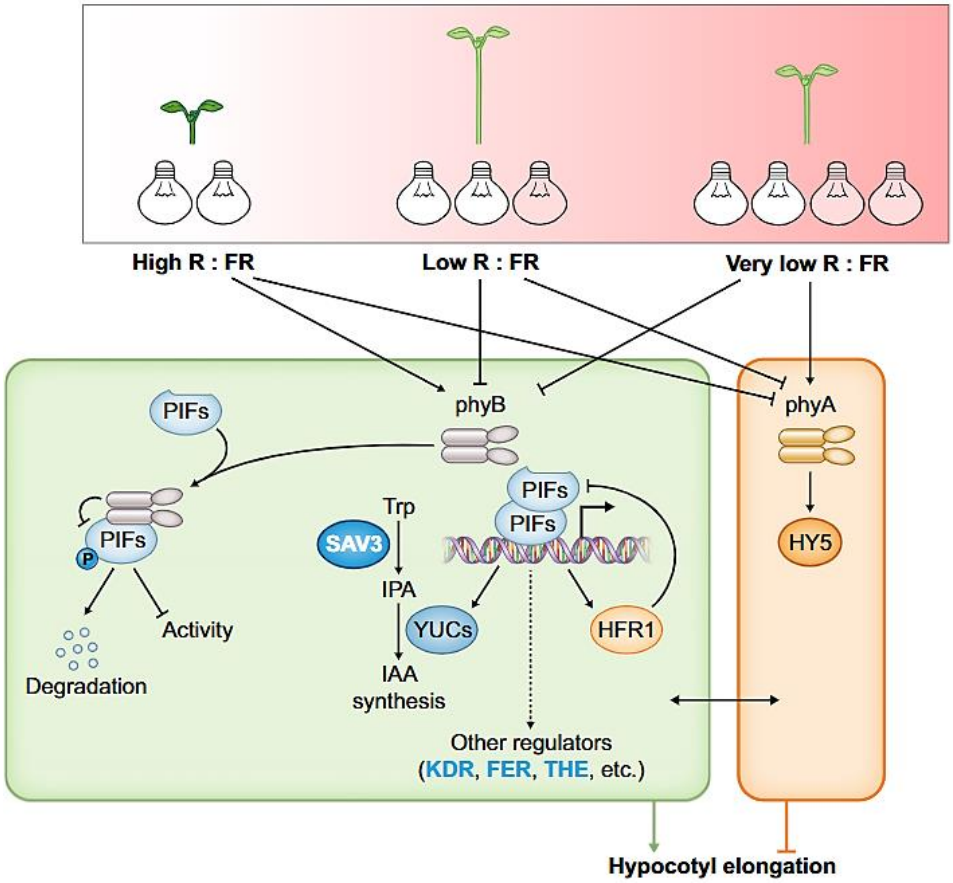

Figure I.3 — Simplified model of shade signaling pathways mediated by phytochromes A and B under different ratios of red to far-red light (R:FR) conditions. *High R:FR maintains phytochrome B (phyB, in green) in its active state, leading to PIF degradation and suppression of shade responses. Under low R:FR, phyB becomes inactive, allowing PIF stabilization and activation of downstream genes, including auxin biosynthesis (SAV3, YUCs) and other regulators (KDR, FER, THE, etc.), which collectively promote shade-induced growth responses. Under very low R:FR, phytochrome A (phyA, in yellow) and HY5 further modulate shade signaling, while negative regulators such as HFR1 help balance the response. Taken from (Martinez-Garcia & Rodriguez-Concepcion, 2023).*

conditions (Galstyan *et al.*, 2011; Martínez-García *et al.*, 2014). This species serves as a prototypical example of plants that perceive vegetative proximity as a signal to rapidly adapt to thrive on these situations. In contrast, the closely related species *Cardamine hirsuta* displays a poor response to shade, reflecting their adaptation to grow in naturally dense and shaded environments (Hay *et al.*, 2014; Lihová *et al.*, 2006). As such,

C. hirsuta is classified as a *shade-tolerant* species. Owing to their close phylogenetic relationship and shared genetic frameworks, both species provide an excellent comparative model system to investigate shade response mechanisms at both molecular and phenotypic levels between the two plant groups (Hay *et al.*, 2014; Martínez-García & Rodriguez-Concepcion, 2023). At the molecular level, *C. hirsuta* attenuated response to shade results from, at least, the enhanced activity of the shade suppressors phyA and HFR1, and likely the reduced activity of PIFs, compared to *A. thaliana* (Molina-Contreras *et al.*, 2019; Paulišić *et al.*, 2021)

The SAS encompasses a set of morphological and physiological adaptations that affect all stages of *A. thaliana* development, from seed germination and dormancy up to flowering and seed production in adult plants (Halliday *et al.*, 1994; Martínez-García *et al.*, 2010; Roig-Villanova *et al.*, 2025; Shinomura *et al.*, 1996). One of the hallmark traits of SAS is hypocotyl elongation at the seedling stage, which portrays shaded plants attempt to outgrow neighboring individuals and access more favorable light conditions (Martínez-García *et al.*, 2014). It is a fast and widely studied response, whose consistency makes it a reliable indicator of SAS. This vertical growth response is often accompanied by upward leaf positioning (hyponasty) (Michaud *et al.*, 2023), reduced lateral branching (González-Grandío *et al.*, 2013), and elongated petioles (Djakovic-Petrovic *et al.*, 2007), all contributing to increased light interception. In parallel, SAS involves a marked downregulation of photosynthetic pigment levels, particularly chlorophylls and carotenoids (Morelli *et al.*, 2021; Roig-Villanova *et al.*, 2007). This reduction is thought to result from both transcriptional repression of pigment biosynthesis genes and/or enhanced pigment turnover (Beisel *et al.*, 2011; Bou-Torrent *et al.*, 2015; Moon *et al.*, 2008; Toledo-Ortiz *et al.*, 2010), and reflects a strategic shift away from investing in full photosynthetic capacity under shade, where light quantity and quality are suboptimal, as the plant prioritizes elongation and foraging for light. Importantly, another key feature of SAS is the attenuation of defense-related pathways, making plants potentially more vulnerable to biotic stress (Cerrudo *et al.*, 2012; Courbier *et al.*, 2021; De Wit *et al.*, 2013). These changes reflect a growth-over-defense trade-off, whereby plants prioritize competitive elongation at the expense of other energy-intensive processes in response to vegetation-driven light cues.

I.4 A volatile output of shade

Beyond the well-characterized morphological and physiological responses triggered by proximity shade (low R:FR), recent advances suggest that plant adaptive strategies to nearby vegetation include the remodeling of their metabolic landscape, including the biosynthesis and emission of VOCs (Ballaré & Pierik, 2017), adding a novel layer to the shade response framework (Ninkovic *et al.*, 2019). In this context, the term *shade volatilome* has been proposed to refer to the specific blend of volatiles produced under proximity shade conditions. Based on the well-established role of VOCs and plant-to-plant communication signals (Fig. I.1), we hypothesize that the shade volatilome might be not just a passive consequence of metabolic rearrangements but an actively regulated response to low R:FR signaling. The emergence of this concept opens new perspectives on the complexity of shade responses by combining physical (low R.FR) and chemical (VOCs) signals that, together, modulate plant acclimation to crowded environments.

Accumulated evidence from several experimental studies has proved that exposure to low R:FR conditions leads to both quantitative and qualitative changes in VOC emission profiles, suggesting that light cues can reprogram metabolic fluxes toward specific volatile outputs. Quantitatively, low R:FR has been associated to reduced total VOCs emission in species such as *A. thaliana* or *Hordeum vulgare* (Kegge *et al.*, 2013, 2015). However, contrasting responses have been reported in *Zea mays*, where long-term low R:FR exposure or mutations in *phyB* result in decrease total VOCs emission, yet short-term exposure can transiently enhance volatile production (Escobar-Bravo *et al.*, 2024). These divergent findings point out to the existence of species-specific regulatory programs, time-dependent dynamics and/or different sets of compounds analyzed in the modulation of VOC output under proximity shade.

The general trend toward reduced volatile emission under low R:FR conditions has been primarily attributed to the downregulation of key volatile families such as terpenoids and GLVs, both of which represent major components of the plant volatilome across diverse species (Kegge *et al.*, 2013, 2015; Pashkovskiy *et al.*, 2024; Reichel *et al.*, 2022). However, while overall VOC emissions often decline under low R:FR conditions, the emission of specific volatile compounds can be selectively upregulated. In the following paragraphs, we will examine particular compounds or

compound classes whose emission has been shown – or is hypothesized – to be modulated by proximity shade, and deepen into their physiological roles.

I.4.1 Ethylene

Ethylene is a gaseous plant hormone that appears among the still short list of individual VOCs whose production has been consistently shown to be modulated by proximity shade. Experimental supplementation with FR light, simulating proximity shade, in a small range of species—including barley (*H. vulgare*) (Kegge *et al.*, 2015), tobacco (*Nicotiana tabacum*) (Pierik, Cuppens, *et al.*, 2004) or *A. thaliana* (Kegge *et al.*, 2013)—has been reported to substantially increase ethylene biosynthesis. These findings suggest that ethylene may constitute an important metabolic output of shade-induced signaling, potentially contributing to plant acclimation in crowded environments.

Ethylene exerts a wide range of physiological effects in plants, acting as a key hormonal signal involved in growth regulation, stress responses, senescence, fruit ripening and defense (Vandenbussche *et al.*, 2012). One of the hallmark phenotypic manifestations of ethylene signaling described in dark-grown seedlings is the so-called *triple response*, first described in *A. thaliana* (Schaller & Kieber, 2002). This response consists of three distinctive traits: (i) inhibition of hypocotyl elongation, (ii) radial swelling of the hypocotyl, and (iii) exaggerated curvature of the apical hook. These morphological changes are thought to protect the meristematic tissues as the seedling pushes through the soil. The triple response has been extensively used to identify and characterize ethylene-related mutants, laying the foundation for our current understanding of the biosynthesis, perception, and transduction pathways of this hormone. Although classically associated with growth inhibition in some contexts such as in darkness, ethylene can also promote elongation responses depending on the developmental stage and environmental conditions (Smalle *et al.*, 1997). Its influence on cell elongation, cell wall remodeling, and hormonal cross-talk makes it particularly relevant during adaptive developmental processes such as those triggered by shade (Le *et al.*, 2005; Merelo *et al.*, 2017; Van de Poel *et al.*, 2015). In this context of low R:FR, ethylene has been linked to elongation growth and other shade-associated traits,

suggesting it may functionally integrate into the SAS alongside other hormonal and transcriptional regulators, in coordination with or parallel to the PIF-driven signaling module (Das *et al.*, 2016). Considering its biosynthetic activation under low R:FR conditions and its gaseous, volatile nature, ethylene may represent a relevant output of shade-responsive metabolism with potential importance in shaping physiological responses to vegetation proximity within the shade volatilome.

Ethylene biosynthesis is a highly regulated and well-characterized metabolic pathway (Fluhr *et al.*, 1996; K. L.-C. Wang *et al.*, 2002), beginning with the amino acid methionine (Fig. I.4). Methionine is converted into S-adenosylmethionine (SAM) by SAM synthetase, which in turn is transformed into 1-aminocyclopropane-1-carboxylic acid (ACC) via ACC synthase (ACS)—the rate-limiting step of the pathway. This enzymatic reaction also produces 5′-methylthioadenosine (MTA), which is recycled back to methionine, maintaining amino acid homeostasis. Finally, ACC is converted into ethylene by ACC oxidase (ACO), completing the biosynthetic process (Fig. I.4). Ethylene production is subjected to multiple layers of regulation (Argueso *et al.*, 2007; Pattyn *et al.*, 2021), including circadian control: peak RNA levels of key biosynthetic genes coincide with maximal ethylene synthesis, all governed by diurnal rhythms. Core clock components such as TIMING OF CAB EXPRESSION 1 (*TOC1*) and CIRCADIAN CLOCK ASSOCIATED 1 (*CCA1*) are required to sustain these rhythmic dynamics by modulating *ACS* gene expression (Thain *et al.*, 2004). In addition, ethylene levels are fine-tuned through negative feedback: elevated ethylene signaling downregulates its own production, while reduced sensitivity enhances it (Booker & DeLong, 2015; Yoshida *et al.*, 2005). This self-regulatory mechanism reinforces the hormone's temporal and quantitative precision. Regarding light regulation, recent findings in *Sorghum bicolor* suggest that phyB plays a direct role in repressing ethylene biosynthesis by inhibiting *ACO* transcription (Finlayson *et al.*, 1998, 1999). Upon exposure to low R:FR conditions—associated with proximity shade and phyB inactivation—ethylene production increases significantly, resembling the phenotype of phyB-deficient mutants. These observations highlight phyB as a key upstream modulator of ethylene biosynthesis under shade, although additional SAS-related regulators may also contribute to this response and remain to be identified.

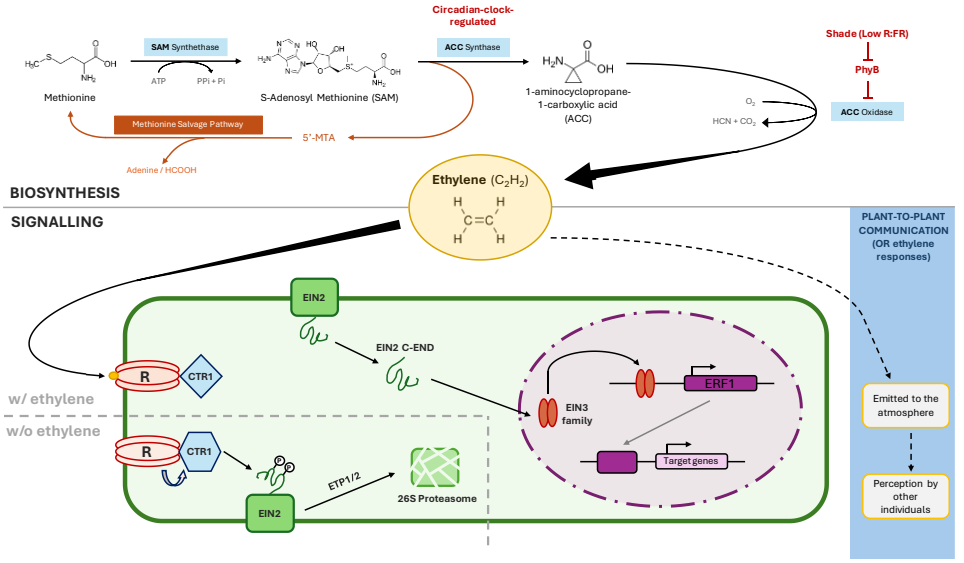

Figure I.4 — Schematic diagram of ethylene biosynthetic pathway, ethylene's signaling mechanism and ethylene's potential role as a plant-to-plant communication signaling molecule. R, ethylene receptor.

The ethylene signaling pathway (Fig. I.4) has been extensively characterized, largely through mutant screens in *A. thaliana* based on the distinctive triple response observed in dark-grown seedlings (H. Guo & Ecker, 2004), as mentioned above. Ethylene is perceived by a family of five membrane-bound receptors localized to the endoplasmic reticulum: ETR1, ERS1, ETR2, ERS2, and EIN4 (Bleecker, 1999). Although these receptors function redundantly, ETR1 has been shown to play a predominant role (Binder *et al.*, 2005). Structurally, they share similarity with prokaryotic two-component histidine kinases (Gamble *et al.*, 1998) and act as negative regulators of the pathway in the absence of ethylene by activating the Raf-like serine/threonine kinase CTR1 (Shakeel *et al.*, 2015). Active CTR1 phosphorylates the C-terminal domain of EIN2, a key positive regulator and main signaling element of the pathway (Alonso *et al.*, 1999), targeting it for 26S proteasome-mediated degradation via the F-box proteins ETP1 and ETP2 (Ju *et al.*, 2012). Ethylene binding inactivates CTR1, presumably through a conformational change that inhibits its kinase activity, thereby preventing EIN2 phosphorylation (Park *et al.*, 2023). As a result, the C-terminal fragment of EIN2 is cleaved and translocates to the nucleus, where it promotes the stabilization and activity of the transcription

factor EIN3 and its homologs EIL1 and EIL2 (Wen *et al.*, 2012). These transcription factors initiate a transcriptional cascade, including activation of *ERF1* and other downstream effectors, culminating in the ethylene response.

I.4.2 Apocarotenoids

Apocarotenoids have emerged as a group of specialized metabolites that can act as signals for plant-to-plant communication both below and aboveground (L. Li *et al.*, 2025; Moreno *et al.*, 2021). These compounds originate from the oxidative cleavage of carotenoids (Fig. I.5)—a pigment class known to be downregulated under shade—so it is expected that degradation of carotenoids following exposure to low R:FR might result in enhanced apocarotenoid production.

Chemically, apocarotenoids comprise a wide variety of molecules, ranging from phytohormones, like abscisic acid (ABA) and strigolactones (SLs), to volatile compounds, such as β-cyclocitral (β-cc) and β-ionone (β-ion) (Fig. I.5). Apocarotenoids can be synthesized either through non-enzymatic or enzymatic pathways. The non-enzymatic route is typically triggered under conditions of photooxidative stress, where carotenoids act as scavengers of reactive oxygen species (ROS), particularly singlet oxygen ($^1O_2$). This interaction leads to the oxidative cleavage of the carotenoid backbone, resulting in the formation of smaller degradation byproducts, apocarotenoids. In contrast, the enzymatic pathway involves a family of enzymes called carotenoid cleavage dioxygenases (CCDs), which catalyze the stereo- and regioselective cleavage of double bonds within carotenoid molecules. Six major CCD sub-families have been described in plants: CCD1, CCD4, CCD7, CCD8, 9-cisepoxicarotenoid dioxygenases (NCED) and zaxinone synthase (ZAS) (J. Y. Wang *et al.*, 2019; S. Zhang *et al.*, 2021). Their function is closely associated with the regulation of carotenoid levels and pigmentation patterns across various plant tissues and organs. In specific, CCD1 enzymes exhibit broad substrate flexibility and double-bond specificity, enabling them to generate a wide variety of volatile compounds and dialdehyde byproducts. This suggests a possible role in the breakdown and scavenging of damaged carotenoids (Ilg *et al.*, 2009). In contrast, CCD4 enzymes show a more selective activity, cleaving specifically at the C9–C10 or C7–C8 double bonds of bicyclic carotenoids

(S. Zhang *et al.*, 2021). CCD7 and CCD8 subfamilies are reported to be key enzymes for the biosynthesis of SLs (Alder *et al.*, 2012); NCEDs are necessary for ABA biosynthesis (Schwartz *et al.*, 2003) and ZASs are responsible for the catalysis of zaxinone production, a recently discovered plant growth regulator in *Oryza sativa* (rice) (J. Y. Wang *et al.*, 2019). All these enzymatic processes are tightly regulated and allow for the controlled production of specific apocarotenoids under defined developmental or environmental conditions.

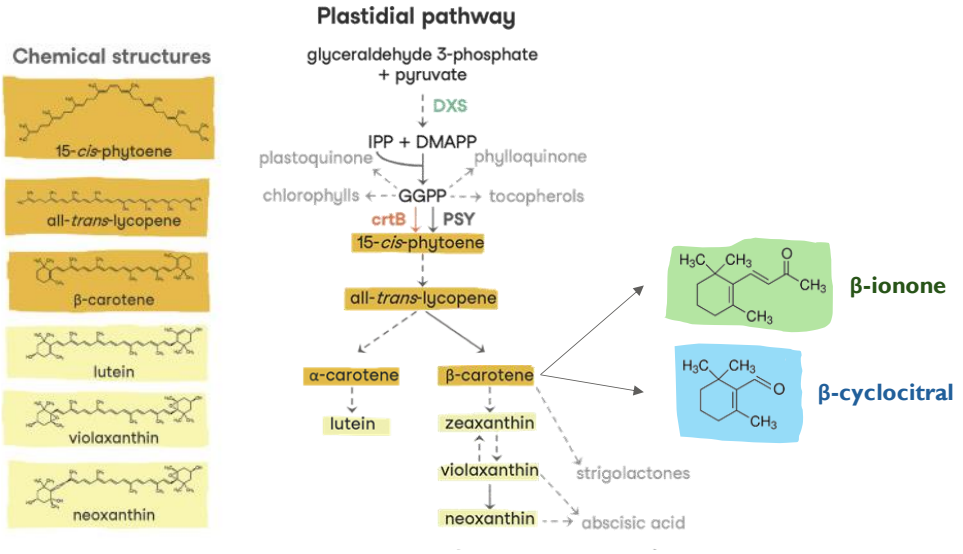

Figure I.5 — Biosynthetic pathway of β-cyclocitral and β-ionone derived from carotenoid metabolism. *Schematic representation of the plastidial carotenoid biosynthetic pathway, highlighting the steps leading from precursor metabolites to carotenoids and their cleavage into apocarotenoids. Chemical structures of representative carotenoids are shown on the left, while the derived apocarotenoids β-cyclocitral (blue) and β-ionone (green) are indicated on the right. Enzymes catalyzing key steps in the biosynthesis of carotenoids are noted in the pathway. Adapted from Torres-Montilla & Rodriguez-Concepcion, 2021.*

Among the volatile products arising from both enzymatic and non-enzymatic pathways, β-cc and β-ion have received particular attention due to their origin from β-carotene (Fig. I.5), one of the most abundant carotenoids in photosynthetic tissues. Both compounds have been observed to be produced under high light stress conditions, as products of

oxidative cleavage of β-carotene, as an attempt to mitigate the damaging of singlet oxygen radicals ($^1O_2$) (Ramel *et al.*, 2012, 2013). By contrast, the role of CCD enzymes for the biosynthesis of β-cc and β-ion in plants appears to be limited and its physiological relevance remains somewhat inconclusive. Both molecules have been reported as products of CCD4 enzymatic activity in species such as *Crocus sativus* or *Vitis vinifera* (vine) (Baba *et al.*, 2015; Meng *et al.*, 2019), pointing toward broad substrate specificity within this enzyme family. This pattern has also been observed in rice, in which overexpression of *OsCCD4b* led to increased accumulation of both these apocarotenoids (Taniguchi *et al.*, 2023). In addition, CCD1 enzymes have also been implicated in β-ion production across several species (Ibdah *et al.*, 2006; Simkin, Underwood, *et al.*, 2004; Y. Wang *et al.*, 2022). In *Solanum lycopersicum* (tomato), β-ion can be synthesized by either CCD1 or CCD4 (Simkin, Schwartz, *et al.*, 2004; Yoo *et al.*, 2023), while recombinant CCD7 of *A. thaliana* has also been shown to produce β-ion (Schwartz *et al.*, 2004). The regulation of *CCD* expression and activity under defined physiological or environmental conditions is still poorly understood and merits further investigation.

Both β-cc and β-ion, despite their relatively recent recognition as bioactive compounds, have already been reported as signaling molecules in plants associated with plant development, defense capabilities and response to stresses. β-cc has been shown to enhance drought tolerance independently of ABA (Deshpande, Manoharan, *et al.*, 2021), reduce ABA biosynthesis while conferring resistance to bacterial blight in rice (Taniguchi *et al.*, 2023), act as a retrograde signal to provide tolerance to photooxidative stress (D'Alessandro *et al.*, 2018), upregulate multiple stress-responsive genes (Deshpande, Purkar, *et al.*, 2021), promote root growth (Dickinson *et al.*, 2019) or optimize growth and defense responses in tomato plants (Deshpande & Mitra, 2023). On the other hand, β-ion has been reported as a volatile deterrent or repellent to insects when emitted by leaves of different species (Gruber *et al.*, 2009; Ômura *et al.*, 2000; S. Wang *et al.*, 1999). Notably, recent findings have shown that β-ion can also enhance resistance to the fungus *Botrytis cinerea* through transcriptomic reprogramming in *A. thaliana*, modulating the expression of thousands of genes involved in stress tolerance, growth, hormone metabolism, photosynthesis or pathogen defense (Felemban *et al.*, 2024).

Together, these findings highlight the signaling potential of the apocarotenoids that might be present in the shade volatilome,

underscoring their relevance as volatile regulators of plant physiology in response to environmental stimuli. Nevertheless, the reported physiological effects of β-cc and β-ion have been typically observed following exogenous application by addition to the growth media or foliar sprays, leaving open questions about their actual impact and perception when naturally emitted into the atmosphere under physiological conditions.

Objectives

Objectives

Over the last decade, mounting evidence has revealed that exposure to altered R:FR ratios—particularly low R:FR conditions mimicking proximity shade—leads to substantial reprogramming of the plant volatilome. These changes, mostly described as reductions in total VOC output, have been primarily associated with the downregulation of terpenoids and GLVs, two major families of constitutively emitted compounds across a wide range of species. This has often been interpreted as a trade-off between growth and secondary metabolism under shade. However, a closer look at individual volatile compounds which do not belong to these two families and whose production is also shade-responsive (Escobar-Bravo *et al.*, 2024; D. Guo *et al.*, 2025; Kegge *et al.*, 2013; Vicherová *et al.*, 2020) suggests a more nuanced and meaningful biological scenario.

Volatile molecules such as ethylene and the apocarotenoids β-cc and β-ion have gained attention for their consistent light-dependent production. Ethylene biosynthesis is directly influenced by light quality, with low R:FR conditions known to enhance its synthesis in several species. In contrast, β-cc and β-ion are typically associated with photooxidative stress resulting from excess light scenarios, like those potentially arising when photosynthetic pigments drop in response to low R.FR without changes in light intensity. These compounds have already been described as functional signals within the emitting plant, regulating diverse physiological processes including root and hypocotyl development, stress acclimation, and defense. However, their potential role in interplant signaling as VOCs remains largely unexplored.

The hypothesis proposed in this work is that the distinct set of VOCs emitted by plants under low R:FR conditions may function as signaling agents in plant-to-plant communication, eliciting specific physiological or developmental responses when perceived by neighboring plants. In this framework, certain volatiles emitted in response to proximity shade could convey information about impending light competition or promoting mutualism or facilitation between plants growing in such high density

conditions, enabling nearby plants to adjust their physiology proactively—even before experiencing the altered light environment themselves. A few recent studies have begun to explore this possibility in bryophytes, barley and maize (Vicherová *et al.*, 2020; Kegge *et al.*, 2015; Escobar-Bravo *et al.*, 2024; D. Guo *et al.*, 2025), although the nature of the signaling molecules and processes remain largely uncharacterized. This points to a relatively new field of research. If confirmed, such a mechanism would represent a previously uncharacterized layer of plant–plant interaction, in which VOCs serve not just as stress or defense mediators, but as social signals conveying information about vegetation density and competitive light environments.

The main objective of this thesis is to test the hypothesis that proximity shade triggers volatile-mediated plant communication processes. To explore this idea, this thesis aims to:

Objective 1: Examine the potential impact of the shade volatilome on the development of nearby non-shaded plants;

Objective 2: Investigate the functional role of specific VOCs—namely ethylene, β-cc and β-ion— on this process;

Objective 3: Dissect the molecular mechanisms by which these VOCs trigger their effects, eventually building a model of VOC-mediated proximity shade signaling.

Through a combination of metabolic, molecular, genetic and phenotypic approaches, the work aims to determine whether, and how, the shade volatilome —and these compounds individually— can act as signaling cues capable of influencing neighboring plant responses. Ultimately, this study seeks to contribute to a broader understanding of plant responses to vegetation proximity, proposing that it may not only rely solely on photoreceptor-mediated processes, but also involve volatile-based communication between plants

Results

Chapter I

Chapter I. Shade-induced plant volatiles act as negative regulators of early seedling development

1.1 The shade volatilome represses elongation of proximal etiolated seedlings

To investigate the potential signaling activities of the VOCs released by shade-exposed plants on neighboring non-shaded individuals, we used adult plants of *S. lycopersicum* (tomato) as the VOC-emitting species (emitter plants or e-plants), and seedlings of *A. thaliana* as the VOC-receiving entity (receiver plants or r-plants). Tomato was selected as an e-plant because its widely-described shade-associated responses (Burbano-Erazo *et al.*, 2025; Ji *et al.*, 2021), rich metabolism (Vogel *et al.*, 2010; L. Liu *et al.*, 2015), broad VOCs production profile (Rambla *et al.*, 2013), and VOC emission in response to diverse stimuli, including light cues (Urdin-Bravo *et al.*, 2024; Cortés *et al.*, 2016; Bleeker *et al.*, 2009). *A. thaliana* seedlings were chosen as r-plants because of their small size, the wealth of information on this developmental stage, and the availability of extensive genetic resources, facilitating a better understanding of potential VOCs effect both at the physiological and molecular level.

We developed a one-box enclosed system to conduct our plant-to-plant communication experiments under controlled conditions (Fig. 1.1). In this initial set-up, both the e- and r-plants were placed within the same unit (a large transparent and hermetically closed box), therefore, sharing the same atmosphere. This “same-box” system did not allow to provide different light conditions to the e-plants and r-seedlings. For that reason, we initially tested the effect of VOCs emitted by tomato e-plants exposed to W or W+FR light on *A. thaliana* r-seedlings that developed in the dark (Fig. 1.1). Petri dishes containing the seeds were placed inside a cardboard case, which was also covered in aluminum foil to guarantee complete darkness in the interior. Both the cardboard cases and the tomato plants (typically, *ca.* one-month old plants grown in individual small

pots) were put together in the box at the same time, and the system was then closed (Fig. 1.1). Sealed boxes were incubated for several days either under W or under W+FR in walk-in growth chambers.

By sharing the same enclosed environment for several days, the differentially produced VOCs emitted by tomato plants exposed to either W or W+FR could diffuse freely and interact with *A. thaliana* seeds while they germinated and developed into etiolated seedlings. Although various developmental traits were considered, we first set our focus onto studying the potential differences on hypocotyl elongation, a well-studied skotomorphogenic response with a wide dynamic range and easy to measure.

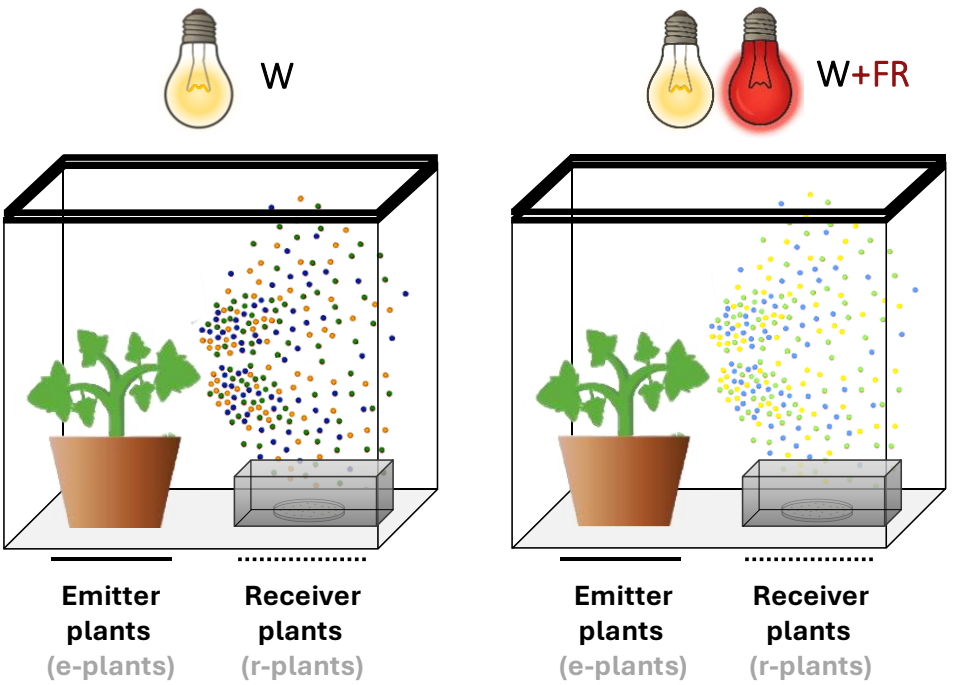

Figure 1.1 — Same-box system for plant-to-plant communication (schematic diagram). *The same-box system consists of emitter plants (e-plants) and receiver plants (r-plants) placed within a single hermetically closed box with transparent top and side walls. Both plant groups share the same airspace, allowing volatiles released by e-plants to diffuse freely toward r-plants. The system can be illuminated under different light regimes: white light alone (W, left) or W supplemented with far-red light (FR) to simulate proximity shade (W+FR; right), affecting e-plants only. E-plants are adult tomato plants grown in pots. R-plants are A. thaliana seedlings grown in Petri dishes inside foil-covered cardboard boxes to exclude light, therefore developing in complete etiolation.*

After 3 days, we observed that hypocotyls of *A. thaliana* r-seedlings exposed to the atmosphere produced by the tomato e-plants under simulated shade (W+FR) were significantly shorter than those treated with the VOCs released by W-exposed tomato plants (Fig. 1.2-A). This trend was consistently observed across independent experiments that varied key parameters (Table 1.S1) – including W or W+FR exposure duration, number of e-plants, number of covering layers surrounding the receivers' cases, etc. (Fig. 1.S1). Despite these variations, etiolated seedlings exposed to shaded-tomato VOCs repeatedly exhibited reduced elongation.

These first results indicate that the VOCs released by tomato e-plants under shade conditions carry environmental information that can be perceived by neighboring *A. thaliana* r-seedlings, influencing their development (suppressing elongation in the absence of light).

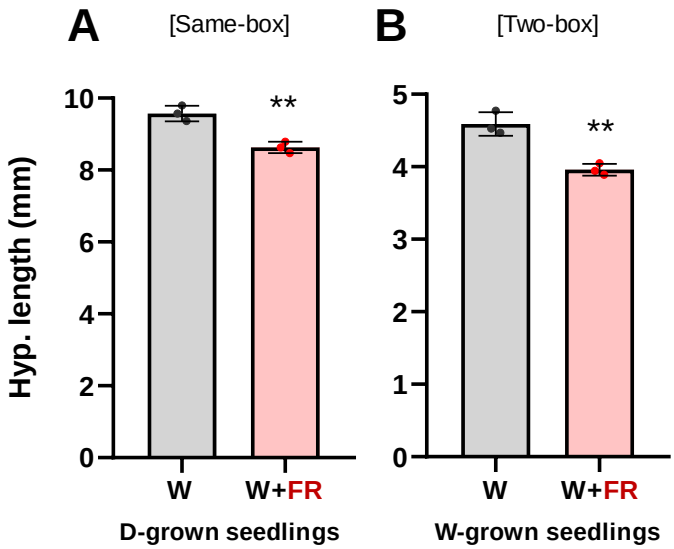

Figure 1.2 — The shade volatilome represses hypocotyl elongation of A. thaliana r-seedlings regardless of light conditions. *Hypocotyl length of etiolated* ***(A)*** *and white light- (W-) grown* ***(B)*** *r-seedlings after exposure to volatiles from emitter plants grown under W (in grey) or W supplemented with far-red light (FR) to simulate shade (W+FR, in pink). Bars represent the mean of 3 biological replicates ± SD of the means. Statistical significance was assessed by unpaired, two-tailed t-tests (*=p<0.05, **=p<0.01). See Tables 1.1 and 1.2 for experimental details.*

1.2 The shade volatilome impairs elongation of light-exposed neighboring seedlings

We next developed a two-box plant-to-plant communication system by connecting a second, smaller box to the box system via silicone tubing (Fig. 1.3). The addition of a separated but connected second box enabled us to physically separate the e- and r-plants, hence allowing the *A. thaliana* r-seedlings to be exposed to independently controlled light conditions (regardless of the irradiation used to treat tomato e-plants) while still receiving the VOCs emitted by W or W+FR exposed tomato plants.

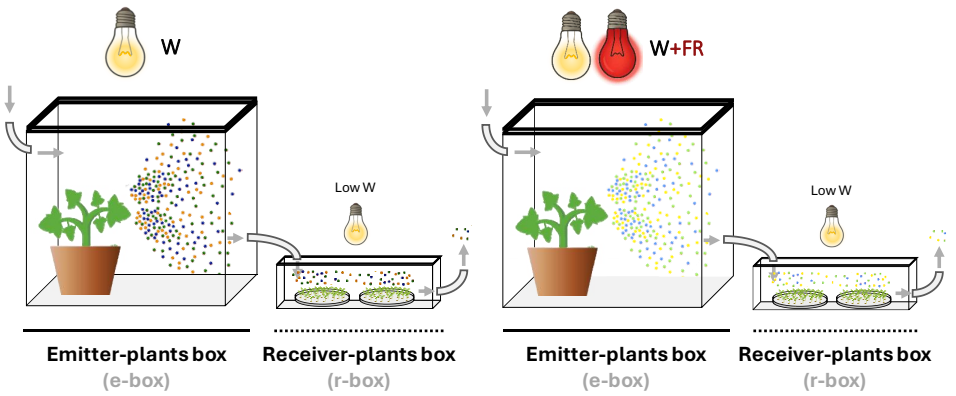

Figure 1.3 — Two-box system for plant-to-plant communication (schematic diagram). *The two-box system consists of tomato plants (e-plants) placed in a large transparent emitter box (e-box) connected by airflow to a much smaller but also transparent receiver box (r-box) containing A. thaliana seedlings (r-seedlings). Volatiles released by e-plants are transported through the air stream (portrayed with grey arrows) into the r-box, where r-seedlings are then exposed to them. Because both boxes are physically separated, e- and r-seedlings can be exposed to independent light treatments. In the experiments shown here, e-plants were illuminated with either white light (W, left) or simulated shade (W+FR, right), while r-seedlings were grown under low white light (low W).*

Initially, we analyzed if the shade volatilome of tomato e-plants impacted hypocotyl elongation of W-grown *A. thaliana* r-seedlings. As light also inhibits hypocotyl elongation, we reasoned that if the W intensity used for the r-seedlings was the same one used for the tomato e-plants (110-140 µmol m^{-2} s^{-1}, long-day photoperiod), it would strongly suppress hypocotyl length, and we probably wouldn't be able to notice any repressive effect driven by the shade-responsive volatilome. Therefore, to maximize the

observable response, we decided to grow the r-seedlings under dim (i.e., low) W. To achieve this, we placed neutral filters (which do not alter light quality) directly above the W-exposed receiver boxes, reducing the intensity of the light penetrating in boxes without affecting its spectral composition (25-27 μmol m^{-2} s^{-1}, long-day photoperiod). This treatment resulted in photomorphogenic (fully de-etiolated) seedlings with relatively long hypocotyls.

Petri dishes with *A. thaliana* seedlings germinated and grown for 2 days under W were placed in the small r-boxes, which were then connected with silicone tubes to the large e-boxes containing the tomato e-plants (Fig. 1.3 and Table 1.S2). While r-boxes were exposed to low W, e-boxes were illuminated with either W or W+FR. An air pump ensured constant air circulation from e- to r-boxes (Fig. 1.3).

After five days of chemical exchange, *A. thaliana* r-seedlings exposed to VOCs from shade-irradiated tomato e-plants elongated significantly less than those exposed to the atmosphere generated by control (W-illuminated) tomato plants (Fig. 1.2-B). This result was consistent with our previous observations in etiolated seedlings (Fig. 1.2-A). This repression under low W conditions was further confirmed by additional experiments (Fig. 1.S2), with varying parameters and conditions. Information regarding these variations can be found in Table 1.S2.

We also examined whether VOC exposure affected photosynthetic performance, using two parameters: ϕPSII (effective quantum yield of PSII, that estimates actual photosynthetic performance) and Fv/Fm (maximum quantum efficiency of PSII photochemistry). No statistical differences were found between *A. thaliana* seedlings exposed to the volatilome of tomato plants grown under W or W+FR (Fig. 1.4), indicating that the shade-associated VOCs did not significantly affect photosynthetic efficiency.

1.3 The shade volatilome induces changes in gene expression that partially overlap with those directly regulated by shade.

Our next step towards the characterization of the role of the shade-produced VOCs as molecular signals in plant-to-plant communication was

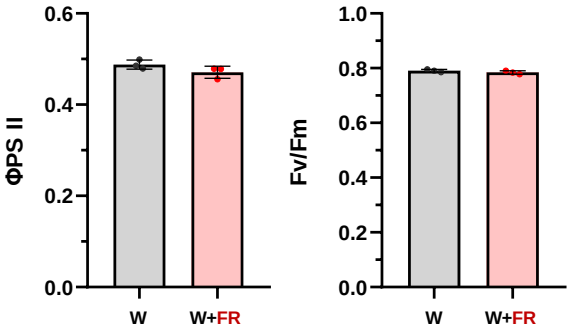

Figure 1.4 — Photosynthetic performance of low W-grown A. thaliana r-seedlings exposed to volatiles from tomato e-plants illuminated with either W or W+FR. *ΦPSII (left) and Fv/Fm (right) of A. thaliana r-seedlings grown under low white light (W) in two-box experiments exposed to the volatiles produced by emitter tomato plants illuminated with white light (W, in grey) or white light supplemented with far-red (W+FR, in pink). Bars represent the mean of 3 biological replicates ± SD of the means. No statistical significances were found conducting unpaired, two-tailed t-tests.*

to analyze the differential impact of shade- and W-produced VOCs of tomato e-plants on gene expression in the *A. thaliana* r-seedlings by performing RNA sequencing. This approach aimed to confirm that shade-induced VOCs contain information that can be perceived by neighboring plants and elicit transcriptional responses.

1.3.1 Sampling, quality and clustering

Using the two-box plant-to-plant communication set-up described above (Fig. 1.3), five-day-old *A. thaliana* seedlings grown under low W conditions (27 µmol m^{-2} s^{-1}, long-day photoperiod) were exposed to VOCs emitted by tomato plants that had been previously illuminated with either W or W+FR light for 24 h. Seedlings were collected at 0, 3, 8, and 24 h (four biological replicates for each time point) following exposure to the two volatilomes for subsequent RNA extraction and sequencing. To verify that the experimental setup was effectively inducing differential volatile production, a subset of *A. thaliana* seedlings was left exposed to the same volatile treatments for five days. As expected, hypocotyl elongation was repressed in response to volatiles from the shade-simulated treatment (Fig. 1.S2-C), reproducing the effects described in the previous section. This phenotypic outcome served as an internal control, confirming the functionality of the emitter plants and the reliability of the system.

Total RNA was extracted from the collected samples and then quality-checked, concentration-normalized, and submitted for sequencing (performed by BGI Genomics™). The sequencing run yielded high-quality data across the total 28 *A. thaliana* samples, with an average of 46.56 million clean reads per sample. Alignment statistics confirmed the robustness of the dataset: on average, 98.25% of reads successfully mapped to the reference genome, with 95.83% mapping uniquely (Table 1.1). These values indicate excellent sequencing depth and specificity, ensuring reliable downstream transcriptomic analyses. Additionally, all samples displayed similar count distributions (Fig. 1.S3), indicating consistent mapping quality and uniform transcriptomic coverage across replicates.

Table 1.1 — Clean reads and alignment to the reference genome

Sample	Total Clean Reads (M)	Total Mapping (%)	Uniquely Mapping (%)
0h_R1	47.4	98.6	96.5
0h_R2	46.9	98.1	96.2
0h_R3	47.3	98.6	96.5
0h_R4	47.2	98.4	96.1
W_3h_R1	47.0	98.4	96.2
W_3h_R2	46.6	98.0	95.8
W_3h_R3	46.5	97.9	95.7
W_3h_R4	47.9	97.9	95.5
FR_3h_R1	45.2	98.2	96.1
FR_3h_R2	47.0	98.4	96.2
FR_3h_R3	47.1	98.2	96.0
FR_3h_R4	47.3	98.6	96.4
W_8h_R1	46.8	98.1	95.2
W_8h_R2	47.8	97.7	94.6
W_8h_R3	47.1	98.5	95.6
W_8h_R4	47.2	98.5	95.5
FR_8h_R1	47.1	98.3	95.2
FR_8h_R2	47.3	98.5	95.5
FR_8h_R3	47.0	98.3	95.2
FR_8h_R4	47.4	98.7	95.7
W_24h_R1	46.7	98.1	95.8
W_24h_R2	46.3	97.7	95.5
W_24h_R3	47.2	98.6	96.3
W_24h_R4	47.3	98.5	96.3
FR_24h_R1	44.4	97.7	95.0
FR_24h_R2	42.3	98.7	96.7
FR_24h_R3	43.7	98.3	96.1
FR_24h_R4	44.7	98.0	95.8
MEANS	**46.56**	**98.25**	**95.83**

To evaluate the overall variation in transcriptomic profiles, we performed a Principal Component Analysis (PCA) together with a Pearson correlation analysis (Fig. 1.5). In the PCA (Fig. 1.5-A), PC1 explained a 64.2% of the total variance, capturing most of the variability in the dataset. This component mainly reflected harvesting time, as circadian or/and diurnal oscillations in gene expression are known to generate important differences between samples collected at different time points (Fig. 1.5-A). Accordingly, samples harvested at 3 h and 8 h separated along the PC1 axis, whereas 0 h and 24 h clustered closely, reflecting their common harvesting time of day (Fig. 1.5-A). Neither PC1 nor PC2 reproduced the differences caused by volatilome treatments. At 3 h and 8 h, W- and W+FR-volatilome samples overlapped, suggesting that the transcriptomic impact of the shade volatilome at these time points was minimal. By contrast, at 24 h, W and W+FR groups showed a consistent separation, indicating that the shade volatilome effect was time-dependent, possibly due to low doses reaching r-seedlings in the two-box system or other technical/biological constraints.

The heatmap of pairwise Pearson correlation coefficients (Fig. 1.5-B) supported these observations. Replicates within each time point showed strong correlation, confirming dataset consistency. As expected, the dendrogram clustered samples primarily by time (8 h, 3 h, and then 0 h and 24 h together), reflecting time-of-day influences on gene expression. Notably, W+FR-volatilome samples at 24 h clustered separately from W-treated samples at 24 h and 0 h (Fig. 1.5-B), again pointing to a treatment effect specific to this time point. Taken together, these results indicate that 24 h is the condition in which transcriptomic responses to the two volatilomes most diverge, and therefore subsequent analyses focused on this time point.

1.3.2 Differential expression and gene enrichment analysis

The next step was to analyze the set of differentially expressed genes (DEGs) at 24 h in response to the shade-volatilome treatment. Applying a threshold of fold change ≥ 1.5 and a Q-value (false discovery rate–adjusted p-value) < 0.05 in DESeq2, a total of 393 DEGs were identified, of which 337 were upregulated and 56 downregulated in W+FR samples relative to W controls (Fig. 1.S4).

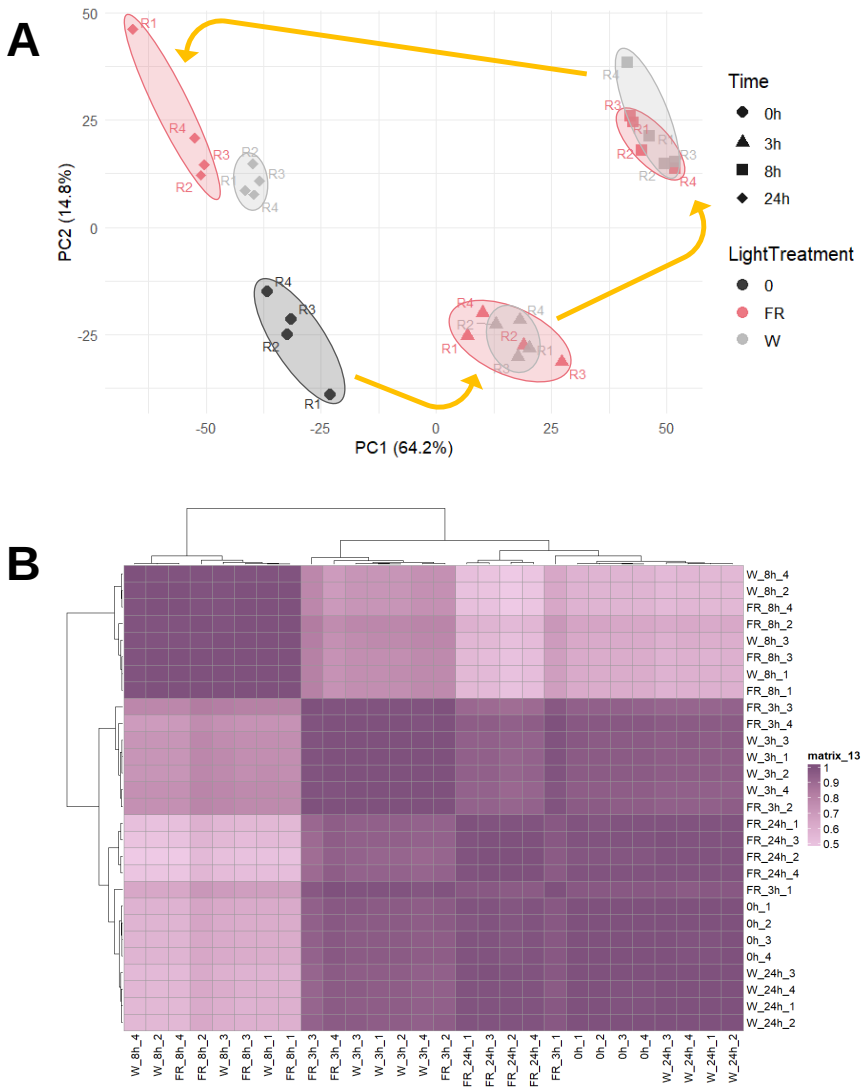

Figure 1.5 — Sample clustering based on gene expression profiles. (A) *Principal component analysis (PCA) of RNA-seq samples from A. thaliana seedlings exposed for the indicated times to the volatilome of tomato e-plants grown under white light (W, grey) or simulated shade (W+FR, pink/red). Each symbol represents a biological replicate (R1–R4), with different shapes indicating sampling times (0, 3, 8 and 24 h). Ellipses were manually drawn to delimit sample groups and highlight differences. Yellow arrows indicate the time progression (0 → 3 h → 8 h → 24 h).* ***(B)*** *Pearson correlation heatmap of the same samples showing pairwise correlation coefficients. Pearson correlation values were calculated across the normalized expression levels of all detected genes, with values close to 1 indicating highly similar transcriptomic profiles, with darker colors indicating higher similarities between two samples.*

To obtain an initial overview of the functional categories significantly represented within the 393 differentially expressed genes (DEGs), we performed a functional enrichment analysis based on Gene Ontology – Biological Process (GO-BP) annotations (Fig. 1.6). This analysis revealed that the shade volatilome significantly impacted the expression of genes involved in responses to hypoxia, oxidative stress, water deprivation, and wounding, among others, while genes related to sulfur compound biosynthesis—particularly glucosinolates derived from methionine—were repressed.

Figure 1.6 — Gene Ontology (GO) biological process (BP) enrichment analysis. *Dot plots showing enriched GO-BPs for upregulated (left) and downregulated (right) DEGs in A. thaliana r-seedlings exposed to W+FR-volatilome compared with W-volatilome after 24 h (p-adj<0.05, FC≥1.5). The x-axis represents gene ratio (proportion of DEGs annotated to each term), while dot size indicates the number of associated genes. Dot color corresponds to the adjusted p-value of the enrichment (pink = more significant).*

Further analyses were considered. However, the relatively small number of DEGs that we could identify in our experimental design, together with the modest magnitude of their expression changes (Tables 1.S3 / 1.S4) inevitably reduced the robustness and biological significance of any additional transcriptomic interpretations. For this reason, we mostly used the 24 h DEG dataset for comparative analyses with transcriptomic responses to other stimuli, both in this and in the following chapters, which allowed us to identify meaningful correlations between the shade volatilome and other treatments.

1.3.3 The shade volatilome and W+FR treatments share transcriptional targets

We next investigated whether the *A. thaliana* genes that were differentially regulated by the tomato shade-triggered VOCs are somehow related with those changing when *A. thaliana* seedlings are directly illuminated with simulated shade (W+FR). To that end, we compared the dataset of 393 DEGs elicited by the shade-related VOCs at 24 hours from our analysis with another dataset of 1144 DEGs regulated by exposure of 7-day-old seedlings to W+FR (compared to W) for 24 h (Moreno-Romero, J., and Martinez-Garcia, J.F., unpublished data).

By crossing both datasets, we found a significant overlap of genes regulated by both direct W+FR irradiation and the shade volatilome (Fig. 1.7-A). Nearly a quarter (97 out of 393, 24.7%) of the genes regulated by the shade-induced VOCs in non-shaded seedlings are also regulated by simulated shade. The significance of this interaction was assessed by performing a Fisher's Exact Test, which confirmed that the overlap between DEGs regulated by shade-volatilome and by simulated shade (W+FR) was highly significant, with an odds ratio of 7.2 (95% CI: 5.6–9.1), indicating a strong enrichment of shared genes relative to random expectation (Fig. 1.7-A). In addition, of the 97 genes regulated by both shade-related VOCs and shade-related low R:FR light, approximately two thirds (63 out of 97, 64.9%) were regulated in the same direction (either up- or down-regulated) in both datasets (Fig. 1.7-B), pointing to a mostly coordinated regulation of the overlapping genes.

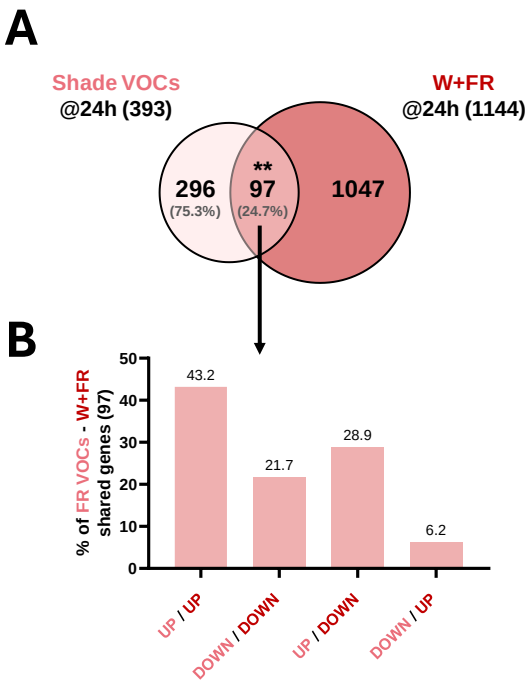

Figure 1.7 — Overlap between DEGs regulated by shade-induced VOCs and simulated shade (W+FR). ***(A)*** *Venn diagram showing the overlap between DEGs regulated by shade-volatilome exposure (pink) and by direct simulated shade (W+FR, dark-red) at 24 h. Numbers indicate the total DEGs in each set and in the overlap, with percentages referring to the fraction of total shade-volatilome DEGs. Asterisks indicate statistically significant enrichment according to Fisher's Exact Test ($p < 2.2 \times 10^{-16}$). The total universe used was 24413, the total amount of genes mapped in the Shade VOCs RNAseq.* ***(B)*** *Directional analysis of the 97 shared DEGs. Bars indicate the proportion of co-regulated (UP/UP or DOWN/DOWN) or counter regulated (UP/DOWN or DOWN/UP) genes by both treatments in relation to the total number of shared DEGs (97).*

In addition, the functional analysis by GO-BP terms of the co-upregulated genes (Fig. 1.S5) showed that the involvement of the shade volatilome in the upregulation of genes controlled by W+FR affected mostly responses to water depravation, wounding, or even specific responses to far-red light. In contrast, the most representative GO-BP category within the co-downregulated DEGs was glucosinolate biosynthetic processes. In fact, 10 out of the 20 most downregulated genes by the shade volatilome (Table 1.S4) are associated with glucosinolate metabolism.

These results together suggest that the shade-related VOCs encode information involved in plants' response to shade at the transcriptomic level. In other words: part of the transcriptomic response of *A. thaliana* to proximity shade can also be elicited by the VOCs emitted when neighboring tomato plants are treated with simulated shade.

Supplemental Information

Table 1.S1 — Summary of conditions tested with the same-box system. HypElo, hypocotyl elongation. GUSstain, GUS staining assay.

Exp. no.	Experimental design			Genotype / Cultivar	no. plants / box	plants age at d0 (d)	Figure
1	72 h in boxes	Tomato (e-plants)		M82	9	36	Fig. 1.2-A
		A. thaliana (r-seedlings)	HypElo	WT		0	
2	72 h in boxes	Tomato (e-plants)		Rio Grande (RG)	6	49	Experiment failed
		A. thaliana (r-seedlings)	HypElo	WT, pifq		0	
3	72 h in boxes	Tomato (e-plants)		M82	7	42	Not shown
		A. thaliana (r-seedlings)	HypElo	WT, pifq, 35S:PIF3-GUS		0	
4	24 h germinating out, 48 h in boxes	Tomato (e-plants)		RG	6	35	Fig 1.S1-A
		A. thaliana (r-seedlings)	HypElo GUSstain	WT, pifq, 35S:PIF3-GUS DR5:GUS; EBSnew:GUS		1	
5	24 h germinating out, 48 h in boxes	Tomato (e-plants)		M82	6	39	Fig 1.S1-B
		A. thaliana (r-seedlings)	HypElo GUSstain	WT, pifq, 35S:PIF3-GUS DR5:GUS		1	
6	36 h germinating out, 48 h in boxes	Tomato (e-plants)		MicroTom	18	32	Fig 1.S1-C
		A. thaliana (r-seedlings)	HypElo	WT, pifq		1.5	
7A	48 h in boxes (d0-d2)	Tomato (e-plants)		M82	6	35	Not shown
		A. thaliana (r-seedlings)	HypElo	Col-0, OX		0	
7B	24h germinating out, 48 h in boxes (d1-d3)	Tomato (e-plants)		M82	6	35	Not shown
		A. thaliana (r-seedlings)	HypElo	Col-0, OX		1	
8A	72 h in boxes (d0-d3)	Tomato (e-plants)		M82	6	35	Not shown
		A. thaliana (r-seedlings)	HypElo	Col-0, OX, ein2-5		0	
8B	24h germinating out, 72 h in boxes (d1-d4)	Tomato (e-plants)		M82	6	35	Fig. 1.S1-D
		A. thaliana (r-seedlings)	HypElo	Col-0, OX, ein2-5		1	
9	R-seedlings 72 h inside e-box or r-box	Tomato (e-plants)		M82	12	36	Not shown
		A. thaliana (r-seedlings)	HypElo	WT		0	

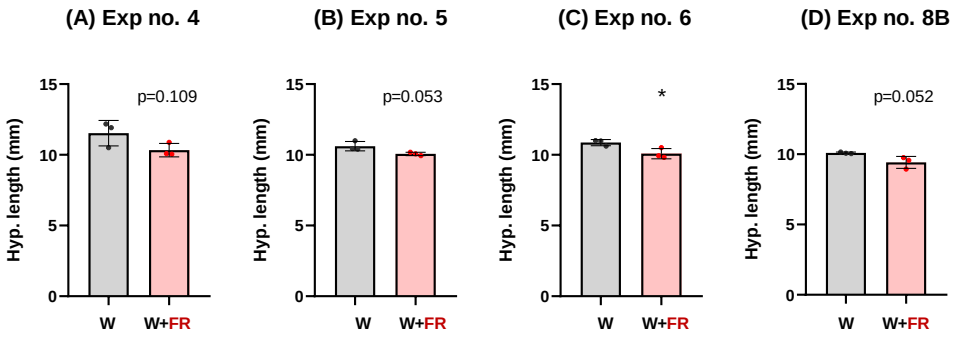

Figure 1.S1 — Hypocotyl length of etiolated A. thaliana r-seedlings in same-box system with tomato e-plants. *Hypocotyl length of etiolated A. thaliana Col-0 r-seedlings exposed to the volatiles produced by tomato e-plants illuminated with white light (W, in grey) or W+FR (in pink). Panels show results from four independent biological experiments (summarized in Table 1.S1). Bars represent the mean of 3 biological replicates ± SD of the means. Statistical significance was assessed by unpaired, two-tailed t-tests (*=p<0.05, **=p<0.01).*

Table 1.S2 — Summary of conditions tested with the two-box system. HypElo, hypocotyl elongation.

Exp. no.	Experimental design			Genotype / Cultivar	no. plants / box	plants age at d0 (d)	Figure
1A	5d in boxes - no recirculating airflow	Tomato (e-plants)		M82	6	32	Fig. 1.2-B
		A. thaliana (r-seedlings)	HypElo	WT		2	
1B	5d in boxes - recirculating airflow	Tomato (e-plants)		M82	6	32	Fig. 1.S2-A
		A. thaliana (r-seedlings)	HypElo	WT		2	
2	5d in boxes - no recirculating airflow	Tomato (e-plants)		M82	6	44	Fig. 1.S2-B
		A. thaliana (r-seedlings)	HypElo	Col-0, bes1-D, ein2-5, phyB		2	
3	5d in boxes - no recirculating airflow - RNAseq Control	Tomato (e-plants)		M82	6	38	Fig. 1.S2-C
		A. thaliana (r-seedlings)	HypElo	Col-0, bes1-D, ein2-5, phyB		2	

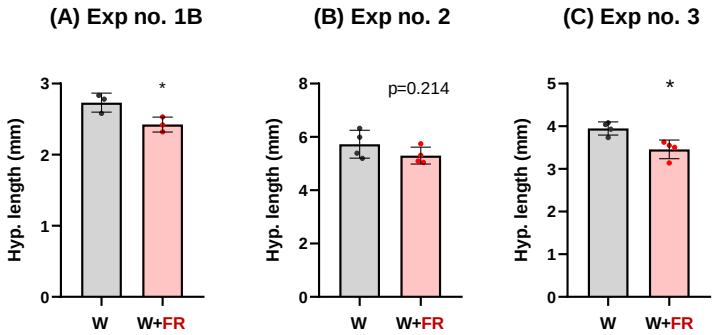

Figure 1.S2 — Hypocotyl length of low W-grown A. thaliana r-seedlings in two-box system with tomato e-plants. *Hypocotyl length of r-seedlings grown under low white light (W) exposed to the volatiles produced by tomato e-plants illuminated with W (in grey) or W+FR (in pink). Panels show results from three independent biological experiments (summarized in Table 1.S2). Bars represent the mean of 3 biological replicates ± SD of the means. Statistical significance was assessed by unpaired, two-tailed t-tests (*=p<0.05, **=p<0.01).*

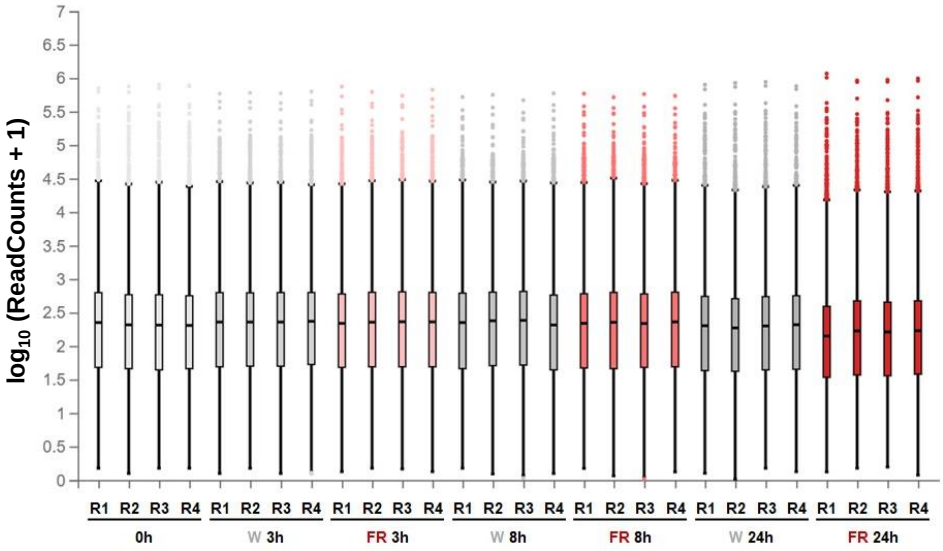

Figure 1.S3 — Distribution of read counts across RNA-seq samples. *Boxplots showing the distribution of log_{10}(ReadCounts + 1) for all detected genes across biological replicates (R1–R4) at different time points (0, 3, 8 and 24 h) under W (shades of grey) or W+FR (FR, pink/red). Each box represents the interquartile range, with horizontal lines indicating the median, whiskers showing 1.5× the interquartile range, and dots representing outliers.*

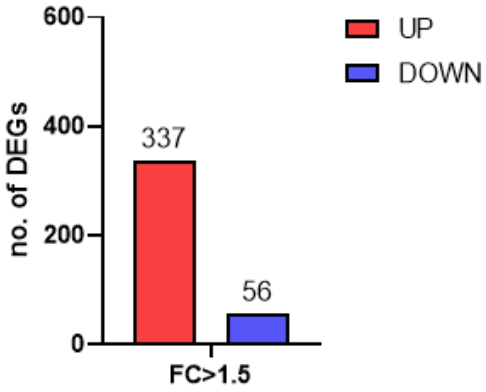

Figure 1.S4 — Differentially expressed genes (DEGs) in response to shade-volatilome exposure. *Number of upregulated (red) and downregulated (blue) DEGs in Arabidopsis r-seedlings exposed to W+FR-volatilome compared with W-volatilome at 24 h. Bars represent the total number of DEGs identified using DESeq2 with adjusted $p < 0.05$ and $|log_2FC| \geq 1.5$ (left) as cut-off values. The actual number of DEGs is written above bars for all cases.*

Table 1.S3 — Most upregulated genes (W+FR vs W, 24 h)

Accession number	Gene ID	W Average TPMs	W+FR Average TPMs	Fold Change	Q-value	Annotation / Gene Description
AT5G20230	BCB	5.94	63.23	12.13	8.4E-20	Encodes an Al-stress-induced gene. Along with TCF, it promotes lignin biosynthesis in response to cold stress. The mRNA is cell-to-cell mobile.
AT1G19530	RGAT 1	2.88	18.10	7.23	4.1E-36	Direct target of RGA, plays an essential role in GA-mediated tapetum and pollen development.
AT1G15040	GAT1_ 2.1	1.718	8.95	5.99	1.3E-24	Encodes a nitrogen regulated putative glutamine amidotransferase that represses shoot branching.
AT1G08630	THA1	6.34	29.31	5.31	7.0E-39	Encodes a threonine aldolase, involved in threonine degradation to glycine. Primarily expressed in seeds and seedlings.

AT1G10070	BCAT-2	5.78	23.49	4.61	4.3E-42	Encodes a chloroplast branched-chain amino acid aminotransferase. Complements the yeast leu/iso-leu/val auxotrohpy mutant. Involved in cell wall development
AT2G05510	-	1.31	4.59	4.56	2.1E-08	Glycine-rich protein family;(source:Araport11)
AT4G08555	-	1.54	5.43	4.06	7.3E-04	hypothetical protein;(source:Araport11)
AT5G21940	-	26.13	77.34	3.44	9.4E-19	hybrid signal transduction histidine kinase M-like protein;(source:Araport11)
AT3G28740	CYP81D11	10.13	28.42	3.27	2.1E-18	Encodes a member of the cytochrome p450 family. Expression is upregulated in response to cis-jasmonate treatment. Overexpression induces synthesis of volatile compounds that affect chemical ecology and insect interactions.
AT5G56550	OXS3	9.14	25.54	3.24	9.4E-19	Encodes OXIDATIVE STRESS 3 (OXS3)， involved in tolerance to heavy metals and oxidative stress.
AT4G30280	XTH18	1.79	4.92	3.17	1.1E-03	Encodes a xyloglucan endotransglucosylase/hydrolase with only the endotransglucosylase (XET; EC 2.4.1.207) activity towards xyloglucan and non-detectable endohydrolytic (XEH; EC 3.2.1.151) activity. Expressed in the mature or basal regions of both the main and lateral roots, but not in the tip of these roots where cell division occurs.
AT5G14180	MPL1	1.34	4.03	3.08	1.7E-08	Myzus persicae-induced lipase 1;(source:Araport11)

AT1G80160	-	1.87	4.97	3.06	2.7E-09	Vicinal oxygen chelate (VOC) superfamily member.
AT3G21720	ICL	14.60	38.57	3.06	2.7E-13	Encodes a glyoxylate cycle enzyme isocitrate lyase (ICL) involved in salt tolerance.
AT3G03341	-	6.33	15.94	3.04	3.0E-04	cold-regulated protein;(source:Araport11)
AT5G14470	GALK2	1.44	3.79	3.02	5.7E-09	Indispensable for oxo-C14-HSL-dependent priming for enhanced resistance. The ALI1 protein may interact with oxo-C14-HSL.
AT2G16005	ROSY 1	1.24	3.13	2.93	1.7E-02	ROSY1 protein contains a MD-2-related lipid-recognition domain. It is rapidly upregulated in response to gravistimulation.
AT3G60140	DIN2	4.93	12.17	2.88	1.8E-16	Encodes a protein similar to beta-glucosidase and is a member of glycoside hydrolase family 1. Expression is induced after 24 hours of dark treatment, in senescing leaves and treatment with exogenous photosynthesis inhibitor. Induction of gene expression was suppressed in excised leaves supplied with sugar. The authors suggest that the gene's expression pattern is responding to the level of sugar in the cell. The mRNA is cell-to-cell mobile.
AT5G39580	PRX62	4.42	10.97	2.85	3.95E-10	Class III peroxidase cell wall-targeted protein localized to the micropylar endosperm facing the radicle. Involved in seed germination.

AT3G07350	-	12.00	28.46	2.78	1.37E-15	Phosphorus (P) stress-inducible DUF506 gene family member.

Table 1.S4 — Most downregulated genes (W+FR vs W, 24 h)

Accession number	Gene ID	W Average TPMs	W+FR Average TPMs	Fold Change	Q-value	Annotation / Gene Description
AT3G19710	BCAT 4	26.13	9	0.402	0.0035	Belongs to the branched-chain amino acid aminotransferase gene family. Encodes a methionine-oxo-acid transaminase. Involved in the methionine chain elongation pathway that leads to the ultimate biosynthesis of methionine-derived glucosinolates.
AT1G16410	CYP 79 F1	14.15	5.50	0.453	0.0224	member of CYP79F The mRNA is cell-to-cell mobile.
AT3G03190	GST F11	8.06	3.29	0.482	0.0083	Encodes glutathione transferase belonging to the phi class of GSTs. Naming convention according to Wagner *et al.* (2002).
AT3G22235	HCYS TM8	28.12	12.14	0.502	0.0000	cysteine-rich TM module stress tolerance protein;(source:Araport11)
AT1G18590	SOT 17	11.49	4.94	0.504	0.0000	encodes a desulfoglucosinolate sulfotransferase, involved in the final step of glucosinolate core structure biosynthesis. Has a broad-substrate specificity with preference with methionine-derived desulfoglucosinolates.

AT1G62560	FMO GS-OX3	3.03	1.35	0.525	0.0103	belongs to the flavin-monooxygenase (FMO) family, encodes a glucosinolate S-oxygenase that catalyzes the conversion of methylthioalkyl glucosinolates to methylsulfinylalkyl glucosinolates
AT1G65860	FMO GS-OX1	2.45	1.14	0.538	0.0063	belongs to the flavin-monooxygenase (FMO) family, encodes a glucosinolate S-oxygenase that catalyzes the conversion of methylthioalkyl glucosinolates to methylsulfinylalkyl glucosinolates
AT2G22500	UCP5	5.63	2.62	0.541	0.0279	Encodes one of the mitochondrial dicarboxylate carriers (DIC): DIC1 (AT2G22500), DIC2 (AT4G24570), DIC3 (AT5G09470).
AT4G17030	EXL B1	6.06	2.82	0.547	0.0028	Encodes EXLB1 (expansin-like B1), a member of the expansin family.
AT5G42530	-	113.22	51.85	0.547	0.0007	hypothetical protein;(source:Araport11)
AT3G02020	AK3	2.29	1.08	0.547	0.0027	encodes a monofunctional aspartate kinase
AT4G12030	BAT5	11.72	5.85	0.568	0.0009	Required for the biosynthesis of methionine-derived glucosinolates. Involved in the transport of 2-keto acids between chloroplasts and the cytosol.
AT1G78370	GSTU 20	94.50	46.25	0.570	0.0017	Encodes glutathione transferase belonging to the tau class of GSTs. Naming convention according to Wagner *et al.* (2002).

AT5G23010	MAM1	49.78	24.50	0.573	0.0031	Encodes a methylthioalkylmalate synthase, catalyzes the condensation reactions of the first two rounds of methionine chain elongation in the biosynthesis of methionine-derived glucosinolates.
AT5G07690	MYB 29	3.95	1.99	0.581	0.0293	Encodes a putative transcription factor (MYB29) that acts as a negative regulator of mitochondrial stress responses.
AT5G14200	IMD1	35.75	17.86	0.582	0.0037	The AtIMD1 is one out of 3 genes encoding the enzyme 3-isopropylmalate dehydrogenase involved in leucine biosynthesis in Arabidopsis. Its subcellular location has been targeted to plastids. Encodes methylthioalkylmalate dehydrogenase. Involved in glucosinolate biosynthesis, in methionine chain elongation.
AT1G29600	ATC3 H10	4.08	2.07	0.584	0.0121	Zinc finger C-x8-C-x5-C-x3-H type family protein;(source:Araport11)
AT3G28080	UMA MIT47	6.22	3.10	0.598	0.0063	nodulin MtN21-like transporter family protein
AT3G58990	IPMI1	32.29	16.69	0.605	0.0284	Small subunit, which together with IPMI SSU1, IPMISSU2 and IPMI LSU1, is a member of heterodimeric isopropylmalate isomerase (IPMI). Together with IPMI SSU3 participates in the Met chain elongation pathway.
AT2G37460	UMA MIT12	3.31	1.75	0.608	0.0205	nodulin MtN21-like transporter family protein

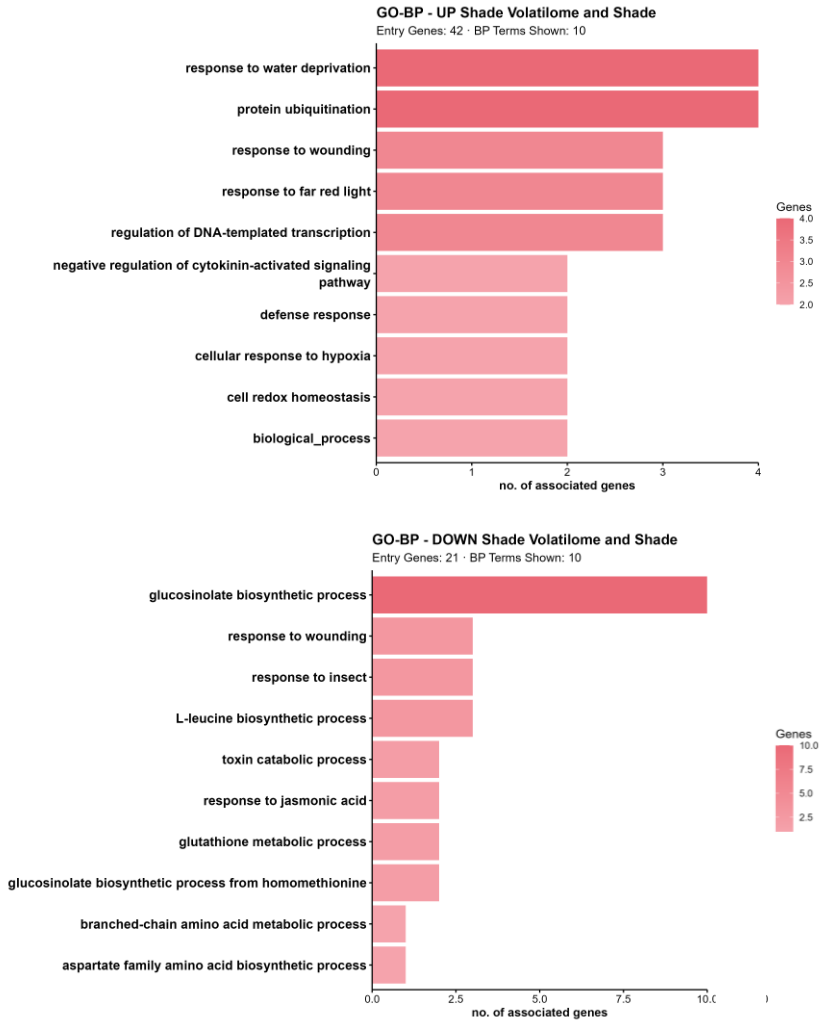

Figure 1.S5 — GO-BP term distribution of co-regulated (UP-UP, top; DOWN-DOWN, bottom) DEGs between shade-volatilome and simulated shade (W+FR). *Barplots showing the most represented GO-BP terms of the differentially expressed genes (DEGs) co-regulated in shade-volatilome and in simulated shade (W+FR). Bar length indicates the number of shared genes in each category, and bar color intensity reflects relative proportion.*

Chapter II

Part of the results presented in this chapter have been published in:

Urdin-Bravo *et al.*, (2024). **Effect of Higher Ethylene Levels Emitted by Shade-Avoider Plants on Neighboring Seedlings.** *Plants*, *13*(22), 3212. https://doi.org/10.3390/plants13223212

All results and figures were merely produced by the author but those from Figure 2.4, for which data combined from experiments performed by both Ángela Sánchez García and the author were displayed.

Chapter II. Dissecting ethylene's role in neighbor communication

2.1 Untargeted analysis of the shade volatilome detects no differentially emitted VOCs

Having confirmed the role of shade-induced tomato VOCs (shade volatilome) as molecular signals mediating plant-to-plant communication and having characterized their phenotypic impact on *A. thaliana* r-seedlings, we next aimed to investigate the composition and differences of the volatilomes emitted by tomato plants upon exposure to control (W) versus simulated shade (W+FR) conditions. Differences between these volatilomes might emerge from the presence or absence of specific compounds (qualitative variation) or from changes in the relative abundance of constitutively emitted VOCs (quantitative variation).

Although we found no reports of VOCs whose biosynthesis solely depends on light signaling, various studies have shown that proximity shade can alter the production levels of individual or entire classes of VOCs (Kegge *et al.*, 2013; Urdin-Bravo *et al.*, 2024). Interestingly, the total amount of VOCs produced under shade conditions has been revealed to rise or decrease depending on the study (Escobar-Bravo *et al.*, 2024; Kegge *et al.*, 2015), pointing to a potential species-specific response pattern and/or differences in the group of VOCs analyzed (i.e., on the system used to adsorb the VOCs produced or emitted).

VOCs production can be inspected using various techniques (Soria *et al.*, 2015). However, while measuring VOC production in plant tissues (e.g., leaves) is physiologically informative, it is VOCs emission that truly reflects the molecular message encoded by plants and sent to their neighbors. Despite being technically more challenging to assess, emission is ultimately a more direct and ecologically meaningful parameter when trying to identify the compounds responsible for plant-to-plant communication.

At the IBMCP in Valencia, we had access to equipment suitable for studying tomato leaf and fruit VOC contents in a broad, untargeted manner. However, we lacked the tools and expertise to adapt our system for reliable VOC emission analysis. To overcome this limitation, we initiated a collaboration with Professor Jonathan Gershenzon's group at the Max Planck Institute for Chemical Ecology (MPI-CE, Jena, Germany), where I conducted a three-month research stay. The laboratory of Dr. Gershenzon assembled a team of experienced personnel along with the necessary equipment to undertake such a strategy, already set up in a fully-equipped greenhouse chamber specifically designed to analyze the capture of VOCs emitted by adult plants which could be adapted to the simulated shade conditions (W+FR) used in our research (Gershenzon, 2007; Holopainen & Gershenzon, 2010; Kigathi *et al.*, 2009, 2019; Medina-van Berkum, 2024).

We first adapted the growth chamber conditions at the MPI-CE to match those used at the IBMCP, particularly regarding light intensity and quality, to ensure comparability between control (W) and shade (W+FR) treatments. Table 2.1 summarizes the similarities and differences of growth conditions in both facilities.

Table 2.1 — Comparison of growth conditions of tomato e-plants between IBMCP (València, Spain) and MP-ICE (Jena, Germany).

Conditions	IBMCP	MPI-CE
Light Intensity	PPFD and R:FR adjusted (see section M.1)	
Daylight regime	Long-day (LD) – 16 h light, 8 h dark	
Diurnal variations (time-of-day)	Day (ZT0) starts at 2 AM	Day (ZT0) starts at 7 AM
Sampling time	9-11 AM (ZT2-ZT4)	
Temperature	22ºC	
Watering	Nutritive solution	Standard water

Approximately 35-day-old tomato plants (cv. M82), grown under similar conditions as in IBMCP, were used as VOCs emitters. A VOCs collection

system was adapted to fit the height and morphology of the tomato plants (Fig. 2.S1). Tomato plants were exposed to either W or W+FR and the VOCs released to their headspace were trapped by adsorption onto PoraPak Q filters for 2 hours every day over a total period of 5 days. The time window used for VOC collection in this experiment (9:00–11:00 h) corresponds to ZT2 – ZT4. The trapped VOCs were then desorbed and analyzed using gas chromatography–mass spectrometry (GC-MS) and gas chromatography with flame ionization detection (GC-FID) for compound identification and quantification, respectively. GC-MS enables separation and structural identification of volatile compounds based on their mass spectra, while GC-FID provides highly sensitive quantification of volatiles through ionization in a hydrogen flame. The identified and later quantified VOCs are listed in Table 2.2.

The detected compounds (listed in Table 2.2) fall primarily into two categories: monoterpenes and sesquiterpenes, with the exceptions of the aldehydes nonanal and decanal. Monoterpenes, typically more volatile, eluted within the first 20 minutes of the chromatograms and constituted the most abundant group of compounds present in the tomato volatilome. Sesquiterpenes, due to their higher molecular weight, appeared later in the chromatograms. When comparing the levels of VOCs emitted by tomato plants under W vs. W+FR, however, the results showed no significant differences in any of the time points sampled (Fig. 2.1). The same compounds were detected in both volatilomes, and no statistically significant differences in the relative or absolute quantities of particular VOCs were observed. Importantly, despite the lack of VOC differences, the 5-day W+FR treatment elicited the characteristic shade-avoidance responses in tomato plants, namely stem elongation and a paler green coloration resulting from pigment degradation (Fig. 2.S2), confirming that the shade treatment was effective.

In addition, an experiment was performed to assess whether differential light treatments could influence VOC emission across the day. For this, another set of tomato plants was grown under the same conditions and exposed to either W or W+FR for 1 day. Keeping the same light treatments, VOC samples were collected every 4 hours starting from the next day, allowing the establishment of a time-course profile of VOC emission. Although the differences between W and W+FR samples were not statistically significant, the results suggest the existence of a peak in VOC production around 4 PM in plants exposed to W+FR (Fig. 2.S3). Notably,

this peak does not align with the time window used for VOC collection in the previous experiment (09:00–11:00 h).

Table 2.2 — List of identified emitted VOCs

Compound	RT-GC	RT-FID	KI observed	KI expected	Class	Response factor
α-pinene	7.201	7.441	933	**937**	Monoterpene	0.73
1,3,5-Cycloheptatriene (3,7,7-trimethyl-)	8.154	8.339	970	**971**	n.s.	1
2-carene	8.918	9.065	1000	**1001**	Monoterpene	0.73
α-phellandrene	9.008	9.156	1004	**1005**	Monoterpene	0.73
α-terpinene	9.332	9.461	1016	**1017**	Monoterpene	0.73
ρ-cymene	9.554	9.662	1025	**1025**	Monoterpene	0.73
ϐ-phellandrene	9.708	9.783	1031	**1031**	Monoterpene	0.73
γ-terpinene	10.415	10.482	1059	**1060**	Monoterpene	0.73
Terpinolene	11.176	11.226	1089	**1088**	Monoterpene	0.73
Nonanal	11.567	11.624	1104	**1104**	aldehyde	1
Carane, 4,5-epoxy-, trans	13.359	13.354	1177	**1179**	Monoterpene	0.73
Dill ether	13.626	13.66	1188	**1188**	Monoterpene	0.73
Decanal	14.066	14.022	1206	**1206**	aldehyde	1
ρ-cumenol	14.567	14.508	1227	**1227**	Monoterpene	0.73
Nonyl-acetate	**16.509**	**16.38**	**1310**	**1308**	**Internal Standard**	**1**
δ-elemene	17.194	17.012	1341	**1338**	Sesquiterpene	0.78
ϐ-elemene	18.402	18.15	1396	**1391**	Sesquiterpene	0.78
ϐ-caryophyllene	19.03	18.782	1425	**1419**	Sesquiterpene	0.78
Guaia-6,9-diene	19.497	19.243	1447	**1443**	Sesquiterpene	0.78
Humulene	19.742	19.479	1459	**1454**	Sesquiterpene	0.78

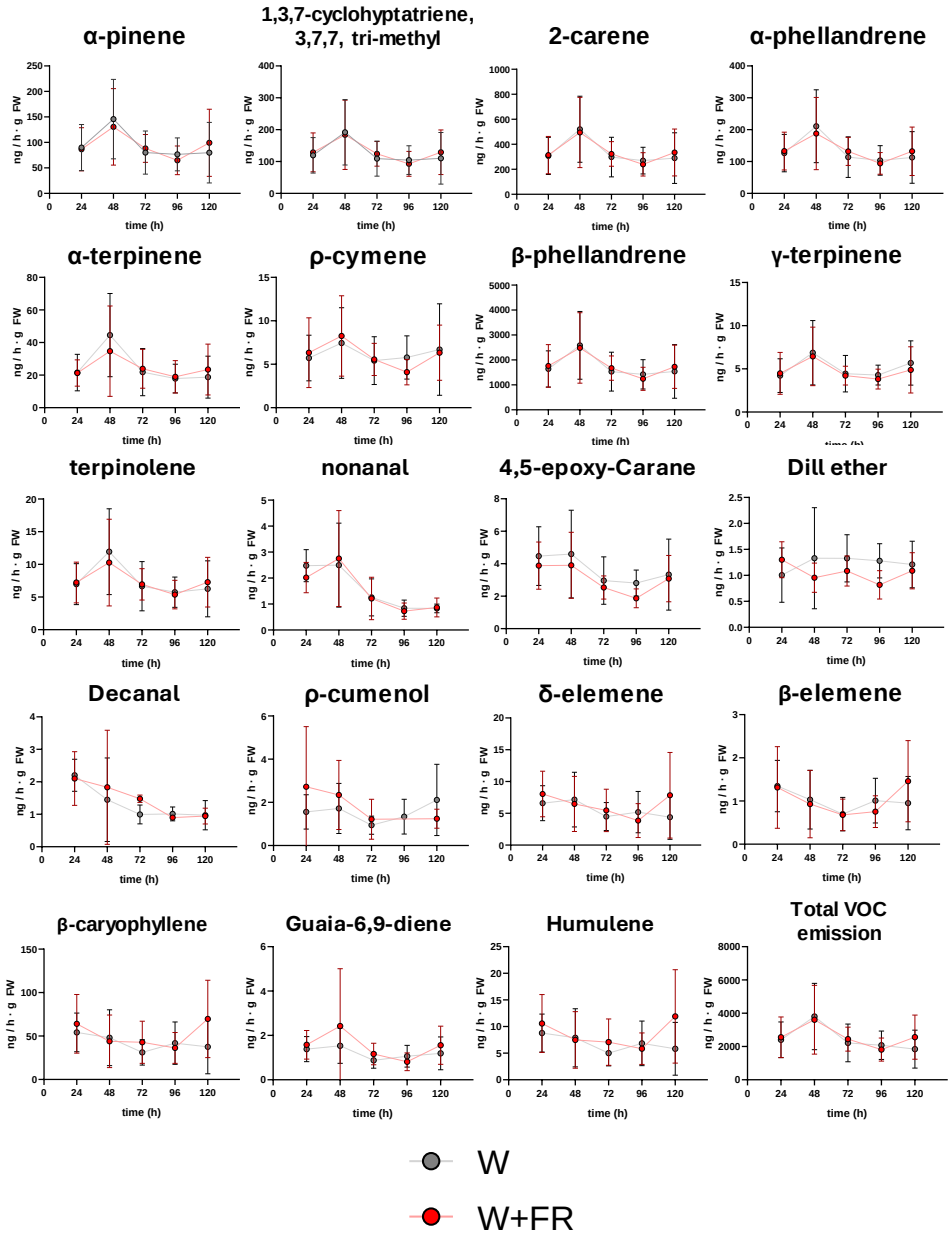

Figure 2.1 — Emission dynamics of volatile organic compounds (VOCs) from tomato plants under W and W+FR conditions. *Time-course emission profiles of the main identified compounds (see Table 2.2) collected from tomato plants exposed to white light (W, grey) or white light supplemented with far-red (W+FR, red). Data are shown as mean ± SD of 8-10 biological replicates collected at 1, 2, 3, 4, and 5 days after treatment. No statistically significant differences were found between light treatments across time points (two-way ANOVA).*

Although our data did not reveal significant changes in the tomato VOC emission profiles or intensities under simulated shade conditions (Fig. 2.1), the biological effects observed in *A. thaliana* r-seedlings (Fig 1.2) suggested that subtle, yet functionally relevant differences, should exist. These could involve trace compounds below the detection threshold, dynamic shifts in emission timing, post-emission modifications not captured in our sampling or VOCs not trapped by the filters used in here. These possibilities will be discussed later on.

2.2 Ethylene emission increases under simulated shade.

At this point we decided to move from untargeted to targeted metabolite profiling, initially focusing on ethylene, a VOC whose synthesis or/and emission had been previously reported to respond to shade in several shade-avoiding plant species, such as tobacco (Pierik, Whitelam, *et al.*, 2004; Finlayson *et al.*, 1998; Thain *et al.*, 2004). We set out to determine whether tomato plants, known to be shade-avoiders, would also exhibit a surge in ethylene production under our W+FR (simulated shade) treatment. Furthermore, we expanded our analysis to *C. hirsuta* (a known shade-tolerant genotype) and used *A. thaliana* (a classic shade-avoider) as a control. By including these closely phylogenetically related species, we aimed to evaluate whether differences across shade responses, concerning avoidance or tolerance, would also encompass ethylene emission.

To measure ethylene emission, leaves from adult tomato (*S. lycopersicum* cv. Microtom and M82), *A. thaliana* (Col-0) and *C. hirsuta* (OX) plants grown on soil under W (long-day photoperiod) were detached and immediately placed in airtight transparent glass tubes (Fig. 2.S4). The tubes were positioned horizontally and continuously illuminated with either W or W+FR for 24 hours. After this period, the ethylene accumulated in the headspace of the tubes containing the leaves was quantified using an ETD-300 ethylene detector. In all three shade-avoider accessions tested, shade-treated leaves released significantly more ethylene in 24 hours than their corresponding W-illuminated controls (Fig. 2.2). In the case of the shade-tolerant *C. hirsuta*, a higher basal ethylene emission under W and a lower increase under W+FR was observed compared to the shade-avoider accessions (Fig. 2.2).

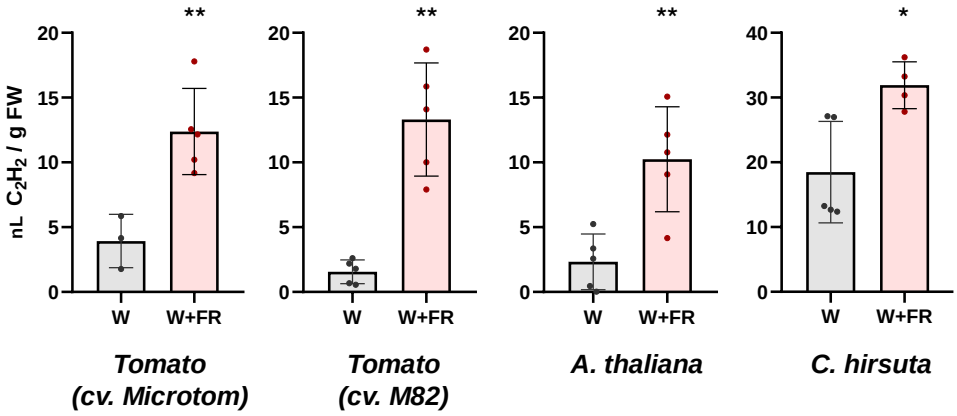

Figure 2.2 — Ethylene levels emitted by leaves from different species. *Ethylene emission was measured in leaves collected from the indicated plant species exposed to white light (W, grey) or white light supplemented with far-red (W+FR, pink) for 24 h. Each bar represents the mean ± SD of 3 to 5 biological replicates, with individual data points shown. Statistical significance was assessed using unpaired, two-tailed t-tests for each species (*p < 0.05; **p < 0.01).*

2.3 Light quality and intensity interact with ethylene to regulate seedling growth.

It is known that an elevated ethylene content influences hypocotyl elongation depending on light conditions: it promotes hypocotyl growth under W irradiation, but strongly inhibits it in etiolated seedlings (Smalle *et al.*, 1997). However, its effects under simulated shade or varying light intensities had not been systematically explored. As a first step to investigate the possible role of the ethylene released by e-plants as a shade-related volatile signal, we designed a group of experiments aimed to understand how increased ethylene levels influence hypocotyl elongation of seedlings growing under different light conditions. In order to determine if this light-dependent integration of ethylene's signal differs between shade-avoider and shade-tolerant species, we included in our experiments both *A. thaliana* Col-0 and *C. hirsuta* OX as model species, and ethylene-insensitive *A. thaliana ein2-5* mutant (Alonso *et al.*, 1999) as a negative control for impaired ethylene signaling.

To stimulate endogenous ethylene production, the wild-type (WT) accessions of *A. thaliana* and *C. hirsuta* were germinated and grown in media supplemented with 1-aminocyclopropane-1-carboxylate (ACC), the

direct biosynthetic precursor of ethylene. Plates with medium lacking ACC were used as controls. After stratification, plates were incubated for 2 days under W and then either transferred to W+FR or maintained under W for 5 more days. At the end of the experiment, hypocotyl length was measured. In the absence of ACC, *A. thaliana* WT and *ein2-5* seedlings treated with W+FR displayed enhanced hypocotyl elongation compared to those grown under W, as expected (Fig. 2.3). When supplemented with ACC, *A. thaliana* seedlings exhibited increased hypocotyl elongation under W, but the response to simulated shade in terms of elongation was repressed (Fig. 2.3). As expected, no impact of ACC was observed in the ethylene-insensitive *ein2-5* mutant. In agreement with its shade-tolerant behavior, in the absence of ACC, *C. hirsuta* hypocotyl elongation in W+FR exposed seedlings was attenuated in comparison with *A. thaliana.* ACC supplementation reduced hypocotyl elongation both under W or W+FR (Fig. 2.3). This result suggests that enhancing ethylene synthesis in *A. thaliana* promotes elongation under W but represses it under W+FR, whereas it represses *C. hirsuta* growth under both W and W+FR.

We next tested the effect of ACC supplementation on these two plant species when growing under varying light intensities. To that end, seeds were germinated on media with or without ACC and incubated for 7 days either in darkness or under different intensities of W (Fig. 2.4). Under dark conditions or low W intensity, ACC supplementation strongly inhibited hypocotyl elongation both in *A. thaliana* and *C. hirsuta*. However, as light intensity increased, ACC treatment resulted in shorter hypocotyls in *C. hirsuta* but longer hypocotyls in *A. thaliana* seedlings. Above a light intensity threshold of 100 µmol $m^{-2} \cdot s^{-1}$, ACC had no measurable effect on *C. hirsuta* hypocotyl length, while it still appeared to promote elongation in *A. thaliana*. Again, no impact was recorded on the *ein2-5* mutant under any condition (Fig. 2.4).

Altogether, these findings support the reported dual role of ethylene in regulating *A. thaliana* hypocotyl elongation in a light-dependent manner. Moreover, they revealed a differential response of the shade-tolerant *C. hirsuta*, suggesting a role for ethylene in the divergent response to vegetation proximity.

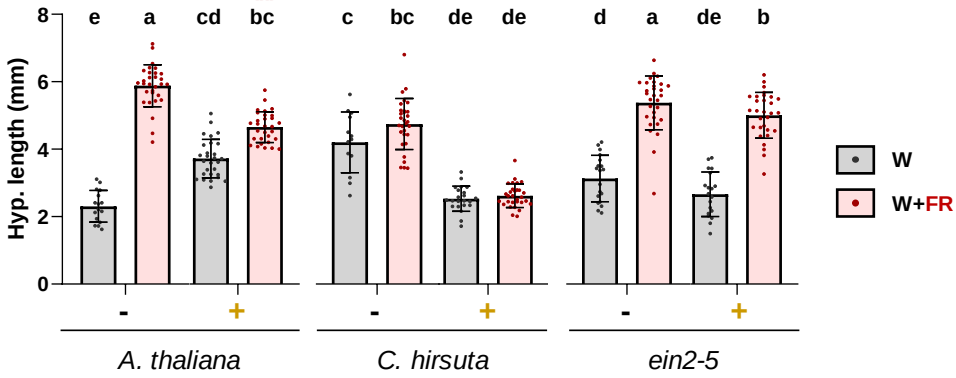

Figure 2.3 — Effect of ACC supplementation on hypocotyl elongation under W or W+FR. *Plots show hypocotyl length measurements of A. thaliana (Col-0 or ein2-5) and C. hirsuta OX seedlings exposed to white light (W, grey) or white light supplemented with far-red (W+FR, pink), when grown with (+) or without (-) supplementation of the ethylene precursor ACC (10 µM). Each bar represents the mean ± SD of 15–30 seedlings, with individual data points shown. Different letters indicate significant differences among groups, according to two-way ANOVA, followed by Tukey's test (p<0.05).*

Figure 2.4 — Effect of ACC supplementation on hypocotyl elongation under a range of W light intensities. *Plots show hypocotyl length of A. thaliana (Col-0 and ein2-5) and C. hirsuta OX seedlings grown under increasing W intensities in the absence (grey) or presence (yellow) of 10 µM ACC. Data are shown as mean ± SD of approximately 20 seedlings' hypocotyl lengths. Asterisks indicate significant differences ACC-treated and control seedlings, according to two-way ANOVA, followed by Sidak's test (**=p<0.05, *=p<0.01).*

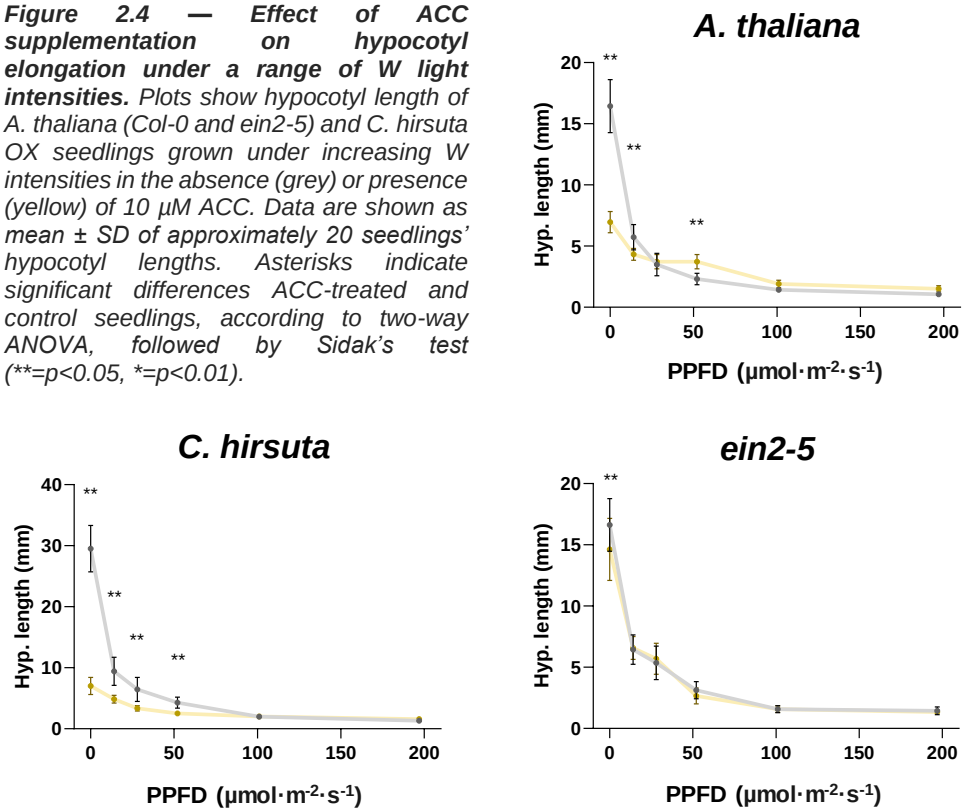

2.4 Ethylene released by shade-treated e-plants might cause changes in r-seedlings

Our next objective was to determine whether ethylene produced by shade-exposed e-plants can be perceived and integrated by neighboring individuals (r-seedlings). Previous studies have evaluated ethylene's effects through two main approaches: using ACC supplementation (as we did to establish ethylene's impact under different light regimes) or by exposing plants to exogenous gaseous ethylene via an airflow system. However, these approaches do not directly address whether exposure to naturally emitted ethylene levels (endogenously produced by e-plants) is sufficient to elicit ethylene-related responses in neighboring individuals.

To investigate this, we employed a dual-compartment plate system, which allows seedlings to grow on physically separated media while sharing the same airspace (Fig. 2.S5). This setup prevents direct physical contact of plants growing in each compartment and focuses exclusively on volatile-mediated communication (e.g., through airborne ethylene). In the e-compartment (containing media supplemented or not with ACC), we placed about either 15 *S. lycopersicum* cv. Microtom seeds or 100 *A. thaliana* seeds. In the adjacent r-compartment, we plated seeds of *A. thaliana* Col-0, the ethylene insensitive *ein2-5* mutant, and the *EBSn:GUS* reporter line (kindly provided by the group of Anna Stepanova and Jose Alonso, North Carolina State University, USA), which expresses the *GUS* gene under the control of an ethylene-induced promoter. Plates were incubated in the dark as the effect of ethylene on *A. thaliana* seedlings was strongest in this condition. This design enabled us to test whether ethylene emitted by seedlings that germinate and grow in the e-compartment can influence growth or activate ethylene-responsive signaling in neighboring seedlings that germinate and grow in the r-compartment.

After incubating the dual compartment plates in darkness for 4 days, we measured the hypocotyl length of etiolated WT and *ein2-5* r-seedlings and assessed ethylene perception by performing GUS staining of *EBSn:GUS* r-seedlings (Fig. 2.5). Col-0 r-seedlings showed reduced hypocotyl elongation when exposed to volatiles from ACC-supplemented e-seedlings, an effect that was completely absent in the *ein2-5* mutant (Fig. 2.5), supporting the conclusion that ethylene is responsible for the observed growth inhibition. In addition, GUS staining of *EBSn:GUS* r-seedlings exposed to volatiles emitted by ACC-grown tomato or *A. thaliana*

e-seedlings showed a visibly stronger GUS signal than those exposed to volatiles from e-seedlings growing without ACC (Fig. 2.5).

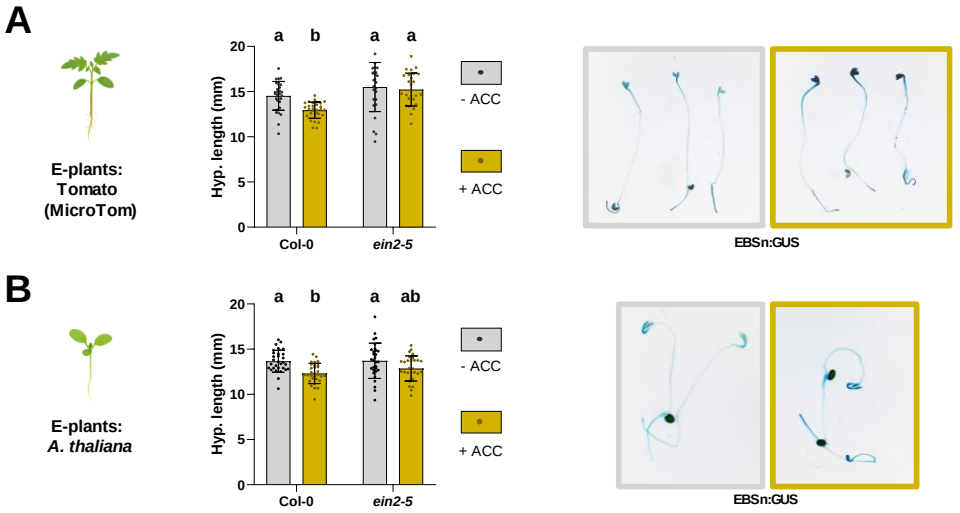

Figure 2.5 — Ethylene-mediated plant-to-plant communication assay. *Results shown follow the experimental setup shown in Fig. 2.S5, using either tomato (A) or A. thaliana seedlings (B) as e-plants. Plots (on the center-left) show hypocotyl length of A. thaliana r-seedlings grown in the dark without ACC in split Petri dishes together with e-plants grown with or without ACC. Data are presented as mean ± SD of at least 20 r-seedlings. Statistical significance was determined by two-way ANOVA followed by Tukey's multiple comparisons test. Different letters indicate significant differences between groups ($p < 0.05$). Panels on the right show histochemical GUS staining of r-seedlings harboring the EBSn:GUS ethylene reporter.*

We then asked whether the ethylene levels produced by seedlings growing under simulated shade conditions would be sufficient to elicit comparable responses in neighboring individuals. First, we sought to compare the amount of ethylene emitted by seedlings under W+FR with that of seedlings grown under W with supplemented ACC. To this end, ethylene emission was quantified after growing 100 *A. thaliana* Col-0 seedlings in 50 mL short wide-mouth sample glass bottles, containing 20 mL of media either supplemented or not with ACC (Fig. 2.6). After stratification, bottles were incubated for 2 days under W light and then either transferred to W+FR or kept under W for 5 additional days. After this period, bottles were sealed with a septum-containing lid and incubated under the same light

conditions for 24 h to allow ethylene accumulation in the headspace. Ethylene levels were then measured using the ETD-300 ethylene detector. As controls, we used bottles containing media with or without ACC, but with no seeds or seedlings (Fig. 2.6).

Our measurements showed that, as expected, only bottles containing seedlings emitted measurable levels of ethylene to the headspace (Fig. 2.6), confirming that ACC alone does not spontaneously convert into ethylene. In the absence of ACC, seedlings exposed to W+FR released approximately twice as much ethylene as their respective W controls (Fig. 2.6). These measurements were consistent with our earlier observations (Fig. 2.2), although ethylene production was lower than that of leaves excised from adult plants. ACC supplementation led to a much stronger induction of ethylene emission, reaching levels that were more than 10-fold higher than those released by controls growing without ACC, regardless of the light treatment (Fig. 2.6). These findings suggest that increased ethylene levels resulting from exposure of e-plants to W+FR might be too low to elicit a visible elongation effect on r-seedlings.

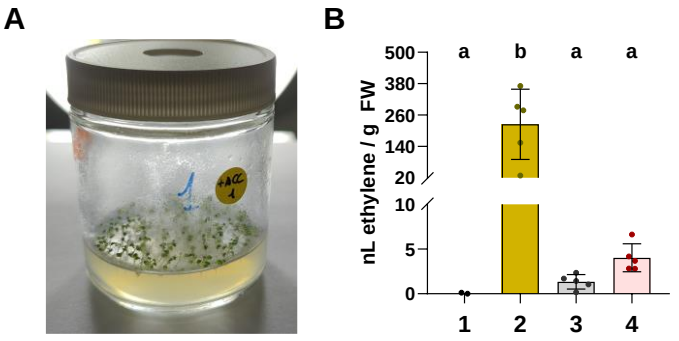

Figure 2.6 — Ethylene accumulation in sealed bottles containing A. thaliana seedlings. *(A) Representative image of the experimental setup for ethylene accumulation assays, consisting of sealed glass bottles containing approximately 100 A. thaliana seedlings grown on agar medium supplemented with or without 10 µM ACC, and exposed to either W or W+FR. (B) Quantification of ethylene levels in bottles under different conditions: (1) medium supplemented with ACC but without seedlings; (2) seedlings grown with ACC; (3) seedlings grown without ACC under white light (W); and (4) seedlings grown without ACC under white light supplemented with far-red radiation (W+FR). Data are presented as mean ± SD of 5 independent bottles (dots indicate biological replicates). Statistical significance was determined by an ordinary one-way ANOVA followed by Tukey's multiple comparisons test. Different letters indicate significant differences between groups ($p < 0.05$).*

Supplemental information

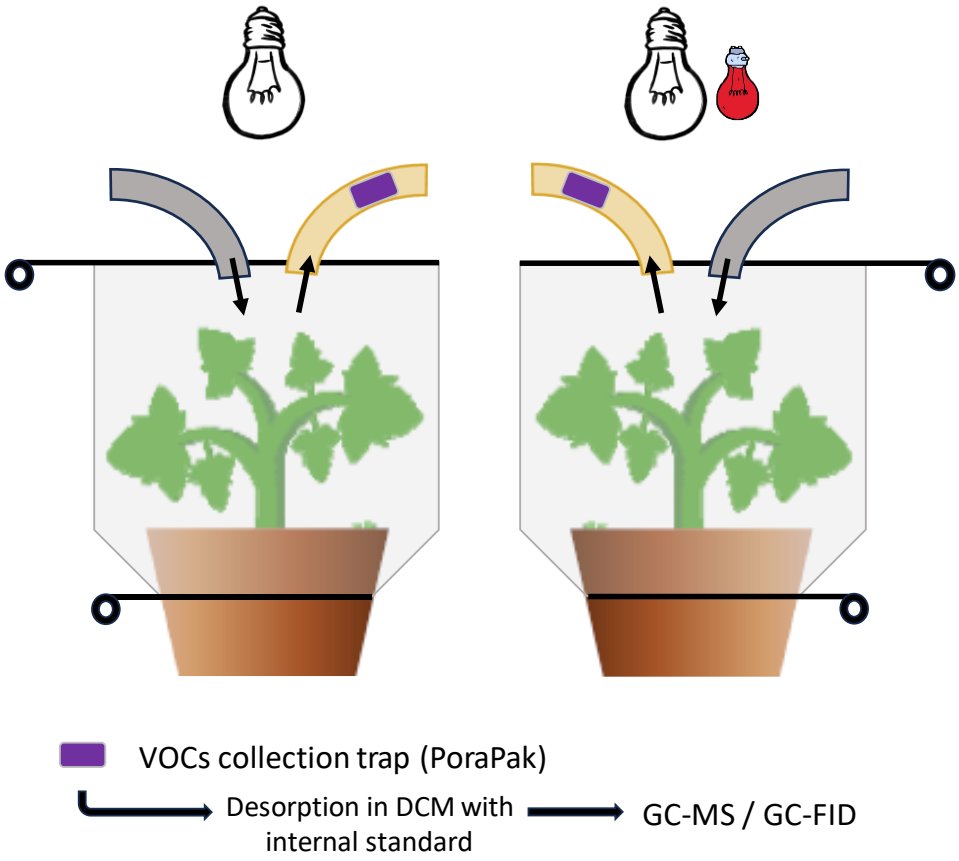

***Figure 2.S1 — Schematic representation of the VOC collection system**. Tomato plants were covered in airtight plastic boxes, and exposed to either white light (W, left) or white light supplemented with far-red radiation (W+FR, right). At the moment of VOC collection, the boxes were closed with cable binders, with two inlets creating an air stream inside the system for 2 hours. Air was pumped continuously through the boxes, with incoming air filtered using activated charcoal (grey) and outgoing air passing through adsorption tubes (yellow) containing an adsorbent material (PoraPak, in purple) to trap emitted volatiles. Flow direction is indicated by arrows. Specifications for VOC capturing are given in its respective Materials and Methods section.*

Figure 2.S2 — Aspect of tomato plants used for VOC emission analysis. *Picture shows representative W-grown tomato plants after exposure to either W (left) or W+FR (right) for 5 days.*

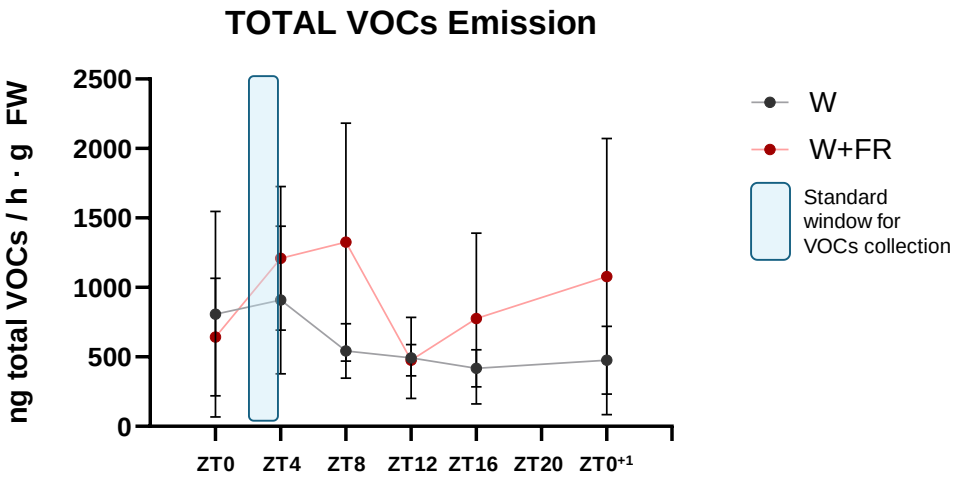

Figure 2.S3 — Analysis of diurnal VOC emissions in tomato plants exposed to either W or W+FR. *Samples were collected every 4 hours across a 24-hour cycle. For each sampling, VOCs were collected in two-hour periods (see section M.7.1). Data represent mean ± SD of 8 biological replicates. A shaded blue area indicates the time window (ZT2–ZT4) used for VOC collection in previous experiments. No statistically significant differences were found between light treatments across time points (two-way ANOVA). ZT, Zeitgeber Time.*

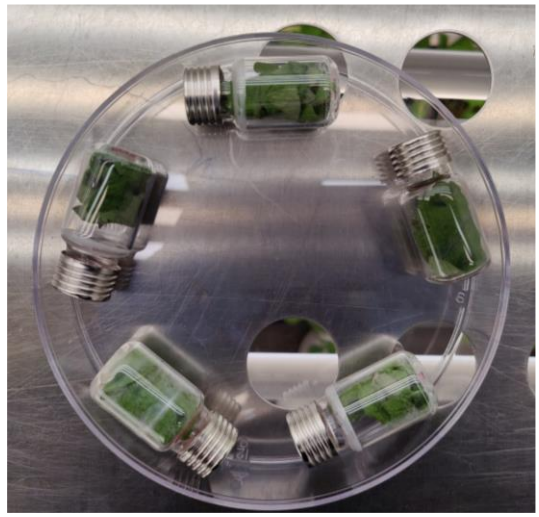

Figure 2.S4 — Experimental set-up for ethylene emission analysis. *Representative image of sealed glass vials containing tomato leaves used for ethylene emission measurements. Vials were placed in a circular rack to ensure stable positioning during the collection period. Specifications are given in the respective Materials and Methods section.*

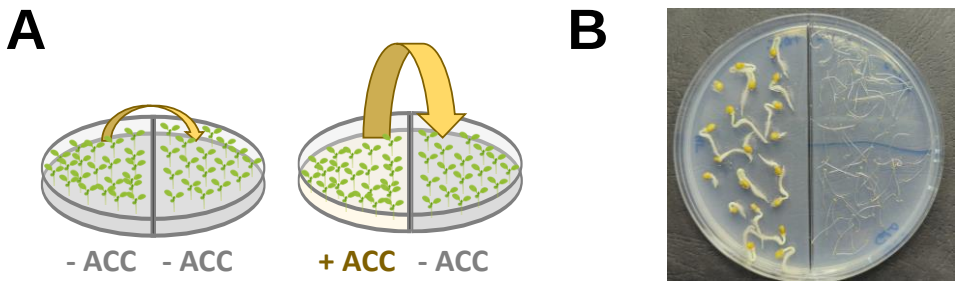

Figure 2.S5 — Schematic (A) and visual (B) representation of the experimental setup for the analysis of ethylene-mediated plant-to-plant communication. *Using compartmentalized Petri dishes, r-seedlings were grown in the absence of ACC (–ACC) (in the right compartments) and e-seedlings were grown in the separated (left) compartment on media with (+) or without (-) ACC. Ethylene (marked in yellow) produced at higher levels by ACC-treated seedlings could diffuse through the shared headspace of the plate, potentially affecting the neighboring untreated seedlings. A representative top-down-view photo is shown (B), with tomato e-seedlings appearing on the left separated (via septum) from the A. thaliana r-seedlings on the right.*

Chapter III

Chapter III. Exploring a role for apocarotenoids in volatile-mediated communication

3.1 Shade-induced carotenoid drop leads to the production of volatile apocarotenoids.

To continue our targeted search for shade-responsive VOCs that could be involved in plant-to-plant communication, we next turned our attention to volatile apocarotenoids. As previously mentioned, exposure to proximity shade is accompanied by a drop in the contents of photosynthetic pigments, including chlorophylls and carotenoids, as plants adjust to altered light conditions (Bou-Torrent *et al.*, 2015; Leschevin *et al.*, 2024; Llorente *et al.*, 2016; Morelli *et al.*, 2021a). From this standpoint, we hypothesized that oxidative breakdown products of carotenoids—collectively referred to as apocarotenoids—might accumulate under proximity shade. Importantly, some of these apocarotenoids are volatile, and hence they could represent a class of VOCs acting as signals of shade conditions.

Within this family of compounds, we initially focused on two volatile apocarotenoids derived from β-carotene degradation: β-cyclocitral (β-cc) and β-ionone (β-ion). The formation of these volatiles can occur via non-enzymatic cleavage, typically under high light stress, where β-carotene reacts with singlet oxygen ($^1O_2$) and other reactive oxygen species (ROS) as part of a photoprotective response (Frank & Cogdell, 1996; Ramel *et al.*, 2012). In addition, enzymatic cleavage by lipoxygenases and/or carotenoid cleavage dioxygenases (CCDs) can also produce β-cc and β-ion; however, the specific CCD enzymes potentially involved (CCD1, CCD4 and CCD7) have only been characterized in a limited number of species (Auldridge *et al.*, 2006). Both β-cc and β-ion have been reported to act as signaling molecules in plants, which made them particularly relevant to our investigation (D'Alessandro *et al.*, 2018; Felemban *et al.*,

2024; Taniguchi *et al.*, 2023; H. Zhang *et al.*, 2022). Still, their potential roles as volatile cues in plant-to-plant communication, including their effects across species and the molecular mechanisms underlying their bioactivity, remain largely unexplored.

We first aimed to assess whether β-cc and β-ion production is promoted in response to proximity shade. To this end, we exposed tomato detached leaves to either W or W+FR conditions and evaluated two key parameters. First, we quantified total carotenoid and β-carotene content using HPLC. Then, contingent on observing a reduction in carotenoids under W+FR—as expected—we performed targeted volatile analysis using solid phase microextraction - GC-MS (SPME-GC-MS) to measure levels of β-cc and β-ion (Fig. 3.1). HPLC analysis confirmed that W+FR induced degradation of carotenoids in tomato leaves, with β-carotene showing the strongest reduction (Fig. 3.1-A). Further analysis of the same leaf tissue showed a moderate increase in the accumulation of both β-cc and β-ion, which was only statistically significant in the case of β-ion (Fig. 3.1-B).

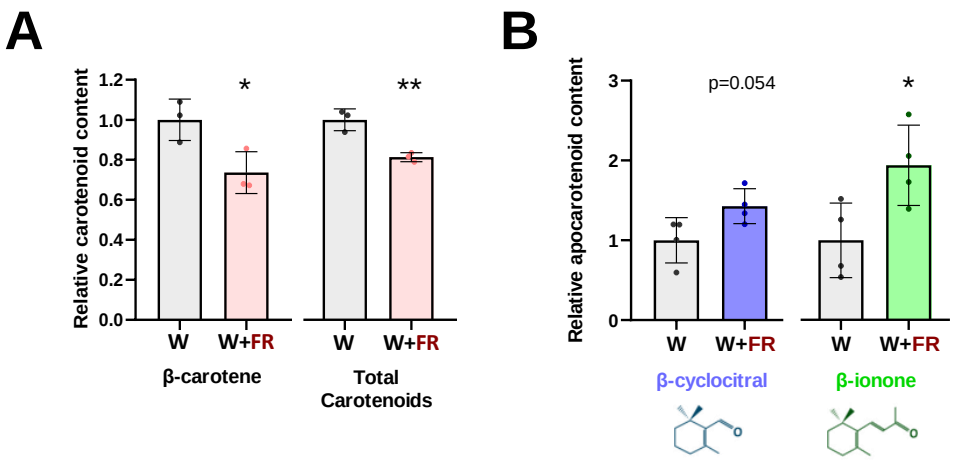

Figure 3.1 — Carotenoid and apocarotenoid quantification in response to simulated shade. *(A) Relative levels of β-carotene and total carotenoids in tomato seedlings exposed to white light (W, grey) or white light supplemented with far-red radiation (W+FR, pink. (B) Relative quantification of β-cyclocitral (β-cc, blue) and β-ionone (β-ion, green), in tomato seedlings exposed to W or W+FR. A tendency towards higher β-cc levels under W+FR was detected (p = 0.054), while β-ion levels were significantly increased. Bars represent mean ± SD of 4–6 biological replicates. In all plots, statistical significance was assessed using unpaired, two-tailed t-tests (*p < 0.05; **p < 0.01).*

3.2 Volatile β-cc and β-ion repress hypocotyl elongation.

Having established that simulated shade exposure enhances the production of β-cc and β-ion, we next sought to determine whether the atmospheric application of either compound could mimic the phenotypic effects previously observed in seedlings exposed to the full shade volatilome. We focused first on hypocotyl elongation, a developmental trait that was consistently repressed in seedlings growing under the influence of shade-derived VOCs (Fig. 1.2) and that is also affected by direct exposure to proximity shade (Pastor-Andreu *et al.*, 2024; Roig-Villanova & Martínez-García, 2016). As r-plants, we used both *A. thaliana* Col-0 (shade avoider) and *C. hirsuta* OX (shade tolerant) seedlings, to compare with the ethylene results reported on the previous chapter.

Concerning the experimental design, it was important to ensure that r-seedlings were only exposed to airborne apocarotenoids. To avoid direct contact between β-cc or β-ion and the growth medium, aliquots of these apocarotenoids were deposited into the cut-off cap of a PCR tube positioned at the center of each Petri dish, acting as a reservoir physically separated from the agar medium where seeds were sown (Fig. 3.S1). At defined time points—depending on the specific experimental conditions—a small volume (10 µL) of a DMSO solution containing a known concentration of either apocarotenoid was placed into the cap. Mock treatments were also performed by adding only DMSO, without any apocarotenoid. Then, each Petri dish was sealed with Parafilm to minimize the escape of airborne apocarotenoids and to maintain a stable volatile environment for the developing seedlings. Preliminary experiments showed that a completely hermetic seal (such as this achieved using Parafilm) prevented seedling development inside the plate (i.e., it resulted in small and short underdeveloped seedlings, Banerjee *et al.*, 2019). To overcome this problem, we found that piercing the Parafilm seal in four equidistant points was sufficient to allow gas exchange for normal seedling development while, likely, restricting volatile apocarotenoid leakage (Fig. 3.S2).

The impact of airborne β-cc or β-ion on the elongation of *A. thaliana* and *C. hirsuta* seedlings was investigated under different concentrations of the apocarotenoids in the 10 µL droplet and various light regimes: W, low W, W+FR and complete darkness (D) (Fig. 3.S3). Our results show that β-ion and, to a lower extent, β-cc, can repress hypocotyl elongation in a dose-

dependent manner in both species (Figs. 3.2, 3.S4). The effect was hardly detectable in control seedlings growing under W (Fig. 3.2-A). However, under light conditions triggering an enhanced elongation response (low W, W+FR or D), apocarotenoid-exposed seedlings elongated less in a concentration-dependent manner, with β-ion consistently exerting a stronger effect compared to β-cc (Figs. 3.2-B, 3.S4). These results correlate with the observed hypocotyl growth repression induced by exposure to the full shade volatilome (Fig. 1.2-A/B).

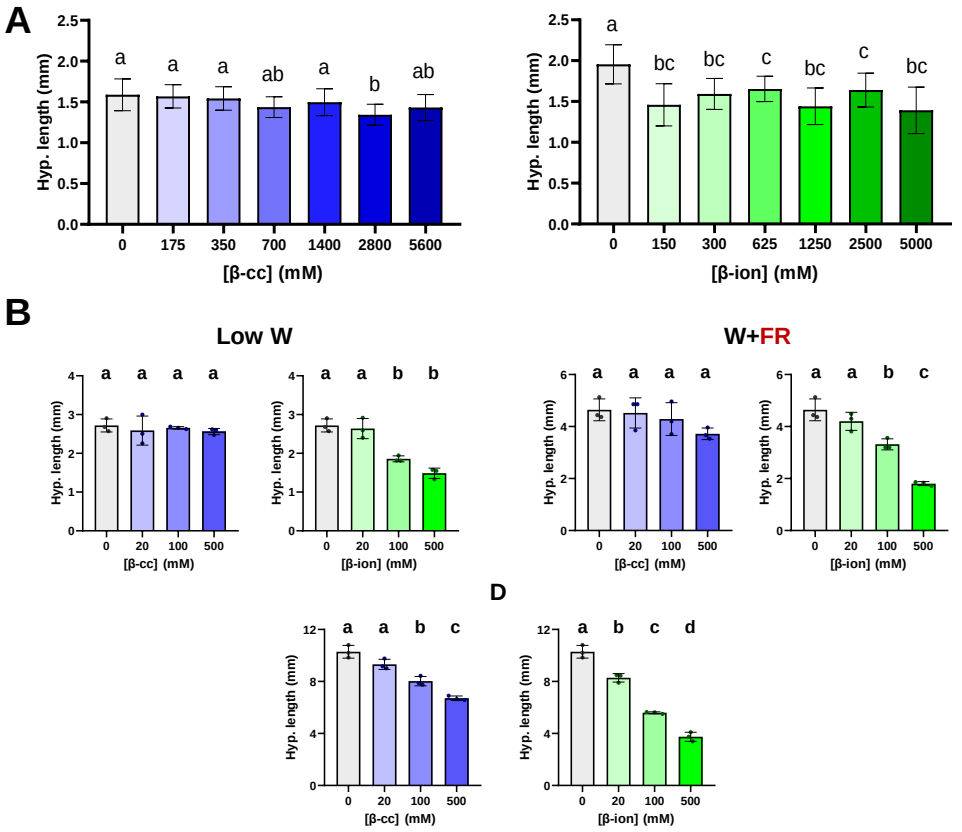

Figure 3.2 — Impact of airborne apocarotenoids on A. thaliana seedling growth under different light conditions. *Hypocotyl length of A. thaliana seedlings exposed to different doses of airborne β-cc (in blue shades) or β-ion (in green shades) under different light conditions: (A) W (48 µmol·m^{-2}·s^{-1}); (B) Low W (28 µmol·m^{-2}·s^{-1}); W+FR (48 µmol·m^{-2}·s^{-1}); and darkness (D). Darker shades represent higher concentrations of apocarotenoids in the tube-caps, which are portrayed along the X axis. In grey, DMSO (Control). Bars represent the mean ± SD of three biological replicates. Different letters indicate significant differences between treatments within each light condition (ordinary one-way ANOVA followed by Tukey's multiple comparisons test, p < 0.05).*

Based on these dose-response analyses, we selected solutions of 500 mM for β-cc and 100 mM for β-ion as our working doses for further experiments using the same setup. Using these working doses, we compared the effects of airborne apocarotenoids on hypocotyl elongation in *A. thaliana* seedlings grown under three W intensities: 49, 28 and 18 µmol $m^{-2} \cdot s^{-2}$ (Fig. 3.3). Our results confirmed that β-ion and β-cc also inhibit hypocotyl elongation under W of moderate intensities (28 and 18 µmol $m^{-2} \cdot s^{-2}$), even though the effect is not observed under the highest intensity, when hypocotyl elongation of Col-0 seedlings is already strongly repressed (Fig. 3.3).

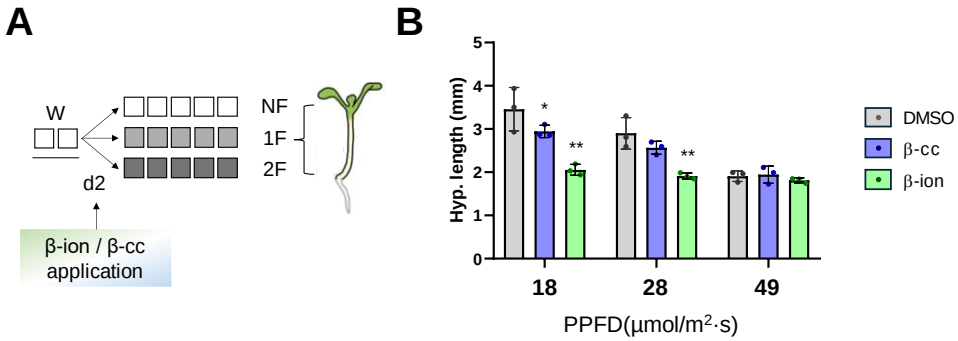

Figure 3.3 — Impact of airborne apocarotenoids on hypocotyl elongation under different W intensities. *(A) Schematic representation of the experimental design. A. thaliana seedlings were exposed to the apocarotenoids evaporated from a 10 µL droplet of 100 mM β-ion, 500 mM β-cc, or DMSO as a control under different W intensities, obtained through the application of no (0), 1 or 2 filter papers above the plates (no filter, NF= 49 µmol m^{-2} s^{-1}, 1F= 28 µmol m^{-2} s^{-1}, 2F= 18 µmol m^{-2} s^{-1}). Timing of β-ion or β-cc drop application is indicated, with every square representing 1 day of experiment. (B) Hypocotyl length of A. thaliana seedlings grown as indicated in (A). Bars represent mean ± SD of three biological replicates. Asterisks indicate significant differences between treatments within each light intensity, compared to DMSO (two-way ANOVA followed by Dunnett's multiple comparisons test, * = p < 0.05, ** = p < 0.01).*

3.3 Air concentrations of exogenously applied apocarotenoids are similar to those produced in shade-exposed plants

As previously mentioned, we used 500 mM β-cc and 100 mM β-ion in the droplet solution in our experimental assays. However, these values only reflect the initial concentrations in the liquid phase (i.e., in the DMSO solution of the tube-cap droplet, Fig 3.S1). In our setup, seedlings are

exclusively exposed to the volatile fraction released from the droplet into the headspace, and therefore, the actual treatment concentration corresponds to the amount of compound present in the vapor phase. To better assess the physiological relevance of our experiments, we next proceeded to determine as accurately as possible the airborne concentration reached by each apocarotenoid under our experimental conditions. This would allow us to potentially link observed biological responses to real atmospheric doses and assess how our system compares to potential natural exposures in plant-plant communication scenarios.

As a first step, we estimated the theoretical maximum concentration in the headspace (HS) assuming full volatilization (Fig. 3.S5). For this, we considered the initial amount of compound applied in the tube-cap droplet—10 µL—and the volume of the HS within the semi-sealed Petri dish. Considering the geometry of the plate and the volume occupied by the growth medium, we estimated the available gas-phase volume to be approximately 50 mL. Considering these assumptions, the maximum theoretical concentrations in the HS would be around 100 µM for β-cc and 20 µM for β-ion. These values represent an upper bound, assuming complete volatilization and no compound loss through absorption or leakage.

Next, we built a standard curve to ultimately estimate real atmospheric concentrations of β-cc and β-ion in our system. This approach correlated the known concentrations of each apocarotenoid in the HS with their corresponding extracted ion current (EIC) peak areas, as measured by GC-MS. To do so, 15 mL GC-MS vials were used as controlled HS chambers. In each vial, we added 10 µL of β-cc or β-ion solutions at defined concentrations in DMSO, ranging from 100 nM to 10 mM in tenfold dilution series (Fig. 3.S6-A). Each vial was sealed and subjected to a standard incubation protocol prior to analysis: 20 minutes of mild shaking and heating (at 40°C) to promote volatilization of the compound into the HS in the presence of the SPME fiber. We assumed that the applied heating treatment transferred the entirety of the apocarotenoid content to the gaseous phase, which was subsequently adsorbed by the SPME fiber. After incubation, HS analysis was conducted by SPME-GC-MS, and the resulting EIC peak areas for each compound were recorded. A log-transformation of the expected HS concentration values yielded a linear relationship with EIC area, which allowed us to fit a standard calibration

curve (Fig. 3.S6-B). This log-linear model could then be used to estimate unknown HS concentrations of β-cc and β-ion in experimental settings by interpolation from the recorded GC-MS signal.

To assess whether SPME fiber saturation or HS saturation could bias our quantification, we monitored the chromatographic response across the tested concentration range. In both β-ion and β-cc (Fig. 3.S6-B), we observed a consistent increase in the EIC area with increasing initial concentrations, suggesting no evident saturation of the fiber or the HS compartment. The log-transformed data showed good linearity in the analyzed (mid-to-high) concentration range, particularly around the values relevant to our standard application doses. Although no replicates or internal standards were used at this stage, the trend and reproducibility of the signal provided a functional framework for interpolating approximate atmospheric concentrations in subsequent plate assays. Further refinements, such as replicate measurements or internal calibration with a volatile reference compound, may improve the precision of these estimates in future experiments.

Finally, we estimated the atmospheric concentration of apocarotenoids in our experimental setup (Fig. 3.S1) (i.e., at 22ºC temperature of seedlings growth with no heating to promote volatilization). Due to the impracticality of inserting SPME fibers into standard circular (9 cm diameter) Petri dishes (where seedlings are grown), we designed an approximation system based on HS enrichment and SPME-GC-MS analysis (Fig. 3.S7) using square Petri plates (12 × 12 cm) with a larger internal HS volume—approximately three times the volume of our regular Petri plates. To maintain proportionality with the standard system, we increased the applied solution volume to 30 µL (3 × 10 µL), using the same concentrations previously used (100 mM β-ion or 500 mM β-cc). The solution was poured in a small open container placed in the center of the square plate. SPME fibers were laid directly on the culture medium, within the same compartment as the volatile source but without direct contact. Plates were sealed with Parafilm (punctured at four equidistant points, as in the standard system) and incubated under identical growth conditions (22°C, D). Fibers were exposed to the HS for different time intervals, with replicate samples collected at each time point. After each incubation, fibers were retrieved and analyzed by GC-MS. The resulting chromatographic EIC peak areas were plotted against vaporization time (Fig. 3.4), and the EIC areas in equilibrium were then interpolated using the linear calibration

curves obtained from standard vials (Fig. 3.S6-B), allowing us to approximate the actual airborne concentration of β-ion and β-cc inside the system.

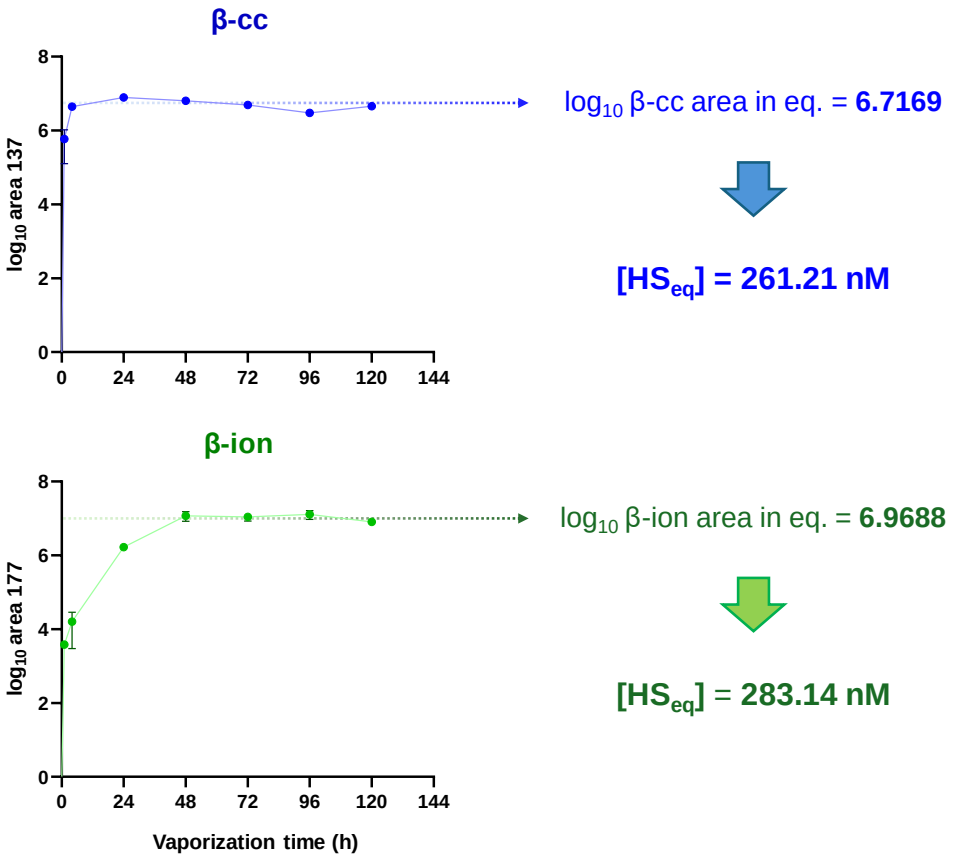

Figure 3.4 — Vaporization dynamics of airborne apocarotenoids and determination of headspace (HS) equilibrium (eq.) concentrations. *Time-course of vaporization for β-cc (above, in blue) and β-ion (below, in green) applied in closed squared Petri-dish systems. GC-MS peak areas of the respective quantifier ions were monitored over time until reaching equilibrium and plotted according to the total vaporization time (from closing the system, to reopening to measure the fibers). Equilibrium HS concentrations were then calculated from the EIC chromatographic areas in equilibrium, based on the linear regression equations obtained from the standard curves (see Fig. 3.S6-B).*

Our semi-quantitative analysis revealed that the HS concentrations of both β-ion and β-cc in the Petri dishes used in our experiments remain in the nanomolar range, significantly below the initial concentrations applied in

the tube-cap droplet (Fig. 3.4). Despite the working concentrations in the droplet were different for β-ion (100 mM) and β-cc (500 mM), the HS concentration turned out to be very similar for both apocarotenoids, about 300 nM (Fig. 3.4). Interestingly, the vaporization dynamics differed between the two compounds. While β-cc rapidly reached its HS equilibrium concentration within the first 4 hours post-application, β-ion exhibited a slower release profile, only reaching a stable concentration around 24 hours after treatment (Fig. 3.S8). These differences suggest distinct physicochemical behaviors in volatilization and/or partitioning to the HS, which could be relevant to their bioactivity over time.

Additionally, we sought to assess the physiological relevance of the HS concentrations of β-cc and β-ion used in our system by comparing them to their endogenous levels in shade-treated plant tissues. Although we were not able to detect or quantify β-cc and β-ion in the HS of tomato plants, we used the apocarotenoid content measured in leaf tissue as a proxy (taken from data portrayed in Fig. 3.1). Our results from SPME–GC–MS measurements of β-cc and β-ion in tomato leaf tissue, compared against the GC–MS area–HS concentration linear relationships established with pure standards (Fig. 3.S6), indicate that one gram of tomato leaf tissue exposed to W+FR accumulates sufficient β-cc and β-ion to theoretically result in HS concentrations of about 6 nM β-cc and 11 nM β-ion (Fig. 3.5).

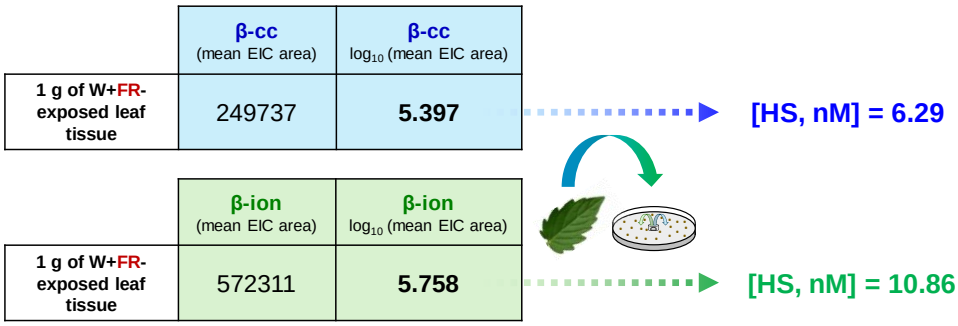

Figure 3.5 — Extrapolation of potential airborne apocarotenoid concentrations from endogenous tissue levels. *Absolute levels of β-cc (in blue) and β-ion (in green) detected per gram of tomato leaf tissue exposed to W+FR are shown in tables as mean extracted ion chromatogram (EIC) areas. Values are also presented after log_{10} transformation. Considering the linear relationship between apocarotenoid [HS] and EIC peak area, obtained from Fig. 3.S6, projected HS concentrations in the system are drawn.*

Although these values fall within the nanomolar range, they remain below the HS concentrations estimated for our Petri dish experimental system. Nevertheless, considering the total leaf biomass of 30–35 day-old tomato plants, together with the fact that our tissue-based approach only provides a snapshot of apocarotenoid content at a given time— rather than a continuous emission profile beyond our analytical resolution—we conclude that the HS concentrations applied in the Petri dish assays may be within the physiologically range.

3.4 Airborne apocarotenoids have effects beyond hypocotyl elongation

3.4.1 β-cc specifically induces seed germination arrest

We next wanted to focus on additional impacts driven by airborne β-cc and β-ion beyond hypocotyl elongation. While analyzing the effects of these apocarotenoids on dark-grown seedlings, we observed a potential influence on seed germination. To further explore this, we monitored the germination dynamics of *A. thaliana* seeds exposed to β-cc or β-ion using the same experimental setup under W or darkness. Germination was assessed based on counting radicle emergence at regular intervals until 100% (or stable) germination was reached in each treatment (Fig. 3.6).

Our results indicate that β-cc consistently delays and even suppresses seed germination in *A. thaliana* under either W (Fig. 3.6-A) or darkness (Fig. 3.6-B). In contrast, β-ion exerted no observable effect on germination. The β-cc impact was further validated in a dose–response assay, where increasing β-cc concentrations induced progressive inhibition of germination in Col-0 seeds (Fig. 3.7). Considering that the bioactivity of β-ion within the first 24 hours of application could be limited by its slower vaporization and consequently lower HS concentrations (Figs. 3.4, 3.S8), we performed an additional experiment where β-ion was applied one day before the standard time point. However, pre-application of β-ion did not alter germination rates (Fig. 3.S9), thereby ruling out a potential role of this compound in germination control. These results highlight the specificity of action between these two apocarotenoids.

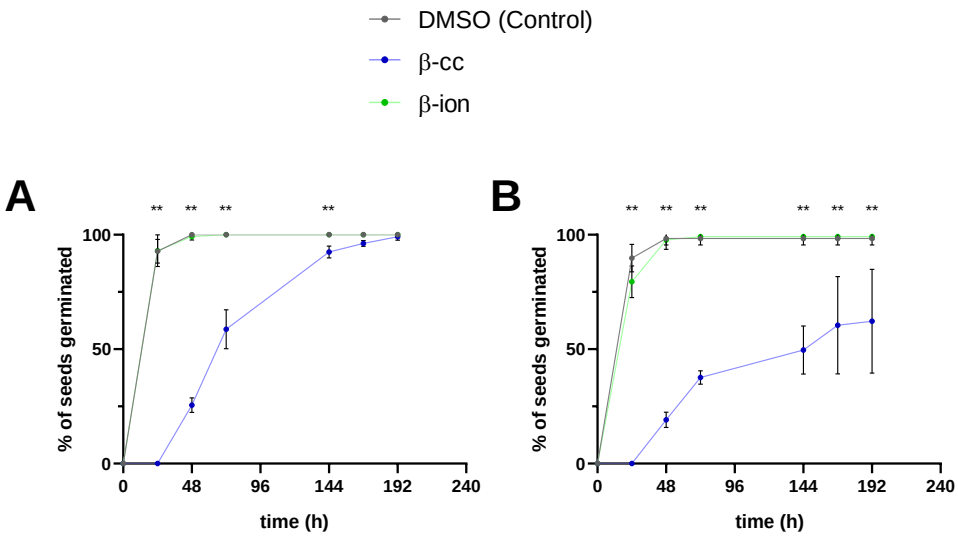

Figure 3.6 — Effect of airborne apocarotenoids on seed germination. *Germination kinetics of A. thaliana Col-0 seeds exposed to airborne β-cc (from 10 µL of 0.5 M β-cc, blue) or β-ion (from 10 µL of 0.1 M β-ion, green) compared with control conditions (10 µL of DMSO, grey) under (A) W or (B) darkness conditions. Data are represented as the cumulative percentage of germinated seeds over time (mean ± SD, n ≥ 3 biological replicates with at least 30 seeds each). Asterisks indicate statistically significant differences compared to controls at the same time point (two-way ANOVA followed by Sidak's multiple comparisons test, *p<0.05, **p < 0.01).*

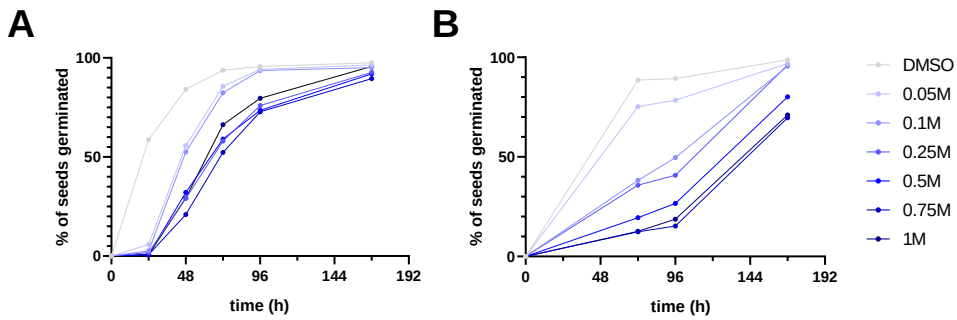

Figure 3.7 — β-cc impact on A. thaliana germination. *Germination kinetics of Col-0 seeds exposed to increasing doses of airborne β-cc under (A) W or (B) darkness conditions, β-cc was applied in sealed Petri-dish systems.*

3.4.2 β-ion enhances photosynthetic performance in a phyB-dependent fashion

We next investigated whether exposure to β-cc or β-ion modulates seedling photosynthesis—a process that in our system appeared unaffected by the complete shade volatilome, yet has been previously reported to respond to proximity shade (Leschevin *et al.*, 2024; Morelli *et al.*, 2021a). In particular, chlorophyll fluorescence parameters such as φPSII and Fv/Fm were measured in *A. thaliana* Col-0 seedlings exposed to airborne β-cc or β-ion under different light conditions (Fig. 3.8). In dose–response experiments conducted under low W and W+FR, β-cc did not induce significant alterations in either parameter across the concentrations tested (Fig. 3.8-A, B). By contrast, β-ion displayed a clear dose-dependent effect: while lower concentrations exerted no detectable influence, our working dose (100 mM in the droplet solution, 300 nM in the HS) enhanced φPSII without affecting Fv/Fm, whereas the highest concentration tested caused a reduction in both parameters (Fig. 3.8-A). Under W+FR conditions (Fig. 3.8-B), the stimulatory effect of β-ion on φPSII was not observed, although the highest dose still negatively impacted photosynthetic efficiency.

Given that the dose–response experiments identified the working dose of β-ion as biologically relevant for modulating photosynthetic traits, we next focused on testing the application of the working doses for β-cc or β-ion (500 mM and 100 mM, respectively) under different intensities of W (Fig. 3.9). This approach allowed us to evaluate whether the effects of airborne apocarotenoids depend on light availability, a key determinant of photosynthetic activity (Böhning & Burnside, 1956; Wimalasekera, 2019). In addition to Col-0, we included the *phyB* mutant, which is hyposensitive to light-mediated developmental cues but still retains a hypocotyl response to these compounds under different W intensities (Fig. 3.S10). Including this mutant provided an opportunity to explore whether the observed effects of apocarotenoids on photosynthetic efficiency require *phyB*-dependent light perception or operate through alternative pathways.

Our results under the different tested intensities of W were consistent with the β-ion working dose impact on ϕPSII (Fig. 3.9). While β-cc did not significantly impact this photosynthetic parameter (consistent with the results reported in Fig. 3.8), β-ion elicited a significant positive effect on the effective quantum yield of PSII of Col-0 seedlings across all W

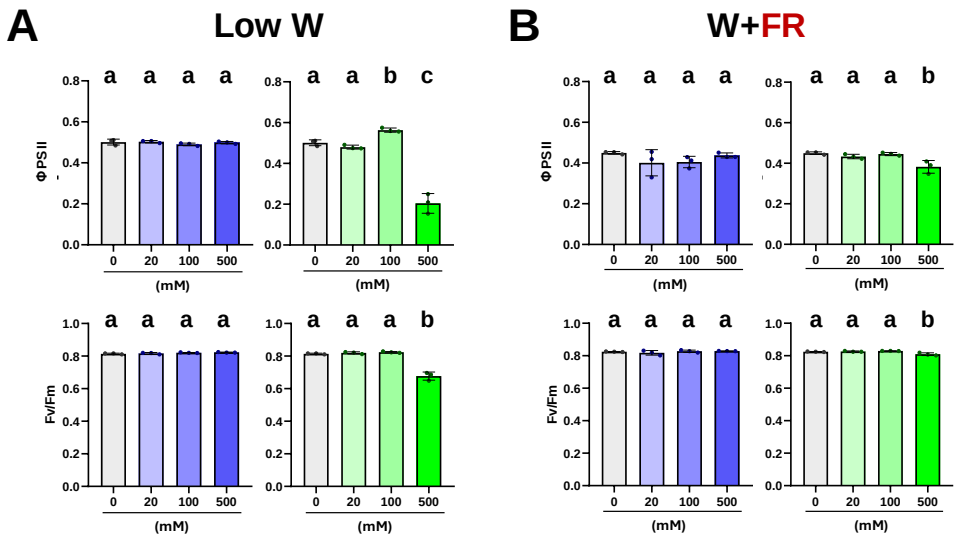

Figure 3.8 — Impact of airborne apocarotenoids on photosynthetic parameters of Col-0 seedlings under different light conditions. *Photosynthetic parameters were measured in Col-0 seedlings exposed to increasing doses of airborne β-cc (blue) or β-ion (green) under (A) low W (28 µmol·m^{-2}·s^{-1}) or (B) W+FR (48 µmol·m^{-2}·s^{-1}). In grey, DMSO (Control). For within each group, effective PSII quantum yield (φPSII, above) and maximum quantum efficiency of PSII photochemistry (Fv/Fm, below) are displayed. Bars represent mean ± SD from three independent biological replicates. Letters indicate statistically significant differences among each light and apocarotenoid treatment (ordinary one-way ANOVA followed by Tukey's multiple comparisons test, p<0.05).*

intensities tested, in comparison to the control. By contrast, this effect was absent in the *phyB* mutant (Fig. 3.9). These results confirm a positive and specific role for β-ion distinct from the response to β-cc. Moreover, they indicate that while the repression of hypocotyl elongation by β-ion does not require PHYB, the enhancement of photosynthetic efficiency does, pointing to a specific dependence on PHYB for this physiological output.

3.4.3 β-ion induces changes in the nuclear disposition of phyB

Given the phyB requirement for some β-ion-related phenotypes, we next asked whether β-ion might modulate phyB behavior at the subcellular level. PhyB is known to form discrete subnuclear structures termed photobodies (PBs) upon photoactivation (M. Chen *et al.*, 2005). These

dynamic assemblies, whose number, size, and composition are influenced by light quality and intensity, are considered hallmarks of phyB signaling

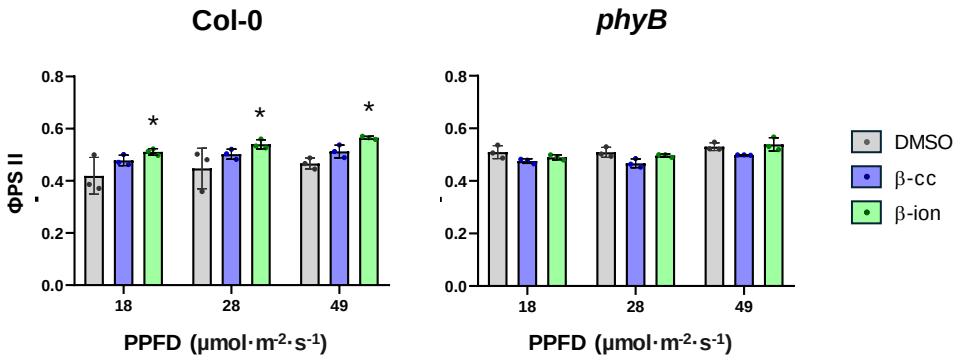

Figure 3.9 — Airborne apocarotenoid impact on photosynthetic performance of A. thaliana seedlings under different W intensities. *Plots represent φPSII of A. thaliana Col-0 (WT, left) and phyB mutant (right) seedlings exposed to β-cc (blue) or β-ion (green) under increasing intensities of W light (PPFD). In grey, DMSO (Control). Bars represent mean ± SD of three biological replicates. Statistical significance was assessed using two-way ANOVA followed by Dunnett's multiple comparisons test. Asterisks different letters denote significant differences compared to DMSO (*p<0.05, **p<0.01).*

activity and may link environmental perception to transcriptional regulation. While the mechanistic relationship between PB dynamics and specific physiological outputs remains incompletely understood, they provide a valuable readout to explore whether β-ion affects phyB signaling capacity.

We used seedlings of the *35S:PHYB-GFP* reporter line and analyzed the presence of PBs in cotyledon cells by confocal microscopy, as described in Ortiz-Alcaide *et al.*, 2019. Seedlings were first maintained for 2 days under white light (W) and then exposed to either DMSO or 100 mM β-ion for 5 additional days, all under continuous W. On day 7, cotyledon epidermal cells were imaged directly by confocal microscopy (Fig. 3.10).

A clear increase in the number of PBs per nucleus was observed in β-ion-treated PBG seedlings compared with DMSO controls (Fig. 3.10-A). Quantification (Fig. 3.10-B) confirmed a significant increase in PB number per nucleus upon β-ion treatment. Further analysis of the distribution of nuclei according to their PB content (Fig. 3.10-C) revealed a shift towards populations with higher PB counts in β-ion-treated seedlings compared to DMSO controls (see also Fig. 3.S11). These data were confirmed in a

subsequent experiment that followed the same experimental design, reproducing the same β-ion-driven effects on PHYB-GFP nuclear distribution (Fig. 3.S12). Altogether, these results indicate that β-ion alters the nuclear distribution of PHYB, potentially linking perception of β-ion, phyB signaling capacity and the photosynthetic performance enhancement observed (Fig. 3.8 / 3.9)

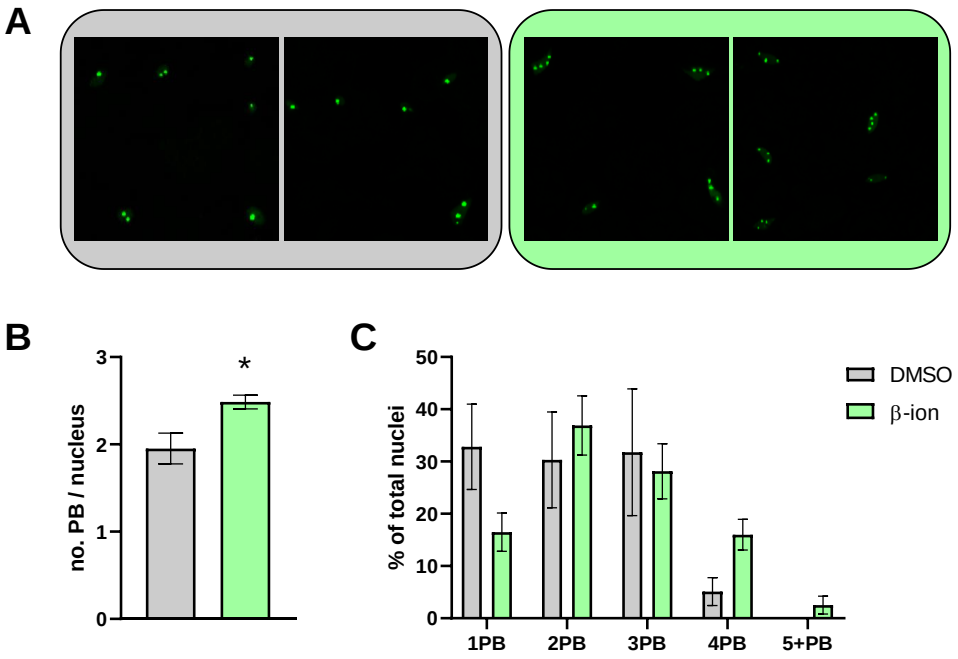

Figure 3.10 — Impact of β-ion on phyB subnuclear distribution. *35S:PHYB-GFP seedlings were exposed to DMSO (control, grey) or airborne β-ion (green) under W for 5 days. (A) Representative confocal images showing two independent fields of nuclei with PHYB-GFP photobodies (PBs). (B) Quantification of PBs. Bars represent mean ± SEM from at least 8 confocal images, each containing a minimum of 10 nuclei. Statistical significance was determined by an unpaired two-tailed t-test. Asterisks denote significant differences between treatments (*p<0.05, **p<0.01). (C) Distribution of nuclei according to PB number (from 1 to ≥5). Bars represent mean percentage ± SEM from the same dataset. No significant differences between treatments were detected (two-way ANOVA test).*

Supplemental Information

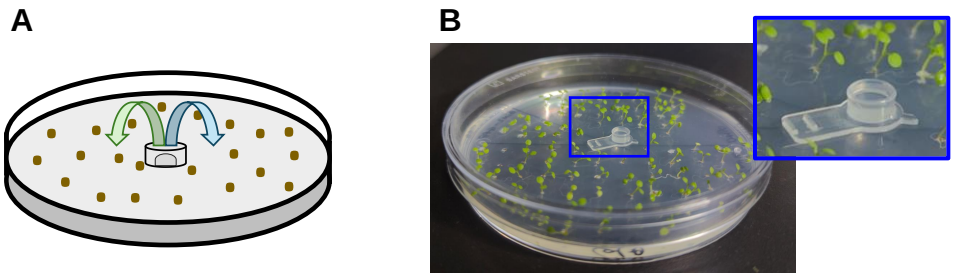

Figure 3.S1 — Schematic depiction of the volatile delivery system used to assess airborne apocarotenoid effects on seedlings. *(A) schematic representation of the placement of a sterilized tube cap in the center of a Petri dish containing seeds, into which a defined volume (10 µL) of apocarotenoid solution is applied, allowing its volatilization. Exchange with the surrounding atmosphere is restricted by Parafilm sealing, which was perforated 4 times to balance air renewal and volatile retention. (B) picture of the actual experimental setup. A magnification of the tube cap in the area boxed in blue is also shown.*

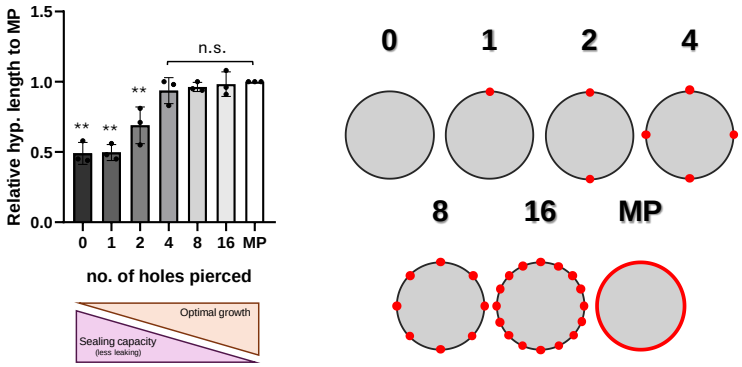

Figure 3.S2 — Optimization of the Petri dish-based volatile delivery system. *Three plates with A. thaliana seeds were sealed using Micropore (MP, allowing free air exchange) or Parafilm with different number of perforations (0, 1, 2 4, 8 and 16) as represented in the cartoon. Then, plates were incubated under W for 7 days. Plots shows relative hypocotyl elongation (to MP sealing). Purple and orange triangles below the X axis represent a schematic summary of the trade-off between sealing capacity (volatile retention) and optimal plant growth, illustrating the need for intermediate perforation. Bars show the mean ± SD of three biological replicates. Statistical significance was determined by an ordinary one-way ANOVA followed by Tukey's multiple comparisons test. Asterisks indicate significant differences against the MP group (** = p < 0.01, * = p< 0.05, n.s. = non-significant).*

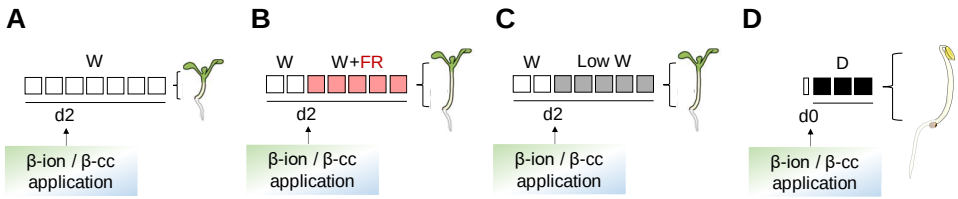

Figure 3.S3 — Schematic representation of experimental designs for hypocotyl elongation assays. *Seedlings were exposed to β-ion or β-cc under different light conditions: (A) continuous W, (B) W+FR, (C) low (dim) W, and (iv) darkness (D). Every square represents 1 day of experiment. Timing of β-ion or β-cc application is indicated.*

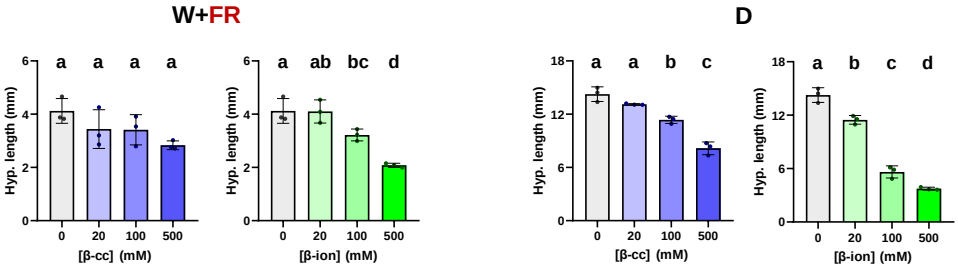

Figure 3.S4 — Impact of airborne apocarotenoids on C. hirsuta seedling growth under different light conditions. *Hypocotyl length of C. hirsuta seedlings exposed to different doses of airborne β-cyclocitral (in blue shades) or β-ionone (in green shades) under different light conditions: W+FR (48 μmol·m^{-2}·s^{-1}, on the left); and darkness (D, on the right). Darker shades represent higher concentrations of apocarotenoids in the tube-caps, which are portrayed along the X axis. In grey, DMSO (Control). Bars represent the mean ± SD of three biological replicates. Different letters indicate significant differences between treatments within each light condition (ordinary one-way ANOVA followed by Tukey's multiple comparisons test, $p < 0.05$).*

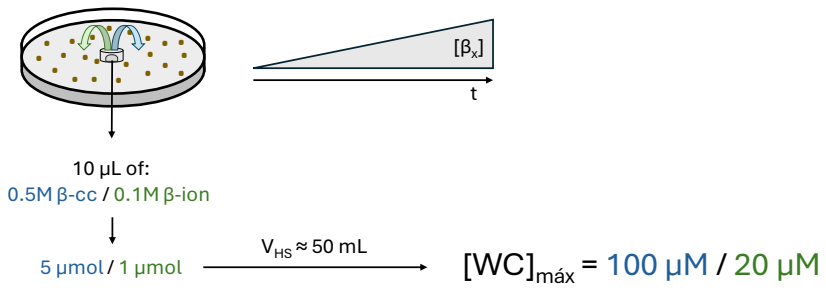

Figure 3.S5 — Determination of the theoretical maximal headspace (HS) concentration of β-cc and β-ion. *Schematic representation of the Petri-dish system used to calculate the theoretical maximal HS concentrations of apocarotenoids applied as volatiles. Known amounts of β-cc (blue, 5 µmol) or β-ion (green, 1 µmol) were applied in sealed systems. Calculations were based on the compound applied to the tube cap and the air volume inside the Petri dish (V_{HS}, 50 mL). Assuming complete volatilization, maximal HS concentrations of ~100 µM for β-cc and ~20 µM for β-ion were obtained. These values represent upper-limit estimates used to guide experimental design. WC, working concentration.*

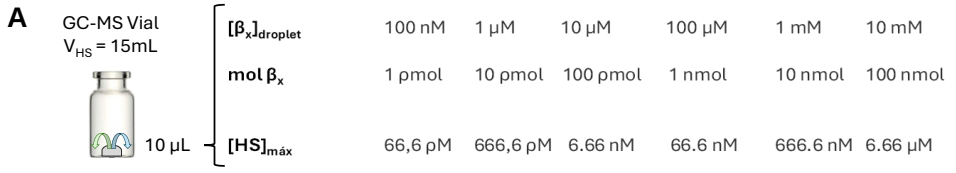

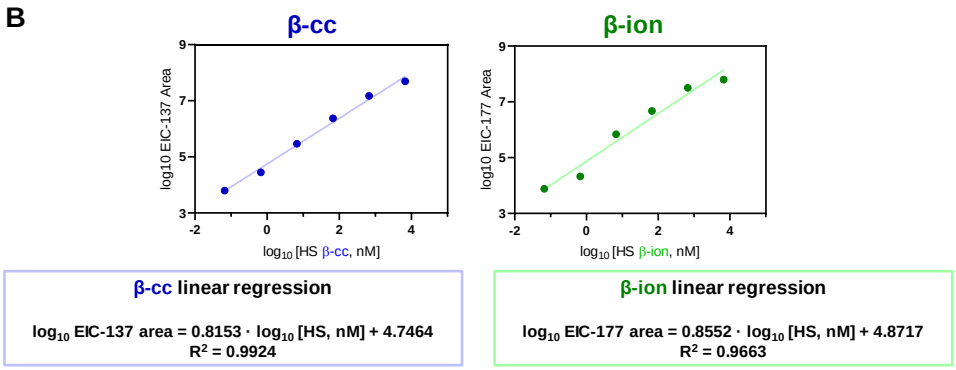

Figure 3.S6 — Standard curves for airborne apocarotenoids. *Establishment of the relationship between headspace (HS) concentration and GC–MS peak area for β-cc (blue) and β-ion (green). (A) Serial dilutions of both those compounds (100 nM–10 mM) were prepared and 10 µL of each were placed in 15 mL sealed vials. Assuming complete volatilization, corresponding HS concentrations were calculated based on vial volume (15 mL). (B) Vials were run on the GC-MS, providing EIC areas for both compounds for each calculated HS concentration. EIC peak areas of quantifier ions were plotted against calculated HS concentrations after a logarithmic transformation, yielding a linear relationship used for quantification of airborne apocarotenoids in subsequent experiments.*

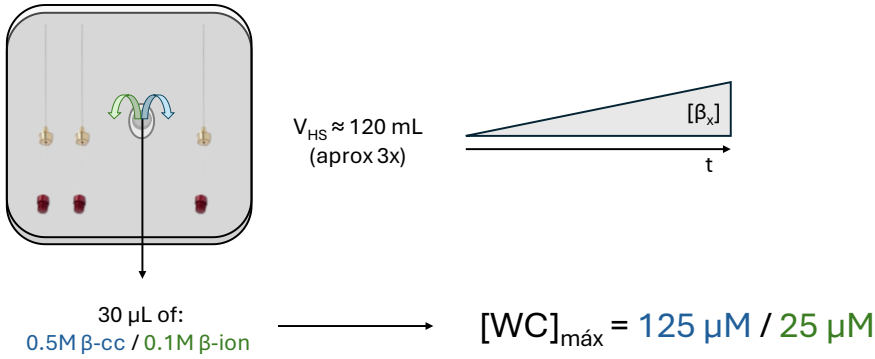

Figure 3.S7 — Schematic representation of the system used to estimate headspace (HS) apocarotenoid concentration. *Known amounts of concentrated stock solutions (0.5 M β-cc and 0.1 M β-ion) were applied onto tube caps positioned inside sealed plates (15 µmol and 5 µmol, respectively). Based on the applied amounts and the estimated air volume within the system (approximately 120 mL), theoretical maximal HS concentrations of ~125 µM for β-cc and ~25 µM for β-ion were derived, assuming complete volatilization.*

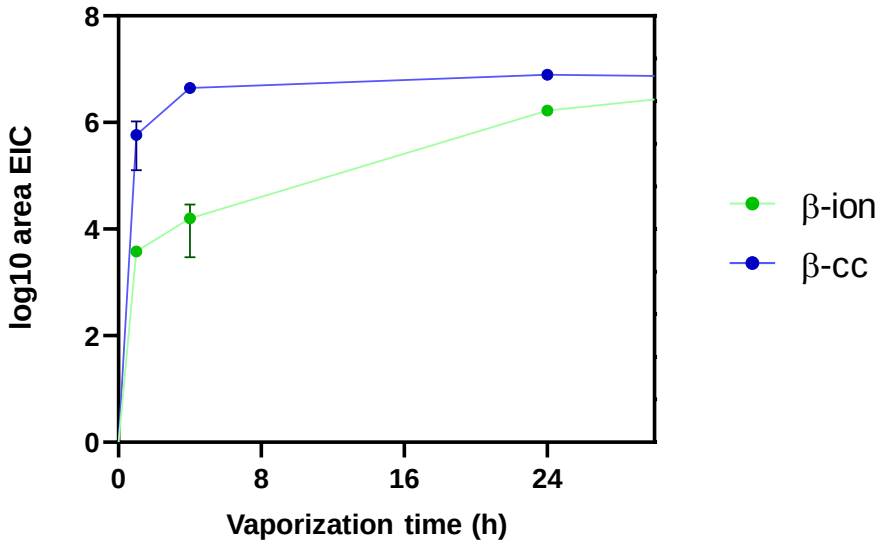

Figure 3.S8 — Early vaporization dynamics of airborne apocarotenoids. *Close-up of the first 24 h of vaporization for β-cc (blue) and β-ion (green), extracted from the dataset in Fig. 3.4. Data show that both compounds rapidly accumulate in the HS within the first hours after application, with β-cc reaching equilibrium way faster than β-ion.*

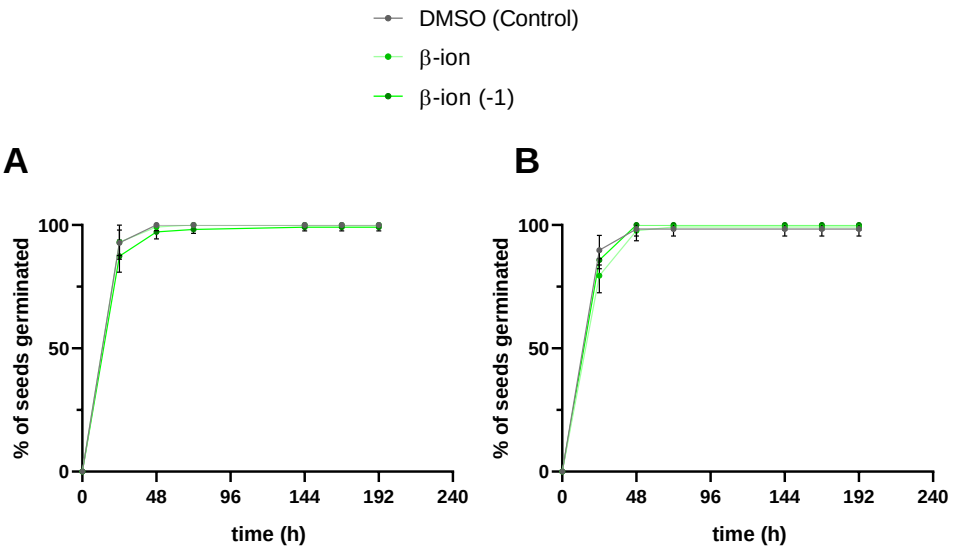

Figure 3.S9 — β-ion does not impact A. thaliana seed germination, even when applied one day prior to sowing. *Germination rates of Col-0 seeds exposed to airborne β-ion (from 10 µL of 0.1 M β-ion), applied either simultaneously with seed sowing or 24 h before sowing (β-ion -1), either (A) under W or (B) under D conditions. No significant differences were observed compared to control treatments, confirming the lack of effect of β-ion on germination regardless of the timing of application.*

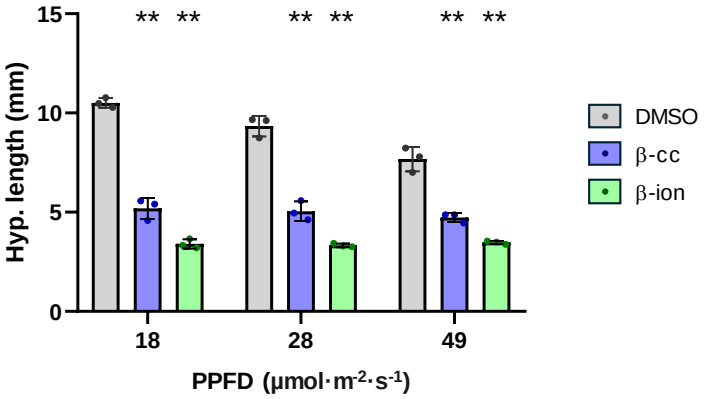

Figure 3.S10 — Impact of airborne apocarotenoids on hypocotyl elongation of phyB seedlings. *Hypocotyl length of A. thaliana phyB mutant seedlings exposed to β-cc (blue) or β-ion (green) under different W intensities (Photosynthetic Photon Flux Density, PPFD, X axis). In grey, DMSO (Control). Bars represent mean ± SD of three biological replicates. Statistical significance was assessed by two-way ANOVA followed by Dunnett's multiple comparisons test. Asterisks denote significant differences compared to DMSO (*p<0.05, **p<0.01).*

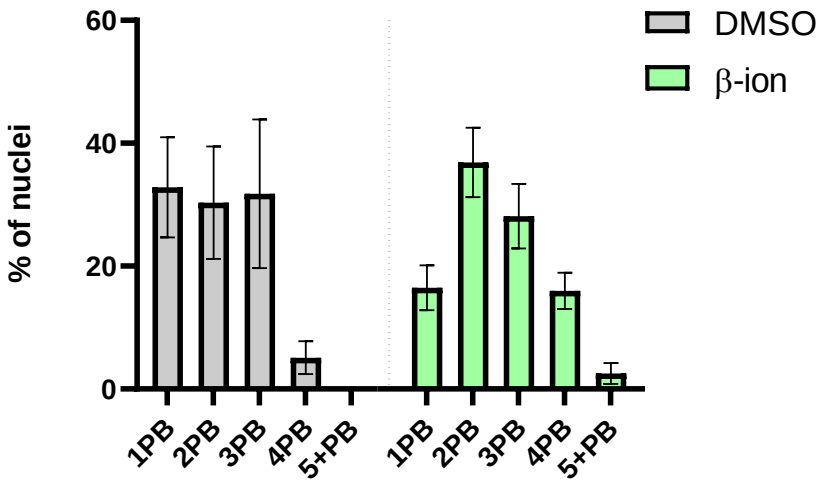

Figure 3.S11 — Distribution of phyB-GFP photobodies (PBs) per nucleus under β-ion exposure. *Quantification of nuclei containing different numbers of PBs (from 1 to ≥5) in 35S:PHYB-GFP seedlings exposed to DMSO (control, grey) or airborne β-ion (green). Bars represent mean percentage ± SEM from at least 8 confocal images, each comprising a minimum of 10 nuclei. This separate representation of the profiles (corresponding to Fig. 3.10C) highlights the trend towards a higher proportion of nuclei containing multiple PBs under β-ion treatment, although no statistically significant differences were detected.*

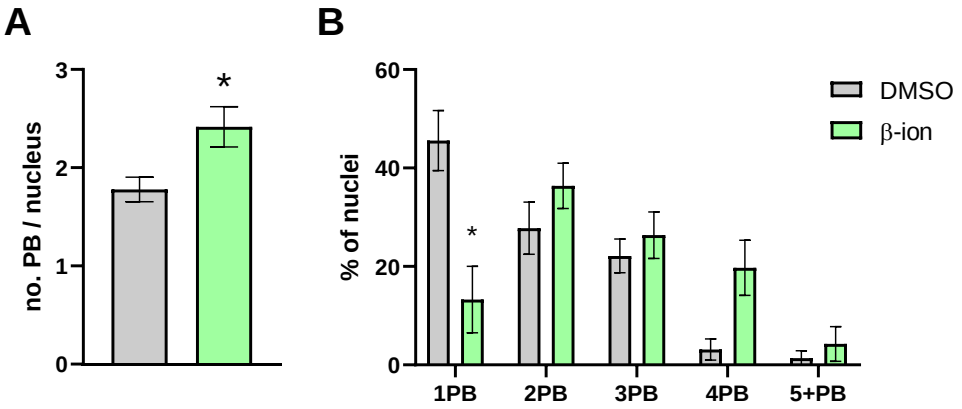

Figure 3.S12 — Impact of β-ion on phyB-GFP photobody dynamics – Confirmation experiment. *Quantification of PB number per nucleus (left, A) and distribution of nuclei according to PB content (right, B) in 35S:PHYB-GFP seedlings exposed to DMSO (control, grey) or airborne β-ion (green), under W. Bars represent mean ± SEM from at least 8 confocal images comprising ≥10 nuclei each. Statistical significance was assessed by (A) an unpaired two-tailed t-test; (B) two-way ANOVA followed by Sidak's multiple comparison test. Asterisks denote significant differences between treatments (*p<0.05, **p<0.01).*

Chapter IV

Chapter IV. Transcriptomic dissection of volatile-mediated responses

In the preceding chapters, we demonstrated that shade-induced VOCs act as signaling molecules capable of reshaping the developmental and transcriptional programs of neighboring plants. This raised the central question of which individual compounds within the volatilome could account for such activity. By examining candidate VOCs whose production is increased by proximity shade, we showed that application of ethylene and the apocarotenoids β-cyclocitral (β-cc) and β-ionone (β-ion) elicited phenotypic responses resembling those of the complex shade volatilome. Notably, the two apocarotenoids elicited distinct effects on diverse physiological processes, underscoring that, although they can converge on some responses, they also exhibit a clear specificity of action.

In this chapter, we extend this search for causal volatiles to the transcriptomic level. First, we integrate volatile-responsive transcriptomes by comparing the RNA-seq results from the shade volatilome with individual datasets of the apocarotenoids β-cc and β-ion (obtained by RNA-seq, own data), and of the volatile hormone ethylene (obtained by microarray, published data), as well as with the combination of all three treatments. This comparative approach aimed to assess the degree of overlap and divergence of the contribution of each compound to the shade volatilome transcriptional signature. In a second step, we perform a functional characterization of β-cc- and β-ion–regulated gene networks, aiming to connect their specific transcriptional profiles with the phenotypic effects previously described.

4.1 Comparative analysis of transcriptomic responses.

4.1.1 Dataset overview and selection

To carry out the comparative analysis, we first defined the transcriptomic datasets to be included. As a reference, the dataset of the transcriptomic

response to the shade volatilome (RNA-seq) was described in Chapter I (section 1.3). For this analysis, we selected the DEG set identified at 24 h of treatment using DESeq2, with a threshold of fold change ≥ 1.5 and a q-value < 0.05, which comprised a total of 393 genes. This dataset was eventually separated into 337 up- and 56 down-regulated genes (Fig. 1.S4).

For ethylene, we relied on an external dataset generated by Das *et al.*, 2016, who performed a microarray-based transcriptomic analysis of one-day old *A. thaliana* seedlings grown under short day photoperiod (9 h light and 15 h darkness) and exposed to exogenous gaseous ethylene for 0, 12, and 24 hours. Their study followed an organ-specific approach, profiling transcriptomic responses in hypocotyls and cotyledons separately. To construct our ethylene-responsive dataset, we selected the data corresponding to 24 h, which most closely matched the airborne apocarotenoid treatment duration in our own RNA-seq experiment. Since our analyses were based on whole seedlings, hypocotyl and cotyledon datasets were merged, combining DEGs regulated in both tissues. The resulting dataset comprised 6213 total DEGs.

For the apocarotenoids β-cc and β-ion, we generated *de novo* RNA-seq datasets. Prior to their integration into the comparative framework, these datasets underwent quality assessment, clustering validation, and DEG identification. The following section details these analyses and the criteria applied to define the final transcriptomic profiles of β-cc and β-ion.

4.1.2 Sampling, quality and clustering analysis of apocarotenoid RNA-seq

Plant material for β-cc and β-ion transcriptomic profiling was grown and treated as described for the shade volatilome RNA-seq analysis (section 1.3). Specifically, *A. thaliana* seedlings grown for five days under low W conditions (27 µmol m^{-2} s^{-1}, long-day photoperiod) were subsequently exposed to airborne β-cc or β-ion, using the same Petri dish system developed for previous experiments. Seedling samples were harvested at two time points following the addition of the apocarotenoid droplet containing the working concentrations (100 mM β-ion or 500 mM β-cc) to the tube cap: 8 h and 24 h after the start of the treatment. A mock-treated control, exposed only to DMSO solution, was included for each time point.

These growth conditions and treatment time-points were selected to align with the RNA-seq analysis performed for the shade-induced volatilome (section 1.3), facilitating direct comparisons. At least 3 biological replicates were collected for every sampling time and treatment combination. Total RNAs extracted from the samples were quality-checked, concentration-normalized, and submitted for sequencing (performed by BGI Genomics™).

Sequencing quality for this RNA-seq dataset was consistently high across all samples. On average, each library yielded an average of 44.89 million clean reads, providing a robust depth for transcriptome analysis (Table 4.1). Alignment efficiency to the *A. thaliana* reference genome reached 98.17%, with 96.22% of reads mapping uniquely, indicating both technical reliability and low background noise in the dataset. In addition, all samples showed a similar profile and distribution on their *Read Counts* (Fig. 4.S1), indicating uniformity across replicates.

To explore the distribution and clustering of the samples based on their transcriptomic profiles, a Principal Component Analysis (PCA) was performed (Fig. 4.1). Slight separations between some replicates among time-treatment groups (e.g., Bcc_8h_R1) were observed in the PCA. However, no technical issues were detected (e.g., library size, mapping rate), and these replicates were therefore retained in the main analysis to preserve biological variability. Using only the transcriptomic data, PC1 - which explained 34% of the total variance- clearly reflected treatment duration (e.g. diurnal-related variations), as it was observed in the first RNA-seq dataset (Fig. 1.5). Samples from 8 h clustered together, as did those from 24 h of treatment duration. This suggests that the time elapsed since the beginning of the treatment accounts for a larger proportion of the transcriptomic variance than the treatment itself at those timepoints. Consequently, treatment-specific responses may be partially masked by broader temporal dynamics, underscoring the importance of comparing treated and control samples at equivalent timepoints when analyzing DEGs. Nonetheless, the differential effects of apocarotenoid treatments appear to be better captured along the PC2 axis, which accounts for 23.9% of the total variance. While β-cc at 24 h and β-ion at 8 h do not show strong separation from their respective control groups, β-cc at 8 h (excluding the outlier sample *Bcc_8_1*) and β-ion at 24 h display a clear divergence along PC2. This pattern suggests that these treatments elicit distinct transcriptomic responses at specific time points. As discussed in Section

3.3, such differences may be partly explained by variations in apocarotenoid vaporization dynamics during the early stages of exposure (Fig. 3.S8).

Table 4.1 — Clean reads and alignment to the reference genome. In samples, first letters refer to treatment (DMSO, control; β-cc, *Bcc*; β-ion, *Bion*). Next number indicates the time of sampling and last two digits refer to the biological replicate.

Sample	Total Clean Reads (M)	Total Mapping (%)	Uniquely Mapping (%)
DMSO_ 8_R1	39.3	98.6	96.1
DMSO_ 8_R2	45.7	98.0	95.7
DMSO_ 8_R3	46.2	98.3	96.0
DMSO_ 8_R4	45.9	98.3	95.9
Bcc_8_R1	45.2	97.7	95.4
Bcc_8_R2	46.2	98.4	96.5
Bcc_8_R3	46.2	98.3	96.4
Bcc_8_R4	46.2	98.2	96.1
Bion_8_R1	46.2	98.3	96.0
Bion_8_R2	45.9	98.1	95.7
Bion_8_R3	46.1	98.1	95.9
DMSO_ 24_R1	45.8	98.3	96.6
DMSO_ 24_R2	45.5	98.0	96.3
DMSO_ 24_R3	46.1	97.5	95.7
Bcc_24_R1	45.6	97.9	96.3
Bcc_24_R2	45.8	98.1	96.5
Bcc_24_R3	31.1	98.7	97.2
Bcc_24_R4	46.2	98.4	96.6
Bion_24_R1	45.8	98.1	96.5
Bion_24_R2	46.0	98.1	96.5
Bion_24_R3	46.1	98.2	96.6
Bion_24_R4	44.7	98.4	96.6
MEANS	**44.89**	**98.17**	**96.23**

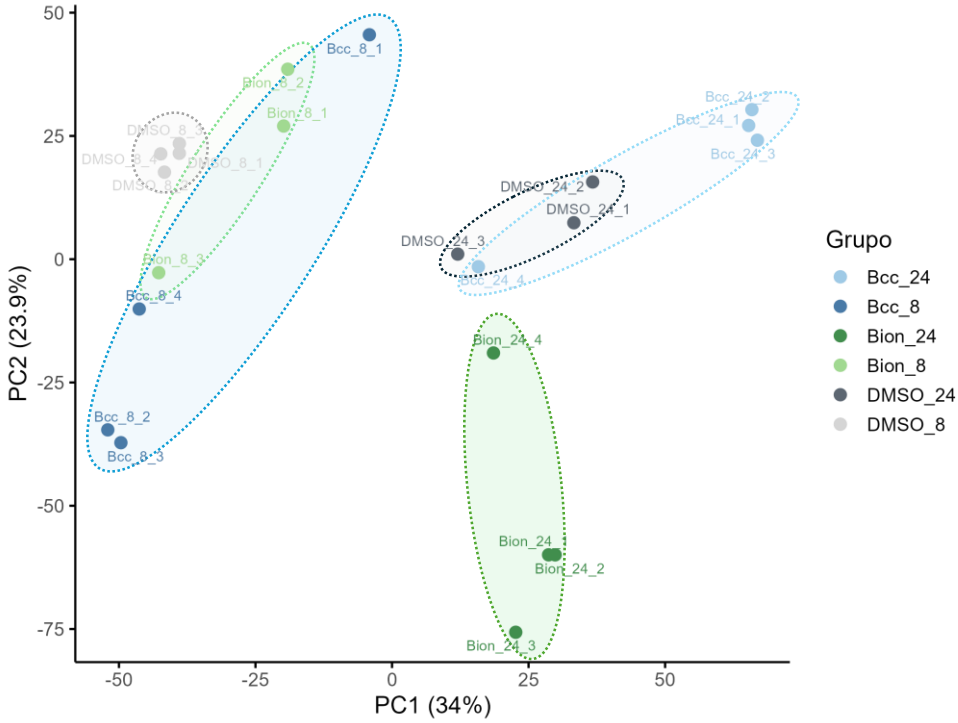

Figure 4.1 — Sample clustering based on gene expression profiles. *Principal component analysis (PCA) of RNA-seq samples from Arabidopsis seedlings exposed to DMSO (control, in grey), β-cc (Bcc, in blue) or β-ion (Bion, in green). Each symbol represents a biological replicate (R1–R4), with different shades of colors indicating sampling times (8 and 24 h). First number after the treatment refers to the time of sampling; last number refers to the biological replicate. Ellipses were manually drawn to delimit sample groups and highlight differences.*

To further evaluate the overall similarity between RNA-seq samples, a heatmap of Pearson correlation coefficients was generated using normalized expression values. The pairwise Pearson correlations were computed between all samples, and the resulting correlation matrix was visualized as a clustered heatmap (Fig 4.2). Samples were again clearly clustered according to their time of treatment (8 h vs. 24 h). Within each time point, β-cc at 8 h formed a distinct cluster, displaying greater divergence in Pearson correlation coefficients relative to both DMSO (control) and β-ion. At 24 h, β-ion also clustered separately from DMSO and β-cc, although the differences in correlation coefficients were less pronounced, and the latter two could not be clearly distinguished. Overall,

clustering patterns observed in the heatmap were generally consistent with the sample groupings revealed by PCA, reinforcing the robustness of the experimental design and the reliability of the RNA-seq data.

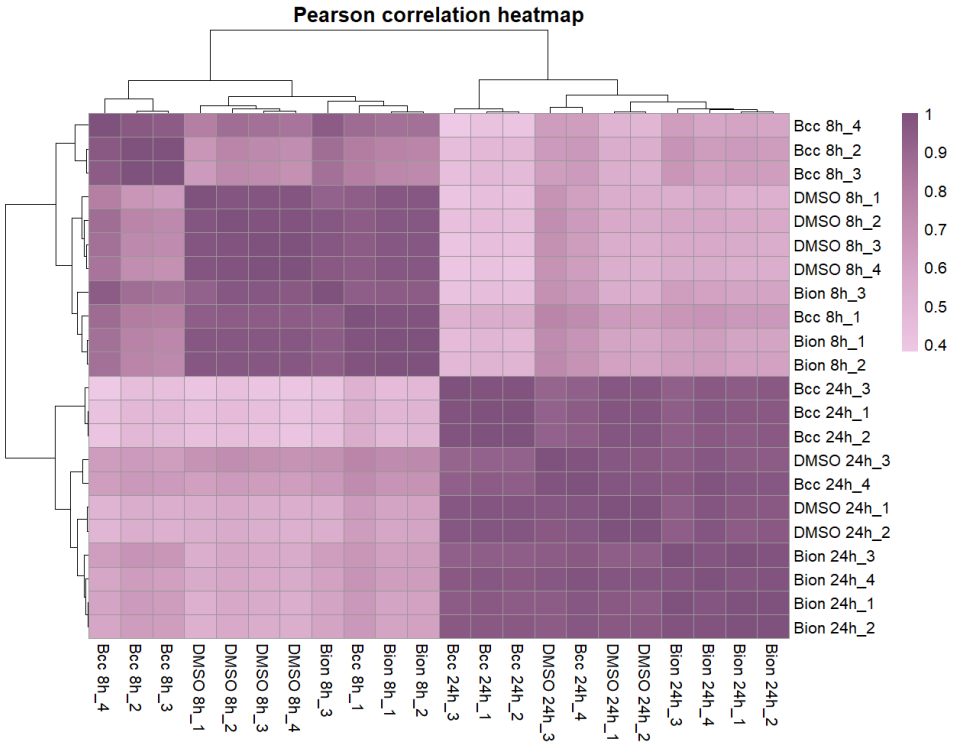

Figure 4.2 — Sample clustering based on Pearson Correlation Coefficients. *Pearson correlation heatmap of the same samples showing pairwise correlation coefficients. Pearson correlation values were calculated across the normalized expression levels of all detected genes, with values close to 1 indicating highly similar transcriptomic profiles, with darker colors indicating higher similarities between two samples.*

4.1.3 Differential expression analysis and selection of apocarotenoid-responsive datasets

The initial analysis of the RNA-seq data revealed that exposure to airborne apocarotenoids significantly alters the transcriptomic profile of *A. thaliana* seedlings. Next, we compared the sets of DEGs identified at 8 h and 24 h after treatment with β-cc or β-ion, applying a threshold of fold change ≥ 1.5 and q-value < 0.05 in DESeq2. A Venn diagram representation (Fig. 4.3-

A) showed that β-cc elicited a markedly stronger transcriptomic response at 8 h, with 2077 DEGs, in contrast to 620 DEGs detected for β-ion at the same time. Interestingly, this trend reversed at 24 h: β-ion triggered a substantially broader transcriptional response (3168 DEGs) than β-cc (747 DEGs).

When focusing on overlaps between treatments, we observed a considerable number of shared DEGs across both apocarotenoids, suggesting the existence of shared transcriptional programs. Nonetheless, most of the DEGs are not shared by both compounds, also highlighting a degree of specificity of both apocarotenoids into regulating distinct programs (Fig. 4.3-A). When focusing on the shared DEGs, the most pronounced overlap occurred between β-cc at 8 h and β-ion at 24 h, with 894 shared DEGs out of a combined total of 5245 (17.04%) (Fig. 4.3-B).

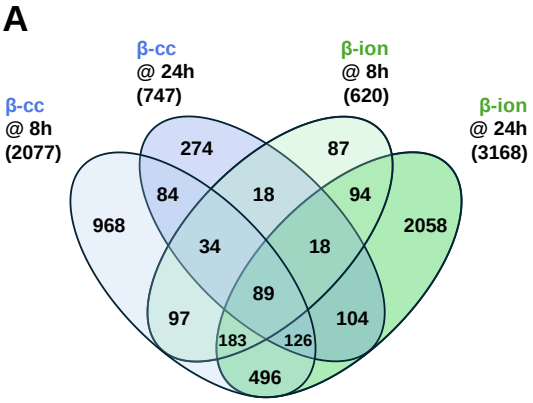

B

		β-ion	
		8h	24h
β-cc	8h	403/2697 (14.94%)	894/5245 **(17.04%)**
	24h	159/1367 (11.63%)	337/3935 (8.56%)

Figure 4.3 — Transcriptomic responses of A. thaliana seedlings to airborne β-cc and β-ion. *(A) Venn diagram representation of differentially expressed genes (DEGs) identified at 8 h and 24 h after treatment with β-cc (shades of blue) or β-ion (shades of green). (B) Table representing the overlap between β-cc and β-ion treatments datasets.*

Based on (1) this substantial overlap of the 8 h (fast) response to β-cc and 24 h (slow) response to β-ion, (2) the fact that these timepoints corresponded to the strongest transcriptional responses for each compound, and (3) the faster vaporization dynamics of β-cc than β-ion during early exposure (Fig. 3.S8), which may influence their temporal bioactivity, we selected these datasets for downstream analyses.

4.1.4 Comparative analysis of volatile-mediated transcriptomic responses supports a relevant role for apocarotenoids within the shade volatilome.

Once the ethylene-, β-cc-, and β-ion–responsive datasets had been defined, we next integrated them with the transcriptomic profile of shade-volatilome–exposed seedlings. This comparative framework aimed to determine the extent to which individual or combination of volatile treatments better reproduce the transcriptional signature of the shade volatilome. To this end, we first assessed the global overlap of DEGs across treatments, followed by a directionality-based analysis to distinguish between co-regulated and counter-regulated genes, thereby providing insights into the degree of convergence or divergence in their transcriptional outputs. A list providing information of overlapping DEGs in all treatments (29) is provided in Table 4.S1.

We first contrasted the ethylene-responsive dataset with the list of DEGs regulated by the shade-volatilome (Fig. 4.4). A significant enrichment was detected in the overlap between both conditions according to Fisher's Exact Test (Fig. 4.4-A), with ethylene alone accounting for 36.9% of the volatilome-responsive genes. This is in agreement with the conclusion that ethylene signaling contributes to the transcriptomic reprogramming triggered by shade VOCs. However, when assessing the regulatory direction of the 148 overlapping DEGs, only 41.2% were co-regulated in both treatments, while the majority were counter-regulated (Fig. 4.4-B). Thus, although ethylene likely contributes to the transcriptional output of the shade volatilome, the prevalence of opposite regulatory patterns argues against a central or major role for ethylene in this process.

GO enrichment analysis of the 148 shared DEGs revealed an overrepresentation of terms associated with stress responses, particularly hypoxia, oxygen- and oxidative stress, as well as processes linked to wounding and salicylic acid (SA) signaling (Fig. 4.4-C). Additionally, several metabolic pathways, including those related to glycosylated and glucosinolate compounds, were also significantly enriched (Fig. 4.4-C). These results parallel the functional signature observed for shade VOCs alone (Fig. 1.6), which also featured a strong enrichment in stress-related processes together with secondary metabolism.

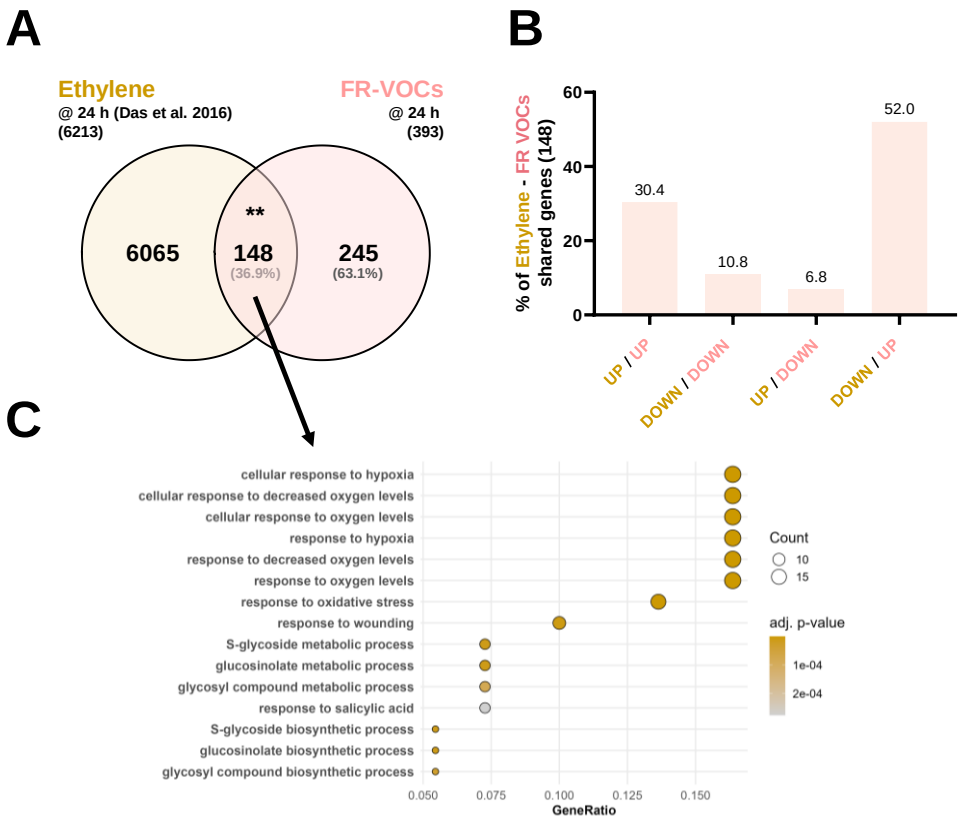

Figure 4.4 — Transcriptomic overlap between ethylene and shade volatilome treatments. *(A) Venn diagram showing the intersection between DEGs regulated by ethylene (yellow) and shade VOCs (pink). Fisher's Exact Test showed a highly significant enrichment ($p = 8.7 \times 10^{-8}$; odds ratio = 1.79, 95% CI: 1.45–2.21). (B) Directionality analysis barplot of the 148 shared DEGs. Bars show the proportion of consistently co-regulated genes (UP/UP or DOWN/DOWN) and counter-regulated genes (UP/DOWN or DOWN/UP) compared to the total volume of shared DEGs (148). (C) GO-BP enrichment dot plot of the 148 overlapping DEGs. The x-axis indicates the gene ratio (fraction of DEGs associated with each term), dot size corresponds to gene counts, and dot color represents adjusted p-values (yellow = higher significance).*

We next compared both apocarotenoid-responsive datasets with the transcriptomic profile shaped by the shade VOCs (Figs. 4.5, 4.6). Fisher's Exact Tests revealed a highly significant enrichment of DEGs induced by each apocarotenoid within the shade volatilome-responsive set. In both cases, the odds ratios (10.18 for β-cc and 4.39 for β-ion) indicated a stronger association with the volatilome response than that observed for ethylene (odds ratio of 1.79). The overlap comprised 183 genes in the case

of β-cc (Fig. 4.5-A), and 152 in β-ion (Fig. 4.6-A), accounting for the 46.6 and 38.7% of the total DEGs regulated by the shade VOCs, respectively. Interestingly, the directionally-based analysis in both sets of overlapping DEGs revealed a remarkable co-regulation of 92.9% induced by β-cc (Fig. 4.5-B), and of 80.9% by β-ion (Fig. 4.6-B). Altogether, these correlations support a relevant contribution for both apocarotenoids in modulating the overall transcriptional responses mediated by the shade volatilome.

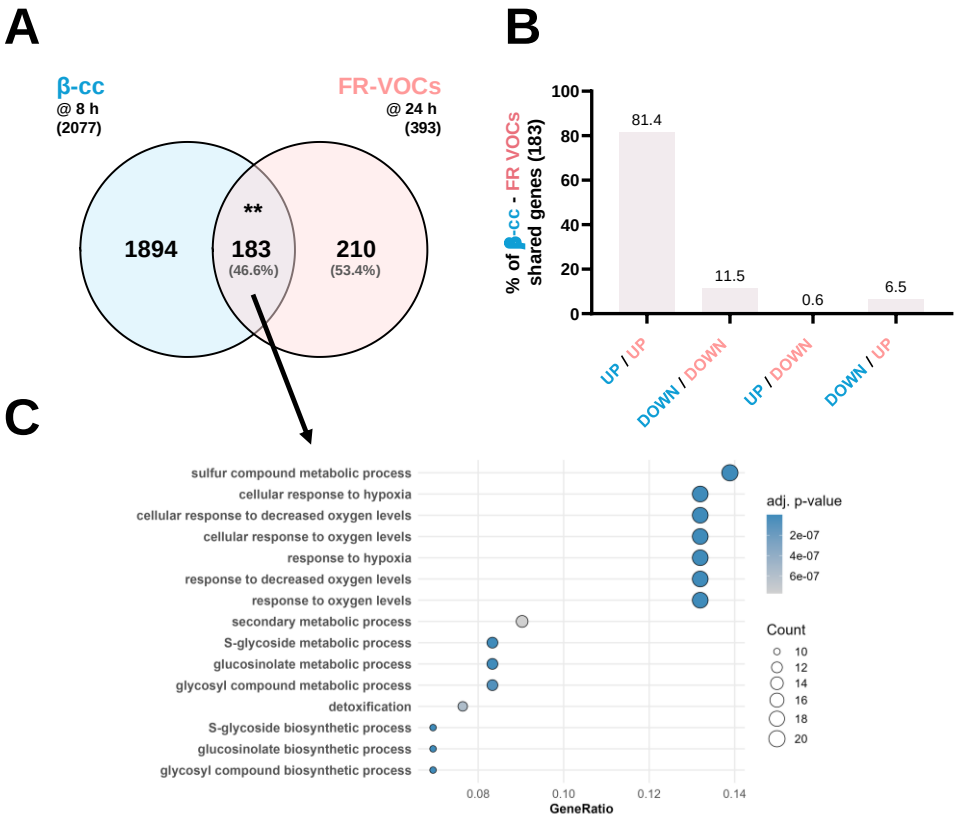

Figure 4.5 — Transcriptomic overlap between β-cc and shade volatilome treatments. *(A) Venn diagram showing the overlap between DEGs regulated by β-cc (blue) and FR-VOCs (pink). Fisher's Exact Test revealed a highly significant enrichment ($p < 2.2 \times 10^{-16}$; odds ratio = 10.18, 95% CI: 8.25–12.54). (B) Directionality analysis of the 183 shared DEGs. Bars indicate the proportion of consistently co-regulated genes (UP/UP or DOWN/DOWN) and counter-regulated genes (UP/DOWN or DOWN/UP). (C) GO-BP enrichment analysis of the 183 overlapping DEGs. The x-axis shows the gene ratio (fraction of DEGs annotated per term), dot size reflects the number of associated genes, and dot color indicates enrichment significance (blue = more significant).*

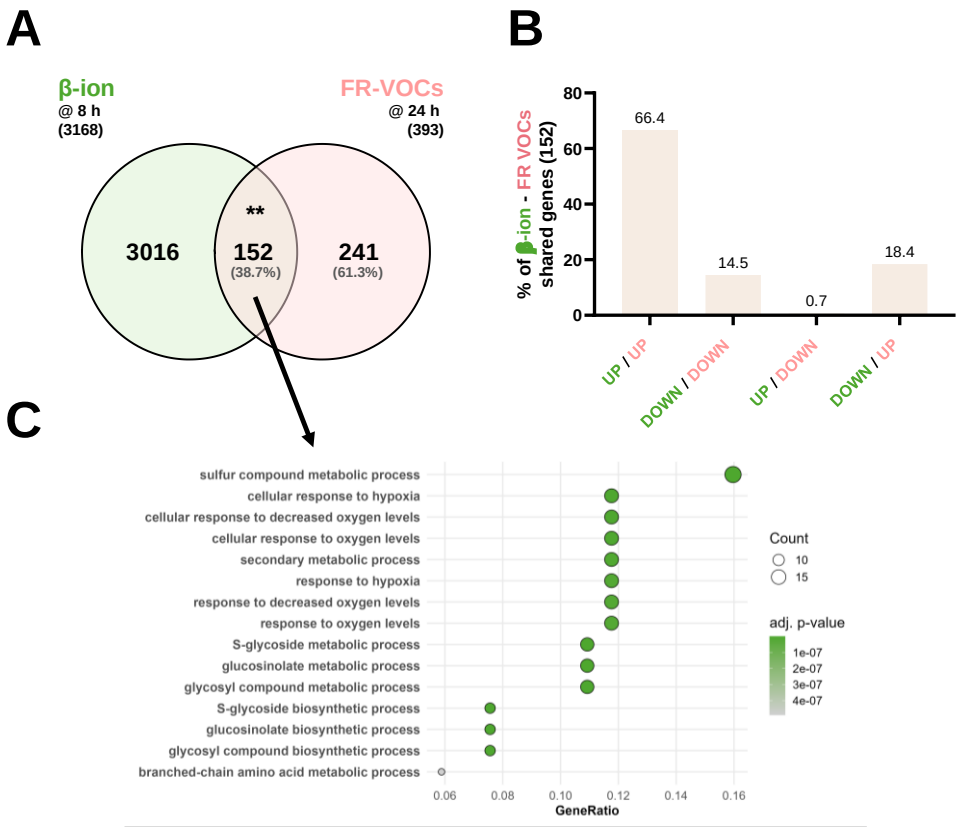

Figure 4.6 — Transcriptomic overlap between β-ion and shade volatilome treatments. *(A) Venn diagram showing the overlap between DEGs regulated by β-ion (green) and FR-VOCs (pink). Fisher's Exact Test revealed a highly significant enrichment ($p < 2.2 \times 10^{-16}$; odds ratio = 4.39, 95% CI: 3.55–5.44). (B) Directionality analysis of the 152 shared DEGs. Bars indicate the proportion of consistently co-regulated genes (UP/UP or DOWN/DOWN) and counter-regulated genes (UP/DOWN or DOWN/UP). (C) GO-BP enrichment analysis of the 152 overlapping DEGs. The x-axis shows the gene ratio (fraction of DEGs annotated per term), dot size reflects the number of associated genes, and dot color represents enrichment significance (green = more significant).*

The GO enrichment analyses of the overlapping DEGs between shade VOCs and β-cc or β-ion revealed a highly consistent functional profile (Figs. 4.5-C, 4.6-C). In both cases, enriched categories were dominated by stress-related responses, including hypoxia, oxygen and oxidative stresses, as well as processes linked to secondary metabolism, such as glucosinolate and glycoside biosynthesis. Sulfur compound metabolism also appeared as a recurrently enriched term. This strong functional convergence indicates that both apocarotenoids recapitulate the same

biological processes enriched in the shade-volatilome overlap (Fig. 1.7), supporting their contribution as key components of the volatilome signature rather than driving distinct or divergent transcriptomic outputs.

In addition to individual treatments, we also assessed combined transcriptomic responses through a directional analysis (Fig. 4.7). For each combination of treatments, the overlap included not only consistently up-regulated or consistently down-regulated DEGs, but also a subset of DEGs showing opposite (crossed) regulation (i.e., up-regulated in one treatment and down-regulated in the other).

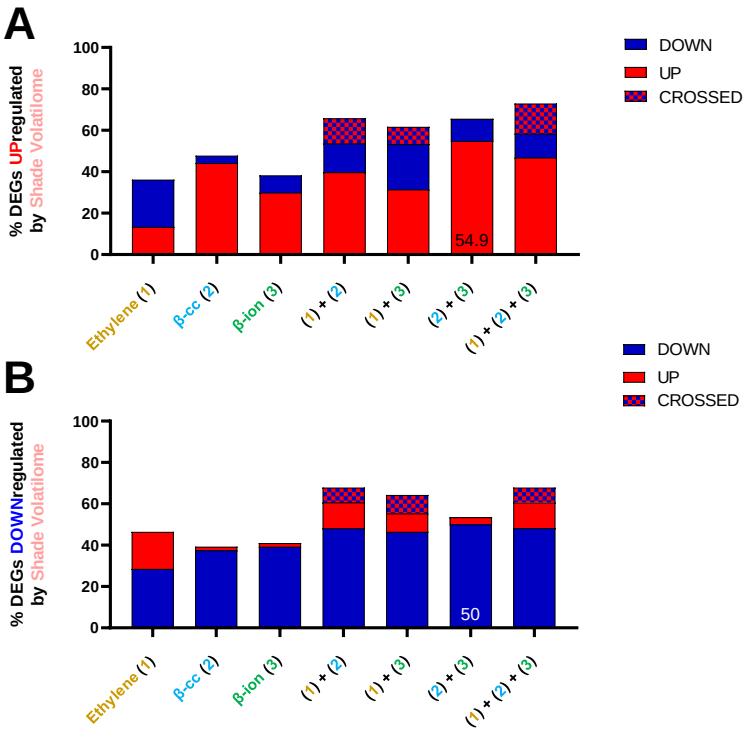

Figure 4.7 — Co-regulation analysis of shade volatilome and individual VOCs, including combinations. *Percentage of (A) up-regulated or (B) down-regulated shade volatilome DEGs covered by individual VOCs or their combinations are shown in the two panels. The X-axis represents ethylene (1, yellow), β-cc (2, blue), β-ion (3, green), and all possible combinations. For each VOC or combination, consistently up-regulated DEGs (in red), consistently down-regulated DEGs (in dark blue), and cross-regulated DEGs (UP/DOWN or DOWN/UP between treatments, in a red–blue checkered pattern) are shown in stacked bars. Percentages indicate the fraction of shade volatilome DEGs accounted for in each case. Maximum covering co-regulation percentages are shown in the corresponding bars.*

The three first bars in Fig. 4.7 plots correspond to the comparisons already described in Figs. 4.4 to 4.6. As noted, β-cc and β-ion align more closely with the directionality of shade-volatilome–induced responses, showing minimal counter-regulation of transcriptomic profiles (Fig. 4.7) This contrasts with ethylene, for which the majority of shared DEGs with the shade volatilome are oppositely regulated. When ethylene is combined with other treatments, these divergences dominate, generating substantial sets of cross-regulated DEGs and preventing a better fit with the shade-volatilome transcriptomic profile. Indeed, ethylene-containing combinations do not improve the coverage of shade-volatilome up-regulated DEGs (Fig. 4.7-A) and only modestly increase the coverage of down-regulated DEGs (Fig. 4.7-B). By contrast, the combination of β-cc and β-ion provides the highest coverage in both categories, accounting for 54.9% and 50% of shade-volatilome up- and down-regulated DEGs, respectively, with the lowest degree of counter-regulation among all combinations. Altogether, the fact that more than half of the genes responsive to the shade volatilome are co-regulated by the two apocarotenoids strongly supports their key role as central contributors to the signaling activity within the shade volatilome.

To complete the comparative analysis, we moved beyond DEGs and examined the distribution of most represented or enriched GO-BP categories across treatments (Fig. 4.8). First, we identified the ten most represented GO-BP terms within the overlap of shade-volatilome DEGs and each individual volatile treatment (Fig. 4.S2). These terms were then compared with the top-25 most represented categories in the shade-volatilome dataset (Fig. 4.8-A). In parallel, we performed the same analysis using enriched GO-BP terms: those identified in the shade volatilome were contrasted with the enriched categories obtained from the overlaps with each volatile treatment (Fig. 4.8-B). This approach provided a broader functional perspective on the extent to which ethylene, β-cc, and β-ion capture the biological responses associated with the shade volatilome.

The results indicate that the most represented GO-BP terms in the shade volatilome correlate with also the most represented categories in all individual VOC treatments (Fig. 4.8-A). Overall, top represented terms by individual VOCs concentrate in the top representative categories driven by

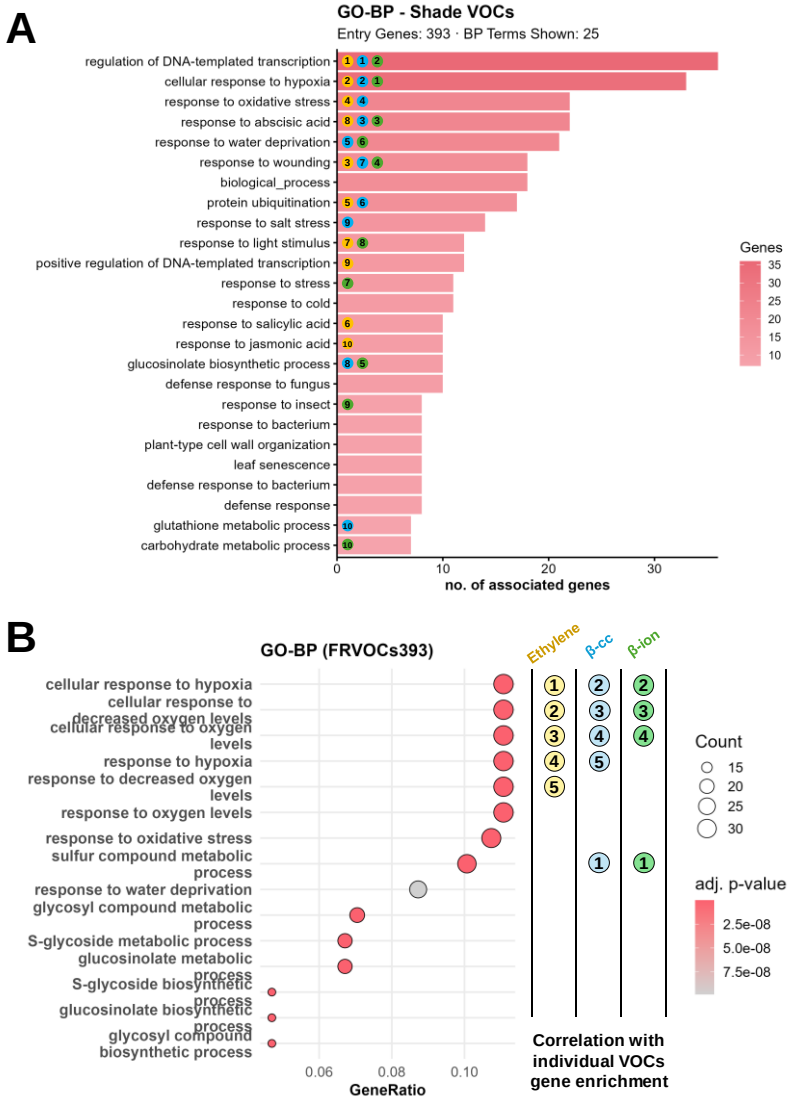

Figure 4.8 — Comparison of top GO-BP term distribution and enrichment of transcriptomic changes triggered by shade volatilome and individual VOCs, *The dataset of 393 DEGs regulated by shade VOCs is visualized according to the 25 most represented GO-BP terms (A) or the 12 most enriched GO-BP annotations (B), both listed along the Y axis. Bar length (A) or dot size (B) reflect the number of DEGs associated with each GO-BP term, whereas color intensity (pink) indicates higher significances. Circles within bars (A) or placed on the right of the dotplot (B) indicate overlap with the top ten GO-BP categories represented (A) or the top five categories enriched (B) in individual volatile treatments; numbers denote rank positions (1–10) in the corresponding distribution (A) an enrichment (B) of transcriptomic changes triggered by individual VOCs: ethylene (yellow), β-cc (blue), and β-ion (green).*

the shade volatilome (Fig. 4.8-A), and specific annotations (unique per each individual VOC treatment) also seem to be present in the 25 most represented terms by the shade volatilome. A similar scenario was observed when comparing the most enriched GO-BP accessions across treatments (Fig. 4.8-B): all individual volatiles regulating the most enriched categories, related with responses to hypoxia, whereas airborne apocarotenoids regulation also comprises sulfur-compound metabolic processes. These transcriptomic analyses further highlight the unequal contribution of the individual VOCs, β-cc and β-ion having a more relevant role than ethylene in the shade volatilome. Therefore, these VOCs appear to modulate the core of the transcriptomic response and shape the overall profile of the shade volatilome GO-BP term distribution.

4.2 Functional analysis of transcriptomic responses

We next sought to investigate the molecular mechanisms underlying the effects of β-cc and β-ion within the shade volatilome. To this end, we separated common and specific transcriptomic responses, using the same pipeline for both groups: first, through gene enrichment analysis (GO-BP and KEGG pathway terms); second, through the identification of genes belonging to the most enriched terms, and later (eventually) evaluating proteomic and metabolic data to link the apocarotenoid-mediated regulation of specific metabolic pathways with the phenotypic responses previously observed.

Additionally, we aimed at identifying potential molecular perception mechanisms of volatile apocarotenoids by screening for proteins able to bind β-ion. To do so, we collaborated with the group of Dr. Aleksandra Skirycz (MSU, USA). Using an *A. thaliana* protein extract library prepared by a colleague from our lab during a research stay, their team performed an isothermal shift assay (iTSA) with β-ion as ligand. This proteome-wide thermal profiling detects proteins whose stability is altered upon ligand binding, thereby pointing to possible modulation of activity. As a result, a list of 173 candidate physical interactors was provided (Table 4.S2). Some of these protein candidates had putative regulatory roles or were previously associated with translation, hormone signaling, or secondary metabolism (Table 4.S2). While we did not functionally validate the potential role of these candidates on β-ion signaling, the list was used as

a supporting tool to draw conclusions based on the analysis of transcriptomic changes, as indicated below.

4.2.1 Common functionalities of both apocarotenoids

We first examined the transcriptomic responses that are commonly regulated by β-ion and β-cc. Both compounds had previously been shown to exert specific and shared effects at the phenotypic level (see sections 3.2 and 3.4). To translate these phenotypic observations into molecular terms, we focused on the subsets of DEGs identified for β-cc at 8 h and for β-ion at 24 h (Fig. 4.3), the conditions in which each compound elicited its strongest transcriptomic impact. By separately crossing the sets of up-regulated and down-regulated DEGs, we were able to identify shared genes consistently co-regulated by both treatments, as well as to later disentangle specific responses unique to each apocarotenoid.

The overlap analysis revealed that even though most of the DEGs from each dataset are apocarotenoid-specific, there was a highly significant number of shared DEGs between β-cc and β-ion, both up- (424 DEGs, odds ratio = 13.05) and down-regulated (455 DEGs, odds ratio = 14.48) genes (Fig. 4.9-A). GO-BP enrichment analysis of the up-regulated overlap showed categories predominantly associated with stress-related processes, including responses to hypoxia, oxygen levels, and catabolic activities (Fig. 4.9-B). By contrast, the down-regulated overlap was enriched in processes linked to cell wall metabolism, including polysaccharide, pectin and galacturonan metabolism, as well as glucosinolate biosynthesis (Fig. 4.9-B). These results indicate that β-cc and β-ion share a substantial common transcriptomic core, also aligned with the transcriptomic response to the shade volatilome (Fig. 1.6), converging on stress-associated activation and repression of specific metabolic pathways. Additionally, KEGG pathway enrichment of the shared DEGs complemented the GO-BP results by mapping the stress-related categories onto specific metabolic routes (Fig. 4.9-C). The up-regulated overlap was linked to central primary metabolism, including carbon metabolism, glycolysis/TCA cycle, amino acid and glutathione metabolism, consistent with a metabolic reprogramming typical of stress responses. Conversely, the down-regulated overlap highlighted the repression of motor proteins, glucosinolate biosynthesis, and related processes, in line with the reduced investment in growth and specialized metabolism. These KEGG associations provided a functional bridge to

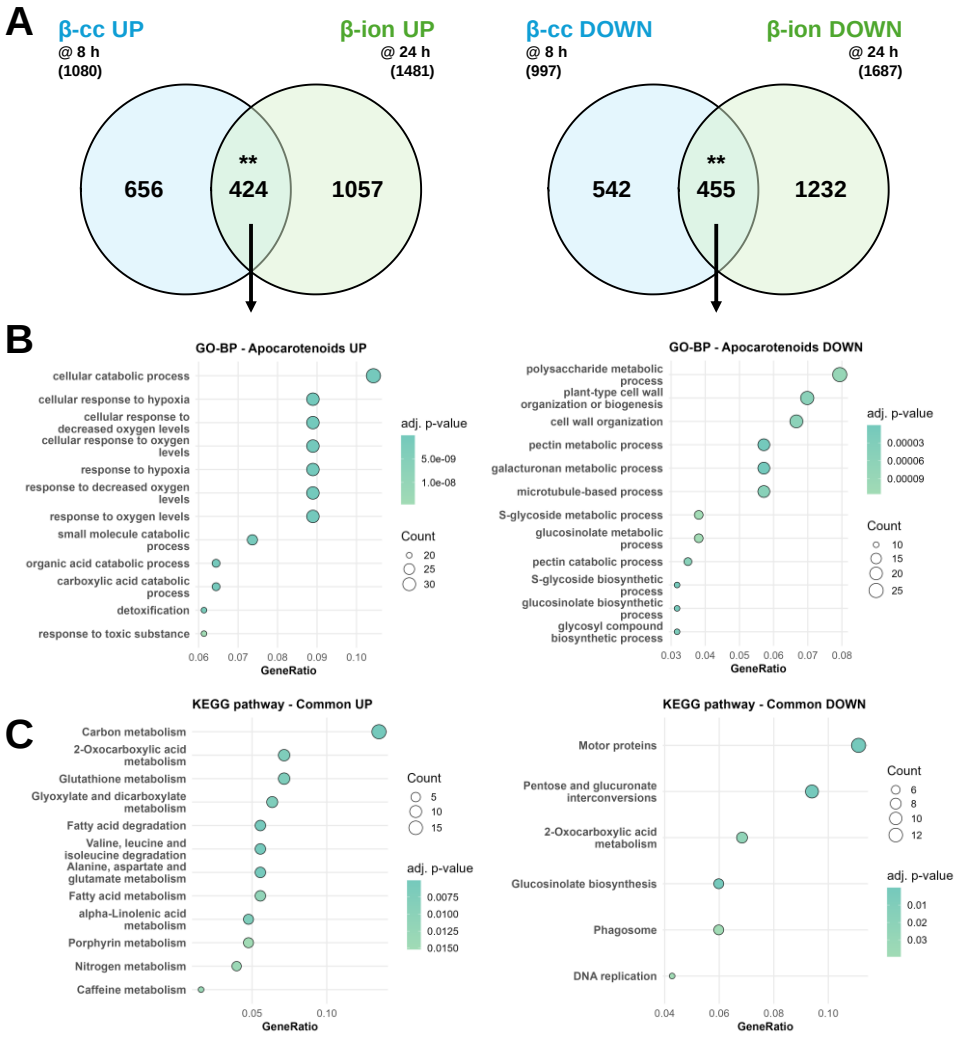

Figure 4.9 — Comparison of airborne-apocarotenoid datasets and GO-BP gene-enrichment analysis of shared up- or down-regulated DEGs. *(A) Venn diagrams showing the overlap between genes up-regulated (left) or down-regulated (right) by β-cc (blue) and β-ion (green). Fisher's Exact Tests indicated a highly significant enrichment of DEGs in both comparisons ($p < 2.2 \times 10^{-16}$ for both; odds ratio UP = 13.05, odds ratio DOWN = 14.48).(B,C) Dot plots representing GO-BP (B) or KEGG pathway (C) gene enrichment analysis of the overlapping up-regulated (left) or down-regulated (right) DEGs. The x-axis shows the gene ratio (fraction of DEGs annotated to each term), dot size reflects the number of genes per category, and dot color represents enrichment significance (turquoise = more significant).*

explore in detail the metabolic adjustments underlying apocarotenoid-driven transcriptional responses. Next, we will comment the different DEGs associated with the identified categories of GO-BP and KEGG enrichment analysis.

4.2.1.1 Carbon metabolism (UP)

Terms associated with metabolic processes of small molecules were observed both in GO-BP and KEGG enrichment analysis (Fig. 4.9): 2-oxocarboxylic acid metabolism, glyoxylate and dicarboxylate metabolism, amino-acid metabolism, etc. We deepened into the *Carbon metabolism* KEGG pathway term, where we observed upregulation of a broad set of genes encoding enzymes related to glycolysis, the TCA cycle and amino acid catabolism, including *GAPDH, SDH2-3, ACO2, ATCS, PPDK*, and *ASP3*, among others (Fig. 4.10). Altogether, these results suggest that both apocarotenoids promote a highly active primary metabolic state in seedlings, which can be interpreted as a metabolic reinforcement typically associated with stress signaling.

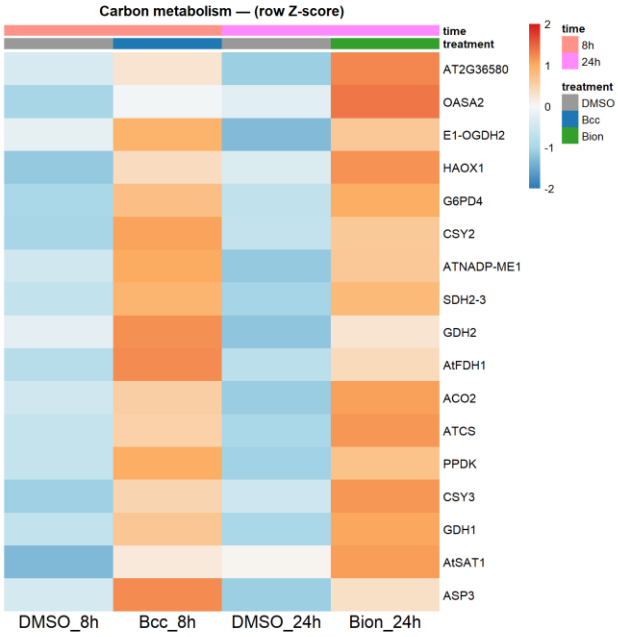

Figure 4.10 — Heatmap of DEGs associated with carbon metabolism in response to apocarotenoid treatments. *Heatmap showing the transcriptional regulation (row Z-score) of genes involved in carbon metabolism upon exposure to 8 h of β-cc or 24 h of β-ion, compared to DMSO controls. Each row represents an individual gene, whose IDs are shown on the right of each row. Colors represent relative expression values (row Z-scores), where red-orange indicates expression levels above the mean of that gene across treatments, and blue indicates expression levels below the mean.*

4.2.1.2 Responses to hypoxia (UP)

Genes annotated to the “response to hypoxia” GO-BP category showed consistent transcriptional induction upon exposure to both apocarotenoids, including well-known markers of low-oxygen adaptation such as ***ADH***, ***DIN10***, and ***ANAC102***, together with several transcription factors (***WRKY22, STOP1, ANAC002***) and signaling components (***MKK9, PERK9***) (Fig. 4.11). Additional genes encoded proteins involved in detoxification and redox homeostasis (***UGT73B3, DOGT1, BBE22***) or in metabolic adjustment (***NRP, SAP2***). Altogether, these results reveal that β-cc and β-ion trigger a broad hypoxia-like transcriptional program, integrating metabolic, regulatory, and detoxification functions to potentially activate prophylactic responses to stress.

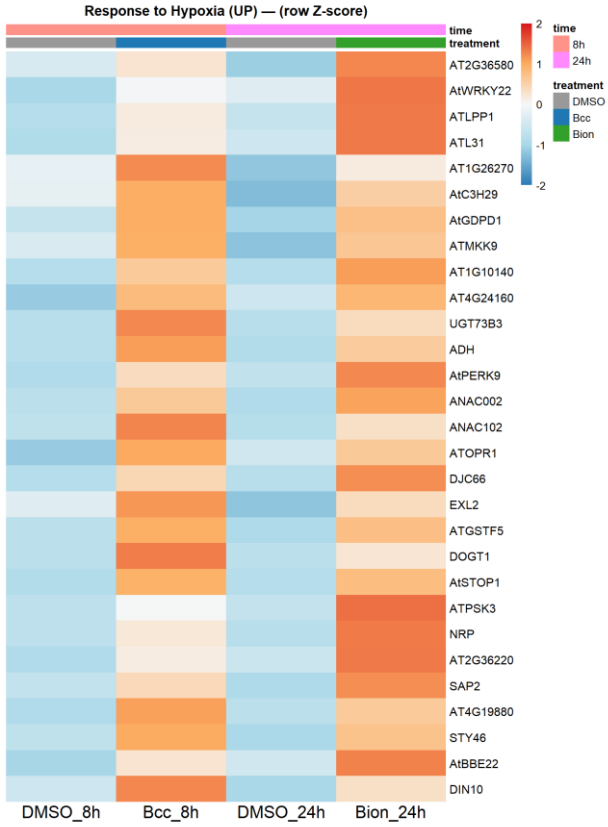

Figure 4.11 — Heatmap of DEGs associated with hypoxia responses in seedlings exposed to apocarotenoids. *Heatmap showing the transcriptional regulation (row Z-score) of genes associated with hypoxia response upon exposure to β-cc (8 h) and β-ion (24 h), compared to DMSO controls. Each row represents an individual gene, with symbols shown when available and ATG IDs otherwise. Colors indicate relative expression values (row Z-scores), where red–orange reflects expression levels above the mean of that gene across treatments, and blue reflects levels below the mean.*

4.2.1.3 Motor proteins (DOWN)

The most enriched down-regulated KEGG pathway common to both apocarotenoids was motor proteins. Genes belonging to this down-regulated group included several tubulins (*TUA*, *TUB*, *TBB*), actins (*ACT3*, *ACT11*) and a kinesin, among others (Fig. 4.12). These components are central to cytoskeletal organization and intracellular transport, processes typically linked to cell elongation and growth. Altogether, their repression suggests that apocarotenoids contribute to the attenuation of growth-related programs through these genes, a phenotype consistent with a reallocation of resources away from development and toward stress-associated responses.

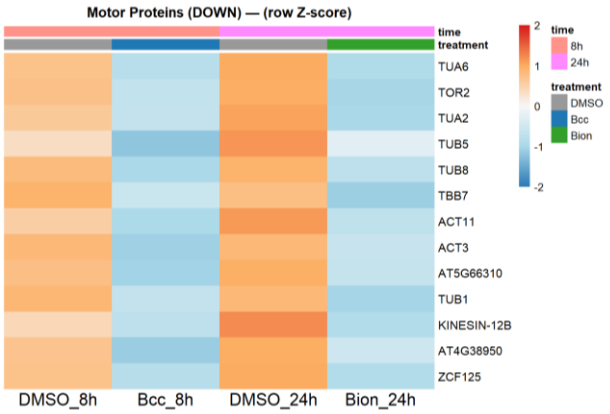

Figure 4.12 — Heatmap of DEGs associated with motor proteins in response to apocarotenoid treatments. *Heatmap showing the transcriptional regulation (row Z-score) of genes encoding motor proteins, including tubulins, actins, and kinesins, upon exposure to β-cc or β-ion compared to DMSO controls. Each row represents an individual gene, with colors indicating relative expression levels (red-orange = above the mean, blue = below the mean).*

4.2.1.4 Glucosinolate biosynthesis (UP and DOWN)

We could observe, both in GO-BP and KEGG enrichment analysis, similar terms associated with glucosinolate biosynthesis. Glucosinolates (GS) represent a branch of specialized defense metabolism, providing nitrogen/sulfur-containing defense compounds against herbivore attack (Halkier & Gershenzon, 2006). There are three main groups of GS: indolic (produced through tryptophan metabolism); aliphatic (synthetized from methionine) or aromatic (derived from phenylalanine or tyrosine). The biosynthesis of indolic and aliphatic GS is summarized in Fig. 4.13.

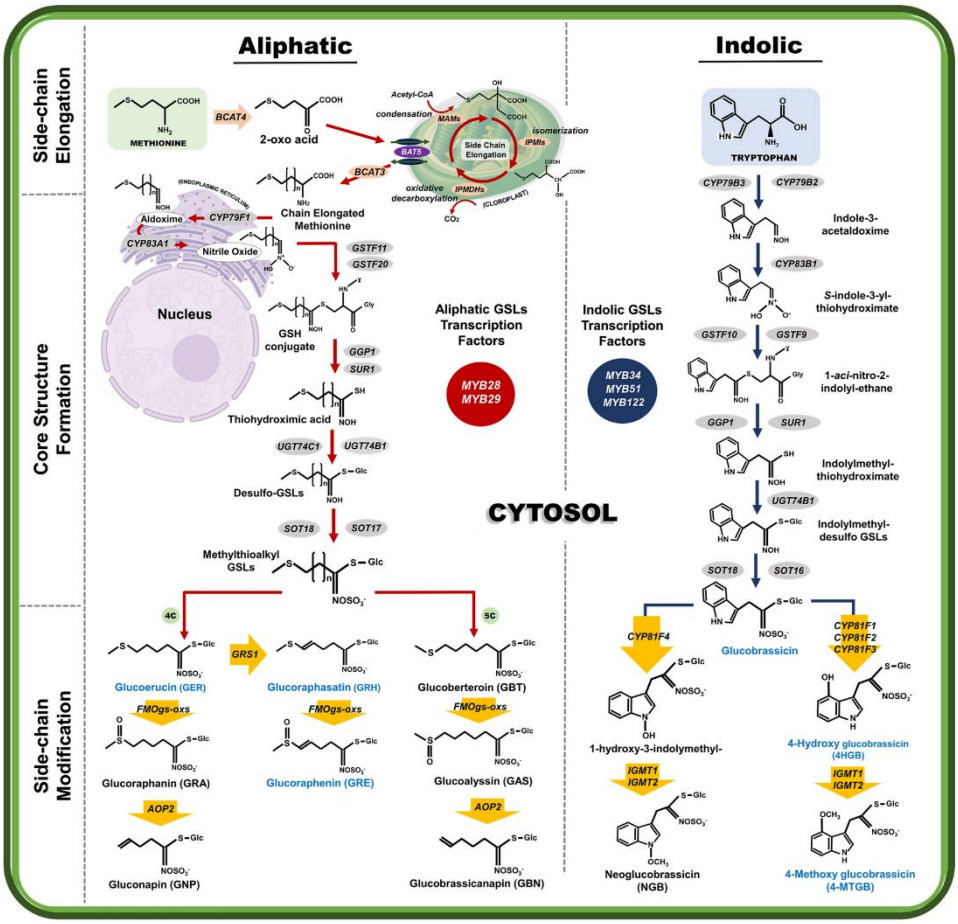

Figure 4.13 — Schematic pathways of aliphatic and indolic GS biosynthesis in Brassicaceae (Taken from Nugroho et al., 2021).

Our results show that both apocarotenoids induce an overall repression of the genes involved in the methionine chain elongation pathway (e.g. *BUS1, BCAT4, IPMI, GSM1, CYP79F2)*, connecting this amino acid with aliphatic GS production (Fig. 4.14). By contrast, genes in the indolic branch—involved in tryptophan metabolism and camalexin biosynthesis, sharing early steps with IAA biosynthesis—showed more heterogeneous responses and in most cases, particularly under β-ion, increased expression (Fig. 4.S3). Genes of the TAA1/YUC auxin biosynthetic pathway were also examined, since they also use tryptophan as the main precursor for auxin production, but no significant regulation was detected (Fig. 4.S4). The differential regulation of aliphatic and indolic GS also

applied to the main transcription factors controlling their biosynthesis (Fig. 4.S5): a general downregulation of genes promoting the biosynthesis of aliphatic GS (e.g. *MYB28, MYB76*) was accompanied by an upregulation of transcription factors controlling the indolic branch of GS (e.g. *MYB51*, *WRKY33*).

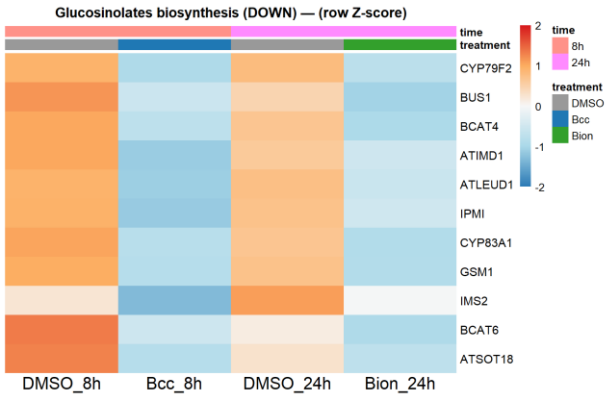

Figure 4.14 — Heatmap of DEGs associated with glucosinolate biosynthesis in response to apocarotenoid treatments. *Heatmap showing the transcriptional regulation (row Z-score) of genes involved in glucosinolate biosynthesis upon exposure to β-cc or β-ion, compared to DMSO controls. Each row corresponds to an individual gene (symbols on the right). Colors represent relative expression values (row Z-scores), with red–orange indicating expression above the mean across treatments and blue indicating expression below the mean.*

In parallel, the list of putative β-ion-binding proteins provided many potential interactors that include enzymes involved in glucosinolate biosynthesis (Table 4.S2, shown highlighted in orange). In fact, β-ion seemed to physically interact with the enzymes IGMT4, IPMI-SSU1, CYP83B1, CYP71A12, TGG1 or SOT17. These interactors span multiple steps of the aliphatic glucosinolate pathway, from core biosynthetic enzymes to those catalyzing side-chain modifications and degradation (Fig 4.13).

To determine whether such potential protein interactions and/or transcriptomic changes were accompanied by changes in metabolite accumulation, we analyzed GS content (including aliphatic, indolic and aromatic compounds) in response to β-cc or β-ion treatments. Seedling

cultivation, glucosinolate extraction and HPLC-MS measurements were conducted in the facilities of the MPI-CE in Jena, Germany, during my research stay. The experimental conditions were adjusted to the ones used growing the samples for RNA-seq, so the output of glucosinolate measurements would be comparable to the transcriptomic data described above. Seedlings of *C. hirsuta* were also included to assess potential species-specific responses to apocarotenoids within *Brassicaceae* species. Certain GS were observed to be species-specific, some of them were exclusive from *A. thaliana*, whereas others could only be detected in *C. hirsuta*. Most strikingly, no significant changes in GS content in *A. thaliana* or *C. hirsuta* were found after treatment with either apocarotenoid, regardless of the molecular species (Fig. 4.15).

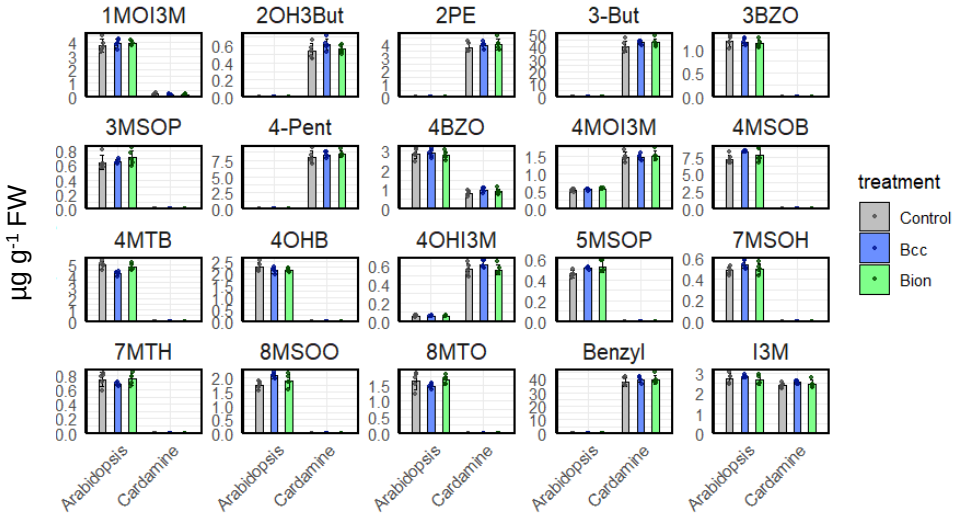

Figure 4.15 — GS content in A. thaliana and C. hirsuta seedlings upon airborne apocarotenoid treatments. *Barplots showing the content (µg g^{-1} FW) of GS molecular species quantified in seedlings of A. thaliana and C. hirsuta exposed to β-cc (blue), β-ion (green), or DMSO (Control, grey). Panels correspond to different GS species, identified by side-chain structure and biosynthetic origin, including indolic GS (e.g., I3M, 1MOI3M, 4MOI3M), aliphatic GS (e.g., 3MSOP, 4MSOB, 7MSOH, 8MSOO, 8MTO), aromatic GS (e.g., 4BZO, 3BZO, Benzyl), and derivatives. No significant differences were detected among treatments (two-way ANOVA) in either species.*

To confirm that the *A. thaliana* new set of seedlings used for GS measurements underwent the same transcriptomic events, RNA was extracted from seedlings and qPCRs were performed exploring the expression of three of the most strongly repressed glucosinolate biosynthetic genes identified previously: *CYP79F2, CYP83A1* and *GSM1*. Although statistical significance was not reached in all cases, the results reproduced the same trend of repression observed in the RNA-seq set, supporting the transcriptomic evidence for downregulation of the aliphatic GS pathway in response to airborne β-cc or β-ion treatment (Fig. 4.S6).

As a summary, both β-cc and β-ion induce the expression of genes involved in primary metabolism and hypoxia-like stress responses, while concurrently repressing genes for growth-associated motor proteins and GS biosynthesis, outlining a coordinated shift toward a stress-adapted transcriptional state. However, the observed changes in gene expression do not parallel changes in metabolite levels, at least in the case of GS metabolites.

4.2.2 Specific responses to apocarotenoids

We next analyzed the specific responses to β-cc or β-ion by assessing individual responses separately (Fig. 4.9). β-cc induced the expression of 656 specific genes and repressed the transcription of other 542 DEGs. On the other hand, β-ion specifically up- and down-regulated 1057 and 1232 DEGs, respectively. All these 4 datasets were subjected to the same GO-BP and KEGG pathway gene enrichment analysis performed in the previous section.

Beyond the shared transcriptional programs, β-cc and β-ion each displayed distinct sets of specifically regulated genes that point to divergent physiological trajectories (Figs. 4.16, 4.17). β-cc-specific effects appear to reinforce the shared core of transcriptomic responses driven by both apocarotenoids, consolidating the common up-regulated categories related to abiotic stress management, such as hypoxia and catabolism, while also concomitantly repressing metabolic pathways associated with jasmonate- and glucosinolate-mediated defense (Fig. 4.16-A). By contrast, β-ion specifically triggered a strong transcriptional activation of immune- and defense-related processes, including defense response to bacterium and symbiont, innate and adaptive immune system processes,

and regulation of defense responses, together with hypoxia/oxygen-associated categories. In contrast, a pronounced repression of growth-associated categories, notably those linked to the cell cycle and cytoskeleton organization, along with water and fluid transport (Fig. 4.17-A). Altogether, these contrasting specific responses highlight that, although both apocarotenoids converge on a common transcriptional core, their individual contributions diverge towards distinct physiological outputs, thereby expanding the functional versatility of the apocarotenoid-associated signaling.

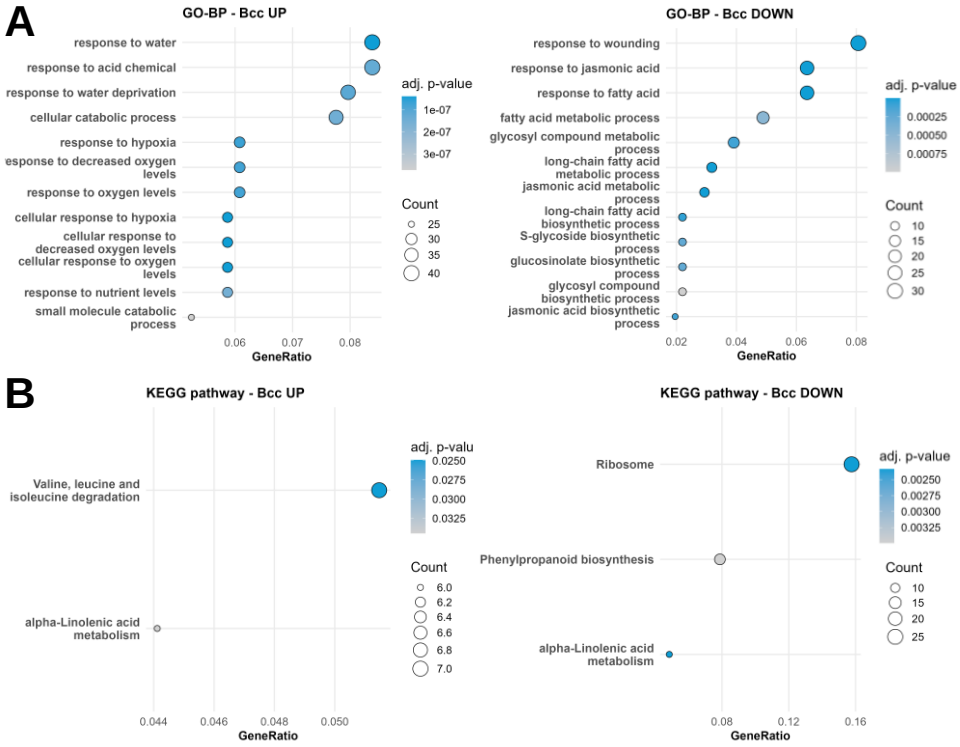

Figure 4.16 — GO-BP and KEGG pathway enrichment of β-cc-specific DEGs. *Dot plots showing the 12 most significantly enriched GO-BP (A) or KEGG pathway (B) categories among the genes specifically regulated by 8 h of β-cc treatment. The x-axis represents the gene ratio (fraction of DEGs annotated to each term), dot size indicates the number of associated genes, and dot color corresponds to the adjusted p-value (blue = higher significance).*

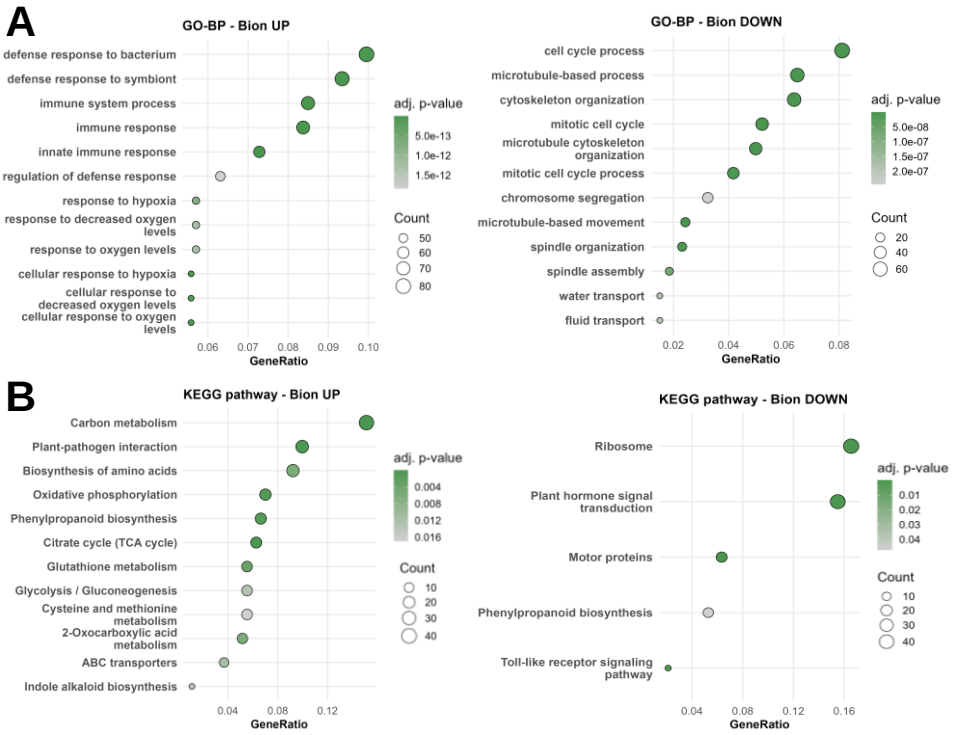

Figure 4.17 — GO-BP and KEGG pathway enrichment of β-ion-specific DEGs. *Dot plots showing the 12 most significantly enriched GO-BP (A) or KEGG pathway (B) categories among the genes specifically regulated by 24 h of β-ion treatment. The x-axis represents the gene ratio (fraction of DEGs annotated to each term), dot size indicates the number of associated genes, and dot color corresponds to the adjusted p-value (green = higher significance).*

To complement the GO-BP enrichment analysis and refine the interpretation of apocarotenoid-specific responses, we further examined KEGG pathway enrichment in the sets of uniquely regulated DEGs (Figs. 4.16, 4.17). This approach allows us to connect the broader biological categories described above with specific metabolic and signaling pathways underlying the contrasting effects of β-cc and β-ion. The KEGG pathway enrichment analysis for β-cc-specific DEGs did not seem to generate a wide range of specific categories (Fig. 4.16-B). In contrast, β-ion-specific enrichment pointed towards a diverse reinforcement of immune and defense signaling, together with the downregulation of core growth-related processes such as ribosome biogenesis or hormone signaling (Fig. 4.17-B). Altogether, KEGG enrichment highlights how the

distinct transcriptional trajectories observed at the GO-BP level are underpinned by the regulation of specific molecular pathways, providing a mechanistic basis for the divergent outputs of each apocarotenoid. Key enriched KEGG pathway terms are further analyzed in the next subsections.

4.2.2.1 Ribosomal proteins biosynthesis (DOWN, β-cc and β-ion)

KEGG pathway 'Ribosome' appeared as down-regulated both in β-cc and β-ion specific gene enrichment analysis. Analysis of ribosome-related transcriptional responses revealed a broad downregulation of genes encoding both 40S and 60S ribosomal subunits upon airborne apocarotenoid treatment (Fig. 4.18).

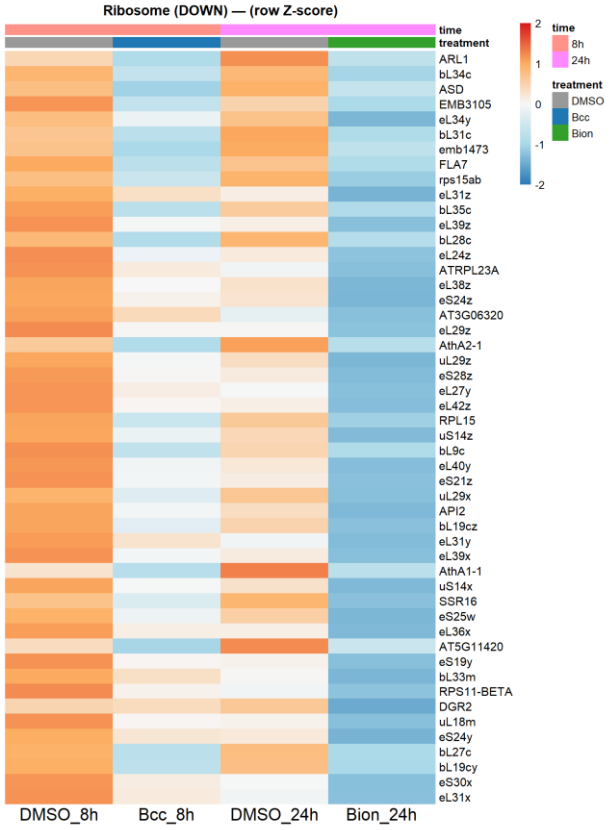

Figure 4.18 — Heatmap of DEGs associated with the KEGG pathway Ribosome in response to apocarotenoid treatments. *Heatmap showing the transcriptional regulation (row Z-score) of genes encoding ribosomal proteins upon exposure to β-cc (8 h) or β-ion (24 h), compared to DMSO controls. Each row represents an individual gene, with gene symbols indicated on the right. Colors represent relative expression values (row Z-scores), where red-orange indicates expression levels above the mean of that gene across treatments, and blue indicates expression levels below the mean. A marked repression of ribosomal protein genes is observed under both apocarotenoid treatments.*

Interestingly, the iTSA results identified several ribosomal proteins as putative β-ion-binding targets (Table 4.S2, highlighted in purple). This group of candidates (in terms of function and protein-type) was the most represented among the potential β-ion interactors, suggesting a possible dual mode of action. The convergence of transcriptomic repression and candidate β-ion protein interactors points to a coordinated modulation of the translational machinery, although the functional link between both layers remains to be established.

4.2.2.2 Phenylpropanoid biosynthesis and Indolic alkaloid biosynthesis (UP, β-ion // DOWN, β-cc and β-ion)

Phenylpropanoid biosynthesis KEGG pathway accession appeared as up-regulated in the case of β-ion and down-regulated in both airborne apocarotenoids specific gene enrichment analysis (Figs. 4.16-B, 4.17-B). This pathway was particularly relevant as it linked to several outputs of our dataset: phenylpropanoids serve as precursors for lignin and flavonoids, two important components of the plant cell wall (a GO-BP category down-regulated by both apocarotenoids; Fig. 4.9-B) with well-described defensive roles. Moreover, the biosynthesis of phenylpropanoids is known to be tightly regulated by precursors from GS biosynthesis (Kim *et al.*, 2015; Shin *et al.*, 2023), a family consistently found among the down-regulated GO-BP/KEGG terms (Fig. 4.9-B, C). Notably, key enzymes in this pathway, including PAL1 and CAD1, also emerged as candidate β-ion interactors in the iTSA dataset (Table 4.S2), raising the possibility that their activity could be directly modulated by apocarotenoid binding.

The phenylpropanoid biosynthesis pathway showed both up- and down-regulated subsets of genes in response to the apocarotenoids (Fig. 4.19). β-ion treatment was associated with the induction of several peroxidases (e.g., *PRX62, PRX52*), laccases (e.g., *LAC4, LAC17*), and BBE-like oxidases (Fig. 4.19-A), while other enzymes of the pathway, including additional peroxidases and ATP-binding proteins, appeared repressed by both compounds (Fig. 4.19-B). In addition, β-ion induces indolic alkaloid biosynthesis (Fig. 4.17-B), which serve as intermediates for indolic GS biosynthesis. These compounds deriving from tryptophan (addressed in Fig. 4.S3) repress phenylpropanoid biosynthesis (Kim *et al.*, 2015), connecting both terms regulated by β-ion. Furthermore, β-ion induces the expression of several Kelch F-Box proteins (Fig. 4.S7), which act as

negative repressors of this pathway by promoting the degradation of phenylalanine ammonia lyases (PALs), rate-limiting enzymes of the pathway (Kim *et al.*, 2020). Altogether, these results indicate that apocarotenoids, and particularly β-ion, modulate different outputs of the phenylpropanoid biosynthetic pathway through selective activation and repression of distinct gene subsets, potentially through the accumulation of GS intermediates.

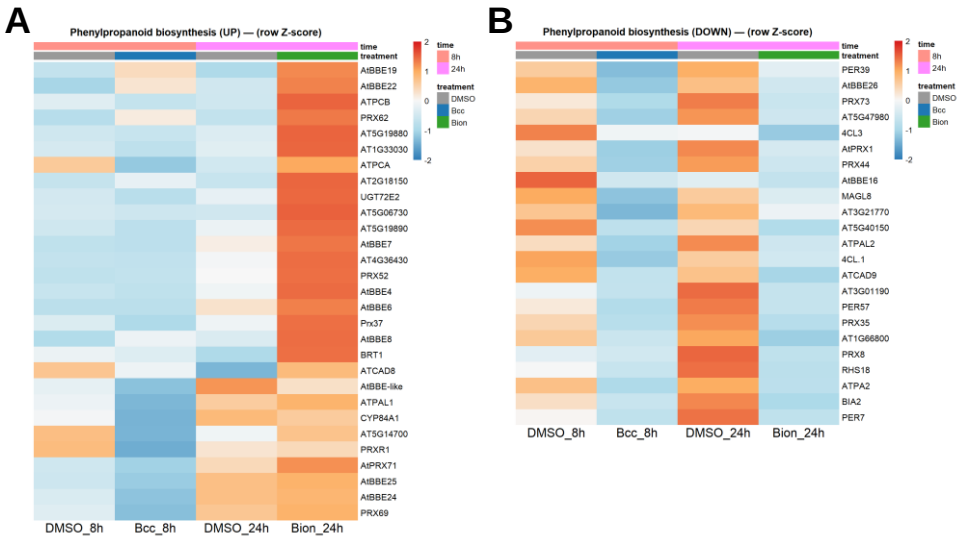

Figure 4.19 — Heatmaps of DEGs associated with phenylpropanoid biosynthesis in response to apocarotenoid treatments. *Heatmaps showing transcriptional regulation (row Z-score) of genes belonging to the phenylpropanoid biosynthesis KEGG pathway upon exposure to β-cc (8 h) or β-ion (24 h), compared to DMSO controls. Each row corresponds to a single gene, with IDs indicated on the right. Color scale represents relative expression values (row Z-scores), where red-orange indicates expression above the mean and blue indicates expression below the mean across treatments. Genes are separated into up-regulated (A, left) and down-regulated (B, right) subsets.*

4.2.2.3 Oxidative phosphorylation and photosynthesis (UP, β-ion)

KEGG enrichment analysis revealed the specific enrichment of the oxidative phosphorylation (OXPHOS) pathway in the β-ion dataset (Fig. 4.17-B). This pathway, central to mitochondrial energy metabolism, comprises components of the electron transport chain and ATP synthase, ensuring ATP production during respiration. The specific enrichment suggests that β-ion (and apparently also β-cc, although not as enriched as

in the case of β-ion) may stimulate respiratory capacity as part of a broader adjustment of cellular energy homeostasis. To explore this response in more detail, we examined the transcriptional regulation of the genes associated with this pathway.

The OXPHOS-related heatmap confirmed a broad transcriptional upregulation of genes encoding mitochondrial electron transport chain components and ATP synthase subunits by both apocarotenoids (Fig. 4.20), suggesting a reinforcement of mitochondrial ATP-generating capacity. Interestingly, β-ion also induced a discrete but consistent upregulation of photosynthesis-related genes, including subunits of photosystem I and ATP synthase (Fig. 4.S8), in agreement with the enhancement in photosynthetic performance observed by β-ion (Fig. 3.8). While this regulation does not extend to the entire photosynthetic apparatus, it points to a coordinated reinforcement of energy-related processes in both mitochondria and chloroplasts. Taken together, these results suggest that β-ion promotes a global bioenergetic boost by enhancing respiratory and photosynthetic capacity, a response that may serve to sustain metabolism under stress while supporting defense-associated transcriptional programs.

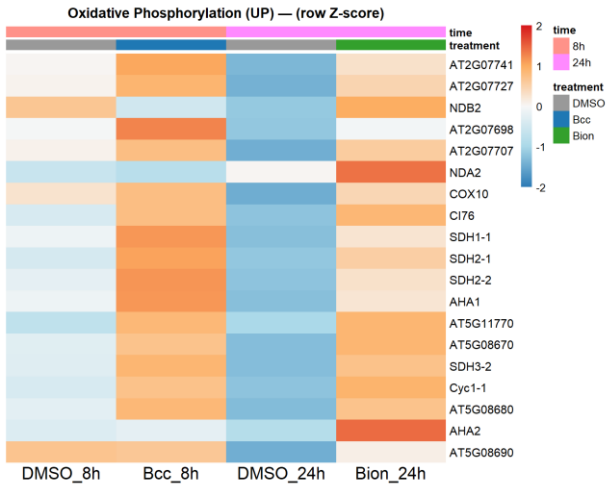

Figure 4.20 — Heatmap of DEGs associated with oxidative phosphorylation in response to apocarotenoid treatments. *Heatmap showing the transcriptional regulation (row Z-score) of genes related to oxidative phosphorylation upon exposure to β-cc (8 h) or β-ion (24 h), compared to DMSO controls. Each row represents an individual gene. Colors represent relative expression values (row Z-scores), where red-orange indicates expression levels above the mean of that gene across treatments, and blue indicates expression levels below the mean.*

4.2.2.4 Plant defense: MAPK pathway and Salicylic Acid (SA) signaling (UP, β-ion)

Among the KEGG pathways specifically enriched in β-ion–regulated DEGs, *plant–pathogen interaction* emerged as a particularly relevant category, which came together with GO-BP terms also enriched as *defense response to bacterium / symbiont, immune response* or *regulation of defense response.* The KEGG pathway integrates perception mechanisms (e.g. pattern-recognition receptors), downstream signaling cascades such as MAPK activation, and hormonal responses involving SA, all of which converge in the orchestration of plant immunity. The enrichment of this term in β-ion–treated seedlings indicates that this apocarotenoid promotes the transcriptional activation of defense-related modules typically associated with pathogen recognition and signaling.

The plant–pathogen interaction KEGG category showed a clear induction of a broad set of genes specifically in response to β-ion (Fig. 4.21). This included receptors such as EFR and several WAKs, calcium-binding proteins (CMLs), and a wide array of WRKY transcription factors, all of which are commonly associated with early defense perception and transcriptional reprogramming during immune responses. The coordinated upregulation of these elements suggests that β-ion enhances defense-related signaling capacity, potentially linking this activation to downstream MAPK signaling cascades and SA-dependent pathways that are central to plant immunity.

In fact, a large set of genes involved in downstream signaling cascades was specifically up-regulated by β-ion (Fig. 4.22). Within the MAPK pathway signaling set, we observed the induction of multiple WRKY transcription factors, receptor-like kinases, and cytochrome P450 genes, which are key regulators of defense-related transcriptional reprogramming (Fig. 4.22-A). In parallel, genes associated with SA signaling, including central regulators such as *NPR1/3/4*, *SARD1*, and the pathogenesis-related protein *PR-5*, also showed enhanced expression under β-ion (Fig. 4.22-B). Together, these results indicate that β-ion not only activates general pathogen perception modules but also reinforces core immune signaling through MAPK- and SA-dependent routes and suggests that this apocarotenoid promotes a defense state reminiscent of systemic acquired resistance.

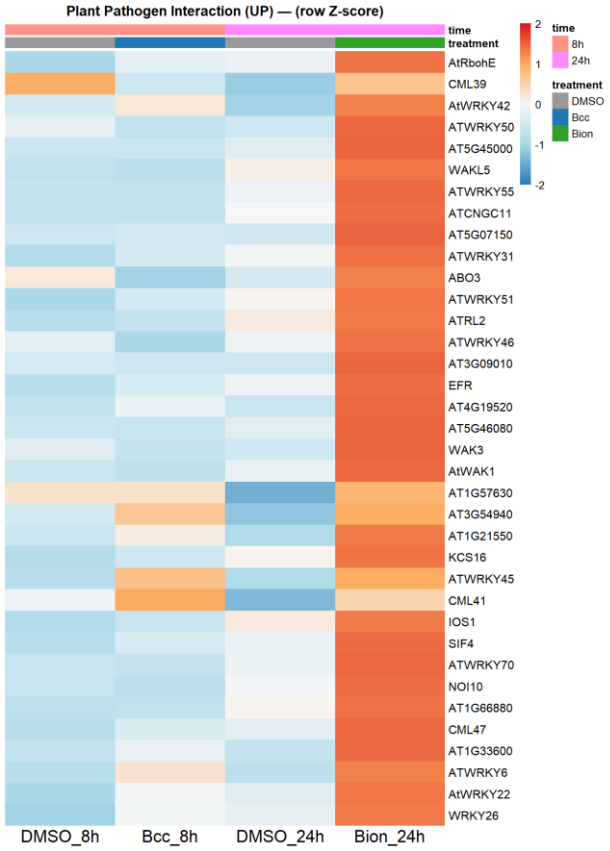

Figure 4.21 — Heatmap of DEGs associated with the plant–pathogen interaction KEGG pathway in response to apocarotenoid treatments. *Heatmap showing the transcriptional regulation (row Z-score) of genes associated with the plant–pathogen interaction pathway in Arabidopsis seedlings exposed to β-ion or β-cc compared to DMSO controls at 24 h and 8 h, respectively. Each row represents an individual gene, with IDs or gene symbols indicated on the right. Colors represent relative expression values (row Z-scores), where red-orange indicates expression levels above the mean of that gene across treatments, and blue indicates expression levels below the mean.*

To test that hypothesis, we expanded our transcriptomic analysis to include SA biosynthetic, glycosylation and signaling genes. Transcriptomic data revealed that β-ion strongly up-regulated the SA biosynthetic pathway derived via isochorismate synthases (ICS1, ICS2) (Fig. 4.23-A), in clear contrast to the phenylpropanoid-derived pathway via PAL (Fig. 4.23-B), which showed no consistent induction. This transcriptomic activation also applied to SA-glycosylation enzymes, (Fig. 4.S6), indicating a broad impact of β-ion on SA metabolism.

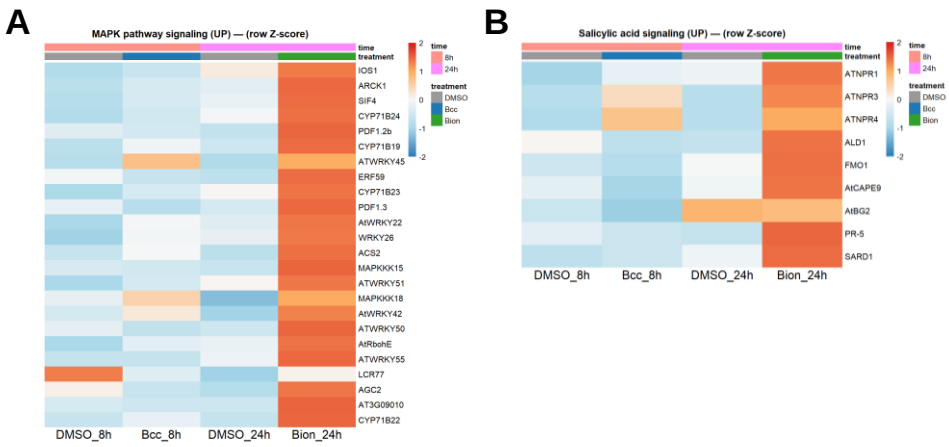

Figure 4.22 — Heatmaps of DEGs associated with MAPK pathway signaling (A) and SA signaling (B) in response to apocarotenoid treatments *Heatmaps showing the transcriptional regulation (row Z-score) of genes associated with MAPK signaling (A, left) and SA signaling (B, right) in response to β-cc (8 h) and β-ion (24 h) treatments compared to their respective DMSO controls. Each row represents an individual gene, with color gradients indicating relative expression (red-orange = above mean expression; blue = below mean expression).*

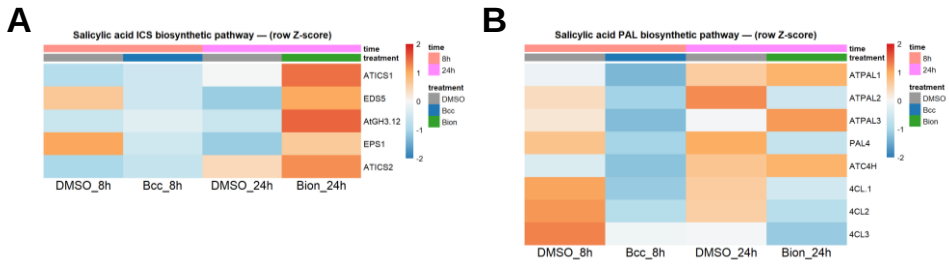

Figure 4.23 — Heatmaps of DEGs associated with SA biosynthetic pathways in response to apocarotenoid treatments. *Transcriptional regulation (row Z-score) of genes belonging to the isochorismate (ICS) (left) and phenylalanine ammonia-lyase (PAL) (right) pathways of SA biosynthesis in seedlings treated with β-cc (8 h) or β-ion (24 h) compared to DMSO controls. Each row represents an individual gene, with higher or lower expression relative to the mean across treatments indicated by red-orange or blue, respectively.*

We next measured SA content together with other phytohormones such as JA or ABA, also involved in other regulated processes related to defense and also water deprivation (Figs. 4.16, 4.17). This analysis was extended to *Cardamine* hirsuta to enable comparisons across *Brassicaceae* species. In agreement with our transcriptomic analyses in *A. thaliana*, we

observed that β-ion treatment increased SA levels both in its free and glycosylated (SA-Glu137) forms (Fig. 4.24). ABA levels were also elevated by β-ion, whereas JA levels remained unchanged in any of its analyzed forms (Fig. 4.24). Although basal levels differed in *C. hirsuta*, a similar impact of β-ion was observed in *C. hirsuta* (Fig. 4.24).

Altogether, the data indicate that β-ion triggers a robust defense-oriented transcriptional program in *A. thaliana*, with activation of MAPK and SA signaling, and a marked accumulation of SA itself. By contrast, β-cc did not strongly impact these pathways, underscoring that only β-ion promotes this defense-specific hormonal output. These findings highlight a functional divergence between both apocarotenoids, where β-ion emerges as a potent inducer of SA-mediated immunity.

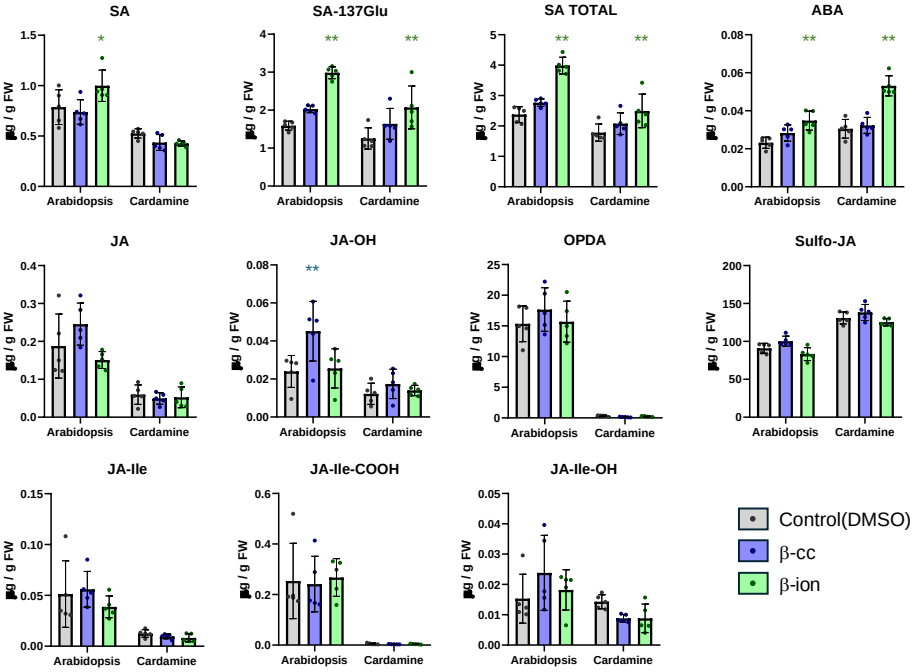

Figure 4.24 — SA, ABA and JA content in A. thaliana and C. hirsuta seedlings exposed to airborne apocarotenoid treatments. *Hormone quantification showing the content (µg g^{-1} FW) of SA, abscisic acid (ABA), and jasmonic acid (JA) and derivatives in A. thaliana (left) or C. hirsuta (right) seedlings treated with β-cc (in blue), β-ion (in green) or DMSO (Control, in grey). Statistical analysis was assessed with a two-way ANOVA followed by a Dunnett's multiple comparisons test. Asterisks indicate significant differences compared to DMSO (**p<0.01, *p<0.05).*

4.2.2.5 Plant hormone signal transduction – SAUR Genes (DOWN, β-ion)

Lastly, among the KEGG pathways specifically enriched in β-ion–regulated DEGs, *plant hormone signal transduction* emerged as a key down-regulated category. This pathway encompasses the transcriptional outputs of major plant hormones, including auxin, cytokinin, gibberellin or abscisic acid, which collectively coordinate developmental processes and growth. The repression of this term in β-ion–treated seedlings points to a broad attenuation of hormone-dependent signaling modules, particularly auxin-related responses, suggesting a potential shift away from growth promotion under apocarotenoid exposure.

Analysis of the KEGG category plant hormone signal transduction revealed a consistent downregulation of multiple genes upon β-ion treatment (Fig. 4.25). Most of these correspond to the SAUR family, well-known auxin-responsive transcripts, together with other members of the auxin signaling network such as IAA3 and IAA6. The repression was particularly evident in seedlings exposed to β-ion at 24 h, while 8 h of β-cc showed slight downregulation as well. This widespread suppression of auxin-associated transcripts points to a negative regulation of auxin signaling outputs, suggesting that β-ion may contribute more specifically to redirecting transcriptional programs away from growth promotion and toward defense-related priorities.

The fact that *SAUR* expression is governed by the interaction of many phytohormones contexts (Ren & Gray, 2015) raised the possibility that the observed repression pattern in β-ion–treated seedlings could result from broader hormonal cross-talk, rather than from a simple auxin-specific effect. To test whether auxin activity is suppressed by the presence of β-ion, we used a DR5:GUS reporter line as a readout of auxin-responsive promoter activity.

Five-day-old DR5:GUS seedlings grown under W conditions were either left in the original plates or transferred to growth media containing Picloram (PIC, an auxin analogue) or epibrassinolide (EBL, a synthetic brassinosteroid). Transfer controls were also included, consisting of seedlings moved to fresh medium without any added compounds. Following transfer, plates were maintained under W for 24 h and exposed to airborne β-ion or DMSO (control). In addition, seedlings that remained in their original plates were either kept under W or were transferred to low

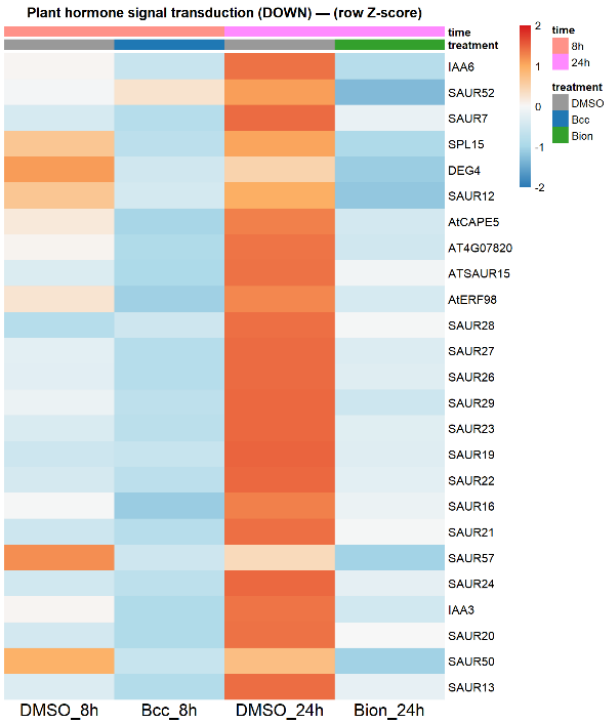

Figure 4.25 — Heatmap of DEGs associated with plant hormone signal transduction in response to apocarotenoid treatments. *Heatmap showing the transcriptional regulation (row Z-score) of genes associated with the KEGG pathway "Plant hormone signal transduction" after exposure to β-cc or β-ion, compared to DMSO controls. Each row represents an individual gene, with IDs and gene names indicated on the right. Colors represent relative expression values (row Z-scores), where red-orange indicates expression levels above the mean of that gene across treatments, and blue indicates expression levels below the mean.*

W or W+FR for the same 24 h period, during which they were also subjected to β-ion or control treatments. Samples were collected at prior to treatment/transfer (0 h), 8 h, and 24 h for all light, pharmacological, and β-ion treatment combinations postulated, after which GUS staining assays were performed to assess DR5 promoter activity.

GUS staining results revealed that β-ion does not directly alter auxin activity *per se*. (Fig. 4.26). Both PIC addition and less strongly W+FR exposure led to enhanced GUS staining driven by DR5 promoter activation, reflecting elevated auxin levels of exogenous (PIC) or endogenous (W+FR) origin (Roig-Villanova & Martínez-García, 2016). In all other conditions, GUS staining remained at baseline levels and displayed a homogeneous distribution across seedlings at 0, 8 and 24 hours. Importantly, β-ion did not reduce GUS staining in seedlings with elevated auxin activity nor in those under standard conditions, ruling out a direct impact of β-ion on auxin-derived activity driven by the DR5 promoter.

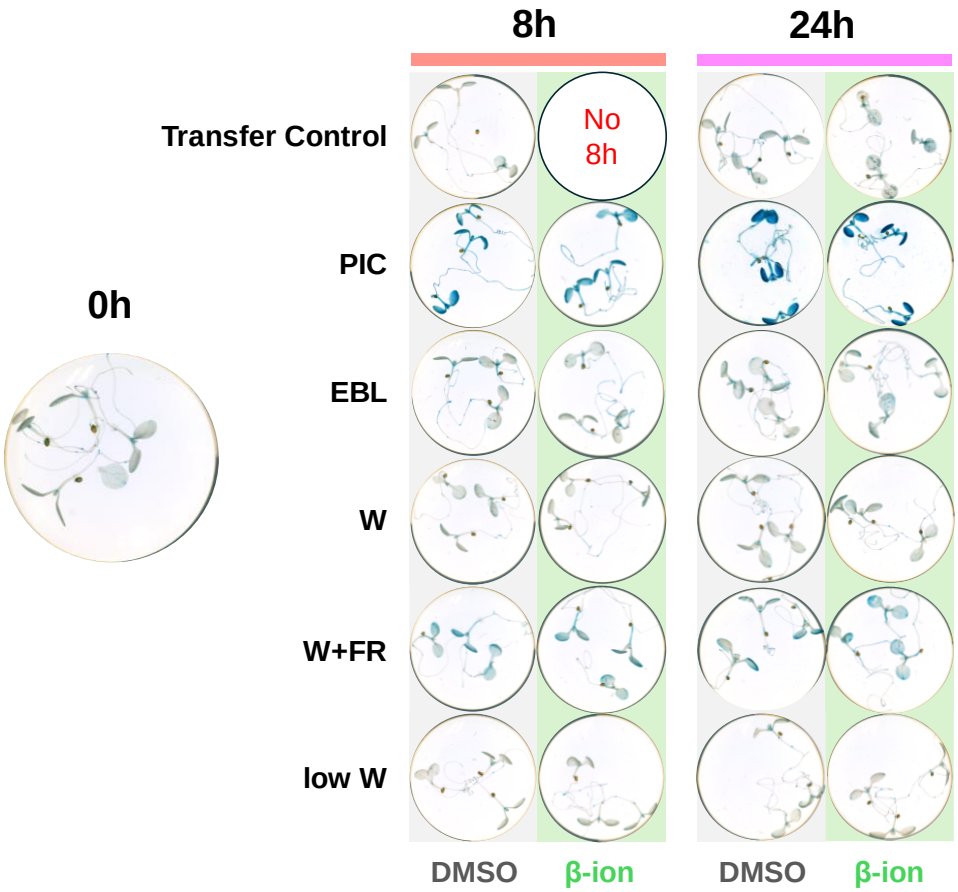

Figure 4.26 — Impact of β-ion exposure on GUS staining of DR5:GUS seedlings in response to hormonal and light treatments. *DR5:GUS seedlings grown under W conditions were exposed for 24 h to airborne β-ion or DMSO (control), either without transfer or after relocation to fresh medium supplemented with picloram (PIC) or epibrassinolide (EBL). Transfer controls and additional treatments under W, low W, or W+FR conditions were included. Samples were collected at 0 h, 8 h, and 24 h for GUS staining analysis of DR5 promoter activity.*

Altogether, our transcriptomic and physiological analyses reveal that although β-cc and β-ion share a common transcriptional backbone centered on stress-associated metabolic adjustments, their specific outputs diverge into distinct physiological programs. β-ion selectively enhanced oxidative phosphorylation and photosynthetic gene expression, consistent with an energetic reinforcement that may sustain its strong activation of immune-related processes, including MAPK and SA signaling

cascades. This defense-oriented reprogramming was further accompanied by the downregulation of *SAUR* genes. On the other hand, β-cc favored specific responses aiming to consolidate the transcriptomic prophylactical response to stresses such as hypoxia, while repressing JA- and glucosinolate-related pathways, outlining a distinct metabolic trajectory. Taken together, these results highlight that β-cc and β-ion, while partially overlapping, drive divergent signaling outcomes: β-ion predominantly primes immune defenses at the cost of growth-related functions, whereas β-cc emphasizes metabolic adjustments more related to abiotic stress resilience.

Supplemental Information

Table 4.S1 — 29 Overlapping DEGs from shade volatilome, ethylene, β-cc and β-ion treatments

Accession number	Gene ID	Annotation / Gene Description
AT1G02850	BETA GLUCOSIDASE 11 (BGLU11)	beta glucosidase 11;(source:Araport11)
AT1G06360	ADS4.2	ADS4.2 has strong desaturase activity on acyl-CoA substrates longer than C32 and product regio-specificity in yeast assays.
AT1G07040	-	plant/protein;(source:Araport11)
AT1G10140	-	Uncharacterized conserved protein UCP031279;(source:Araport11)
AT1G21680	-	DPP6 N-terminal domain-like protein;(source:Araport11)
AT1G52290	PROLINE-RICH EXTENSIN-LIKE RECEPTOR KINASE 15 (PERK15)	Encodes a member of the proline-rich extensin-like receptor kinase (PERK) family. This family consists of 15 predicted receptor kinases (PMID: 15653807).
AT1G54100	ALDEHYDE DEHYDROGENASE 7B4 (ALDH7B4)	Aldehyde dehydrogenase
AT1G78370	GLUTATHIONE S-TRANSFERASE TAU 20 (GSTU20)	Encodes glutathione transferase belonging to the tau class of GSTs. Naming convention according to Wagner *et al.* (2002).
AT1G80440	KISS ME DEADLY 1 (KMD1)	Encodes a member of a family of F-box proteins; called the KISS ME DEADLY (KMD) family; that targets type-B ARR proteins for degradation and is involved in the negative regulation of the cytokinin response. Also named as KFB20; a member of a group of Kelch repeat F-box proteins that negatively regulate phenylpropanoid biosynthesis by targeting the phenylpropanoid biosynthesis enzyme phenylalanine ammonia-lyase.
AT2G05380	-	glycine-rich protein 3 short isoform (GRP3S) mRNA; complete. The mRNA is cell-to-cell mobile.
AT2G27830	-	hypothetical protein;(source:Araport11)
AT2G36800	DON-GLUCOSYL-TRANSFERASE 1 (DOGT1)	Encodes a DON-Glucosyltransferase. The UGT73C5 glycosylates both brassinolide and castasterone in the 23-O position. The enzyme is presumably involved in the homeostasis of those steroid hormones hence regulating BR activity. Transgenic plants overexpressing UGT73C5 show a typical BR-deficient phenotype.
AT2G44130	KISS ME DEADLY 3 (KMD3)	Encodes a member of a family of F-box proteins; called the KISS ME DEADLY (KMD) family. Component of SCF ubiquitin protein ligase; interacts with phenylalanine ammonia-lyase. AtKFB39 is a homolog of previously identified AtKFB50 (At3g59940) and specifically interacts with Arabidopsis PAL3 and PAL4 in vitro.

AT3G01970	WRKY DNA-BINDING PROTEIN 45 (WRKY45)	member of WRKY Transcription Factor; Group I
AT3G13310	DNA J PROTEIN C66 (DJC66)	Chaperone DnaJ-domain superfamily protein;(source:Araport11)
AT3G19710	BRANCHED-CHAIN AMINO-TRANSFERASE4 (BCAT4)	Belongs to the branched-chain amino acid aminotransferase gene family. Encodes a methionine-oxo-acid transaminase. Involved in the methionine chain elongation pathway that leads to the ultimate biosynthesis of methionine-derived glucosinolates.
AT3G50890	HOMEOBOX PROTEIN 28 (HB28)	homeobox protein 28;(source:Araport11)
AT3G54600	DJ1F	Glyoxalase I with low activity.
AT3G59940	KISS ME DEADLY 4 (KMD4)	Encodes a member of a family of F-box proteins; called the KISS ME DEADLY (KMD) family; that targets type-B ARR proteins for degradation and is involved in the negative regulation of the cytokinin response. Also named as KFB50; a member of a group of Kelch repeat F-box proteins that negatively regulate phenylpropanoid biosynthesis by targeting the phenylpropanoid biosynthesis enzyme phenylalanine ammonia-lyase.
AT4G02380	SENESCENCE-ASSOCIATED GENE 21 (SAG21)	Encodes SAG21, also known as LEA 5. Has a role on oxidative stress tolerance. mRNA levels are elevated in response to various stresses.
AT4G12030	BILE ACID TRANSPORTER 5 (BAT5)	Required for the biosynthesis of methionine-derived glucosinolates. Involved in the transport of 2-keto acids between chloroplasts and the cytosol.
AT4G15530	PYRUVATE ORTHOPHOSPHATE DIKINASE (PPDK)	Encodes a dual-targeted protein believed to act as a pyruvate; orthophosphate dikinase. These enzymes are normally associated with C4 photosynthesis which does not occur in Arabidopsis. However, PPDK may play a role in remobilizing nitrogen during leaf senescence in Arabidopsis.
AT4G16190	RD19C	Member of the papain-like cysteine proteases known for its participation in anther development after its maturation by VPE (vacuolar processing enzyme); interacts with SBP1 (selenium binding protein 1).
AT4G34138	UDP-GLUCOSYL TRANSFERASE 73B1 (UGT73B1)	UDP-glucosyl transferase 73B1;(source:Araport11)
AT4G36040	DNAJ11 (J11)	DNA J protein.
AT5G13330	RELATED TO AP2 6L (Rap2.6L)	encodes a member of the ERF (ethylene response factor) subfamily B-4 of ERF/AP2 transcription factor family. The protein contains one AP2 domain. There are 7 members in this subfamily.
AT5G49690	UDP-GLYCOSYL-TRANSFERASE 91C1 (UGT91C1)	UDP-glycosyltransferase that can act upon sulcotrione herbicide. Overexpression confers resistance to herbicide.
AT5G61000	(RPA70D)	Replication factor-A protein 1-like protein;(source:Araport11)
AT5G61820	NODULIN 19 (NOD19)	P1-interacting host factor required for robust virus infection.

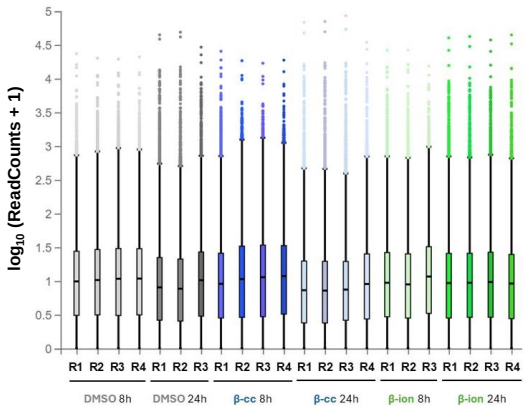

Figure 4.S1 — Distribution of read counts across RNA-seq samples. *Boxplots showing the distribution of log_{10}(ReadCounts + 1) for all detected genes across biological replicates (R1–R4) at different time points (8 and 24 h) under control treatment (DMSO, shades of grey), β-cc (shades of blue) or β-ion (shades of green) treatments. Each box represents the interquartile range, with horizontal lines indicating the median, whiskers showing 1.5× the interquartile range, and dots representing outliers.*

Figure 4.S2 — Distribution of Gene Ontology Biological Process (GO-BP) terms among individual volatile treatments. *Barplots showing the 10 most represented GO-BP categories among the datasets of DEGs in Arabidopsis r-seedlings exposed to ethylene (in yellow), β-cc (in blue) or β-ion (in green). Bar length indicates the number of genes associated with each category, while color intensity corresponds to the relative frequency within the dataset.*

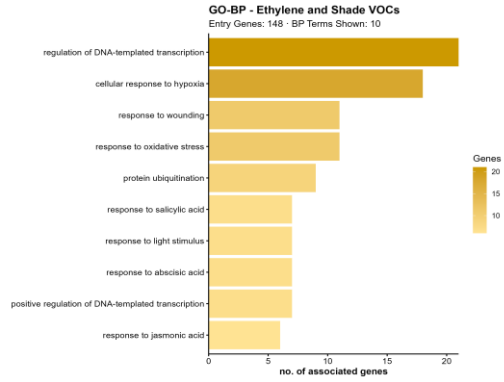

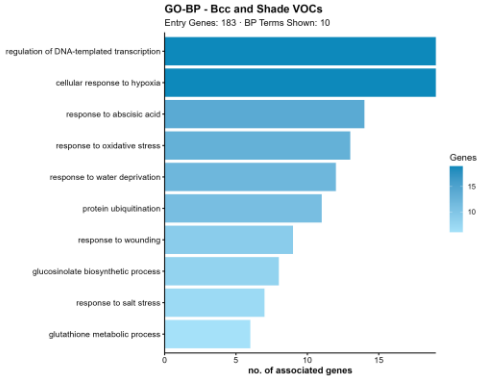

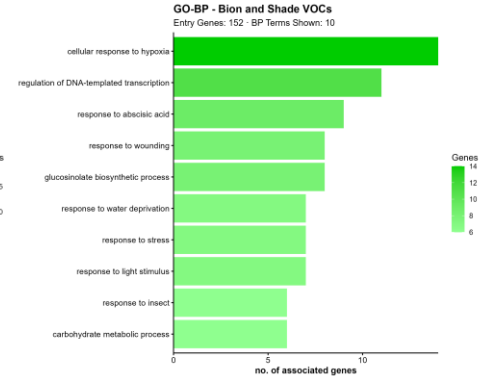

Table 4.S2 — Putative β-ion protein targets. Highlighted in **purple**: Ribosomal proteins. Highlighted in **orange**: Enzymes involved in glucosinolates or phenylpropanoid biosynthesis. Highlighted in **beige**: Overlap with BIN2-interacting proteins. Highlighted in **yellow**: RACK1A.

ATG ID	Gene Name	Annotated Functions (GO-BP)	Binding score / p-value	Fold Change (FC)
AT3G60245	**RPL37AC**	Translation	0.0002523	1.520
ATMG00070	**NAD9**	-	0.0002554	1.341
AT4G32470	**QCR7-1**	Mitochondrial electron transport	0.0006915	0.000
AT3G44110	**ATJ**	Photoperiodism, flowering, response to stress,(…)	0.0007669	0.816
AT2G34480	**RPL18AB**	Translation, Pollen tube growth, Embryo development	0.0009218	1.359
AT3G56130	**BLP3**	-	0.0010648	1.287
AT4G33580	**BCA5**	Carbon utilization	0.0012478	1.135
AT1G21130	**IGMT4**	Methylation	0.0023476	1.152
AT5G42190	**SKP1B**	Auxin activated signaling pathway, response to JA and ethylene, (…)	0.0023659	1.578
AT3G51600	**LTP5**	Lipid transport	0.0024898	0.888
AT3G13120	**RPS10**	Translation	0.0024900	1.520
AT5G04850	**VPS60-2**	Protein transport, Vesicle budding, Endosomes	0.0025046	-
AT3G53900	**UPP**	Uracil Salvage	0.0025053	0.879
AT5G45620	**RPN9A**	-	0.0025529	0.821
AT1G12050	**FAH**	Cell death, Catabolic processes	0.0027751	1.149
AT5G37510	**EMB1467**	Photorespiration	0.0027939	0.828
AT2G37040	**PAL1**	Phenylpropanoids biosynthesis, defense response, (…)	0.0028290	1.068
AT2G27460	**SEC23D**	Endoplasmic reticulum to Golgi vesicle-mediated transport	0.0028466	2.140
AT1G43890	**RABC1**	Protein transport	0.0038722	0.685
AT1G01100	**RPP1A**	Translational elongation	0.0040983	1.911
AT4G32760	**TOL9**	Protein transport, Vesicle budding, Endosomes	0.0043671	1.331
AT1G13060	**PBE1**	Proteasome-mediated protein catabolic process	0.0045171	1.334
AT3G55590	**CYT1**		0.0047864	0.550
AT2G25840	**OVA4**	Reproductive structure development	0.0051426	0.727
AT4G13840	**CER26**	Fatty acid biosynthesis, cell wall organization	0.0055654	-
AT2G35370	**GDCH**	Glycine decarboxylation, photorespiration	0.0063645	1.701
AT2G43090	**SSU1**	Glucosinolate biosynthetic process	0.0065261	1.085
AT3G10350	**GET3B**	Chloroplast biogenesis	0.0070399	0.966
AT1G10370	**GSTU17**	Glutathione metabolic process	0.0070764	2.497

AT1G72680	**CAD1**	Lignin biosynthesis, Osmotic tolerance	0.0071718	1.740
AT2G27050	**EIL1**	Ethylene response pathway	0.0080397	0.832
AT5G44070	**PCS1**	Response to cadmium, Arsenite transport	0.0081881	0.838
AT4G31500	**CYP83B1**	Tryptophan biosynthetic process, Glucosinolates biosynthesis, (…)	0.0081984	0.639
AT3G02875	**ILR1**	Auxin metabolic process	0.0085928	5.823
AT1G60710	**ATB2**	-	0.0097711	1.280
AT1G65310	**XTH17; XTH18; XTH19**	Cell wall biogenesis, Lateral root development	0.0102002	0.453
AT5G49215	**PGF16**	-	0.0104626	0.702
AT4G29830	**VIP3**	Flower development	0.0105759	2.182
AT1G69830	**AMY3**	Starch catabolic process	0.0107971	-
AT3G12500	**CHI-B**	Chitin catabolic process, defense response	0.0108361	1.166
AT2G36620	**RPL24A**	Translation	0.0110289	2.034
AT2G23610	**MES3**	Oxylipin biosynthetic process	0.0113671	1.329
AT2G01520	**MLP328**	Defense response, response to phenylpropanoid	0.0113897	2.324
AT3G04720	**HEL**	Defense response	0.0113906	1.762
AT1G18080	**RACK1A**	Phytohormone regulation, seed germination, seedling development (…)	0.0114236	1.526
AT1G09070	**SRC2**	Defense response, Cellular response to hypoxia	0.0114385	1.469
AT2G27450	**CPA**	Putrescine biosynthetic process	0.0114637	1.238
AT5G42890	**SCP2**	Fatty acid biosynthesis, Intracellular lipid transport	0.0114696	1.242
AT1G51390	**NIFU5**	Iron-Sulfur cluster assembly	0.0115426	0.869
AT5G20070	**NUDT19**	-	0.0116506	1.380
AT5G55730	**FLA1**	Root development	0.0120045	1.182
AT4G37930	**SHM1**	Circadian rhythm, photorespiration, glycine biosynthesis	0.0122458	1.086
AT3G15356	**LEC**	Cellular response to chitin, ethylene or JA	0.0124415	0.929
AT5G07440	**GDH2**	Amino acid metabolic process	0.0126313	1.161
AT5G62000	**ARF1**	Auxin signaling	0.0128793	1.258
AT1G30720	**BBE10**	Cellular response to hypoxia, Cell wall organization	0.0128857	1.219
AT5G18170	**GDH1**	Amino acid metabolic process	0.0132893	1.039
AT3G18060	**AIP1-2**	-	0.0136809	1.143
AT1G75330	**OTC**	Arginine biosynthesis	0.0149473	1.385
AT2G44040	**DAPB1**	Diaminopimelate biosynthetic process	0.0149603	1.524
AT5G08410	**FTRA2**	Photosynthesis	0.0152609	0.941
AT5G23310	**FSD3**	-	0.0154168	1.261
AT2G30750	**CYP71A12**	Indolic Glucosinolates Metabolism	0.0155072	0.752
AT3G49720	**CGR2**	Pectin metabolic process, Cell wall modification, (…)	0.0159296	0.000

ATCG01060	**psaC**	Photosynthesis	0.0160894	1.672
AT1G03870	**FLA9**	Root development, cell adhesion	0.0161262	1.600
AT3G14600	**RPL18AC**	Translation	0.0162828	1.809
AT3G16420	**PBP1**	Protein Folding	0.0168139	1.119
AT2G34510	**ATHB-1**	-	0.0174968	1.229
AT5G17020	**XPO1**	Pollen development	0.0179289	3.400
AT5G11950	**LOG8**	Cytokinin biosynthesis	0.0179883	0.829
AT3G16050	**PDX12**	Pyridoxal phosphate biosynthetic process	0.0180302	1.103
AT3G63170	**FAP1**	Fatty acid metabolic process	0.0187021	1.204
AT3G48890	**MSBP2**	-	0.0188790	0.772
ATCG00760	**RPL36**	Translation	0.0191930	1.115
AT5G13370	**GH3.15**	Auxin conjugate metabolic process	0.0192380	1.538
AT2G17120	**LYM2**	Defense response	0.0202128	0.310
AT5G47700	**RPP1C**	Translational elongation, defense responses	0.0213026	2.053
AT5G60360	**ALEU**	Defense response, Apoptosis signaling pathway	0.0216402	1.477
AT4G31300	**PBA1**	Proteasome-mediated protein catabolic process	0.0217616	1.139
AT4G26260	**MIOX4**	Inositol Catabolic process	0.0235068	-
AT5G16710	**DHAR3**	Ascorbate glutathione cycle	0.0237571	1.345
AT3G10410	**SCPL49**	Proteolysis	0.0241391	0.624
AT4G02380	**SAG21**	Senescence	0.0243593	2.373
AT3G23400	**PAP6**	Chloroplast organization	0.0243863	0.790
AT3G46780	**PTAC16**	Circadian rhythm	0.0245684	0.772
AT5G26000	**TGG1**	Abscisic acid signaling pathway, glucosinolate metabolism	0.0247262	1.228
AT4G39520	**DRG3**	-	0.0256554	0.821
AT1G02780	**RPL19A**	Translation	0.0258619	2.701
AT3G02560	**RPS7B**	Translation	0.0259434	0.666
AT3G55830	**GMT1 / EPC1**	-	0.0261544	1.106
AT2G42520	**RH37**	-	0.0266085	0.457
AT3G05820	**INVH**	Carbohydrate metabolic process	0.0267459	1.267
AT5G64300	**RIBA1**	Riboflavin biosynthesis	0.0269432	0.868
AT4G12420	**SKU5**	Cell tip growth	0.0270710	1.182
AT3G16990	**TENA_E**	Thiamine biosynthesis	0.0279372	1.467
AT3G43270	**PME32**	Cell wall modification, pectin catabolism	0.0284767	0.786
AT5G20570	**RBX1A**	Ubiquitin-mediated degradation, response to AUX and JA	0.0289981	2.681
AT1G18590	**SOT17**	Glucosinolate biosynthetic process	0.0294084	0.850
AT5G51050	**APC2**	AMP/ADP/ATP transport	0.0296922	0.675
AT2G39730	**RCA**	Leaf senescence, response to light	0.0296994	1.177

AT4G18100	**RPL32A**	Translation	0.0298317	1.105
AT4G27000	**RBP45C**	mRNA processing	0.0302071	1.110
AT1G37100	**CGE2**	-	0.0303720	1.364
AT1G04510	**PRP19A**	Defense response, innate immune response	0.0305808	1.683
AT5G24400	**PGL3**	Carboxylate metabolism	0.0308341	1.199
AT4G21445	**CRR9**	-	0.0322624	1.641
AT5G20280	**SPS1**	Sucrose biosynthesis	0.0323536	0.858
AT4G32520	**SHM3**	Glycine biosynthesis	0.0324493	1.201
AT3G02780	**IPP2**	Photosynthesis, Chlorophyll Biosynthesis	0.0326272	0.902
AT5G49510	**PFD3**	Response to gibberellin, cold acclimation	0.0329098	6.692
AT1G31230	**AKHSDH1**	Lysine Biosynthesis, Methionine biosynthesis	0.0331925	0.839
AT3G53230	**CDC48D**	Cell division, Protein Catabolism	0.0332126	-
AT3G01340	**SEC13A**	Protein transport, Vesicle-mediated transport	0.0336746	1.644
AT4G33350	**TIC22**	Protein transport	0.0337520	0.751
AT4G15510	**PPD1**	Photosystem I Assembly	0.0338376	2.324
AT1G51710	**UBP6**	Proteasome-mediated protein catabolic process	0.0340576	0.840
AT1G76300	**SMD3A**	mRNA splicing, via spliceosome	0.0343348	1.341
AT5G61170	**RPS19C**	Translation	0.0347661	1.393
AT3G54050	**CFBP1**	Photosynthesis, Pentose-phosphate cycle	0.0348575	0.953
AT3G02530	**CCT6A**	Response to zinc ion	0.0348812	0.939
AT3G50960	**PLP3A;**	-	0.0350203	4.739
AT5G54160	**OMT1**	Circadian rhythm, methylation, (…)	0.0359167	1.086
AT3G04610	**FLK**	Flower development	0.0361235	0.941
AT3G17240	**LPD2**	-	0.0362449	1.247
AT1G02170	**AMC1**	Defense response	0.0367213	3.373
AT3G62940	**OTU5**	Proteolysis	0.0374059	1.164
AT5G47870	**RAD52-2**	Double-strand break repair	0.0379281	1.443
AT4G29410	**RPL28C**	Translation	0.0379358	0.746
AT1G31330	**PSAF**	Photosynthesis	0.0380458	0.000
AT2G38140	**RPS31**	Plastid translation	0.0382509	1.100
AT3G27310	**PUX1**	Organ growth, protein-containing complex disassembly	0.0385837	0.827
AT5G57655	**XYLA**	D-xylose metabolic process	0.0388547	1.366
AT1G48320	**DHNAT1**	Phylloquinone biosynthesis	0.0396724	1.099
AT4G20860	**BBE22**	Response to JA, Defense response	0.0399240	1.110
AT1G08550	**VDE1**	Chlorophyll metabolism, Fatty acid metabolism	0.0399877	0.896
AT3G07390	**AIR12**	Auxin signaling pathway	0.0402276	1.357

AT2G26080	**GLDP2**	Glycine catabolism	0.0407694	0.887
AT2G42490	**CuAO-Z**	Lateral root formation, response to ABA, JA and SA	0.0409185	1.219
AT4G26300	**EMB1027**	Arginyl-tRNA aminoacylation	0.0411090	0.789
AT3G58500	**PP2A4**	Protein dephosphorylation, defense response	0.0411440	1.324
AT2G30260	**U2B''**	Cis-assembly of pre-catalytic spliceosome	0.0413038	1.165
AT1G14610	**TWN2**	Embryo development, valyl-tRNA aminoacylation	0.0413166	1.117
AT3G09500	**RPL35A**	Translation	0.0423364	1.197
AT3G12600	**NUDT16**	-	0.0426475	0.801
AT1G24020	**MLP423**	ABA signaling, defense response	0.0426847	0.952
AT5G42950	**EXA1**	Defense responses	0.0427418	1.381
AT5G20720	**CPN20**	Negative regulation of ABA signaling	0.0432443	1.096
AT1G29880	**-**	glycyl-tRNA aminoacylation	0.0433490	0.927
AT5G50250	**CP31B**	Innate immune response, mRNA processing	0.0435844	1.111
AT4G26870	**-**	Aspartyl-tRNA aminoacylation	0.0437063	0.740
AT5G19760	**DTC**	Dicarboxylic acid transport	0.0440431	0.374
AT5G59880	**ADF3**	Actin filament depolymerization	0.0440908	1.366
AT3G17810	**PYD1**	Uracil Catabolism	0.0443744	1.296
AT1G67280	**GLYI6**	Methylglyoxal catabolism	0.0448451	1.194
AT3G63490	**RPL1**	Translation	0.0449811	0.856
AT4G25550	**CFIS2**	mRNA processing, rRNA processing	0.0457306	0.677
AT2G01530	**MLP329**	defense response	0.0462000	1.684
AT1G32990	**RPL11**	Translation	0.0464765	1.085
AT4G35450	**AKR2A**	Protein targeting to chloroplast	0.0471382	1.282
AT1G64790	**ILA**	Defense response	0.0471619	0.600
AT1G78570	**RHM1**	Auxin export, cell wall organization	0.0475506	0.883
AT3G48390	**MRF4**	-	0.0476160	1.644
AT3G48930	**RPS11A**	Translation	0.0482051	0.934
AT4G16155	**-**	Response to arsenic	0.0485103	0.886
AT1G62810	**CuAOγ1**	ABA signaling, response to ABA, AUX, JA, SA, (…)	0.0485807	1.746
AT1G32200	**ATS1**	Phosphatidylglycerol biosynthesis	0.0486306	1.563
AT5G03290	**IDH5**	Isocitrate metabolism	0.0488746	0.904
AT3G13580	**RPL7D**	Translation	0.0489713	1.079
AT1G32470	**GDH3**	Glycine decarboxylation	0.0491171	1.914
AT1G35680	**RPL21**	Translation, chloroplast organization	0.0494098	0.833
AT2G28610	**PRS1; PRS2**	-	0.0494812	-
AT1G19160	**ICF1**	-	0.0495095	0.764

Figure 4.S3 — Heatmap of DEGs associated with tryptophan metabolism and indolic glucosinolate biosynthesis in response to apocarotenoid treatments. *Heatmap showing the transcriptional regulation (row Z-score) of genes involved in tryptophan metabolism and indolic glucosinolate biosynthesis upon exposure to β-cc (8 h) or β-ion (24 h), compared to DMSO controls. Each row represents an individual gene (symbols on the right). Colors indicate relative expression values (row Z-scores), with red–orange denoting expression above the mean across treatments and blue indicating expression below the mean.*

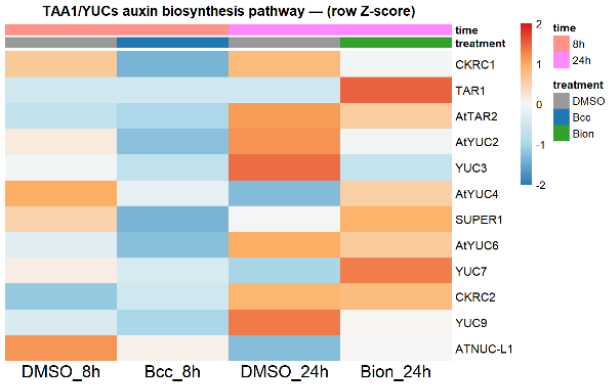

Figure 4.S4 — Heatmap of DEGs associated with the TAA1/YUCs auxin biosynthesis pathway. *Heatmap showing the transcriptional regulation (row Z-score) of genes involved TAA1/YUCs auxin biosynthetic pathway upon exposure to β-cc (8 h) or β-ion (24 h), compared to DMSO controls. Each row represents an individual gene (symbols on the right). Colors indicate relative expression values (row Z-scores), with red–orange denoting expression above the mean across treatments and blue indicating expression below the mean.*

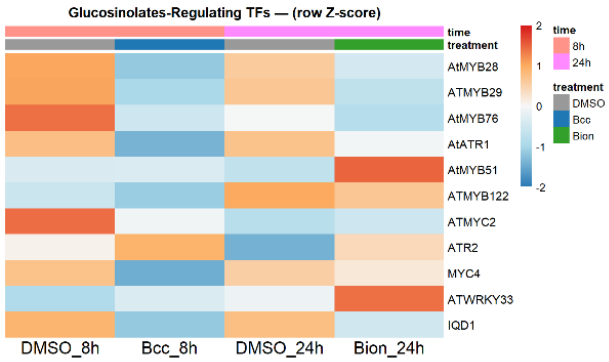

Figure 4.S5 — Heatmap of DEGs encoding transcription factors regulating glucosinolate biosynthesis in response to apocarotenoid treatments. *Heatmap showing the transcriptional regulation (row Z-score) of TFs involved in glucosinolate biosynthesis upon exposure to β-cc (8 h) or β-ion (24 h), compared to DMSO controls. Each row corresponds to an individual TF (symbols on the right). Colors indicate relative expression values (row Z-scores), with red–orange denoting expression above the mean across treatments and blue indicating expression below the mean.*

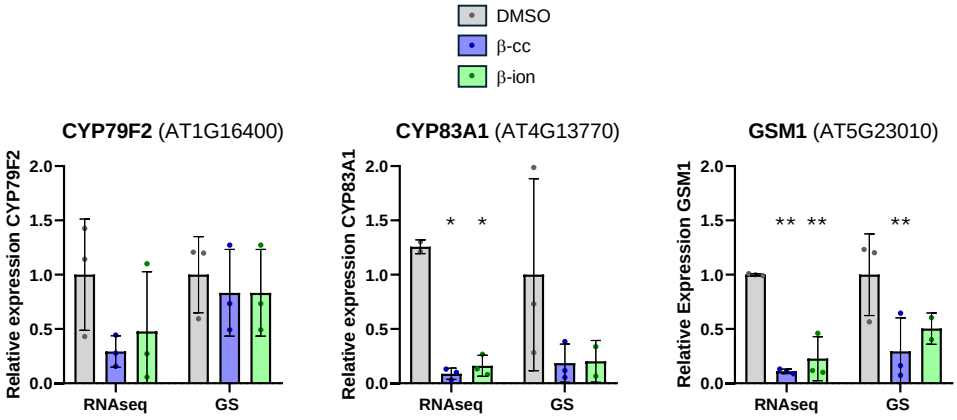

Figure 4.S6 — Comparison of relative expression of aliphatic GS biosynthetic genes between RNA-seq and qPCR analyses. *Barplots showing the relative transcript abundance of selected aliphatic GS biosynthetic genes in A. thaliana seedlings exposed to β-cc (blue), β-ion (green), or DMSO (Control, grey). In each panel, left bars panels correspond to RNA-seq data (log_2 fold-change values, relativized to DMSO), while bars on the right side (GS) show independent validation by qPCR using material derived from the same biological samples used for GS content quantification (Fig. 4.14). Both approaches revealed consistent trends of downregulation across most tested genes, confirming the robustness of RNA-seq–based observations regarding the repression of aliphatic GS biosynthetic pathways under apocarotenoid exposure.*

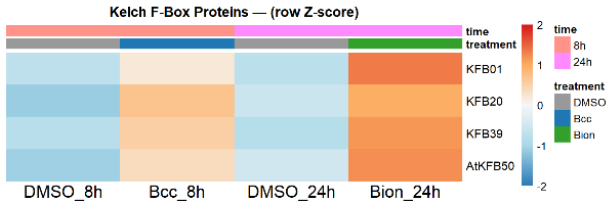

Figure 4.S7 — Heatmap of DEGs encoding Kelch F-box proteins in response to apocarotenoid treatments. *Heatmap showing the transcriptional regulation (row Z-score) of Kelch F-box protein (KFB) genes upon exposure to β-cc (8 h) or β-ion (24 h), compared to DMSO controls. Each row corresponds to an individual gene (symbols on the right). Colors indicate relative expression values (row Z-scores), with red–orange denoting expression above the mean across treatments and blue indicating expression below the mean.*

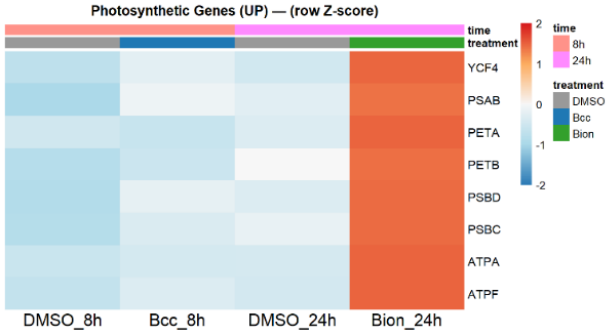

Figure 4.S8 — Heatmap of DEGs associated with photosynthesis in response to apocarotenoid treatments *Heatmap showing transcriptional regulation (row Z-score) of photosynthetic genes in Arabidopsis seedlings exposed to β-cc or β-ion, compared to DMSO controls. Genes include subunits of photosystem I (PSAB, PSBC) and ATP synthase (ATPA, ATPF). Warmer colors indicate higher expression relative to the mean, and cooler colors indicate lower expression.*

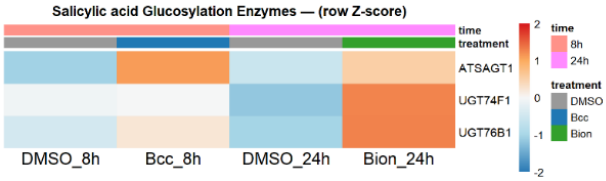

Figure 4.S9 — Heatmap of DEGs associated with SA glycosylation enzymes in response to apocarotenoid treatments. *Heatmap showing the transcriptional regulation (row Z-score) of genes encoding SA-glucosyltransferases (ATSAGT1, UGT74F1, and UGT76B1) in seedlings exposed to β-cc or β-ion, compared with DMSO controls. Colors indicate relative expression values, with red–orange representing expression levels above the gene mean and blue indicating lower values. Upregulation of these genes was particularly evident in response to β-ion, suggesting an active modulation of SA homeostasis through glycosylation processes.*

Chapter V

Chapter V. Molecular mechanisms underlying β-ionone (and β-cyclocitral) effects

In the previous chapters, β-ionone (β-ion) and β-cyclocitral (β-cc) have been shown to be key signaling molecules within the shade volatilome. Additionally, a functional transcriptomic analysis coupled with proteomic and metabolic data revealed that both compounds induce a series of stress-related common responses, while also triggering specific responses. In this chapter, we evaluate key signaling elements that could be critical for the underlying molecular mechanisms of the shade-responsive VOCs. Therefore, here we aim to propose mechanistic models that could explain the biological impact of shade-responsive apocarotenoids. A particular emphasis is placed on β-ion, for which a deeper experimental characterization has been conducted.

5.1 A role for brassinosteroids on apocarotenoid signaling

The results reported in Chapter IV showing a lack of a detectable effect of β-ion on auxin-responsive DR5:GUS staining (Fig. 4.26) suggest that the repression of *SAUR* genes may not be directly mediated by auxin signaling. This opened the possibility that other phytohormones with known roles in *SAUR* gene regulation could be involved in β-ion signaling. Among these, gibberellins (GAs) and brassinosteroids (BRs) stand out as major promoters of elongation growth. Both pathways converge, at least in part, on transcriptional modules that activate *SAUR* expression (Ren & Gray, 2015), albeit through distinct upstream regulators. GAs generally promote elongation via DELLA protein degradation, relieving repression on growth-associated transcription factors (Stamm & Kumar, 2013), while BRs act through BES1 and BZR1 to directly activate a large subset of *SAUR* genes (Kono & Yin, 2020). Disruption of either GA or BR signaling typically leads to reduced *SAUR* expression and impaired elongation

growth, phenocopying aspects of the β-ion-induced repression observed in this work. These functional parallels led us to hypothesize that β-ion (and/or β-cc) might exert its growth-repressive effect by interfering with one or both hormonal pathways.

5.1.1 Apocarotenoids have no effect in brassinosteroid-treated seedlings

We evaluated the impact of airborne apocarotenoids (β-cc and β-ion) on the growth of seedlings growing under W in media supplemented with picloram (PIC, an auxin analog), gibberellic acid (GA_3, an active gibberellin) or epibrassinolide (EBL, an active brassinosteroid) (Fig. 5.1). Under these conditions, apocarotenoid treatment alone had no measurable impact on hypocotyl elongation because of the strong inhibitory effect of light (W) on growth, as shown (Fig. 3.2-A). Nonetheless, in all phytohormone-supplemented conditions, hypocotyl elongation was promoted, and the apocarotenoid effect became apparent. Both β-cc and β-ion repressed the growth promoted by exogenous auxins and gibberellins but had no effect in the case of EBL (Fig. 5.1). These results suggest that, in terms of hypocotyl elongation, β-ion and β-cc alter brassinosteroid signaling, and that exogenous activation of this signaling pathway might be sufficient to override the growth inhibitory effect of volatile apocarotenoids.

A further dose–response assay revealed that exogenous brassinosteroid supplementation can similarly override the repressive effect of β-cc and β-ion on hypocotyl elongation at all concentrations tested (Fig. 5.S1), suggesting a dose-independent effect. This observation argues against a simple competitive inhibition at the BR receptor level, since lower hormone doses would be expected to reveal partial repression if such a mechanism were in place. Instead, the data are more consistent with β-cc and β-ion acting downstream or in parallel to the BR receptor, at a point in the signaling cascade where a sufficiently strong BR input can saturate the pathway and bypass the inhibitory effect.

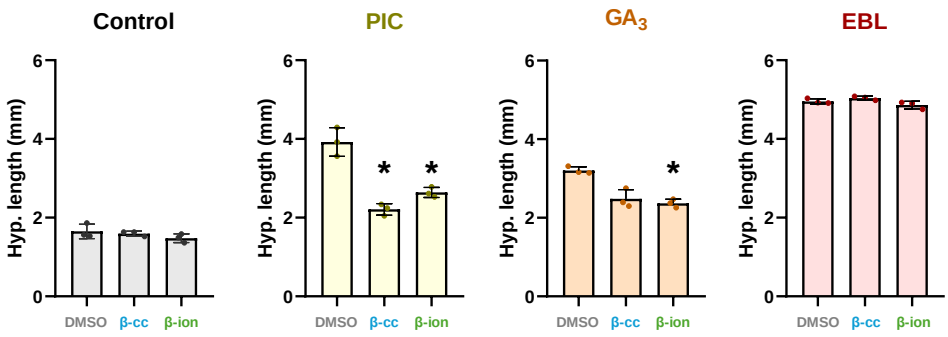

Figure 5.1 — Impact of airborne apocarotenoids on hypocotyl elongation promoted by hormonal treatments. *Plots represent hypocotyl length of A. thaliana W-grown seedlings exposed to airborne β-cc (10 µL 500 mM) or β-ion (10 µL 100 mM) (or 10 µL DMSO as a control) under different hormonal treatments (applied to the growth media): PIC, 5 µM picloram; GA_3, 10 µM gibberellic acid: EBL, 1 µM epibrassinolide. W provided a PPFD of 49 µmol·m^{-2}·s^{-1}. Bars represent the mean ± SD of three biological replicates. Asterisks indicate significant differences driven by apocarotenoids compared to DMSO (two-way ANOVA followed by Dunnett's multiple comparisons test, **p<0.01, *p<0.05).*

5.1.2 BES1 as a key component for apocarotenoid signaling

In order to test whether β-cc and β-ion act downstream of BR signaling, we explored the role of BZR1 and BES1, the main transcription factors mediating BR-responsive gene expression that act as key regulators of BR-induced developmental responses. We performed hypocotyl elongation experiments using two constitutively active mutants in the BR pathway: *bzr1-D* and *bes1-D* (Yin *et al.*, 2002) . Both *bzr1-D* and *bes1-D* carry mutations that mimic the dephosphorylated, active form, leading to constitutive activation of BR signaling even in the absence of exogenous BRs. In addition, we included a GA-signaling mutant lacking the five DELLA proteins present in Arabidopsis - GAI, RGA, RGL1, RGL2, and RGL3 - (hereinafter referred to as *dellaKO*) and an ABA sextuple receptor mutant (*pyr1 pyl1 pyl2 pyl4 pyl5 pyl8,* Gonzalez-Guzman *et al.*, 2012) (hereinafter referred to as *ABAm*), to enable comparisons across different phytohormone pathways. Seedlings were grown under different light regimes (W or darkness, D), and also under W or D supplemented with EBL, GA_3, or a combination of EBL+GA_3, in the presence or absence of β-cc or β-ion. Two batches of Col-0 seedlings were used to discard any age-related issue from the seeds: one for the *dellaKO* mutant, and another for the rest of mutants.

Hypocotyl measurements were represented as scatter-dot barplots showing either absolute values (Fig. 5.2) or values relative to the DMSO control (Fig. 5.S2). Under D conditions, β-cc severely repressed germination as described in section 3.3 (Fig. 3.6), preventing hypocotyl measurements. In the case of β-ion, it strongly repressed hypocotyl growth across genotypes (Fig 5.2). However, the *bes1-D* mutant showed partial tolerance to β-ion (Fig. 5.S2). In the dark, EBL supplementation caused a pronounced repression of hypocotyl elongation across all genotypes tested (Fig 5.2 / 5.S2) (Reed *et al.*, 2018), largely overriding apocarotenoid effects. A notable exception was *dellaKO*, where EBL-driven repression was milder, suggesting that DELLA proteins partially contribute to BR-mediated inhibition of elongation in darkness. In *dellaKO*, the inhibitory effects of β-ion on hypocotyl growth remained detectable even in the presence of EBL (Fig. 5.2).

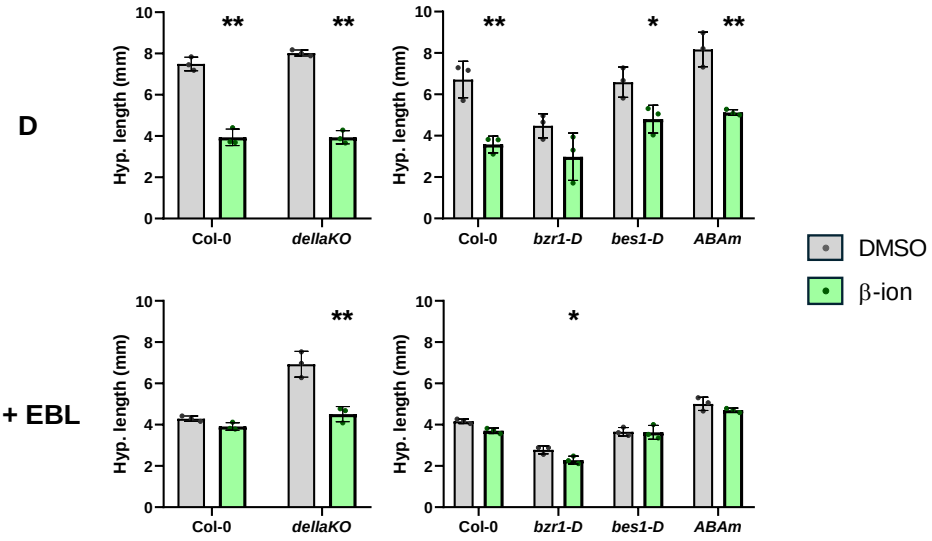

Figure 5.2 — Hypocotyl elongation of D-grown hormone-related mutant seedlings exposed to airborne β-ion. *A. thaliana Col-0 and hormone-related mutants were germinated and grown for 3 days under D either without (top) or with EBL (bottom) and exposed to airborne β-ion (10 µL 100 mM, in green) or DMSO (Control, 10 µL, in grey) during the complete growth period. Bars represent the mean ± SD of three biological replicates. Asterisks indicate significant differences compared to DMSO (two-way ANOVA followed by Dunnett's multiple comparisons test, **p<0.01, *p<0.05).*

BR-mediated growth repression in darkness has been associated with enhanced ethylene biosynthesis and signaling (I.-J. Chen *et al.*, 2013; Jiroutová *et al.*, 2019). To assess whether our apocarotenoids interact with the BR–ethylene regulatory module, seedlings of Col-0 and the ethylene-insensitive mutant *ein2-5* were grown in darkness with or without EBL. In the absence of apocarotenoids, EBL strongly repressed elongation in etiolated Col-0 seedlings, whereas *ein2-5* was largely insensitive to this effect, confirming that EIN2-dependent signaling is indeed necessary for BR-induced repression under these conditions (Fig. 5.3). In contrast, β-ion repressed elongation in *ein2-5* to a similar extent as in Col-0, regardless of EBL supplementation, similar to that observed with *dellaKO* seedlings (Figs. 5.2, 5.S2). Together, these results suggest that β-ion inhibits hypocotyl growth via a pathway that is largely independent of both gibberellins (DELLAs) and ethylene (EIN2) and is therefore mechanistically distinct from BR-mediated repression in darkness.

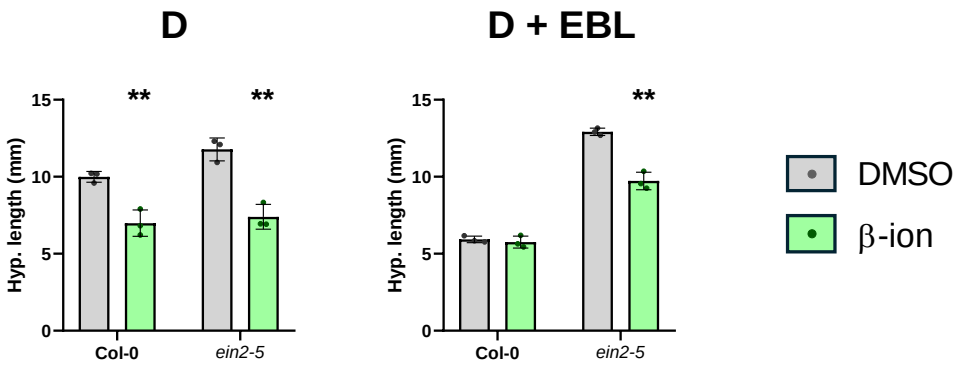

Figure 5.3 — Hypocotyl elongation of Col-0 and ethylene-insensitive 2-5 (ein2-5) D-grown seedlings exposed to airborne β-ion and EBL. *A. thaliana Col-0 and ein2-5 seedlings were germinated and grown for 4 days under D conditions in media without (D, left) or supplemented with EBL (D+EBL, right), and exposed to airborne β-ion (in green) or DMSO (Control, in grey) during the complete growth period. Bars represent the mean ± SD of three biological replicates. Asterisks indicate significant differences compared to DMSO (two-way ANOVA followed by Dunnett's multiple comparisons test, **p<0.01, *p<0.05).*

Under W conditions (Figs. 5.4, 5.S3), both β-cc and β-ion repress hypocotyl elongation across all genotypes tested. However, *bes1-D* seedlings displayed a clear tolerance to both compounds (Fig. 5.S3), suggesting that constitutive activation of BR signaling can mitigate

apocarotenoid-mediated repression. EBL supplementation, as previously described, induced hypocotyl elongation to a degree that surpassed apocarotenoid impact in most cases, excluding the *dellaKO* mutant. In this mutant, EBL-driven elongation was stronger than in other backgrounds (Fig. 5.4), indicating that DELLAs normally attenuate BRs-dependent hypocotyl elongation under W, likely by restraining BRs-driven growth. When this DELLA-mediated growth attenuation disappears, elongation is further enhanced, and the suppression elicited by the volatile apocarotenoids becomes fully apparent again. These results indicate that only the DELLA-restrained component of BR-induced elongation can counteract the repressive effect of β-cc and β-ion, and that removal of this restraint restores apocarotenoid-mediated inhibition.

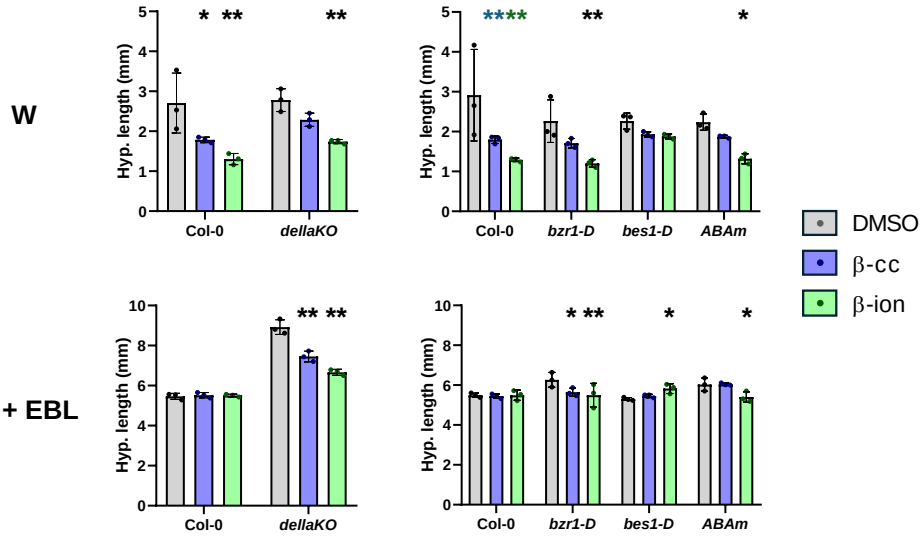

Figure 5.4 — Hypocotyl elongation of W-grown hormone-related mutant seedlings exposed to airborne β-cc and β-ion. *A. thaliana Col-0 and hormone-related mutant seedlings were germinated and grown for 7 days under W without (W, top) or supplemented with EBL (W+EBL, bottom), and exposed to airborne β-cc (in blue), β-ion (in green) or DMSO (Control, in grey) after the second day. Bars represent the mean ± SD of three biological replicates. Asterisks indicate significant differences compared to DMSO (two-way ANOVA followed by Dunnett's multiple comparisons test, **p<0.01, *p<0.05).*

GA_3 supplementation was used to phenocopy the *dellaKO* mutant across all genotypes, and hypocotyl elongation was measured accordingly (Figs. 5.5, 5.S4). As expected, GA_3 had no effect on *dellaKO*, but strongly promoted elongation in all other lines. Notably, *bes1-D* displayed hypersensitivity to GA_3, with a greater elongation response than any other genotype. Although β-cc and β-ion still repressed growth under GA_3, the magnitude of repression appeared partially alleviated, suggesting that GA-dependent growth promotion can counteract, at least in part, apocarotenoid-induced inhibition. The combination of GA_3 with EBL restored strong repression by the apocarotenoids, with the exception of *bes1-D* again (Fig. 5.S4).

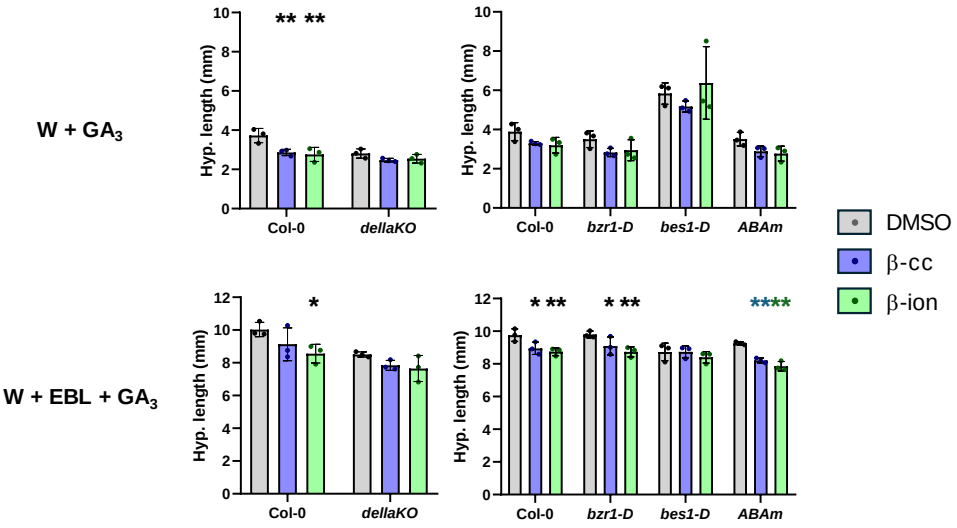

Figure 5.5 — Hypocotyl elongation of W-grown hormone-related mutant seedlings exposed to airborne β-cc and β-ion*. A. thaliana Col-0 and hormone-related mutants (dellaKO, bzr1-D, bes1-D, ABAm) seedlings were grown under W+GA₃ (top) or W+EBL+GA₃ (bottom), exposed to airborne β-cc (in blue), β-ion (in green) or DMSO (Control, in grey). Bars represent the mean ± SD of three biological replicates. Asterisks indicate significant differences compared to DMSO (two-way ANOVA followed by Dunnett's multiple comparisons test, **p<0.01, *p<0.05).*

To further examine BES1 involvement, Col-0 and *bes1-D* seedlings were grown under low W or W+FR light, both of which promote elongation, and apocarotenoid effects were evaluated (Fig. 5.6, 5.S5). Under low W, β-cc

and β-ion strongly repressed elongation in Col-0, whereas this effect was absent in *bes1-D*. Under W+FR, where elongation is largely driven by auxin signaling, repression by β-ion was still reduced in *bes1-D* compared to Col-0, indicating partial tolerance, while β-cc effects remained similar across genotypes.

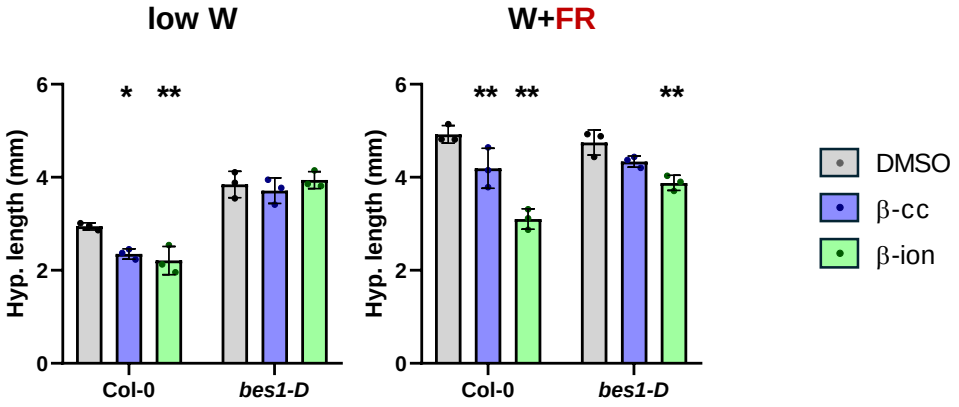

Figure 5.6 — Hypocotyl elongation of Col-0 and bes1-D A. thaliana seedlings exposed to airborne β-cc and β-ion under different light conditions*. A. thaliana Col-0 and bes1-D seedlings were grown under low W (left) or W+FR (right), exposed to airborne β-cc (in blue), β-ion (in green) or DMSO (Control, in grey). Bars represent the mean ± SD of three biological replicates. Asterisks indicate significant differences compared to DMSO (two-way ANOVA followed by Dunnett's multiple comparisons test, **p<0.01, *p<0.05).*

Altogether, our results show that constitutively active BES1 confers consistent tolerance to β-cc and β-ion (based on hypocotyl elongation data across hormonal and light-promoting contexts). This interaction underscores BES1 as a critical point of interception for specific apocarotenoid signals, especially under diverse light conditions.

5.1.3 Apocarotenoids differentially control cell elongation along the hypocotyl in WT and *bes1-D* seedlings

To complement the hypocotyl elongation assays described above, we next sought to dissect the spatial nature of apocarotenoid-mediated growth regulation in WT (Col-0) and *bes1-D* hypocotyls. While total hypocotyl length provides an integrated readout of elongation, it does not reveal

whether the effect of apocarotenoid or BR signaling is uniform along the hypocotyl axis or if specific cell populations are differentially affected (Pastor-Andreu *et al.*, 2024). We therefore addressed three related questions: (1) Is the repression triggered by β-cc and β-ion homogeneous across all hypocotyl cells, or are some regions more strongly affected than others? (2) Do β-cc and β-ion display distinct spatial patterns of action, potentially targeting different regions along the hypocotyl? (3) In the case of the *bes1-D* mutant, is the observed tolerance to airborne apocarotenoids in light-grown conditions due to a complete absence of repression at the cellular level, or does it result from a redistribution of cell elongation along the axis?

To address these questions, WT Col-0 and mutant *bes1-D* seedlings were grown for 2 days under W, after which airborne apocarotenoid treatments were initiated as plates were transferred to either low W or W+FR for 5 additional days. Samples were taken after 3 (2+1) and 7 (2+5) days from germination. Seedlings grown under W for the whole 7-day experiment were used as basal elongation controls. To analyze cell length in the hypocotyls of harvested seedlings, cotyledons and roots were removed, and hypocotyls were fixed in paraformaldehyde (PFA) under vacuum infiltration, followed by washing in ClearSee solution for at least one week. Samples were then stained with Calcofluor White, mounted on glass slides, and imaged using a confocal microscope (Fig. 5.7). For each treatment, at least five hypocotyls were processed and imaged. The resulting images (a representative one is shown in Fig. 5.S6) were post-processed for optimal visualization and used for cell length quantification along the hypocotyl axis.

To establish a reference for basal elongation, we first examined the hypocotyl cell length profiles of W-grown Col-0 seedlings (Fig. 5.7). At day 3, all hypocotyl cells showed a quite similar length, but the longest cells were located in the basal region near the root–hypocotyl junction (Fig. 5.7). These basal cells showed little further elongation between day 3 and day 7, a period in which growth occurred mainly in the central portion of the hypocotyl (Fig. 5.7). Next, we analyzed hypocotyl cell length in Col-0 seedlings that elongated under low W with or without apocarotenoids (Fig. 5.7). Elongation of mock-treated seedlings was mainly supported by growth of cells from the central region of the hypocotyl (cells at positions 6 to 17), with two peaks observed for cells at positions 10-12 and 15-16. A

clear repression of cell elongation in this central region was observed in response to both β-ion and β-cc, which also inhibited cell growth in the apical region (positions 18-20) but had no effect in the basal cells (positions 1-4) of the hypocotyl (Fig. 5.7). No clear differences were detected between the effect of β-ion and β-cc in the spatial repression profile, even though the β-ion treatment was more efficient to repress growth in the central region (Fig. 5.7). In contrast to the Col-0 WT, elongation of *bes1-D* seedlings under low W was mainly supported by growth of cells in the apical region of the hypocotyl, with a decreasing contribution in a basipetal pattern (Fig. 5.7). The cell elongation profile of β-ion- and β-cc–treated seedlings was overlapping closely with the mock control, consistent with the lack of growth-repressing activity of these apocarotenoids (Fig. 5.7).

When seedlings were grown under simulated shade (W+FR), hypocotyl elongation was strongly promoted compared to low W, with cell length profiles showing higher values across the axis (Fig. 5.7). The growth distribution profile was also different, as the second peak of maximum growth observed under low W at positions 15-16 was missing in seedlings exposed to W+FR. Under both light treatments, however, apocarotenoids mainly reduced growth in the central and apical regions, with β-ion exerting a stronger repressive effect than β-cc (Fig. 5.7).

To directly compare light-driven promotion of elongation with apocarotenoid-mediated repression, we calculated cell length differences relative to DMSO and/or W controls (Fig. 5.8). Under low W, the elongation normally promoted by light [$DMSO_{low\ W} - DMSO_{w}$] was completely offset by both β-ion and β-cc [$DMSO_{low\ W} - \beta\text{-cc/}\beta\text{-ion}_{low\ W}$], resulting in profiles that overlapped with the basal W condition (Fig. 5.8, top). In contrast, under W+FR, elongation was more strongly promoted, and although β-ion and β-cc reduced cell lengths, the repression did not fully counteract the FR-induced growth condition (Fig. 5.8, bottom). The effect was particularly pronounced for β-ion, which exerted a stronger repression than β-cc, yet still failed to restore basal W levels.

Altogether, these analyses show that (1) the repression of elongation triggered by β-cc and β-ion is not homogeneous across all hypocotyl cells but it is stronger in the most actively growing cells, inhibiting promoted elongation without affecting basal growth, (2) β-cc and β-ion display similar spatial patterns of action, and (3) the observed tolerance of the *bes1-D*

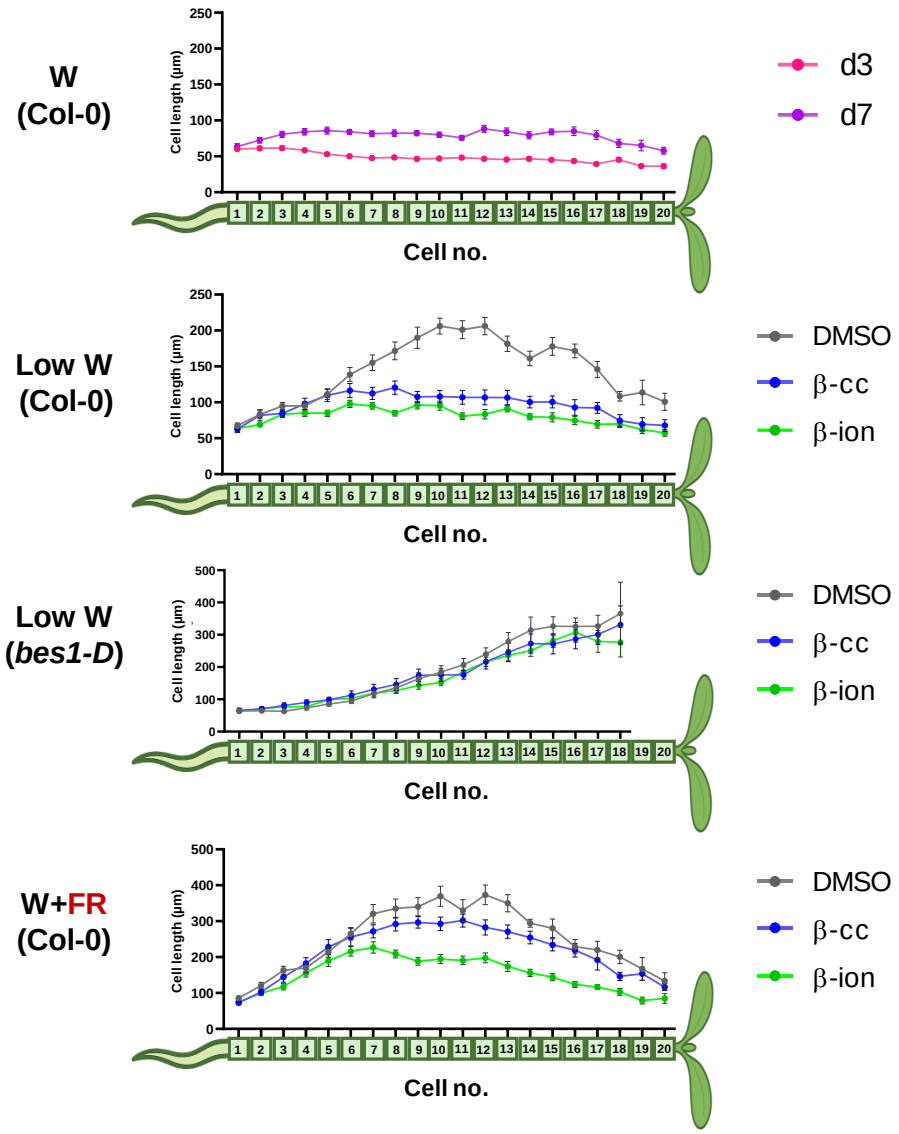

Figure 5.7 — Absolute cell length distribution along the hypocotyl axis of seedlings exposed to different light and apocarotenoid treatments. *Hypocotyls were divided up to 20 (cells) from the root–hypocotyl junction (cell 1, left) to the cotyledons (up to cell 20, right). From top to bottom: Col-0 seedlings grown under W (48 µmol·m^{-2}·s^{-1} R:FR = 4.5) for 3 (light purple) or 7 days (dark purple); Col-0 and bes1-D (only 18 cells could be measured in this case) seedlings grown under low W (28 µmol·m^{-2}·s^{-1} R:FR = 4.5) with DMSO (Control, in grey), β-ion (in green), or β-cc (in blue); Col-0 seedlings grown under W+FR (48 µmol·m^{-2}·s^{-1}, R:FR = 0.15) with DMSO (Control, in gray), β-ion (in green), or β-cc (in blue). Data represent mean cell length ± SE (n ≥ 15; at least five hypocotyls per treatment and three measurements per hypocotyl).*

mutant to airborne apocarotenoids is due to the absence of growth response of elongating cells but not to a redistribution of cell elongation along the axis.

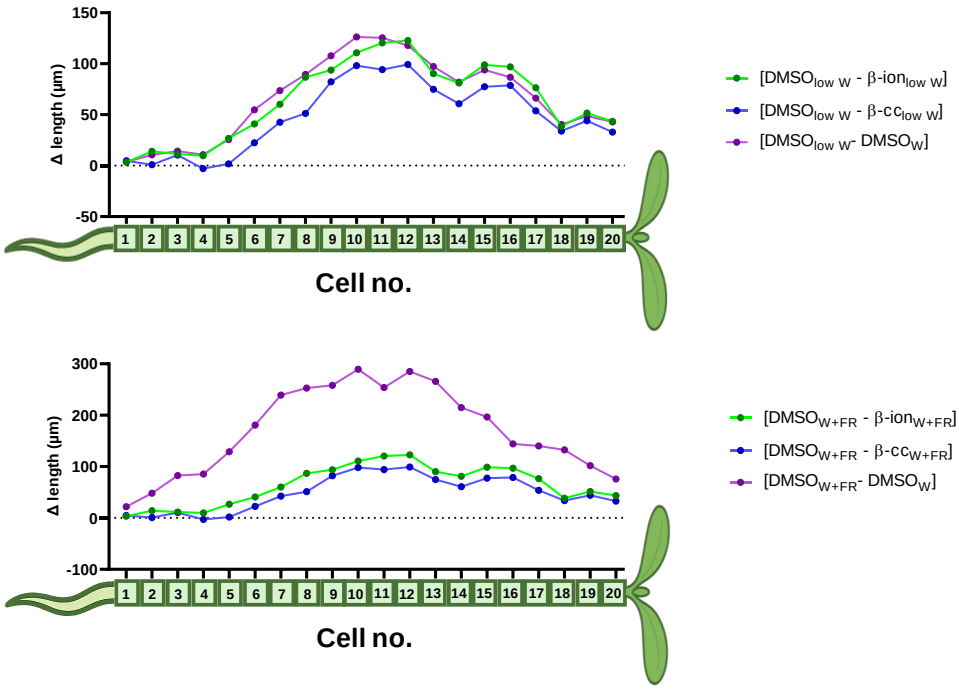

Figure 5.8 — Differences in Col-0 cell length profiles along the hypocotyl axis under apocarotenoid treatments. *Hypocotyls were divided into 20 bins from the root–hypocotyl junction (bin 1, left) to the cotyledons (bin 20, right). On top, differences between cell lengths of DMSO-treated low-W grown seedlings with those treated with β-ion under low W (in green), with β-cc under low W (in blue) and with those treated with DMSO under W (in purple). On the bottom, cell lengths of DMSO-treated W+FR grown seedlings with those treated with β-ion under W+FR (in green), with β-cc under W+FR (in blue) and with those treated with DMSO under W (in purple).*

5.2 Candidates for binding β-ion and transduce the signal to BES1

5.2.1 Identification of candidate proteins

A strategy to investigate the connection between β-ion perception and BR signaling was to screen the list of proteins found to bind this apocarotenoid (Table 4.S2) to look for proteins with a known role in hormone signaling

and light-regulated cell elongation. Among them, we identified the scaffold protein RACK1A (Receptor for Activated C Kinase 1A) (Table 4.S2). RACK1A belong to a small multigene family in *A. thaliana*, comprising three highly homologous isoforms — RACK1A, RACK1B, and RACK1C. While all three share high sequence identity and overlapping functionalities, RACK1A is the most abundantly expressed. RACK1 proteins serve as integrative hubs for diverse signal transduction pathways (Su *et al.*, 2015) .RACK1A mediates responses to several hormones, including brassinosteroids, gibberellins and auxins (J.-G. Chen, 2006). Loss of RACK1A has been shown to impact seed germination (Fennell *et al.*, 2012), hypocotyl elongation (Fu *et al.*, 2024), photosynthesis (Kundu *et al.*, 2013), and defense through MAPK pathway (Cheng *et al.*, 2015), which are processes that we found modulated by apocarotenoid treatments, particularly β-ion. Moreover, RACK1A has reported physical/functional connections to key regulators in this study, including BES1/BZR1 and phyB (Z. Li *et al.*, 2023; W. Zhu *et al.*, 2024). Interestingly, 13 of the proteins known to interact with RACK1A (a total of 295 are found in the *BioGRID* protein-protein interaction platform) are also able to bind β-ion in iTSA assays (Fig. 5.S7), and in-silico docking revealed a good fit for β-ion in the center of the RACK1A pocket (Fig. 5.S8). Taken together, the multifunctional role of RACK1A at the crossroads of hormone and light signaling, and its potential capacity to bind β-ion or/and interact with other proteins that bind this apocarotenoid, make it a plausible mediator of apocarotenoid (β-ion) responses.

5.2.2 RACK1A-defective mutants show unaltered response to apocarotenoids

To experimentally assess whether RACK1A participates in the apocarotenoid signaling pathways responsible for the observed effects, we used three RACK1-defective mutant genotypes in the Col-0 background: single *rack1a* (*rack1a-2* allele), double *rack1a rack1b* (hereinafter referred to as *rack1ab*), and double *rack1b rack1c* (hereinafter referred to as r*ack1bc*), a kind gift from Stéphanie Robert (Ma *et al.*, 2024). To ensure that RACK1A participates in orchestrating light-mediated hypocotyl elongation, we initially performed a screening across different W intensities to compare our RACK1 mutant lines' growth patterns with those reported previously (Fu *et al.*, 2024). In that work, RACK1A was described as a

positive regulator of hypocotyl elongation under all tested light conditions: any loss-of-function mutant showed reduced elongation, whereas overexpressing RACK1A lines promoted growth relative to controls. We used different light conditions that mimic some of the ones used in that article to confirm RACK1A role on hypocotyl elongation. Seeds from Col-0 and the mutants *rack1a-2*, *rack1ab* and *rack1bc* were sowed, vernalized, and grown for 4 days under different light intensities, ranging from D (0 µmol m^{-2} s^{-1}) to W (54 µmol m^{-2} s^{-1}). The growth measurements of mutant seedlings were plotted against Col-0 hypocotyl elongation (Fig 5.9). Our RACK1-defective mutant lines matched the same reported behavior under D conditions: reduced elongation in RACK1A-deficient mutants, with no or little impact in the case of *rack1bc*. However, under several low W intensities we observed the opposite of the published trend: surprisingly, *rack1a-2* and *rack1ab* elongated more than Col-0 (Fig. 5.9).

Figure 5.9 — Hypocotyl elongation of RACK1-defective mutants across white light intensities. *Col-0 (in grey), rack1a-2 (in blue), rack1ab (in orange), and rack1bc (in red) seedlings were grown for 4 days under darkness (D, 0 µmol·m⁻²·s⁻¹) or increasing intensities of W (PPFD = 6–54 µmol·m⁻²·s⁻¹). Statistical significance was assessed by two-way ANOVA followed by Sidak's multiple comparisons test. Asterisks denote significant differences compared to DMSO (*p<0.05, **p<0.01).*

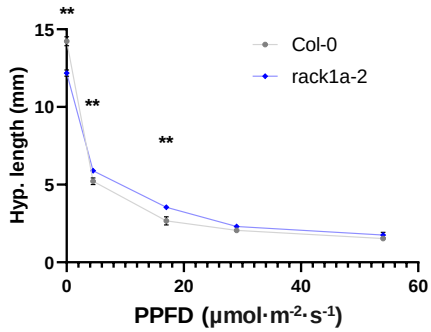

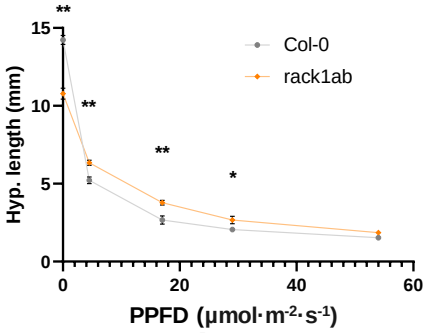

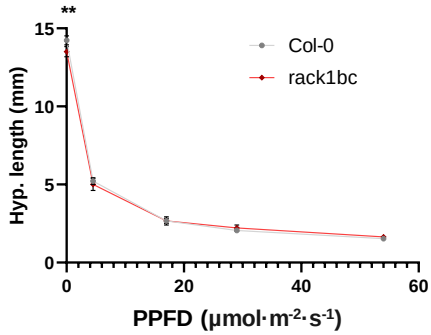

Despite the surprising behavior of the mutants, we decided to proceed with the analysis of their sensitivity to airborne apocarotenoid treatments. First, we evaluated their germination performance in the presence of β-cc or β-ion. Although the germination-repressing effect among apocarotenoids is exclusive to β-cc (Fig. 3.6), and no clear evidence supports β-cc binding to RACK1A, the involvement of RACK1A in germination control made it a relevant target for investigation.

Seeds were sown on plates, subjected to stratification, and subsequently grown either under W or darkness (D) conditions in the presence or absence of apocarotenoids. Germination was monitored as in section 3.4, using radicle emergence as the criterion for completion. For each condition, the proportion of germinated seeds was calculated over time and plotted to visualize the progression of germination (Fig. 5.10).

Germination assays in Col-0, *rack1a-2, rack1ab*, and *rack1bc* mutants under W and D conditions revealed a consistent pattern across genotypes (Fig 5.10). Among the apocarotenoids tested, only β-cc reproducibly delayed and reduced germination, whereas β-ion had no detectable impact. Differences between genotypes were observed regardless of treatment, with *rack1a-2* and especially *rack1ab* displaying lower basal germination rates (Fig. 5.S8), consistent with the known role of RACK1A in seed germination (Fennell *et al.*, 2012). However, the magnitude of β-cc–induced inhibition was comparable across all genotypes and light conditions (Fig. 5.10), indicating that the repression mechanism triggered by β-cc is independent of RACK1-mediated signaling.

To next assess whether RACK1A was implicated in β-cc or β-ion growth inhibition, the same set of RACK1 mutants (*rack1a-2, rack1ab, rack1bc*) were used. After stratification, plates either stayed in D for 4 days (etiolated seedlings) or were transferred for 2 days to W before applying the apocarotenoids and subsequently transferring them to low W or W+FR treatments for the next 5 days (photomorphogenic seedlings). The hypocotyl elongation measurements indicated that loss of RACK1 isoforms has an impact in D conditions, as all three mutants showed shorter hypocotyls, with *rack1a-2* showing the strongest effect (Figs. 5.11, 5.S10). When comparing apocarotenoid treatments, β-cc (applied on d0, immediately after the stratification) caused germination arrest in all genotypes under D, precluding hypocotyl measurements (Fig. 5.11). β-ion reduced elongation in D to a similar extent across WT and mutant

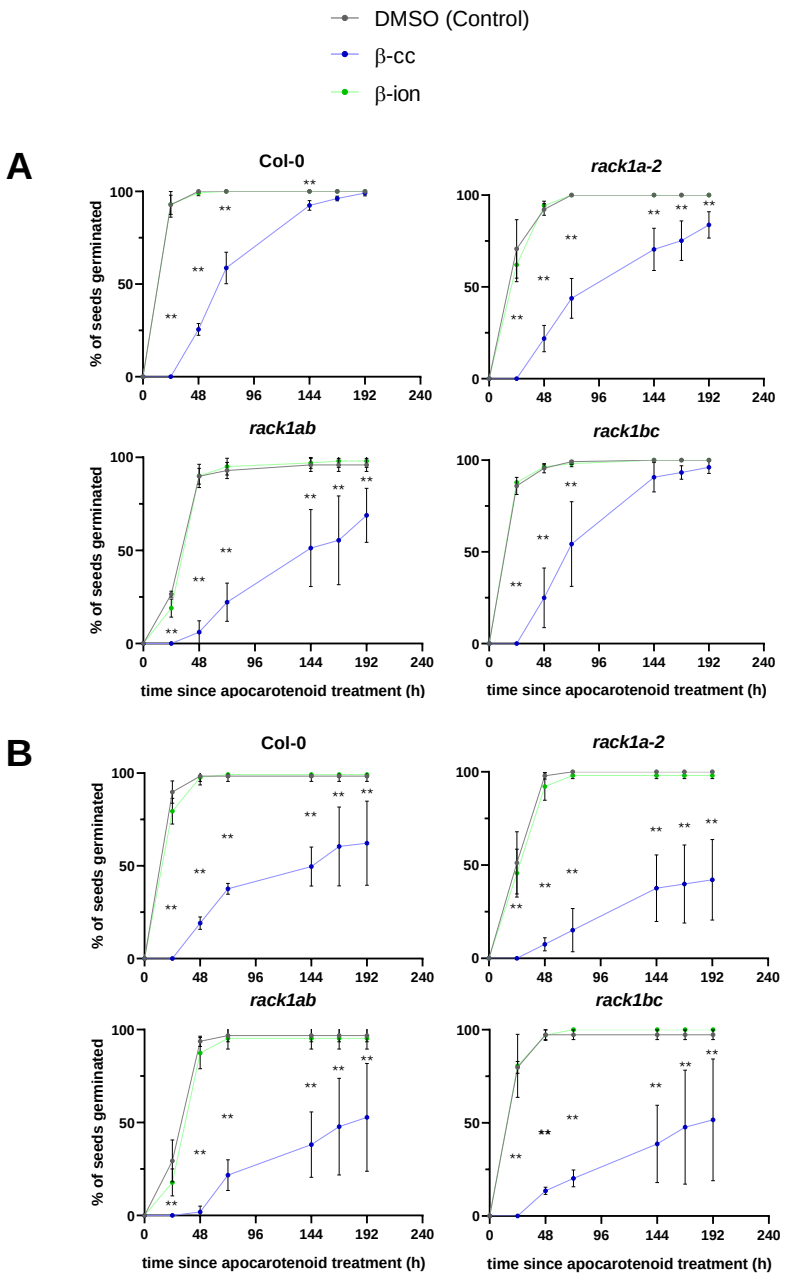

Figure 5.10 — Germination of RACK1-defective mutants exposed to airborne apocarotenoids. *Germination time courses are shown for Col-0, rack1a-2, rack1ab, and rack1bc under white light (A) or under darkness (B) conditions, in the presence of DMSO (Control, in grey), β-cc (in blue), or β-ion (green). Statistical significance was assessed by two-way ANOVA followed by Dunnett's multiple comparisons test. Asterisks denote significant differences compared to DMSO (*p<0.05, **p<0.01).*

genotypes, indicating no major role for RACK1 paralogs in β-ion signaling under these conditions. Under low W, most mutants elongated similarly to Col-0 (except for *rack1ab*), making it unclear whether RACK1A plays a consistent role in hypocotyl elongation in these conditions (Fig. 5.11). Under low W and W+FR, both apocarotenoids inhibited elongation in all genotypes, with two exceptions: *rack1ab* appeared hypersensitive to β-ion only under W+FR, and *rack1bc* showed tolerance (hyposensitivity) to β-cc under low W and hypersensitive to β-cc only under W+FR (Figs. 5.11, 5.9).

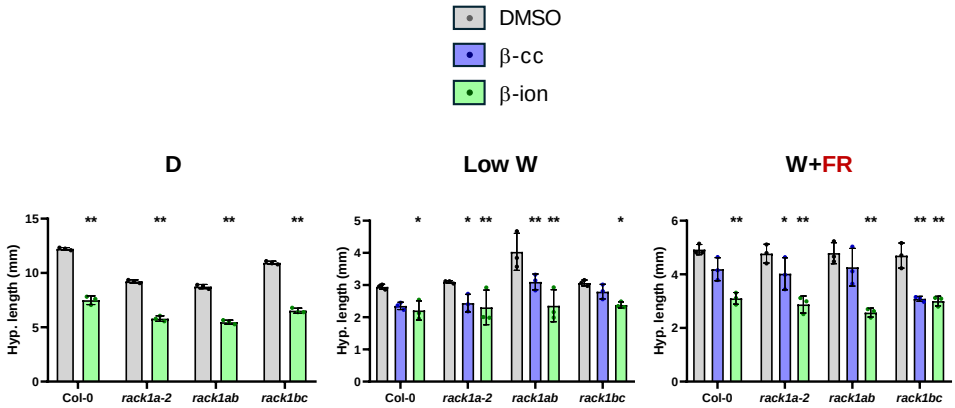

Figure 5.11 — Role of RACK1A in hypocotyl elongation under apocarotenoid treatments. *Hypocotyl lengths of Col-0, rack1a-2, rack1ab, and rack1bc seedlings grown under D (left), low W (center) or W+FR (right), and treated with DMSO (Control, in grey), β-cc (in blue), or β-ion (in green). Bars represent mean ± SD of three biological replicates. Statistical significance was assessed by two-way ANOVA followed by Dunnett's multiple comparisons test. Asterisks denote significant differences compared to DMSO (*p<0.05, **p<0.01).*

5.2.3. BIN2-binding proteins

To more specifically focus on potential components upstream of BES1 that might participate in the β-ion response, we next compared the set of proteins identified as putative β-ion interactors (Table 4.S2) with a list of reported interactors of BR signaling components, ranging from the receptor BRI1 to the BIN2 kinase that phosphorylates and destabilizes BES1 (Fig. 5.S11-A). This analysis only obtained overlapping hits in the case of BIN2, likely because a much higher number of proteins are listed

as BIN2 interactors compared to those known to bind other components of the BR signaling pathway (Fig. 5.S11-B). In particular, 9 proteins were found to be listed as β-ion and BIN2 interactors (Fig. 5.12), which may represent candidate mediators linking β-ion perception with BIN2 activity.

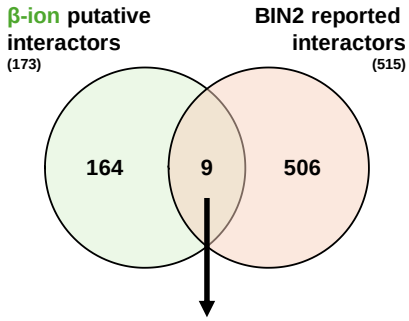

Accession number	Gene ID	Annotation / Gene description
AT1G09070	**SRC2**	SRC2 specifically binds the peptide PIEPPPHH; and moves from ER to a vacuole fraction where it gets internalized. Involved in Protein Storage Vacuole targeting. The mRNA is cell-to-cell mobile.
AT1G51710	**UBP6**	Ubiquitin-specific protease 6 (UBP6). Deubiquinating enzyme. Interacts with calmodulin.
AT2G37040	**PAL1**	Encodes PAL1; a phenylalanine ammonia-lyase. Arabidopsis has four PALs: AT2G37040 (PAL1); AT3G53260 (PAL2); AT5G04230 (PAL3) and AT3G10340 (PAL4).
AT3G44110	**ATJ3**	Homologous to the co-chaperon DNAJ protein from E coli. Member of the HSP40 family. Interacts with HSP70-4(AT3G12580) to mediate heat shock response. Formation of HSGs is dependent on the farnyslation status of J3.
AT4G32760	**TOL9**	Encodes a member of the Arabidopsis TOL (TOM1-LIKE) family of ubiquitin binding proteins that acts redundantly in the recognition and further endocytic sorting of a PIN-FORMED (PIN)-type auxin carrier protein at the plasma membrane; modulating dynamic auxin distribution and associated growth responses.
AT4G33580	**BCA5**	Encodes a putative beta-carbonic anhydrase. Expressed at lower levels than other gene family members. Mutants display stunted growth in normal CO2 environments.
AT4G35450	**AKR2**	A molecular chaperone that binds to the transmembrane domains of interacting proteins to prevent aggregation and direct them to the right location after translation.Involved in targeting of chloroplast outer membrane proteins to the chloroplast. Double mutants of AKR2A and the highly homologous AKR2B have yellow leaves; significantly reduced chloroplast proteins; and no thylakoid membranes.
AT5G42950	**EXA1**	EXA1 is a GYF domain-containing gene of the SMY2 subgroup. Mutants exhibit resistance to potexviruses.
AT5G62000	**ARF2**	Encodes an auxin response factor. Mutants have many defects including enlarged rosette leaves; reduced fertility; later senescence; hypocotyl elongation defects; enlarged seeds and enlarged cotyledons. May not mediate auxin effects. Increase in seed size due to increased cell proliferation. The mRNA is cell-to-cell mobile.

Figure 5.12 — Venn diagram showing the overlap between proteins identified as putative interactors of β-ion (left, green) and reported BIN2 interactors (right, orange). *A total of nine proteins were common to both datasets, representing candidate elements potentially linking β-ion binding with BIN2 activity (description in table below).*

Supplemental Information

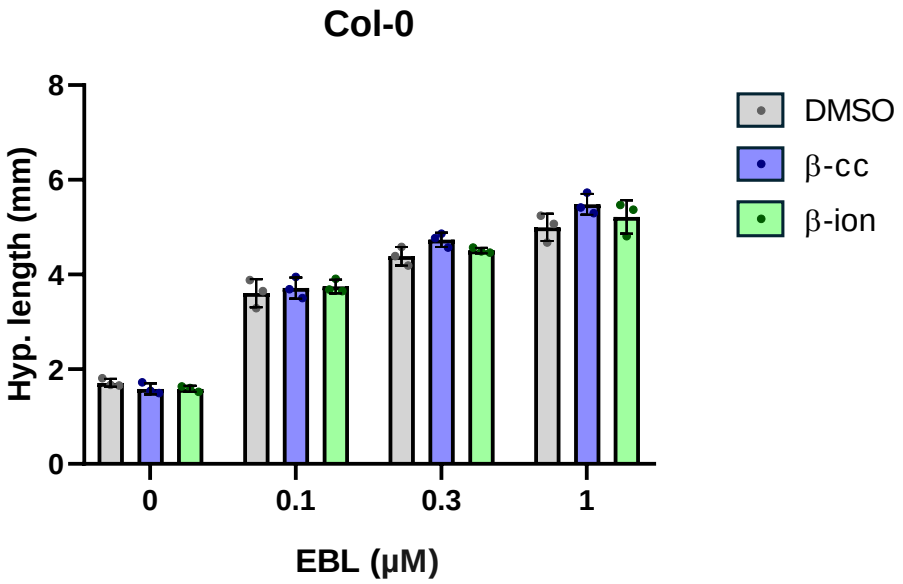

Figure 5.S1 — Hypocotyl elongation of seedlings grown under different EBL concentrations upon exposure to airborne apocarotenoids. *Hypocotyl length of A. thaliana W-grown seedlings exposed to airborne DMSO (Control, in grey), β-cc (10 µL of 500 mM, in blue) or β-ion (10 µL 100 mM, in green) in the presence of different doses of brassinosteroids (EBL) applied to the growth media. W provided a PPFD of 49 µmol·m^{-2}·s^{-1}. Bars represent the mean ± SD of three biological replicates. A two-way ANOVA followed by Dunnett's multiple comparisons test did not provide statistical differences across treatments.*

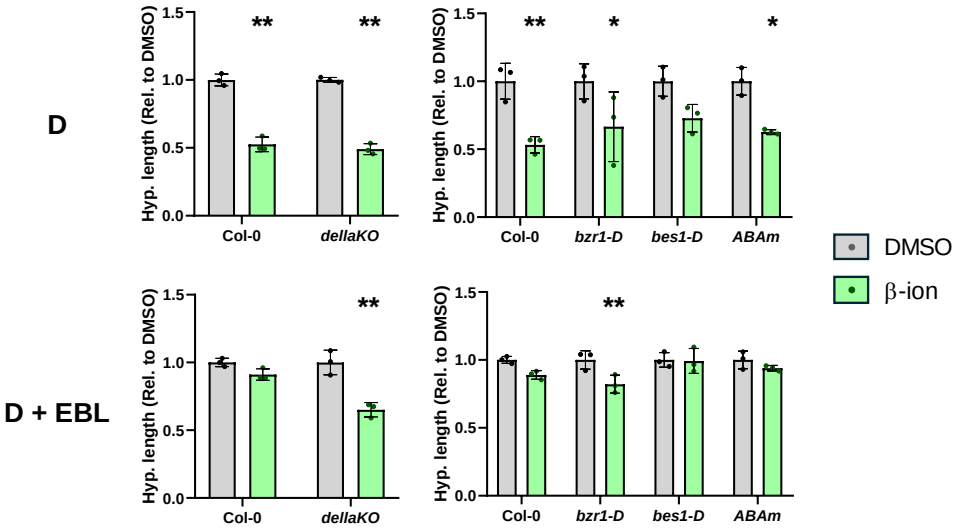

Figure 5.S2 — Relative hypocotyl elongation of hormone-related mutant D-grown seedlings exposed to airborne β-ion. *A. thaliana Col-0 and hormone-related mutants (dellaKO, bzr1-D, bes1-D, ABAm) seedlings were grown in D (top) or D+EBL (bottom), exposed to airborne β-ion (in green) or DMSO (Control, in grey). Relative elongation was calculated by normalizing hypocotyl length of treated seedlings to their respective DMSO controls. Bars represent the mean ± SD of three biological replicates. Asterisks indicate significant differences compared to DMSO (two-way ANOVA followed by Dunnett's multiple comparisons test, **p<0.01, *p<0.05).*

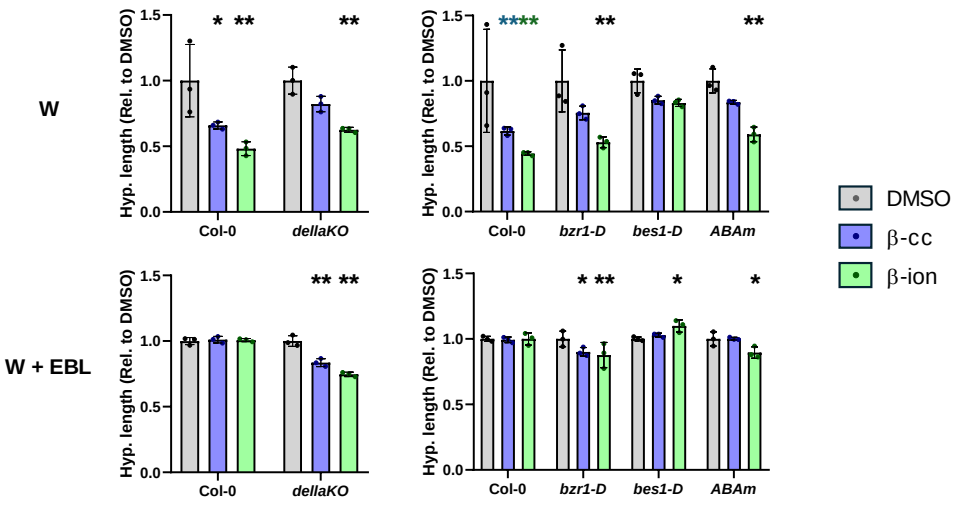

Figure 5.S3 — Relative hypocotyl elongation of hormone-related mutant W-grown seedlings exposed to airborne apocarotenoids. *A. thaliana Col-0 and hormone-related mutants (dellaKO, bzr1-D, bes1-D, ABAm) seedlings were grown under W (top) or W+EBL (bottom), exposed to airborne β-cc (in blue), β-ion (in green) or DMSO (Control, in grey). Relative elongation was calculated by normalizing hypocotyl length of treated seedlings to their respective DMSO controls. Bars represent the mean ± SD of three biological replicates. Asterisks indicate significant differences compared to DMSO (two-way ANOVA followed by Dunnett's multiple comparisons test, **p<0.01, *p<0.05).*

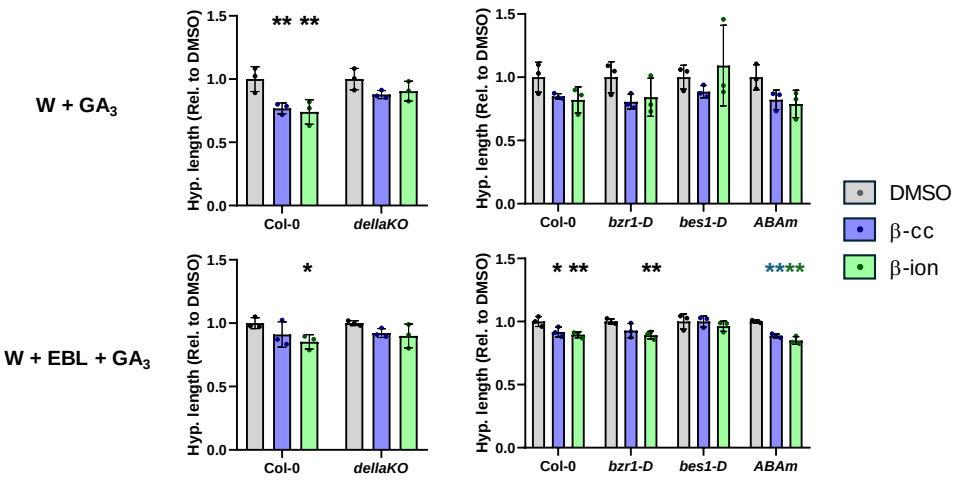

Figure 5.S4 — Relative hypocotyl elongation of hormone-related mutant W-grown seedlings exposed to airborne apocarotenoids. *A. thaliana Col-0 and hormone-related mutants (dellaKO, bzr1-D, bes1-D, ABAm) seedlings were grown under W+GA$_3$ (top) or W+EBL+GA$_3$ (bottom), exposed to airborne β-cc (in blue), β-ion (in green) or DMSO (Control, in grey). Relative elongation was calculated by normalizing hypocotyl length of treated seedlings to their respective DMSO controls. Bars represent the mean ± SD of three biological replicates. Asterisks indicate significant differences compared to DMSO (two-way ANOVA followed by Dunnett's multiple comparisons test, **p<0.01, *p<0.05).*

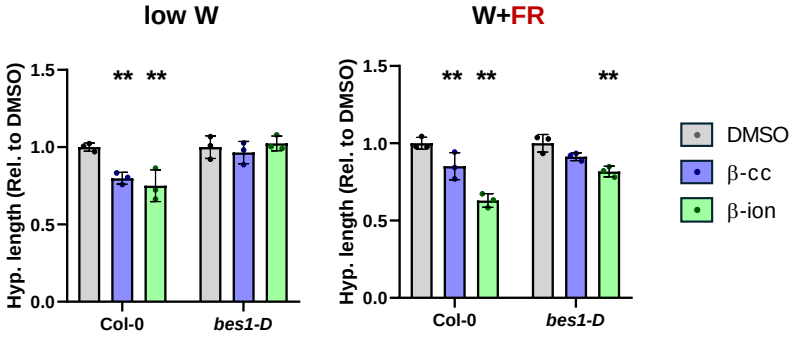

Figure 5.S5 — Relative hypocotyl elongation of Col-0 and bes1-D A. thaliana seedlings exposed to airborne apocarotenoids under different light conditions*. A. thaliana Col-0 and bes1-D seedlings were grown under low W (left) or W+FR (right), exposed to airborne β-cc (in blue), β-ion (in green) or DMSO (Control, in grey). Relative elongation was calculated by normalizing hypocotyl length of treated seedlings to their respective DMSO controls. Bars represent the mean ± SD of three biological replicates. Asterisks indicate significant differences compared to DMSO (two-way ANOVA followed by Dunnett's multiple comparisons test, **p<0.01, *p<0.05).*

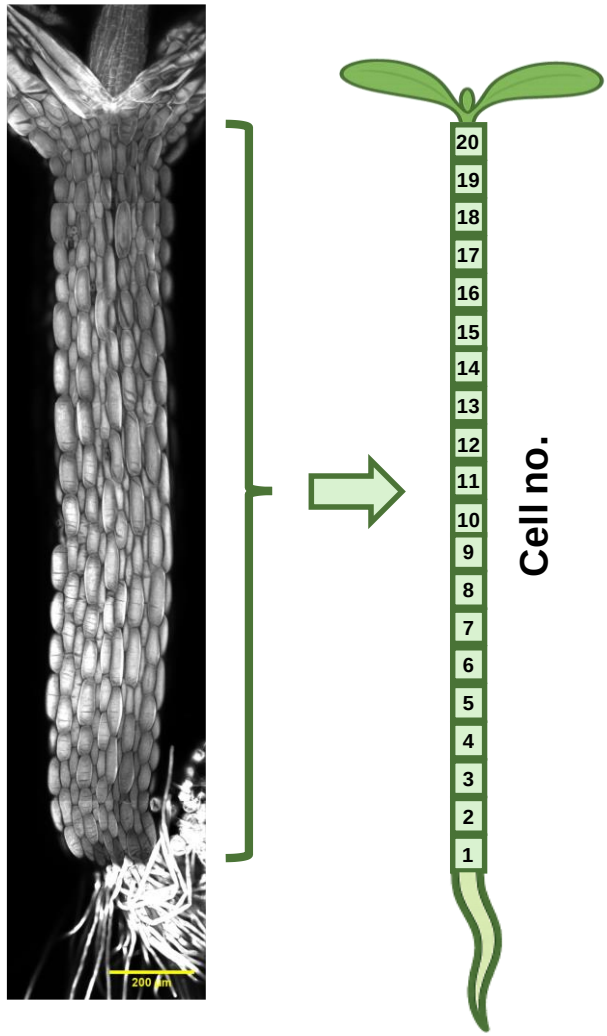

Figure 5.S6 — Representative confocal image of a Calcofluor-white-dyed seedling (left). *Cells in the epidermis are colored in white, and the bottom and top edges of each cell, starting with from the radical meristem (Cell no. 1) to the apical meristem (up to Cell no. 20) are used to measure cell length along the hypocotyl. A schematic diagram of a hypocotyl is later used to illustrate the hypocotyl axis.*

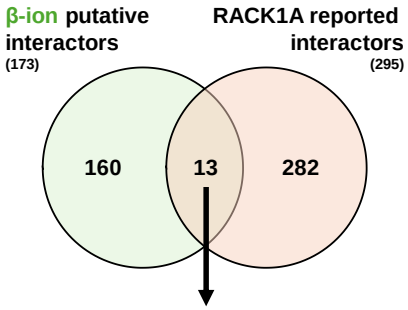

Accession number	Gene ID	Annotation / Gene description
AT1G09070	**SRC2**	SRC2 specifically binds the peptide PIEPPPHH; and moves from ER to a vacuole fraction where it gets internalized. Involved in Protein Storage Vacuole targeting. The mRNA is cell-to-cell mobile.
AT1G12050	**FAH**	Encodes a fumarylacetoacetase that converts fumarylacetoacetate to acetoacetate and fumarate and is likely to be involved in tyrosine catabolism.
AT1G29880	**CLSC12**	glycyl-tRNA synthetase / glycine-tRNA ligase;(source:Araport11)
AT1G31230	**AK-HSDH1**	Encodes a bifunctional aspartate kinase/homoserine dehydrogenase. These two activities catalyze the first and the third steps toward the synthesis of the essential amino acids threonine; isoleucine and methionine.
AT1G31330	**PSAF**	Encodes subunit F of photosystem I.
AT1G78570	**RHM1**	Encodes a UDP-L-Rhamnose synthase involved in the biosynthesis of rhamnose; a major monosaccharide component of pectin. Catalyzes the conversion of UDP-D-Glc to UDP-L-Rha. The dehydrogenase domain of RHM1 was shown to catalyze the conversion of UDP-D-Glc to the reaction intermediate UDP-4-keto-6-deoxy-D-Glc using recombinant protein assay but the activity of the full-length protein was not determined as it could not be expressed in E. coli.
AT2G23610	**MES3**	Encodes a protein shown to have carboxylesterase activity; methyl IAA esterase activity; and methyl jasmonate esterase activity in vitro. This protein does not act on methyl salicylate; MeGA4; or MEGA9 in vitro.
AT2G27450	**NLP1**	Encodes N-carbamoylputrescine amidohydrolase that is involved in putrescine and polyamine biosynthesis.
AT3G23400	**FIB4**	Encodes FIBRILLIN 4 (FIB4). The fibrillins are a large family of chloroplast proteins that have been linked with stress tolerance and disease resistance. FIBRILLIN 4 is required for plastoglobule development and stress resistance.Iinvolved in plastoquinone transport.
AT3G44110	**ATJ3**	Homologous to the co-chaperon DNAJ protein from E coli. Member of the HSP40 family. Interacts with HSP70-4(AT3G12580) to mediate heat shock response. Formation of HSGs is dependent on the farnyslation status of J3.
AT4G20860	**BBE22**	involved in the generation of H2O2 from reduced compounds
AT5G16710	**DHAR3**	DHAR3 protein undergoes thiolation following treatment with the oxidant tert-butylhydroperoxide.Encodes 30-40% of extractable leaf GSH-dependent DHAR activity. Single knockout mutants show unaltered ascorbate and glutathione status in optimal and oxidative stress conditions.Makes a minor contribution to glutathione oxidation in response to increased intracellular hydrogen peroxide (catalase deficiency) (PMID:28381499).
AT5G18170	**GDH1**	Encodes the 43 kDa alpha-subunit of the glutamate dehydrogenase with a putative mitochondrial transit polypeptide and NAD(H)- and alpha-ketoglutarate-binding domains. Mitochondrial localization confirmed by subcellular fractionation. Combines in several ratios with GDH2 protein (GDH-beta) to form seven isoenzymes. Catalyzes the cleavage of glycine residues. May be involved in ammonia assimilation under conditions of inorganic nitrogen excess. The enzyme is almost exclusively found in the mitochondria of stem and leaf companion cells.

Figure 5.S7 — Overlap between β-ion interactors identified in the proteomic screen and reported interactors of RACK1A. *Venn diagram shows the number of unique proteins in each dataset and the 13 shared candidates.*

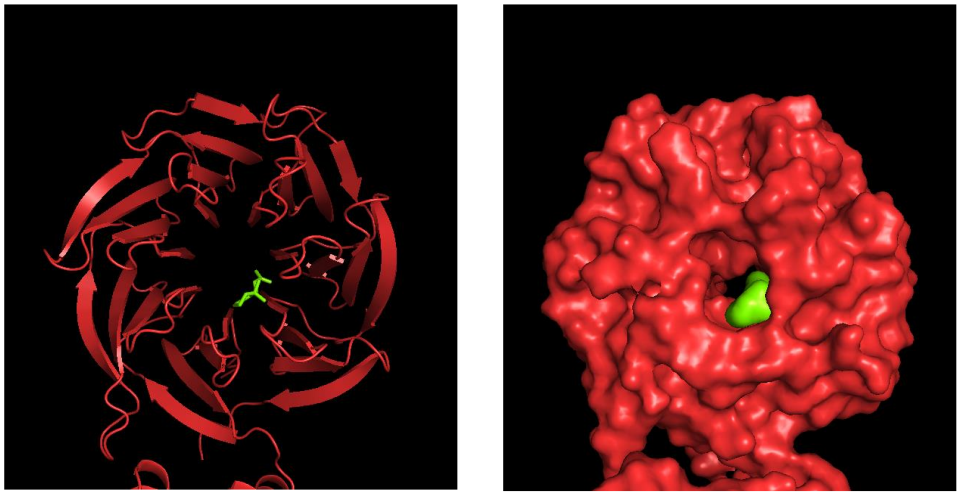

Figure 5.S8 — In silico docking of β-ion with RACK1A. *Left, ribbon representation of the RACK1A structure (red) showing β-ionone bound within a central cavity (green). Right, surface representation highlighting the same binding pocket. Docking simulations were performed with AutoDock Vina and visualized with PyMol.*

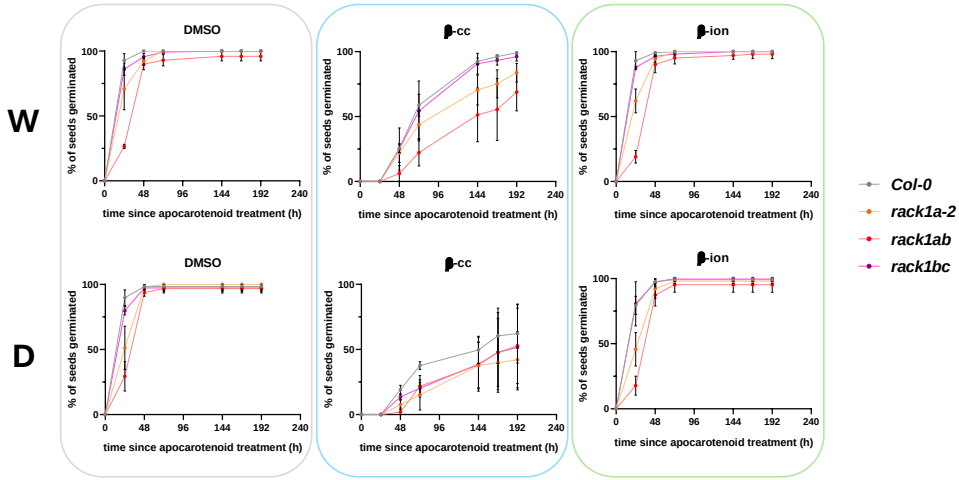

Figure 5.S9 — Germination of Col-0 and RACK1 mutant genotypes grouped by treatment. *Germination time courses under D and W are shown for DMSO (control), β-ion, and β-cc treatments. Across all treatments, rack1a-2 and rack1ab exhibited reduced basal germination compared to Col-0 and rack1bc, consistent with the role of RACK1A in seed germination. The inhibitory effect of β-cc was comparable across genotypes, while β-ion had no detectable impact.*

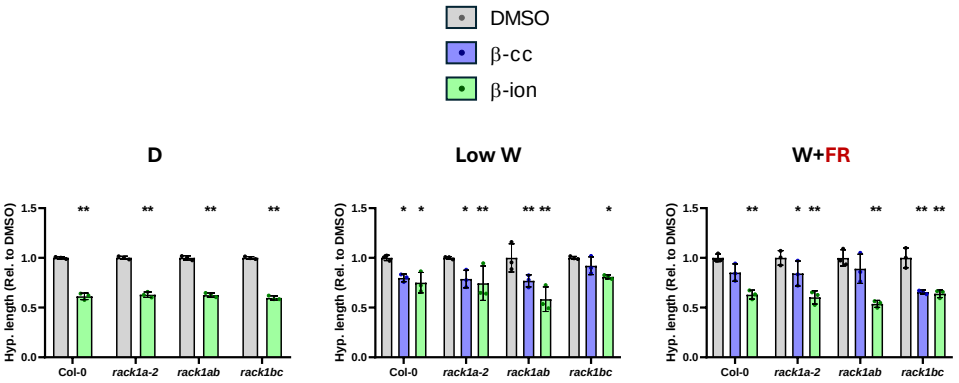

Figure 5.S10 — Relative hypocotyl elongation of RACK1A mutants under apocarotenoid treatments. *Relative hypocotyl lengths (compared to DMSO) of Col-0, rack1a-2, rack1ab, and rack1bc seedlings grown for 7 days under D (left), low W (center) or W+FR (right), treated with DMSO (Control, in grey), β-cc (in blue), or β-ion (in green). Hypocotyl elongation of seedlings exposed to β-cc in the dark could not be measured due to germination issues. Bars represent mean ± SD of three biological replicates. Statistical significance was assessed by two-way ANOVA followed by Dunnett's multiple comparisons test. Asterisks denote significant differences compared to DMSO (*p<0.05, **p<0.01).*

A

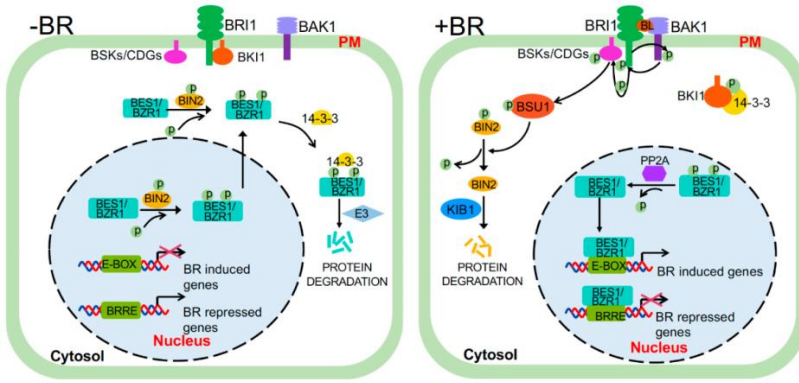

B

BR signaling element	Number of reported interactors
BRI1	45
BAK1	71
BSK1	10
CDG1	6
BKI1	1
BSU1	4
BIN2	515
BES1	30
BZR1	84

Figure 5.S11 — (A) Schematic representation of brassinosteroids signaling pathway, taken from Mao & Li, 2020. *Perception from brassinosteroids (BL) by BRI1 (via BAK1 recruiting) induces a phosphorylation cascade involving BSKs and CDGs that phosphorylates BSU1, a phosphatase that becomes active and dephosphorylates BIN2, leading to degradation to this protein. BIN2 is then unable to phosphorylate BES1 and BZR1, the main transcription factors that, when non-phosphorylated, accumulate in the nucleus and regulate the expression of different brassinosteroid responsive elements (BRRE).* ***(B) Table containing the number of reported interactors of different brassinosteroid (BR) signaling elements (shown in A), obtained from the BioGRID protein-protein interaction platform.***

Discussion

Discussion

Plants, as sessile organisms, rely on complex signaling networks to perceive and respond to nearby vegetation. Light and volatile organic compounds (VOCs) are central cues to integrate this developmental regulation. While the role of light quality—particularly reduced red to far-red ratios (low R:FR)—in triggering acclimation responses such as shade avoidance syndrome (SAS) is well established, that of other components such as VOCs remains less explored. In this thesis, we addressed this gap through integrated physiological, chemical, and molecular analyses. Our findings show that, even without major shifts detected in global VOC profiles, plants exposed to simulated proximity shade (W+FR, low R:FR) emit volatiles that are able to impact gene expression and alter development of nearby non-shaded plants. Our results further unveil specific apocarotenoids—β-ionone and β-cyclocitral— as biologically meaningful signals in the shade volatilome regulating key physiological processes in neighboring plants. In the following sections, these findings will be discussed within the broader context of plant–plant communication.

Plants speak in fragrant volatiles: the response to proximity shade

The discovery that reduced R:FR ratios can specifically shape VOC emissions (Ballaré & Pierik, 2017; Ninkovic *et al.*, 2019) opened the possibility of volatile-mediated signaling within shaded plant communities. Previous studies on shade-derived VOCs (that we refer to as the shade volatilome) remain scarce as they have used only a few different plant species, and have yielded inconclusive patterns: some indicate that VOC levels are globally reduced while others conclude that specific components of the volatile are enhanced, such as ethylene, previously linked to shade responses (Escobar-Bravo *et al.*, 2024; Kegge *et al.*, 2015; Vicherová *et al.*, 2020). Our experiments indicate that simulated proximity shade conditions (W+FR) indeed have a clear impact on increasing ethylene

levels in several plants, including the shade tolerant *C. hirsuta* (Fig. 2.2), expanding the number of species displaying this shade response (Kegge *et al.*, 2013, 2015; Pierik *et al.*, 2004). However, our W+FR treatment appeared to have a very limited impact on reshaping the global spectrum of VOC emissions (both abundance and composition) of adult tomato plants (Figs. 2.1, 2.S1). This outcome contrasts with the well-documented volatilome remodeling triggered by many biotic and abiotic stresses—such as herbivory, pathogen attack, or drought—which typically induce marked increases in green leaf volatiles, terpenoids, or defense compounds (Heil & Karban, 2010; Kost & Heil, 2006; Maffei *et al.*, 2011; Niinemets *et al.*, 2013).

The absence of broad differences in VOC profiles might reflect technical constraints inherent to the GC-MS-based untargeted approach that we followed. Factors such as the stage of development of the e-plants, short collection period (Fig. 2.S1), sampling during a restricted circadian window (Fig. 2.S3), poor detection of low-molecular-weight volatiles (e.g., ethylene, undetectable by standard GC–MS but quantifiable using a dedicated detector), and biases introduced by the PoraPak matrix likely limited sensitivity. These issues underscore the challenges of fully resolving complex volatilomes with standard headspace GC–MS and suggest that subtle but biologically relevant changes could have escaped detection. This rationale led us to explore specific candidate (targeted) volatiles with prior evidence or mechanistic plausibility, to account for the phenotypic and transcriptomic responses observed.

Among the shade-related candidate VOCs, three compounds emerged as particularly relevant: ethylene, β-cyclocitral (β-cc), and β-ionone (β-ion). As mentioned, ethylene has long been linked to shade responses (Kegge *et al.*, 2013, 2015; Pierik, Whitelam, *et al.*, 2004). In contrast, β-cc and β-ion are apocarotenoids with limited precedent in shade literature (Vicherová *et al.*, 2020). The levels of these two apocarotenoids, derived from the degradation of carotenoids such as β-carotene present in the leaves of e-plants, were enhanced under proximity shade in our experiments (Fig. 3.1). Their detection was enabled by SPME-GC-MS, which, through longer accumulation periods and 24 h treatments, overcame key limitations of the untargeted approach, revealing these molecules as strong candidates for conveying shade-derived information.

Together, these observations suggest that the apparent stability of the volatilome under shade masks selective increases in a restricted number of compounds. Ethylene, β-ion, and β-cc emerge as strong candidates because they not only bypassed many of the technical limitations that hampered the untargeted profiling, but also displayed shade-enhanced production and impacted growth of non-shaded r-plants. Their identification underscores the idea that the shade volatilome may rely on a few key signals, rather than broad-spectrum shifts, to convey biologically meaningful information (Fig. D.1).

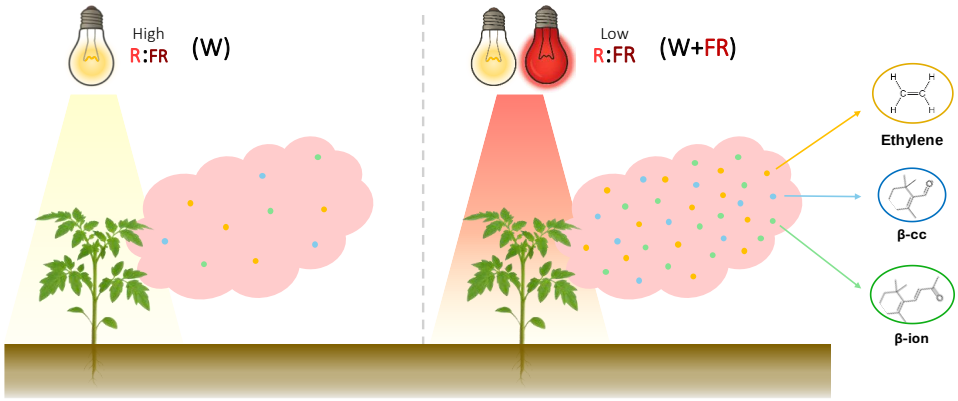

Figure D.1 — Shade conditions selectively enhance the emission of specific volatiles. *Schematic representation of volatilome profiles under W (Control, left) and W+FR (Simulated shade, right). While overall emissions appear similar, shade promotes the production of a restricted set of compounds, including ethylene (in yellow), β-cc (in blue), and β-ion (in green), highlighting their potential role as key informational signals.*

The shade volatilome contains environmental information

In our system, emissions from shaded tomato e-plants consistently reduced hypocotyl elongation in neighboring non-shaded r-seedlings growing in the dark (D) (Fig. 1.2-A) or under dim light (low W) (Fig. 1.2-B). The consistent outcome across contrasting photic environments indicates that (i) the inhibitory message emitted by shaded plants is robustly perceived regardless of the receiver's light status and (ii) the shade volatilome encodes a constitutive signal rather than a condition-specific artifact. Shade-derived VOCs from the barley 'Alva' cultivar have been

shown to increase the biomass of neighboring ‘Kara’ barley plants (Kegge *et al.* 2015). However, stem length remained unchanged, suggesting a shift in carbon allocation rather than genuine VOC-induced growth promotion. Discrepancies may also reflect species-specific biases in volatile communication, as plant responses can differ markedly between conspecific and heterospecific interactions, or differences in the stage of development of the r-plants (adult plants vs. seedlings).

Our transcriptomic analyses showed that, beyond its phenotypic impact on non-shaded seedlings, exposure of r-seedlings to the volatiles emitted by tomato e-plants induced consistent transcriptomic reprogramming, further supporting the signaling nature of the shade volatilome (Fig 1.2). The modest number of differentially expressed genes (DEGs) might reflect technical limitations of the two-box system (e.g., dilution effects, VOC leakage, reduced airflow, spatial heterogeneity) (Figs. 1.1, 1.3) and/or time-dependent dynamics of volatile signaling. Principal component and correlation analyses showed that diurnal rhythms strongly influenced transcript abundance, but only after 24 h a clear separation did emerge between shade- and control-volatilome treatments (Fig. 1.5). The fact that differences became evident only after prolonged exposure underscores the time-dependent nature of volatile signaling, with effects that intensify over time.

The transcriptomic 24 h dataset comprised only 393 DEGs (Fig. 1.S4). Many categories that did emerge were broad or sparsely represented, complicating functional interpretation. Nonetheless, certain patterns were evident: genes linked to oxidative stress, hypoxia, and catabolic processes were upregulated, whereas those associated with sulfur-compound metabolism, particularly glucosinolates, were downregulated (Fig. 1.6). These trends, although limited, gain relevance when considered alongside phenotypic responses and in comparison with larger transcriptomic datasets, as will be discussed in subsequent sections. Importantly, a reduced subset of the induced DEGs by the shade volatilome also responded to direct low R:FR exposure, indicating that volatile signals can recruit part of the genetic program underlying the SAS (Fig. 1.7). This partial overlap suggests that the shade volatilome emerge as one mechanism—among others—through which shade information detected by a few individuals is disseminated within plant communities. Nonetheless, it is important to note that the set of genes not overlapping

with canonical shade responses was more abundant. The downstream effects of these DEGs may also contribute to shade-associated phenotypes through alternative molecular pathways or, potentially, act in opposition to the classical SAS program. Clarifying the functional roles of these non-overlapping responses remains an open question for future research.

Ethylene might not be a major driving force of shade volatilome effects

Having identified ethylene, β-cc and β-ion as shade-enhanced volatiles, the key question was whether these compounds act as airborne signals capable of explaining the biological effects attributed to the shade volatilome. To address this question, we compared their individual phenotypic and transcriptomic impacts with those elicited by the shade volatilome.

Ethylene has traditionally been considered a central regulator of developmental plasticity under diverse light conditions (Rodrigues *et al.*, 2014). Genetic analyses indicated that exposure to reduced R:FR promotes ethylene biosynthesis in many species, contributing to elongation growth, leaf hyponasty, and other SAS-associated traits through broad hormonal crosstalk (Das *et al.*, 2016; Le *et al.*, 2005; Pierik, Whitelam, *et al.*, 2004; Van de Poel *et al.*, 2015). Whether ethylene could function as a neighbor detection signal, however, had not been explored. As ethylene is a volatile plant hormone, it would be expected that ethylene emitted by shaded e-plants could potentially account for both the phenotypic effects of shade volatiles on elongation (Fig. 1.2) and the subset of DEGs shared between direct shade signaling and volatilome exposure in receiver plants (Fig. 1.7). To test ethylene's contribution to hypocotyl elongation, we supplemented media with ACC to grow *A. thaliana* and *C. hirsuta* seedlings under D, low W, W and W+FR conditions. Ethylene produced by ACC-grown tomato or Arabidopsis e-seedlings was found to be detected by nearby r-seedlings growing without ACC, as indicated by the GUS staining of the ethylene-specific *EBSn:GUS* marker line (Fig. 2.5). In *A. thaliana*, ethylene promoted elongation under W light but repressed it in darkness (Fig. 2.4), in agreement with previous reports (Schaller & Kieber, 2002; Smalle *et al.*, 1997). Under our low W (PPFD ≈

28 $\mu mol \cdot m^{-2} \cdot s^{-1}$), ACC effect became negligible (Fig. 2.4), marking the transition between repression (D) and promotion (W). Additionally, under W+FR, ACC supplementation even repress hypocotyl elongation (Fig. 2.3), contradicting the hypothesis of ethylene being a promoter of shade-induced elongation. Consistently, the ethylene insensitive *ein2-5* mutant does elongate in shade, evidencing that ethylene's signaling is not needed for shade-related growth (Fig. 2.3). In the shade-tolerant *C. hirsuta*, basal production of ethylene is higher, and endogenous levels do not change much when exposed to shade (Fig. 2.2). The elevated ethylene levels emitted by *C. hirsuta* leaves even under non-shaded conditions, similar to those of *A. thaliana* under W+FR, suggest that enhanced ethylene emission might be a SAS-related response that is constitutively activated in this shade-tolerant species. Elevated ethylene levels correlated with weaker shade-induced elongation, and ACC supplementation further constrained the response in both species (Fig. 2.3), suggesting that ethylene accumulation may actually attenuate elongation (contributing to shade tolerance in *C. hirsuta*) and an attenuated elongation in a range of light conditions even in the shade-avoider *A. thaliana*. Whether this pattern generalizes to other tolerant species, or reflects dose-dependent regulation of elongation, remains unresolved.

The unnoticeable effect of ethylene on hypocotyl elongation under low W (Fig. 2.4) indicates that, in our two-box plant-to-plant communication set-up (Fig. 1.3), ethylene alone cannot explain the repression caused by shade volatiles (Fig. 1.2-B). In the single-box system (Fig. 1.1), however, ethylene could theoretically contribute to the suppression observed in etiolated (D-grown) seedlings (Fig. 1.2-A). Indeed, ACC-supplemented seedlings emitted enough ethylene to be perceived and modestly affect the growth of neighboring etiolated seedlings (Fig. 2.5), suggesting some potential as a shade-related cue. Yet, the levels naturally produced under shade were insufficient to drive measurable repression responses in neighboring r-plants (Fig. 2.6). However, large groups of shaded adult plants, in crowded and very dense natural environments might concentrate ethylene at localized pockets (Heilman, M. D. *et al.*, n.d.; Pierik, Whitelam, *et al.*, 2004). In shaded settings dominated by shade-tolerant species, even higher levels of ethylene might be produced, which could have a more relevant impact on the development of small plants or seedlings growing closeby.

Crosses of transcriptomic data reported strong correlations between shade- and ethylene-induced gene expression changes (Das *et al.*, 2016), suggesting a close association between the two signals. The comparison of DEGs regulated by 24 h of ethylene treatment (Das *et al.*, 2016) with those regulated by 24 h of exposure to the shade volatilome (Fig. 1.7), however, suggested a limited contribution of this volatile to the shade volatilome (Fig. 4.4), likely diluted or overshadowed by other VOCs enhanced under shade conditions. In summary, our results do not allow us to claim a central role for ethylene in mediating elongation responses within the signaling activity of the shade volatilome (Fig. D.2).

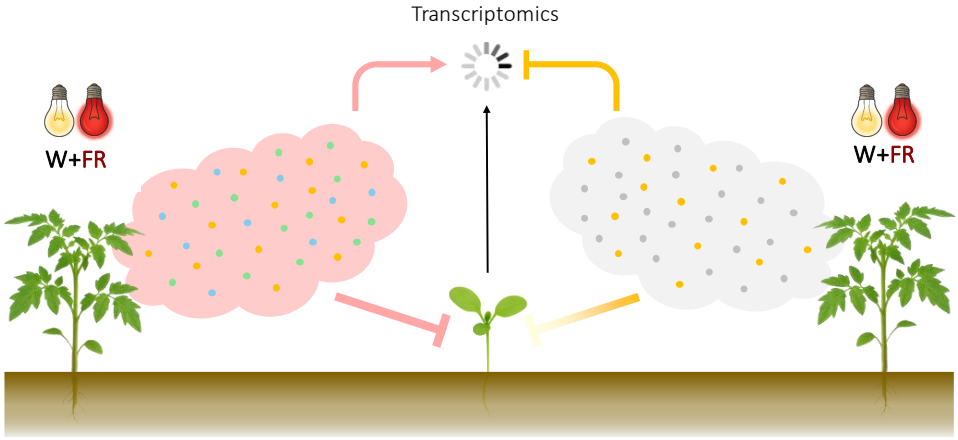

Figure D.2 — Responses to the shade volatilome (left, in pink) do not seem to be reproduced by ethylene (right, in yellow). *Ethylene is unlikely to play a central role in mediating elongation responses within the signaling framework of the shade volatilome, and its transcriptomic regulation patterns mostly oppose to those of the shade volatilome.*

Apocarotenoids emerge as key molecules within the shade volatilome

The findings described above suggest that other volatiles besides ethylene must carry the main weight of shade-volatilome signaling. Our focus therefore turned to the apocarotenoids β-cc and β-ion, both of which showed shade-enhanced emissions (Fig. 3.1). Although relatively recent in their recognition as bioactive metabolites, both compounds have been linked to the regulation of plant development (Deshpande & Mitra, 2023;

Dickinson *et al.*, 2019), defense (Felemban *et al.*, 2024; Taniguchi *et al.*, 2023), and stress responses (D'Alessandro *et al.*, 2018; Deshpande, Purkar, *et al.*, 2021). However, their roles as volatile signals remain poorly understood, since most studies have tested them via media supplementation or spraying rather than true airborne exposure. Within this framework, we analyzed their effects as VOC cues to evaluate their potential as key mediators of shade-volatilome signaling.

Our set-up, developed from Petri dish in which seedlings were exposed exclusively via volatilization from compound-containing solutions (Figs. 3.S1, 3.S2), proved consistent across experiments and adaptable to different doses and time points, likely by minimizing compound loss while maintaining normal growth, also enabling stable solution–atmosphere equilibria (Fig. 3.4). Experimental evidence indicated that β-cc and β-ion distributed evenly in the headspace, with no detectable distance-dependent effects, consistent with their high volatility and rapid saturation of the headspace. Finally, given that vaporization dynamics critically shape effective exposure, we next sought to quantify headspace (HS) concentrations and temporal accumulation patterns of β-cc and β-ionone.

By combining standard solutions, simple mathematical models, SPME fibers as probes and monitored airborne accumulation dynamics through GC-MS, we established distinct kinetics for β-cc and β-ion (Fig 3.S8): within the first 4 h, β-cc had already reached equilibrium—reflecting its higher volatility—with HS levels nearly 100-fold higher than β-ion (Fig. 3.S8); and by 24 h, concentrations of the two compounds began to converge, and equilibrium was reached for both by 48 h (Fig. 3.4). Assuming comparable signaling activity, this disparity implies that β-cc would exert effects hours before β-ion could reach effective concentrations. Whereas for long-term assays (hypocotyl elongation or photosynthetic efficiency) cumulative exposure reduces the impact of these differences, early responses (RNA-seq profiles or germination) appeared as highly sensitive to differences in vaporization dynamics, making careful experimental design essential to capture each compound's contribution during the first 24 h of exposure.

Semi-quantitative analyses indicated that β-cc and β-ion reached HS equilibrium concentrations in the nanomolar range (~300 nM each; Fig. 3.4), far below the molar concentrations of the working solutions (0.5 M and 0.1 M, respectively). Direct HS-GC–MS detection (i.e., physiological

emissions) was not feasible as previously discussed, so we estimated tissue apocarotenoid content by SPME-GC–MS (Fig. 3.1) and related these values to their potential scalable HS concentrations in the experimental system (Figs. 3.S1, 3.S5). Calculations suggested that a shaded tomato plant could reproduce a concentration of ~5–10 nM per g of leaf in the headspace (it is assumed that all its content is released to the HS of the system and complete volatilization, but their dynamic production is not considered). Consequently, they indicate that the concentrations used could fall within a physiologically plausible range. Confirmation would require direct quantification methods.

The analyses of the effects of β-cc and β-ion on seedling growth in both *A. thaliana* and *C. hirsuta* indicated that exposure to airborne apocarotenoids repressed hypocotyl elongation under all light regimes tested - when elongation was sufficiently promoted - (Figs. 3.2, 3.S4). The results suggest a dose–response relationship: the stronger the elongation drive imposed by light conditions, the more pronounced the repression mediated by apocarotenoids (under the highest W conditions tested their effects were mild, likely because elongation was already strongly suppressed by high irradiance). The differences in the repression magnitude of seedling elongation between the apocarotenoids and the shade volatilome itself (Fig. 1.2) may reflect dosage or additional compounds within the blend.

The involvement of these apocarotenoids in mediating developmental responses in seedlings has been scarcely explored, with only β-cc reported as a conserved promoter of root elongation when supplied in the growth medium (Dickinson *et al.*, 2019). In contrast, our results—focused on a distinct developmental trait, hypocotyl elongation—support an opposite regulatory outcome. These differences may stem from tissue-specific responses, but they could also reflect divergent mechanisms of action, as β-cc perception in roots from a liquid phase likely differs from its sensing as an airborne signal, thereby eliciting distinct physiological outputs.

Analyses of these growth responses at the cellular level (Fig. 5.S6) showed that both apocarotenoids selectively repressed elongation promoted by low W or W+FR (Fig. 5.7), consistent with microscopic observations (Fig. 3.2-B). Even in the most affected seedlings, cell lengths did not fall below basal W levels, where apocarotenoids had no macroscopic effect (Figs. 5.7, 5.8). The spatial pattern of repression

mirrored the elongation profile induced by low W (Fig. 5.8), indicating complete counteraction of this signal, while in W+FR the effect was partial, as cells elongated beyond W levels. Altogether, these findings show that apocarotenoids do not suppress basal growth but act as selective antagonists of light-induced elongation, with their impact scaling to the strength of the elongation drive.

Germination and photosynthetic performance also emerged as apocarotenoid-sensitive traits. Importantly, germination arrest was specifically induced by β-cc but not by β-ion (Fig. 3.6). The differences between vaporization dynamics of both compounds did not explain the lack of impact of β-ion on germination induction (Figs. 3.S8, 3.S9), pointing to functional divergence between the two structurally related compounds (Fig. 3.7). In the two-box system (Fig. 1.3), germination in *A. thaliana* is completed before seedlings interact with tomato emitters, meaning that β-cc could only act through repression of elongation (Figs. 1.2-B, 3.2-B). By contrast, in the same-box system (Fig. 1.1), shorter hypocotyls in etiolated receivers (Fig. 1.2-A) could result from either direct repression (Fig. 3.2-B) or an indirect effect of delayed germination (Figs. 3.6, 3.7). Although volatilome exposure did not detectably alter germination rates, a subtle β-cc-driven delay at early stages cannot be fully excluded.

The specificity of apocarotenoid effects was also evident in photosynthetic efficiency: only β-ion increased φPSII under low W in a dose-dependent manner (Figs. 3.8A, 3.9). In contrast, the shade volatilome did not alter photosynthetic performance (Fig. 1.4). This discrepancy is best explained by dosage, paralleling the β-cc–induced germination arrest: the concentrations required to elicit detectable effects when compounds are applied individually may not be reached within the natural volatilome, or their impact may be masked by other metabolites present in the blend.

The distinct vaporization kinetics of β-cc and β-ion (Fig. 3.S8) were reflected in their transcriptomic profiles (Figs. 4.1, 4.2): β-cc showed earlier divergence from controls (8 h), whereas β-ion responses became evident later (24 h). Based on these dynamics, β-cc at 8 h and β-ion at 24 h were selected as representative conditions for subsequent comparisons with each other and with the shade volatilome. Comparative analyses indicated partly distinct yet convergent programs (Fig. 4.3), reinforcing the view that their contributions are complementary rather than redundant. Altogether, the phenotypic and molecular effects of airborne apocarotenoids can

converge—such as their consistent repression of hypocotyl elongation and DEGs—or diverge in specific processes like germination and photosynthesis. These dualities suggest that β-cc and β-ion may act synergistically in some contexts while assuming distinct, specialized roles in others, likely through selective modulation of different pathways.

When comparing their transcriptomic profiles with those induced by shade-volatilome exposure at 24 h, the time point when volatilome signaling becomes most evident (Fig. 1.5), both β-cc and β-ion showed strong convergence with volatilome-regulated DEGs (Figs. 4.5-A, 4.6-A), with shared genes not only overlapping but also co-regulated in the same direction (Figs. 4.5-B, 4.6-B). Importantly, combining β-cc and β-ion accounted for more than 50% of the DEGs modulated by the volatilome (Fig. 4.7), whereas adding ethylene did not improve this correlation. These common subsets were enriched in the gene families most characteristic of the shade volatilome, notably hypoxia-responsive genes and those involved in glucosinolate metabolism (Fig 4.8). These results indicate that β-cc and β-ion jointly capture the majority of the transcriptomic signature of the shade volatilome, strongly supporting, together with their phenotypic outputs, their role as its principal signaling components within the shade volatilome (Fig. D.3).

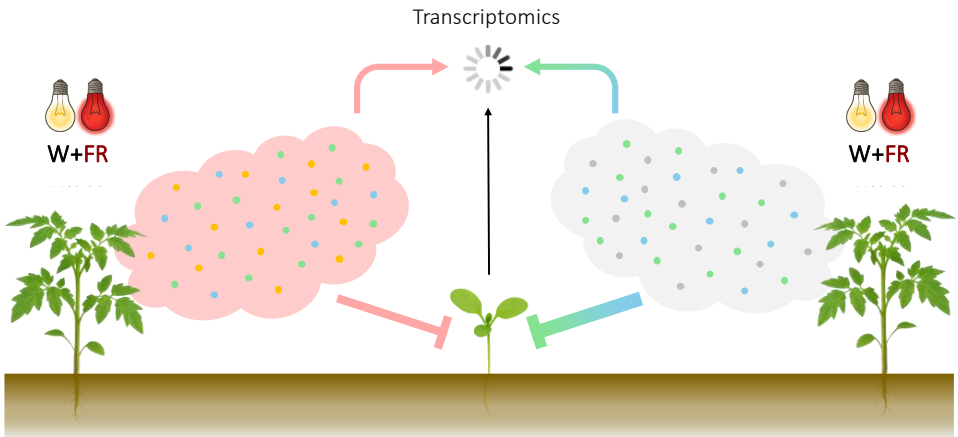

Figure D.3 — Reponses to the shade volatilome (left, in pink) are partially reproduced by the combination (right) of the apocarotenoids β-cc (in blue) and β-ion (in green). *Phenotypic and transcriptomic analysis support a key contribution of airborne apocarotenoids within the shade volatilome.*

Apocarotenoids promote a stress-like transcriptional state in r-seedlings, reinforced by β-cc

Having established β-cc and β-ion as key components of the shade volatilome, we consider how their shared and specific actions converge into broader molecular and functional outcomes. A recurring signature of both apocarotenoids is a stress-like transcriptional state that couples enhanced primary metabolism with hypoxia-related signaling. Genes linked to glycolysis, the TCA cycle, and amino-acid catabolism were broadly upregulated (Fig. 4.10), a pattern typical of stress acclimation where rapid carbon turnover supplies energy and intermediates for defense, detoxification, and repair rather than pure growth (Bolton, 2009; Nunes-Nesi *et al.*, 2010). Consistent enrichment of auxiliary metabolic routes (e.g., glyoxylate, nitrogen; Fig. 4.9-C) and induction of oxidative phosphorylation (Fig. 4.20) further point to an energy-supportive adjustment.

In parallel, hypoxia programs were activated (Fig. 4.11)—including markers such as *ADH, DIN10*, and *ANAC102*—together with TFs and signaling components tied to redox and detoxification (e.g., *WRKY22, STOP1, ERF/AP2, MKK9; UGT73B3, DOGT1, AtBBE22*). Interestingly, β-cc had also been previously associated with the induction of *ANAC102* (D'Alessandro *et al.*, 2018), proposed by these authors as a pivotal element for a photooxidative-stress-driven detoxification response. This lies in agreement with the fact that β-cc has been suggested to function as a signaling molecule coordinating acclimatory responses such as in high-light stress, where it is known to accumulate (Ramel *et al.*, 2012, 2013).

It should be noted that the semi-closed configuration used to maintain stable headspace concentrations (Figs. 3.S1 / 3.S2) may impose a mild hypoxic baseline, which could in part facilitate the detection of hypoxia-related transcriptional signatures across treatments. Nonetheless, since all samples including DMSO controls shared identical conditions, the consistent reinforcement of these pathways under β-cc and β-ion exposure suggests genuine modulation of hypoxia- and stress-associated programs rather than an artifact of the system. Overall, β-cc and β-ion shift receiver seedlings toward anticipatory stress preparedness: instead of amplifying SAS, they reconduct seedling development and pre-condition resilience.

Relative to β-ion, β-cc elicited a more delimited yet internally coherent response that reinforces this shared primed state rather than opening new functional trajectories (Fig. 4.16). β-cc specifically upregulated hypoxia-, water-deprivation- and catabolic-related processes (Fig. 4.16-A), while selectively repressing jasmonate- and glucosinolate-associated categories, suggesting a functional trade-off that prioritizes generalized stress readiness over specialized biotic defenses. These results correlate with β-cc being reported as a master regulator of multiple stress reporter genes in tomato plants, mediating mostly drought tolerance (Deshpande, Manoharan, *et al.*, 2021; Deshpande, Purkar, *et al.*, 2021).

This specific modulation matches the distinct features of its phenotypic footprint: β-cc strongly delays germination but exerts weaker effects on post-germinative elongation (Figs. 3.6, 3.7). Although germination-related DEGs were not detected (RNA-seq sampled post-germination seedlings), the data support a model in which β-cc acts as an early checkpoint—delaying emergence under unfavorable cues while equipping established seedlings with enhanced stress resilience. Thus, the programs observed here likely reflect a broader signaling role for β-cc that extends beyond shade interactions to conditions demanding tight control of growth, metabolism, and stress tolerance. In sum, β-cc operates less as a broad-spectrum growth repressor and more as a strategic fine-tuner of developmental timing and stress accommodation within a β-ion–supported primed background (Fig. D.4).

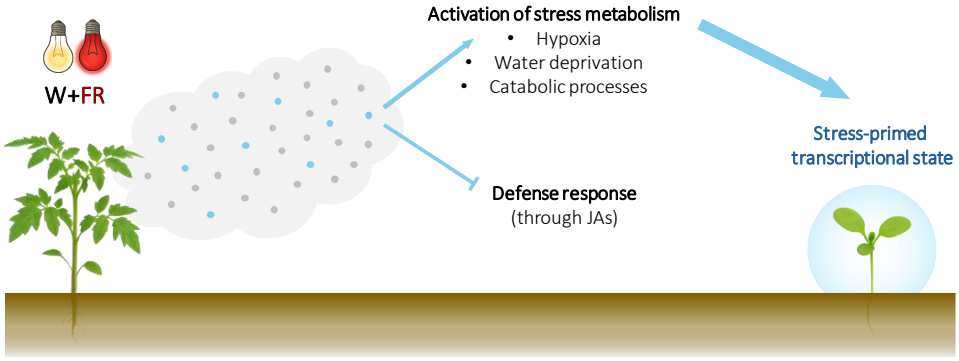

Figure D.4 — β-cc strategically reinforces seedlings for a stress-alert state. *In this state, stress-related genes are transcriptionally activated or poised for activation, providing enhanced readiness for subsequent challenges.*

β-ion is revealed as a versatile immune signal that counteracts shade-induced susceptibility

In contrast to β-cc, which primarily reinforces a stress-primed metabolic state, β-ion triggers a broader transcriptional reprogramming consistent with a growth–defense trade-off. Acting as a volatile immune cue, it activates multiple layers of plant defense even in the absence of pathogens, promoting metabolic and transcriptional changes that anticipate biotic stress. These include the modulation of secondary metabolism—particularly glucosinolates and phenylpropanoids—alongside the induction of canonical defense modules such as MAPK cascades, WRKY transcription factors, and salicylic acid (SA) signaling. Together, these responses outline β-ion as a multifaceted priming agent that redirects metabolic and signaling priorities from growth to defense.

At the transcriptomic level, β-ion orchestrates a selective rewiring of tryptophan metabolism (Fig. 4.S3) and glucosinolates biosynthesis (shared with β-cc; Fig. 4.14) that potentially reflects a strategic reallocation of cellular resources toward defense. The repression of aliphatic glucosinolate synthesis (Fig 4.14), together with the strong induction of the indolic branch (Fig. 4.S3) and its associated phytoalexin camalexin (via *CYP71B15* and WRKY33*;* Figs. 4.S3 / 4.S5*)*, suggests that β-ion shifts metabolic fluxes from constitutive to inducible chemical defenses. This redirection, mirrored also by the regulation of indolic / aliphatic master regulators (*MYB28/29/51/76;* Fig. 4.S5), channels tryptophan toward protective outputs rather than toward auxin biosynthesis (Fig 4.S4), thereby decoupling defense activation from growth promotion. Interestingly, this metabolic reprogramming stands in direct opposition to the low R:FR response, which promotes auxin biosynthesis at the expense of indolic defense metabolites, increasing susceptibility to pathogens such as *Botrytis cinerea* (Cargnel *et al.*, 2014; Felemban *et al.*, 2024).

Beyond glucosinolates, β-ion also remodels phenylpropanoid metabolism (Fig. 4.19). Upregulation of peroxidases, berberine bridge enzymes (BBEs), and lignification-associated genes suggests a strengthening of structural and antimicrobial barriers, while simultaneous repression of early pathway enzymes (Fig. 4.19) and induction of PAL-targeting F-box proteins (Fig. 4.S7) indicates a tightening of upstream flux control. Rather than a global activation, β-ion appears to impose a refined redistribution of metabolic output—favoring lignin deposition and the synthesis of

antimicrobial compounds over the maintenance of broad phenylpropanoid activity. Given the documented metabolic and regulatory coupling between glucosinolate and phenylpropanoid biosynthesis (Kim *et al.*, 2015, 2020; Shin *et al.*, 2023), the identification of PAL1 and GS-pathway enzymes among β-ion interactors suggests that this apocarotenoid may influence the balance between these pathways. Such modulation could favor the redirection of precursor flux toward indolic and phenylpropanoid-derived defense compounds, fine-tuning the trade-off between general metabolism and specialized immunity.

Additionally, β-ion orchestrates a coordinated activation of the salicylic acid (SA) pathway, both at the transcriptional (Fig. 4.21) and metabolic (Fig. 4.24) levels, consolidating its role as a specific priming cue for defense. The selective upregulation of the isochorismate synthase (ICS) branch (Fig. 4.23-A)—together with enhanced SA glycosylation (Fig. 4.S9) and induction of SA-responsive genes (Fig. 4.22-B)—points to a controlled activation strategy, where β-ion promotes the accumulation of a mobilizable SA reservoir rather than triggering an immediate defense burst. Notably, SA signaling is repressed by proximity shade (De Wit *et al.*, 2013), marking again this counteraction between β-ion and the low R:FR signal. Upstream, the concurrent activation of MAPK cascades (Fig. 4.22-A) and WRKY transcription factors (Figs. 4.21 / 4.22-A) provides a mechanistic framework linking apocarotenoid perception to SA-dependent defense signaling.

This fine-tuned activation driven by β-ion ensures readiness while compromising growth, a hallmark of primed immunity. Importantly, such β-ion–driven defense mechanisms oppose the attenuation of immunity typically imposed by proximity shade, illustrating how this apocarotenoid counterbalances shade-induced susceptibility and reinforces resilience within dense canopies (Fig. D.5).

β-ion balances shade-induced trade-offs by reinforcing phyB-dependent photosynthetic efficiency

While β-ion primes seedlings for defense, it simultaneously enhances photosynthetic efficiency—hinting at a coordinated strategy that sustains the energetic demands of immunity without compromising metabolic

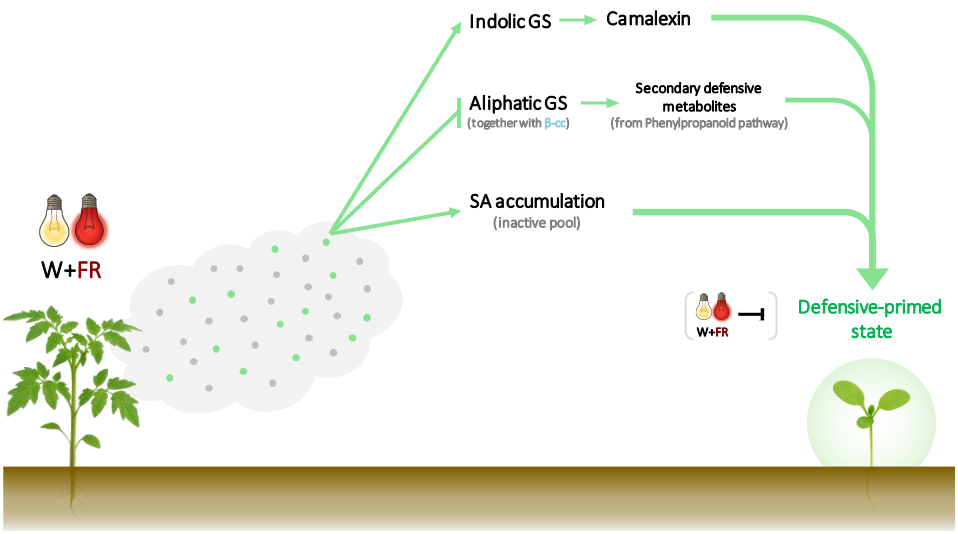

Figure D.5 — Model of β-ion-mediated transcriptional reprogramming towards defense. *Schematic representation of the specific responses induced by β-ion. This VOC specifically triggers defense-associated pathways including the induction of camalexin via indolic GS biosynthesis, reinforcement of phenylpropanoid metabolism (via repression of aliphatic GS biosynthesis, common with β-cc) and increased content of SA and SA-glycosylated. These coordinated responses converge into a defensive-primed state in receiver seedlings, counteracting shade-induced elongation and enhancing readiness against potential biotic stress.*

balance. Consistent with the observed stimulation of ΦPSII (Fig. 3.8-A/3.9), β-ion also induced a subset of photosynthesis-related genes, including components of PSI, PSII, the cytochrome b6f complex, and ATP synthase (Fig. 4.S8). This coordinated transcriptional upregulation suggests enhanced electron transport and ATP production capacity, aligning with the β-ion-specific stimulation of oxidative phosphorylation (Fig. 4.19). Rather than a wholesale remodeling of the photosynthetic apparatus, β-ion appears to fine-tune energy metabolism to support the defensive state it induces. In this way, reinforcement of photosynthetic and respiratory functions provides the energetic framework for sustained immunity, explaining the improved photosynthetic efficiency observed at the physiological level.

The transcriptional profile induced by β-ion points to a functional reconfiguration that enhances the efficiency of light energy utilization. This contrasts with proximity shade, where photosynthetic efficiency is typically

reduced as plants acclimate to altered light quality (Morelli *et al.*, 2021). Such shade-driven adjustments are largely orchestrated by the photoreceptor phyB, a central regulator of light-dependent control of both growth and photosynthesis (Kreslavski *et al.*, 2018). Given this key role, we next tested whether phyB-mediated signaling also underlies the β-ion response.

Hypocotyl elongation assays in the *phyB* mutant showed that both β-cc and β-ion continued to repress growth across diverse light regimes, including W+FR, where phyB is inactive (Figs. 3.2-B / 3.S10). This demonstrates that the growth-suppressive activity of apocarotenoids is largely phyB-independent, in contrast to the canonical shade-avoidance pathway, which requires phyB inactivation to promote elongation. By contrast, phyB proved essential for the photosynthetic branch of the β-ion response. The enhancement of ΦPSII observed in Col-0 under multiple light intensities (Fig. 3.9) was completely abolished in *phyB* mutants, as well as in Col-0 seedlings exposed to W+FR, where phyB activity is suppressed (Fig. 3.8-B). Thus, β-ion improves photosynthetic performance only in the presence of an active phyB photoreceptor. Taken together, these results reveal a functional split in β-ion signaling: elongation repression engages BR-related modules independently of phyB, whereas photosynthetic enhancement requires phyB activity. This duality highlights that β-ion operates not as generic cue but as a finely tuned modulator, targeting distinct regulatory hubs to counterbalance shade-induced trade-offs between growth and energy capture.

β-ion exposure also altered phyB nuclear dynamics: using a 35S:PHYB-GFP line, we observed a significant increase in photobody (PB) abundance per nucleus under β-ion treatment (Figs. 3.10-A, 3.10-B). Since PBs are widely regarded as hubs of phyB signaling, often linked to PIF degradation and transcriptional control of light responses (Van Buskirk *et al.*, 2012; Willige *et al.*, 2024), this nuclear reorganization provides a mechanistic basis for the observed phyB dependency of β-ion–mediated photosynthetic enhancement.

From an ecological perspective, this effect can be viewed as a strategy to counteract proximity shade, where FR-rich conditions normally promote PB disassembly and weaken phyB outputs (Ortiz-Alcaide *et al.*, 2019). By increasing PB accumulation, β-ion may reinforce phyB signaling under conditions that would otherwise compromise photosynthetic performance,

redirecting the balance from shade-driven elongation toward sustained energy capture. While further work is needed to establish a causal chain from PB remodeling to photosynthetic enhancement, the current findings position β-ion as a volatile cue capable of modulating phyB activity at its nuclear signaling hubs (Fig. D.6).

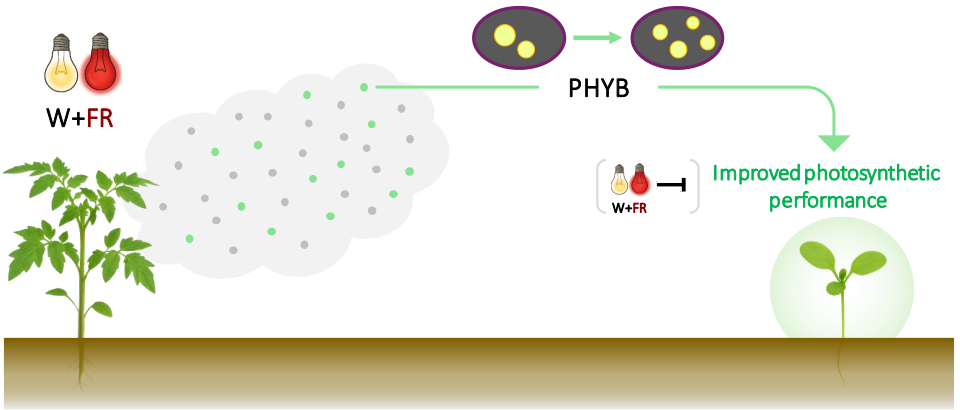

Figure D.6 — Model linking β-ion signaling with enhanced photosynthesis and phytochrome B activity. *Schematic representation of how β-ion promotes a transcriptional program that reinforces photosynthetic performance, through potentially stabilizing or increasing PHYB activity. Together, these responses converge to counteract shade-induced lower photosynthetic rates.*

Apocarotenoids counteract the shade-avoidance syndrome through BR/BIN2-mediated growth repression, independently of RACK1A

Having characterized the distinct physiological effects of β-cc and β-ion on stress adaptation, defense activation, and photosynthetic performance, we next aimed to uncover the molecular components that mediate their shared signaling outputs—particularly those responsible for growth repression.

Given the broad range of physiological processes modulated by both apocarotenoids—including growth, hormone signaling, and photosynthesis—we considered that these effects might converge on a common regulatory hub. RACK1A, a multifunctional scaffold protein integrating hormonal and environmental cues, emerged as a plausible candidate (J. Guo & Chen, 2008; Islas-Flores *et al.*, 2015). Its presence

among top β-ion interactors in the proteomic screen (Table 4.2), the enrichment of known RACK1A partners (Fig. 5.S7), and the predicted β-ion binding pocket (Fig 5.S8) coupled to RACK1A potential to bind small molecules (Ma *et al.*, 2024; Ullah *et al.*, 2019) supported the idea of a potential molecular connection. Moreover, RACK1A directly interfaces with BES1, phyB (W. Zhu *et al.*, 2024), and MAPK signaling (Cheng *et al.*, 2015)—precisely the modules involved in β-ion–driven elongation, photosynthetic, and defense responses—making it an attractive integrative hypothesis.

However, functional analyses did not support a direct role for RACK1A in apocarotenoid signaling. Mutant assays revealed no differential responses to β-cc or β-ion during germination (Figs. 5.10) or hypocotyl elongation (Figs. 5.11 / 5.S10), and the few genotype-specific effects were inconsistent across light conditions and largely explained by basal growth variation. Combined with the likely redundancy among isoforms and discrepancies with published data (Fu *et al.*, 2024), these results indicate that apocarotenoid-mediated growth repression operates independently of RACK1A. Nevertheless, given the strong convergence of transcriptomic (Fig. 4.18) and proteomic (Table 4.2) data on translational and ribosomal regulation—processes where RACK1A plays a structural role (Nielsen *et al.*, 2017)—it may still contribute indirectly through its function at the ribosome, coordinating global translational reprogramming rather than acting as a primary signaling target.

With RACK1A excluded as a key mediator, we next turned to the transcriptional responses themselves to identify candidate mechanisms underpinning apocarotenoid-induced repression of elongation. Both β-cc and β-ion downregulated *SAUR* genes (Fig. 4.25)—rapid auxin-responsive factors that drive cell expansion by activating proton pumps and promoting cell-wall loosening (Stortenbeker & Bemer, 2019). This repression was markedly stronger under β-ion, in agreement with its more pronounced inhibition of hypocotyl elongation (Fig. 3.2-B), and extended to additional categories associated with cell division, cytoskeletal organization, and microtubule dynamics (Fig. 4.12), that could also explain this behavior. Such patterns suggest that β-ion may inhibit elongation not only through hormonal interference but also by directly modulating the cellular machinery underlying anisotropic growth. At the signaling level, *SAUR* repression represents a molecular mirror image of proximity shade,

where *SAUR* induction by auxins and other phytohormones promotes elongation (Ren & Gray, 2015; Roig-Villanova & Martínez-García, 2016). Thus, apocarotenoids, and particularly β-ion, appear again to act as antagonistic cues that counterbalance shade-induced transcriptional programs, shifting developmental priorities from rapid expansion toward restrained, stress-adaptive growth. This connection prompted us to investigate which hormone pathways known to regulate *SAUR* expression mediate this volatile-driven repression of elongation.

Despite the strong repression of *SAUR* genes by β-ion and β-cc (Fig. 4.25), auxin response, the main hormone controlling the expression of *SAUR* genes, did not appear to be directly affected. DR5:GUS reporter assays showed no change in auxin-responsive activity under any light or pharmacological condition (Fig. 4.26), indicating that apocarotenoids do not interfere with auxin perception or ARF-mediated transcription. Functional assays further clarified this hormonal context: both apocarotenoids suppressed hypocotyl elongation promoted by auxin or gibberellin (GA_3) supplementation, yet elongation driven by brassinosteroids (BRs) remained fully resistant to inhibition (Fig. 5.1). Application of 2,4-epibrassinolide (EBL) restored growth even in the presence of β-ion or β-cc, and this effect persisted across a wide concentration range (Fig. 5.S1), pinpointing BR signaling as the pathway most directly targeted by apocarotenoid repression. Consistent with the role of BRs and GAs as major upstream activators of *SAUR* expression—via BES1/BZR1 and DELLA degradation, respectively (Kono & Yin, 2020; Ren & Gray, 2015; Stamm & Kumar, 2013)—these results suggest that β-ion and β-cc dampen elongation by disrupting BR-dependent growth signaling rather than auxin-mediated transcription. Importantly, BRs exert contrasting effects depending on the light environment: they promote elongation under W (Tanaka *et al.*, 2003) but repress it in D (Chory & Li, 1997; Clouse, 2001), a duality that provides a useful framework to interpret the interaction with apocarotenoids, which may shift BR signaling toward its inhibitory mode to counteract shade-induced elongation.

Genetic analyses across BR, GA, and ABA signaling mutants revealed that β-ion–induced repression of elongation operates independently of DELLAs and EIN2, yet converges on the BR pathway. Under white light, BES1 emerged as a central node: the constitutively active *bes1-D* mutant displayed partial tolerance to both apocarotenoids (Fig. 5.4), consistent

with enhanced BR signaling counteracting their inhibitory effects (Fig. 5.1). Conversely, in *dellaKO* seedlings, apocarotenoid repression persisted even in the presence of EBL, indicating that only the DELLA-restrained component of BR-driven elongation can oppose this volatile inhibition. Supporting this view, GA_3 supplementation—which promotes DELLA degradation—partially relieved apocarotenoid repression across genotypes (Fig. 5.5), while the strong hypersensitivity of *bes1-D* to GA_3 highlighted the close interplay between DELLAs and BES1 (Fig. 5.5). Combined GA_3 and EBL treatments restored elongation in most backgrounds except *bes1-D* and *dellaKO*, reinforcing the dual requirement of both components for BR-mediated rescue.

The tolerance of *bes1-D* seedlings extended across light conditions: under low W, apocarotenoid repression was nearly abolished (Fig. 5.6), and cell-level analyses confirmed that constitutive BES1 activity reshaped elongation patterns and prevented inhibition at the cellular level(Fig. 5.7). Similarly, under W+FR, *bes1-D* showed strongly attenuated repression relative to Col-0 (Fig. 5.6). Together, these findings indicate that apocarotenoids act downstream of BR perception but converge on BES1-dependent transcriptional control of elongation.

The overlap between putative β-ion interactors and known BIN2 interactors highlights BIN2 as a potential convergence point between apocarotenoid perception and BR signaling (Fig. 5.12). BIN2 is a central regulator of BES1 activity, and its modulation would provide a direct route for β-ion to influence hypocotyl elongation. Among the nine interactors identified in common between β-ion and BIN2, two belong to the auxin pathway. TOL9 encodes an ubiquitin-binding protein involved in the endocytic sorting of the auxin efflux carrier PIN2, thereby influencing auxin transporter localization (Korbei *et al.*, 2013). ARF2 encodes an auxin response factor that functions as a transcriptional repressor in auxin signaling (Okushima *et al.*, 2005). These two elements constitute direct regulators of auxin-related processes, a pathway that is known to interact with BR signaling.

Beyond auxin-related interactors, other β-ion–BIN2 candidates suggest that this volatile may influence BIN2 through protein stability, folding, and metabolic integration. UBP6 and ATJ3 point to links with protein turnover and quality control, processes that could affect BIN2 abundance or the stability of its downstream effectors. PAL1, central to phenylpropanoid

biosynthesis, may connect apocarotenoid signaling with metabolic adjustments that feedback onto BR–BIN2 activity, for example through redox or structural constraints. Meanwhile, BCA5, AKR2, and EXA1 highlight potential inputs from carbon metabolism, protein targeting, and translational regulation, respectively, all of which could alter the efficiency or specificity of BIN2-dependent signaling. While conclusions remain very speculative at the moment, these candidates raise the possibility that β-ion might not act by directly blocking BIN2, but by shaping the cellular environment that defines its activity window, integrating metabolic and proteomic states with hormonal outputs.

Taken together, our findings support a model in which β-cc and β-ion repress seedling elongation by interfering with BR signaling downstream of perception but upstream of BES1 (Fig. D.7). Constitutively active BES1 confers strong tolerance, while genetic and pharmacological evidence highlight BIN2 and its regulatory partners as likely interception points, potentially modulated through crosstalk with auxin-related proteins or ubiquitin-dependent turnover. Although the exact molecular entry point remains to be defined, the evidence consistently points to apocarotenoids acting on central hubs of growth regulation, dampening both light- and hormone-induced elongation. In doing so, β-cc and β-ion emerge as volatile cues that antagonize the shade-avoidance program, redirecting developmental priorities from rapid elongation toward more conservative, stress-adaptive strategies.

Ecological context and future perspectives

All in all, the results discussed in the previous sections should be framed within a naturally occurring scenario: high-density plant communities where proximity shade signals are triggered. In such environments, plants undergo a profound physiological reprogramming that affects growth and development, photosynthesis, defense, and other processes (Roig-Villanova & Martínez-García, 2016). Light, in this scenario, is a principal environmental input: plants frequently remodel entire developmental programs to maximize its capture, even at the expense of reproduction or defense. These mechanisms are particularly evident in shade-avoider species, which perceive proximity shade as a light-competitive scenario, striving to outgrow their neighbors. By contrast, shade-tolerant plants do

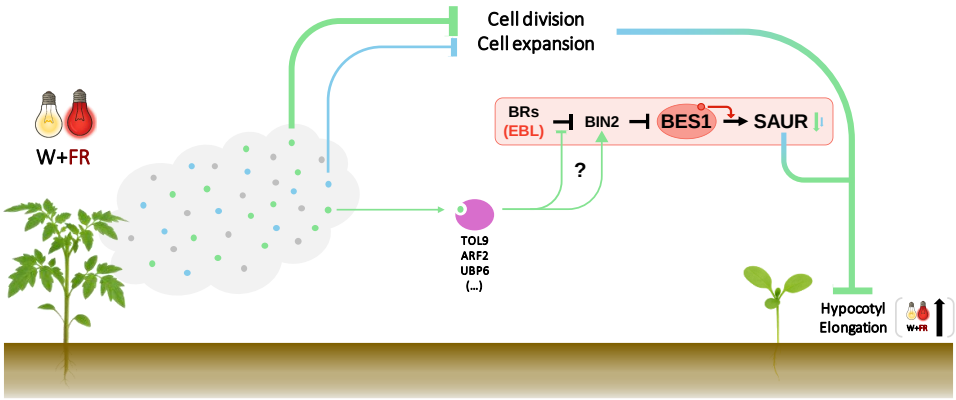

Figure D.7 — Model for apocarotenoid-mediated repression of hypocotyl elongation. *Schematic representation of the proposed mechanism by which airborne β-cyclocitral (β-cc) and β-ionone (β-ion) antagonize shade-induced elongation. Both compounds act downstream of BR perception but upstream of BES1, with BIN2 emerging as a potential interception point. By repressing BES1-dependent activation of SAUR genes, apocarotenoids suppress cell expansion and hypocotyl elongation. Exogenous BR input (EBL) can override this repression, whereas constitutively active BES1 (bes1-D) confers tolerance to β-cc and β-ion. Overall, these volatiles counteract the shade-avoidance program by directly interfering with BR-driven elongation growth.*

not interpret proximity shade the same way, and have evolved to attenuate shade avoidance responses, adjusting their physiology to avoid the costs of excessive elongation (Martinez-Garcia & Rodriguez-Concepcion, 2023). These divergent strategies raise the possibility that additional and/or alternative layers of regulation exist in crowded plant communities.

This is the biological context in which we have framed what we term the *shade volatilome*. In addition to canonical shade responses, recent studies have begun highlighting the potential role of VOCs. While shade-induced shifts in VOC emission have been documented, their biological significance has remained elusive. We revealed that the specific set of VOCs released in response to proximity shade act as environmental signals, triggering responses in neighboring individuals and thereby establishing a form of plant-to-plant communication. Our plant-to-plant communication system was designed to replicate, as closely as possible, the conditions of natural environments, while still providing the level of control required for standardized experimentation. We acknowledge that real ecological contexts involve a far greater degree of complexity, with multiple interacting variables that cannot be fully captured under laboratory

settings. Nevertheless, communication through volatiles within dense plant communities appears highly plausible: the reduced spacing among individuals not only facilitates VOC diffusion to neighboring plants but also increases the likelihood of surpassing the perceptual thresholds required to trigger biologically meaningful responses.

All in all, from an ecological perspective, the differential emission of VOCs under proximity shade raised key questions: why are they released, and what purpose do they serve? In receivers, the effect is robust—reduced elongation coupled with transcriptomic reprogramming—demonstrating that the shade volatilome operates as a consistent and meaningful signal. Two non-exclusive ecological interpretations could be proposed (Fig. D.8).

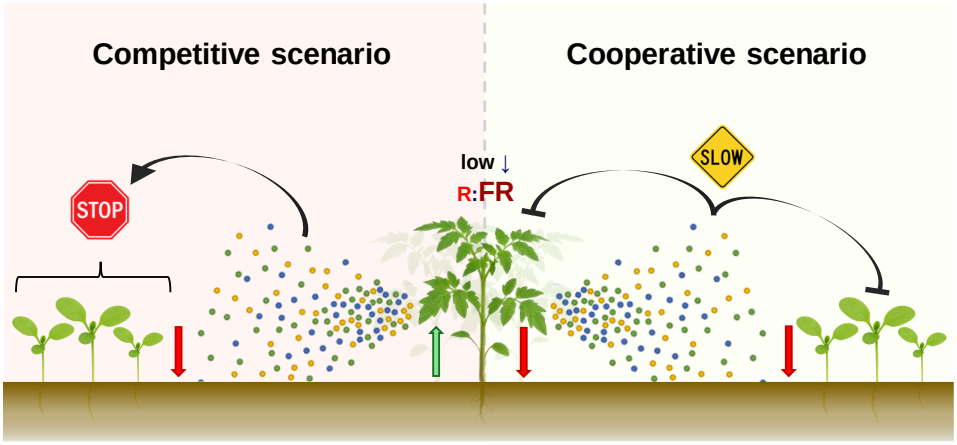

Figure D.8 — Hypothetical ecological outcomes of shade-induced volatile emission.

A *competitive scenario* (Fig. D.8) portrays that shaded plants emit VOCs to restrict elongation in neighboring individuals, thereby gaining a competitive advantage under proximity shade while continuing their own upward growth toward direct sunlight. The interspecific evidence, with tomato acting as emitter and *Arabidopsis* as receiver, further strengthens this hypothesis. Nonetheless, one limitation of this hypothesis lies in the possibility that shaded plants could also perceive and respond to their own emitted volatiles. Such a scenario complicates the purely competitive view.

Alternatively, a *cooperative view* (Fig. D.8) postulates that these volatiles act as a community-level cue, functioning as a potential regulatory layer to

temper excessive shade-associated responses. This perspective accommodates the idea of plants acting simultaneously as emitters and receivers, thereby contributing to collectively adjusting the growth under crowded conditions facing the shade-associated detrimental impacts.

A definitive test for this second hypothesis would require assessing volatile-mediated responses in receiver plants that are themselves growing under proximity shade, where such communication is most likely to be relevant. However, our approaches were directed to respond to different questions, aiming mostly to decipher the shade volatilome biological message at the molecular level. To test so, the use of different conditions and treatments, most times uncoupled from shade treatment or shade signaling processes, were mostly useful. Nonetheless, this research gap is something worth testing, and that would give the ultimate proof that would validate that hypothesis. Regardless of strategy, the recognition of the shade volatilome as a plant-to-plant signal marks a milestone in the study of volatile-mediated communication.

From an ecological perspective, the combined action of shade-responsive β-cc and β-ion, the two principal regulators within the shade volatilome according to our results, suggests that the shade volatilome functions not to reinforce shade-avoidance, but rather to counteract it. This antagonism can manifest in two complementary ways: directly, by repressing the very same growth-related pathways that are activated under low R:FR, such as SAUR-driven elongation or specific defense pathways; or indirectly, by modulating distinct processes that lead to opposite outcomes, such as the reinforcement of other defensive routes and photosynthesis, all at the expense of elongation. In either case, the overall effect is to temper the investment in shade-induced growth, redirecting resources toward survival and resilience.

In this light, we propose that the shade volatilome sparks a cooperative community-level strategy, functioning as a complex chemical cue that dampens shade avoidance and promotes a form of shade tolerance across neighbors (Fig. D.9). By restraining elongation and strengthening resilience traits, these volatiles may help plants allocate resources more effectively under crowded conditions, reducing investment in futile elongation and ensuring a more balanced adjustment to proximity shade. This scenario and their key roles within the shade volatilome underlines the ecological versatility of shade-derived apocarotenoids.

Looking ahead, much remains to be uncovered about the precise mechanisms by which β-cc and β-ion are perceived and transduced. The identity of their primary receptors, the confirmation of specific nodes of hormonal and signaling crosstalk they engage with, and the extent to which these responses operate under natural proximity shade conditions are questions that require further exploration. Yet, the results presented here provide a solid framework: they demonstrate that shade-derived apocarotenoids can act as potent airborne signals, shaping growth, defense, and photosynthetic outputs in ways that counterbalance shade avoidance. By doing so, they expand our understanding of volatile-mediated communication beyond stress cues, highlighting its role in modulating plastic developmental strategies within dense plant communities.

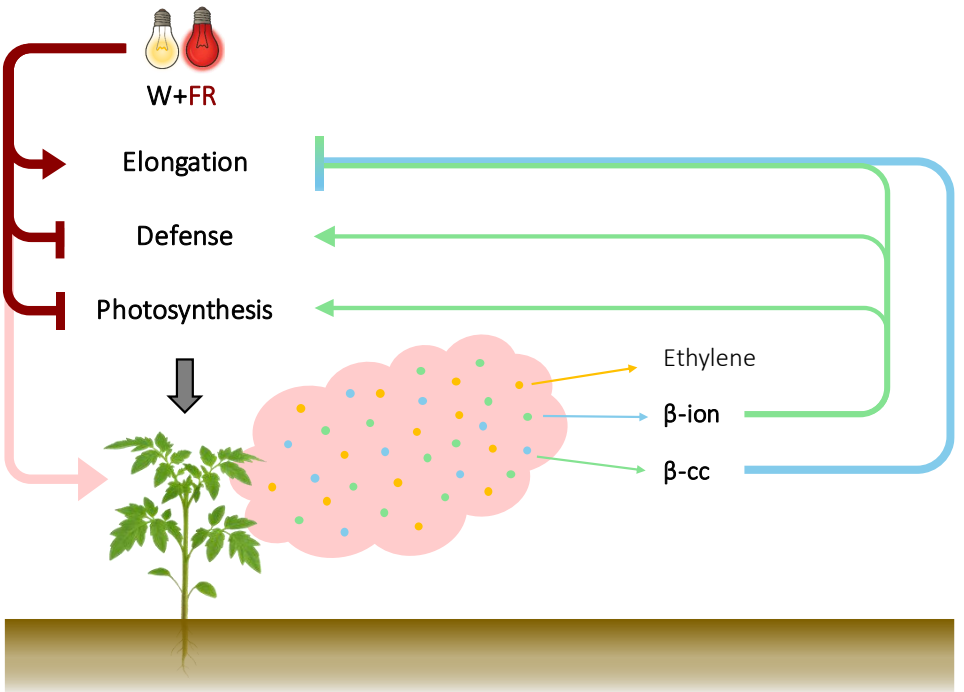

Figure D.9 — Integrative model of shade-induced volatile signaling. *Low R:FR conditions perceived by plants trigger the canonical responses of SAS (Promotion of elongation, repression of defenses and photosynthetic capacities), as well as the production of specific VOCs, prominently ethylene, β-cc and β-ion. Once released, the apocarotenoid volatiles act as airborne signals functioning as a community-level cue, shaping developmental and molecular responses in any plant exposed to them. Altogether, this model illustrates how shade volatiles counteract classical shade-avoidance outputs and contribute to community-level regulation of plant plasticity.*

Conclusions

Conclusions

1. Proximity shade changes the emission profile of volatile organic compounds (VOCs). The resulting blend, referred to as the shade volatilome, represses growth and reprograms transcriptional responses in non-shaded neighboring seedlings.
2. Shade-related transcriptional programs are partially conveyed through shade-responsive VOCs that carry environmental information.
3. The shade volatilome is enriched in ethylene and the apocarotenoids β-cyclocitral (β-cc) and β-ionone (β-ion).
4. Ethylene alone does not seem to account for the main physiological and transcriptional effects triggered by the shade volatilome.
5. β-cc and β-ion consistently mirror the physiological and transcriptional responses induced by the shade volatilome, positioning them as central signaling components of this communication system.
6. Each apocarotenoid compound elicits both common and distinct responses indicative of functional specificity.
7. β-cc appears to function as a fine-tuning signal that enhances stress resilience and adaptive transcriptomic reprogramming.
8. β-ion simultaneously primes defense and modulates phyB signaling, providing a physiological counterbalance to shade-avoidance signaling.
9. β-cc and β-ion jointly antagonize shade-induced elongation by interfering with brassinosteroid activity, likely through BES1-dependent signaling.
10. All in all, the shade volatilome, with a major contribution of β-cc and β-ion, represents an additional regulatory layer of SAS responses, contributing to plant-to-plant communication within crowded canopies.

Materials and Methods

Materials and Methods

- In order of appearance in the manuscript –

M.1 Plant material and growth conditions

M.1.1 Plant-to-plant communication experiments

M.1.1.1 Receiver seedlings

Arabidopsis thaliana wild type (WT, Col-0) and *Cardamine hirsuta* WT (OX) seedlings were used as model plants for volatile reception analyses. All A. thaliana mutants employed were generated in the Col-0 background, unless specified otherwise.

In a laminar flow hood, seeds were surface-sterilized by immersion in a 10% (v/v) bleach solution supplemented with 0.02% (v/v) Tween-20 for 10 min. Afterwards, they were rinsed five times with sterile distilled water and sown onto plates containing half-strength Murashige and Skoog (0.5× MS) medium solidified with 1% (w/v) agar, without sucrose. For treatments requiring chemical supplementation, compounds were incorporated into the medium during preparation; concentrations are specified in the corresponding sections. The rounded edge of the plates was covered with Micropore (3M) tape, allowing air exchange from the inside and outside of the plate.

Plates with *A. thaliana* or *C. hirsuta* seeds were stratified in darkness at 4 °C for 2–3 days before being transferred to growth chambers under long-day (16 h of light, 8 h of darkness) conditions. Unless otherwise indicated, seedlings were cultivated under the standardized light regimes detailed below:

- **D (Darkness):** PPFD = 0 µmol m^{-2} s^{-1}
- **Low W (Low White light):** PPFD = 25-27 µmol m^{-2} s^{-1}; R:FR = 4-5.5

For D conditions, seeds were pre-irradiated with white light for 2 h to trigger germination, then covered with two layers of aluminum foil and placed

inside a closed cardboard box to ensure complete darkness. Under these conditions, etiolated seedlings were grown for 3–4 days.

For Low W conditions, seeds germinated and grew for 5 days under low W before being connected to the corresponding volatilome treatment. Specifications for each experiment are given in figure legends.

M.1.1.2 Emitter plants

Solanum lycopersicum WT plants (cv. M82 and cv. Micro-Tom) were used as model species for volatile emission analyses. Seeds were surface sterilized as described previously for *A. thaliana.* Tomato seeds did not require stratification.

Seeds were initially incubated for 3 days under darkness (D conditions) and subsequently transferred to white light (W). By day 7 post-sowing, germinated seedlings at comparable developmental stages were transferred to a greenhouse chamber and planted in 12-cm round pots. Seedlings were cultivated for an additional 3–4 weeks under a long-day (LD) photoperiod of 16 h light / 8 h dark, at 24 °C and controlled relative humidity (60 % RH).

Light conditions in the greenhouse were as follows:

- **W (White light):** PPFD = 110-140 µmol m^{-2} s^{-1}; R:FR = 3.6-5
- **W+FR (simulated shade):** PPFD = 110-140 µmol m^{-2} s^{-1} ; R:FR = 0.12-0.16

M.1.2 Petri-dish system for volatile exposure

Arabidopsis thaliana wild type (WT, Col-0) and *Cardamine hirsuta* WT (OX) seedlings were used as model plants for volatile reception analyses. All A. thaliana mutants employed were generated in the Col-0 background, unless specified otherwise.

In a laminar flow hood, seeds were surface-sterilized by immersion in a 10% (v/v) bleach solution supplemented with 0.02% (v/v) Tween-20 for 10 min. Afterwards, they were rinsed five times with sterile distilled water and sown onto plates containing half-strength Murashige and Skoog (0.5× MS)

medium solidified with 1% (w/v) agar, without sucrose. For treatments requiring chemical supplementation, compounds were incorporated into the medium during preparation; concentrations are specified in the corresponding sections. The rounded edge of the plates was covered with Micropore (3M) tape, allowing air exchange from the inside and outside of the plate.

- **D (Darkness):** PPFD = 0 µmol m^{-2} s^{-1}
- **W (White light):** PPFD = 45-53 µmol m^{-2} s^{-1}; R:FR = 3.2-4.4
- **Low W (Low White light):** PPFD = 25-31 µmol m^{-2} s^{-1}; R:FR = 3.8-5.5
- **W+FR (simulated shade):** PPFD = 37-48 µmol m^{-2} s^{-1} ; R:FR = 0.04-0.06

For D conditions, seeds were pre-irradiated with white light for 2 h to trigger germination. After this time period, the airborne apocarotenoid treatment is applied and the plates are then covered with two layers of aluminum foil and placed inside a closed cardboard box to ensure complete darkness. Under these conditions, etiolated seedlings were grown for 3–4 days.

In the cases of W, low W or W+FR conditions, seeds germinate and grew under W for 2 days. After this time period, the airborne apocarotenoid treatment is applied and the plates are subsequently transferred to their respective light conditions, where they grow and develop. Five days later (day 7), the effects of airborne apocarotenoid exposure are measured.

M.2 Plant-to-plant communication set-ups

Informative tables (Tables 1.1 / 1.2) were generated for each plant-to-plant communication experiment, specifying the conditions of individual trials. The tables include variations in experimental design, genotypes and varieties used, number and age of emitter plants, among other parameters. Hereinafter, the standard experimental designs for both systems are described.

M.2.1 Same-box system (Fig. 1.1, Table 1.S1)

Plexiglass boxes (41 x 41 x 45.5 cm; e-boxes) were used to perform same-box plant-to-plant communication experiments, in which both emitter

tomato plants and receiver *A. thaliana* seedlings were placed alongside each other in the same receptacle to conduct the experiments.

Emitter tomato plants were prepared as described in section M.1.2 and transferred into the boxes at ~30–40 days of age. Petri dishes containing stratified A. thaliana seeds were irradiated under W for 2 h to induce germination, then covered with two layers of aluminum foil and subsequently enclosed in cardboard boxes to ensure etiolated growth (D). These dishes were placed at the base of the plexiglass boxes, next to the pots containing tomato plants.

Once both emitter and receiver plants were positioned, the system was hermetically closed and placed under greenhouse W or W+FR conditions. After 3 days of volatile-mediated interaction, the boxes were opened, and the hypocotyl length of etiolated A. thaliana seedlings was measured.

M.2.2 Two-box system (Fig. 1.3, Table 1.S2)

E-boxes were used in this case exclusively as receptacles for emitter tomato plants. Each e-box was connected through silicon tubes (TYGON 3350®) to a smaller plexiglass box (19x19x5.5 cm; r-boxes), in which up to 4 Petri dishes containing *A. thaliana* receiver seedlings could be placed at the base.

Emitter tomato plants were prepared as described in section M.1.2 and transferred into e-boxes at ~30–40 days of age. Receiver *A. thaliana* seedlings were germinated and grown for 2 days under W conditions before being transferred into the r-boxes. Once emitter and receiver plants were positioned in their respective boxes, the systems were sealed and exposed to their corresponding light regimes (W or W+FR for emitter plants; Low W for receiver seedlings).

An air pump (Fisherbrand™ UFB70155) generated a unidirectional airflow from the e-box to the r-box at a rate of 9.2 L min^{-1}. After 5 days of volatile-mediated interaction, the airflow was stopped, the boxes were opened, and receiver seedlings were analyzed for hypocotyl elongation and photosynthetic performance.

M.2.3 Shade volatilome RNAseq: variation in the experimental design

The experimental design to obtain samples for RNA-seq was based on the two-box system described above, with specific modifications. In this case, emitter tomato plants of the same age were transferred into e-boxes and acclimated for 1 day under W or W+FR conditions prior to connecting the boxes, in order to promote differential volatile emissions before the onset of plant-to-plant communication.

Stratified *A. thaliana* receiver seedlings were placed into r-boxes, where they germinated and grew for 5 days under Low W conditions. After this period, e-boxes and r-boxes were connected via silicone tubing and airflow was initiated using a pump. Samples corresponding to time 0 h were collected immediately before communication started. Receiver boxes were then opened for sample collection at 3 h, 8 h, and 24 h, and later used for RNA extraction and sequencing.

In addition, a second r-box was subsequently connected in parallel to the system, following the same experimental design as above (M.1.2), and used as a control for shade-volatilome effects.

M.3 Hypocotyl elongation measurements

After the respective treatments, seedlings were carefully laid on Petri dishes and photographed. A 2-cm ruler was included in each image as a scale reference. Unless otherwise specified, experiments comprised three biological replicates, each consisting of at least 25 seedlings per treatment or genotype.

Hypocotyl length was measured from calibrated images using ImageJ software (NIH, USA), which allowed standardized, reproducible, and unbiased quantification of seedling growth parameters. Data from the different biological replicates were averaged and represented in scatter bar plots, showing the mean values of the three biological replicates together with their associated standard deviations (SD), except when stated differently.

M.4 Photosynthetic efficiency analysis

Photosynthetic efficiencies were assessed through chlorophyll fluorescence measurements, which were performed with a MAXI-PAM fluorometer (Heinz Walz GmbH) following a protocol adapted from the manufacturer's standard rapid light curve program. After a period for dark adaptation (at least 30 min), minimal fluorescence (F_0) was recorded over 5 s with a measuring light, and maximal fluorescence (F_m) was determined by applying a saturating pulse of 800 ms duration. Subsequently, actinic light was applied for 90 s. Actinic illumination was provided at instrument setting 24 (Act1, MAXI-PAM; Heinz Walz GmbH), corresponding to the manufacturer's standard rapid light curve protocol, which translated in an intensity of PPFD = 21 µmol m^{-2} s^{-1}. During this 90s period, steady-state fluorescence (Fs) was monitored. At the end of the actinic illumination period, a second saturating pulse (800 ms) was applied to determine maximal fluorescence under light (Fm′).

The maximum quantum yield of PSII (F_v/F_m) was calculated as (F_m–F_0)/F_m. The effective quantum yield (ΦPSII) was calculated as (Fm′–Fs)/Fm′. Unless otherwise specified, measurements were performed on 3 biological replicates per treatment, with 8 technical repeats (individual seedlings) each. Data from the different biological replicates were averaged and represented in scatter bar plots, showing the mean values of the three biological replicates together with their associated standard deviations (SD).

M.5 Gene expression analysis

Total RNA was extracted from fresh seedling tissue (approximately 50 mg per sample) using the PureLink® RNA Mini Kit (Ambion, Life Technologies™), following the manufacturer's instructions. RNA concentration and purity were assessed with a NanoDrop spectrophotometer (Thermo Scientific), and RNA integrity was evaluated by loading 2 µL of each sample on an agarose gel. RNA concentrations were subsequently normalized to 100 ng $µL^{-1}$.

cDNA synthesis was performed using the NZY First-Strand cDNA synthesis Kit (Nzytech®). Quantitative real-time PCR (RT-qPCR) was conducted on a QuantStudio 3 Real-Time PCR system (Thermo Scientific)

using SYBR Green chemistry in 20-µL reactions set up in 96-well plates. Primer sequences are listed in Table M5.4.

Relative transcript levels of target genes were calculated using the comparative Ct method (ΔΔCt), with AtEF1α employed as the reference gene.

Table M5.1 – cDNA synthesis

Reagent	Volume (µL)	Thermocycling conditions
Template RNA (1 µg)	1-10	5 minutes at 65ºC, then 1 min in ice
10x Annealing Buffer	1	
Oligo dT	1	
Nuclease free water	Up to 10	
NZYRT Master Mix	10 (prepared in previous step)	30 minutes at 50ºC, Inactivation for 5 minutes at 85ºC
NZYRT Enzyme Mix	2	
Nuclease free water	8	

Table M5.2 – qPCR mix reaction

Reagent	Volume (µL) for 96-well plates
SYBR Green Master Mix 2x	10
Template cDNA (100 ng)	1
Oligo Fw	0.6
Oligo Rv	0.6
Nuclease free water	7.8
Final Volume	20

Table M5.3 – qPCR program

Step	Temperature	Time	Cycles
Polymerase activation	95ºC	10 minutes	1x
Denaturation	95ºC	15 seconds	40x
Annealing + Extension	60ºC	1 minute	

Table M5.4 – qPCR primers

Oligo	5' → 3'	Gene ID
MUO7	GTTACGCCAGACGAAATCAAAG	AT1G16400 (CYP79F2)
MUO8	CCAAGTGTCCACTCCATGTTA	
MUO9	CAAAGCCGTCATCTTGGATATTG	AT4G13770 (CYP83A1)
MUO10	TCAACACTTGTGGGTACTTCAT	
MUO11	CCATTAAGACCATCGCCAAGA	AT5G23010 (GSM1; IMS3; MAM1)
MUO12	AGCTATGGCGCATATCACAG	
SPO102	ATGATTACTGGTACCTCCCAGGC	AT5G30690 (EF1α)
SPO103	CTCACGGGTCTGACCATCCT	

M.6 RNAseq Analysis

RNA was extracted as described for gene expression analysis, up to concentration normalization phase. Two independent RNA-seq datasets (Shade volatilome and Airborne apocarotenoids, 28 and 30 samples, respectively) were processed identically by BGI Genomics (Shenzhen, China) using the *DNBSEQ* platform (paired-end, 150 bp reads; Phred+33 encoding). Both datasets underwent the same bioinformatic pipeline up to functional enrichment analysis. Read processing, alignment, gene quantification, and the initial differential expression analysis were performed by BGI. Based on these processed data, we carried out sample clustering and functional enrichment analyses. Details of these steps, whether performed by BGI or by us, are described in the following subsections.

M.6.1 Read processing

Raw reads were quality-checked and filtered using *SOAPnuke* (v1.5.6) (Y. Chen *et al.*, 2018). Reads containing adapter sequences, reads with an ambiguous base ratio (N) >0.1%, and reads in which >20% of bases had quality scores below Q15 were removed. Across samples, >95% of reads passed filtering, with >92% of bases exceeding Q30.

M.6.2 Read alignment

Clean reads were aligned to the Arabidopsis thaliana reference genome (*Araport11*, release v2201) using *HISAT2* (v2.2.1) with default sensitive parameters and strandedness set to RF. In addition, *Bowtie2* (v2.5.0) was employed to align reads to the reference gene set, with unique mapping rates exceeding 87% on average.

M.6.3 Gene quantification

Transcript abundances were estimated with *RSEM* (v1.3.1), providing both raw gene counts and transcript-per-million (TPM) normalized expression values. Across samples, more than 24,000 expressed genes were detected.

M.6.4 Differential expression analysis

Differential expression analysis was performed in R (v4.4.1) using the *DESeq2* package (v1.49.4) (Love *et al.*, 2014). Raw gene counts obtained from *RSEM* were first filtered to remove lowly expressed genes (retaining those with at least 10 counts in ≥2 samples). Data were normalized by library size, and variance-stabilizing transformation was applied for exploratory analyses (e.g., PCA).

Differential expression was tested using *DESeq2*'s Wald test within a multifactorial design that included time, treatment, and their interaction (design = ~ time + treatment + time:treatment). Pairwise contrasts between treatments at given time points were extracted by subsetting the dataset

accordingly and re-fitting the model. To improve effect-size estimation, $\log_2$ fold changes were shrunk using the *apeglm* method (A. Zhu *et al.*, 2019).

Genes were considered differentially expressed if they met the following criteria:

- Q-values ≤ 0.05
- A log2FC threshold > 0.585 (FC>1.5) was explored to balance sensitivity and specificity. The set of genes tested in the DE analysis served as the background.

M.6.5 Exploratory analysis (PCA and sample clustering)

To assess overall transcriptome variation across conditions, principal component analysis (PCA) was performed on variance-stabilized counts obtained from *DESeq2*. Sample-to-sample similarity was further evaluated by calculating Pearson correlation coefficients and representing them as clustered heatmaps.

M.6.6 Functional enrichment

Functional enrichment analyses were performed in R (v4.4.1) using the *clusterProfiler* package (v4.14.6) (Wu *et al.*, 2021). Differentially expressed genes (DEGs) were separated into up- and down-regulated subsets according to the thresholds defined in section M.6.4 (FDR ≤ 0.05, $|\log_2 FC| \geq 0.585$).

For Gene Ontology (GO) enrichment, biological process (BP) categories were tested using a hypergeometric test with false discovery rate (FDR) correction. Only terms with Q-values ≤ 0.05 and a minimum of three genes per term were considered significant.

For KEGG pathway analysis, enrichment was carried out with *clusterProfiler::enrichKEGG*, using the Arabidopsis thaliana annotation (organism code “ath”). Background gene sets were defined as all expressed genes retained after filtering. Results were visualized as dot plots ranking the most significantly enriched pathways.

M.7 VOCs Emission Analysis

Volatile organic compound (VOC) emission assays were performed at the facilities of the Max Planck Institute for Chemical Ecology (MP-ICE, Jena, Germany), in a greenhouse growth chamber specifically adapted for this purpose. Growth conditions for tomato plants were adjusted to closely match those employed in Valencia; a comparative summary of growth parameters between both facilities is provided (Table 2.1).

Solanum lycopersicum cv. M82 plants at a comparable developmental stage (30–35 days old) were used as VOC emitters. A total of twenty plants were employed for VOC collection. Two days before sampling, each tomato plant was covered with a custom-made plastic bag designed to fully enclose the aerial tissues. On the following day, ten of the bagged plants were transferred to W+FR light conditions, which was defined as time zero (T_0).

VOC sampling was carried out every 24 h for up to 5 consecutive days, starting at day 1 (T_1). During each collection period, the bags were hermetically closed, and two ports were connected to the system: the inlet port was connected to provide charcoal-filtered air, while the outlet was connected to a cartridge containing 25 mg of PoraPak Q (Supelco) serving as a VOC adsorbent trap. Airflow was adjusted to 0.7 L min^{-1} (inlet) and 0.4 L min^{-1} (outlet). VOC collection was performed for 2 h daily, from 09:00 to 11:00.

After each collection period, cartridges were removed, and VOCs were desorbed using 200 µL dichloromethane (DCM) containing nonyl acetate (10 ng μL^{-1}; Sigma-Aldrich) as an internal standard. Extracted VOCs were analyzed using an Agilent 6890 series gas chromatograph (GC) coupled to either an Agilent 5973 MSD for qualitative identification, or to a flame ionization detector (FID) for quantitative determination. The GC was operated with helium as carrier gas at 1 mL min^{-1} under splitless injection mode (220 °C, 1 µL). Separation was achieved on a DB-5MS column (30 m × 0.25 mm, 0.25 µm film, J & W Scientific, Folsom, CA, USA), and a temperature program: initial hold at 40 °C for 2 min, ramp at 7 °C min^{-1} to 155 °C, then 60 °C min^{-1} to 300 °C, and a final hold at 350 °C for 2 min. The GC was coupled to a single quadrupole MS operated in electron impact (EI) mode (70 eV), with transfer line at 270 °C and scan range m/z 40–350.

VOC identification was achieved by comparing retention times and mass spectra with reference profiles from the NIST Mass Spectral Library, and further validated by calculating Kovats retention indices against published values or by authentic standards. Quantification was performed from GC–FID data based on peak areas relative to the internal standard. Relative response factors were obtained with authentic standards or estimated using the effective carbon number concept, and values were normalized to plant fresh weight (FW) and sampling duration, expressed as ng h^{-1} g^{-1} FW.

M.7.1 Diurnal Emission Analysis

To investigate diurnal emission patterns over a 24-h period, tomato plants were grown as specified in M.6 at the Max Planck Institute for Chemical Ecology (MP-ICE, Jena, Germany). Sixteen *Solanum lycopersicum* cv. M82 plants at a comparable developmental stage (30–35 days old) were used as VOC emitters. Plants were covered with tailored plastic bags two days before sampling, and the following day (day 0), eight of the bagged plants were transferred to W+FR light conditions, defined as time zero (T_0).

VOC sampling was carried out every 4 hours, starting at day 1. Collections longed for 2 hours, conducted at 6:00AM (T_1), 10:00AM, 2:00PM, 6:00PM, 10:00PM and 6:00AM^{+1} (T_6). VOC collection, desorption and GC-MS analysis were performed as described in M.6.

M.8 Ethylene Quantification Analysis

Leaves for ethylene quantification were obtained from plants grown in soil (10 × 10 cm square pots) at 22 °C under greenhouse W long-day conditions for 4 weeks. Rosette leaves (in *A. thaliana* and *C. hirsuta*) or leaflets of fully expanded tomato leaves were excised, weighed, and placed inside 15 mL transparent glass vials that did not alter light quality. Vials containing the samples were sealed and placed horizontally under either W or W+FR conditions for 24 h (Fig. 2.S4).

For seedling assays, approximately 100 surface-sterilized A. thaliana seeds were sown on 0.5x MS medium in 50 mL short wide-mouth bottles. Bottles were initially closed with transparent Petri dish lids and sealed with

Micropore tape (3M). Following stratification and germination at 22 °C under W or W+FR conditions for 7 days, lids were replaced with airtight caps fitted with silicone septa to allow gas sampling. Seedlings were incubated for 24 h under the specified light conditions before measurement.

Ethylene accumulation in vials (detached leaves) and bottles (seedlings) was quantified using an ETD-300 photoacoustic ethylene detector (Sensor Sense, Nijmegen, The Netherlands). Ethylene production rates were normalized to fresh weight of the plant material.

M.9 GUS Staining Assays

Two GUS reporter lines were used in this study (EBSn:GUS / DR5:GUS). The experimental designs and growth conditions associated with these assays are described in the corresponding sections above. Following sample collection, GUS staining was performed as follows:

Seedlings were first transferred to 90% (v/v) acetone and incubated at 4 °C for at least 24 h. Samples were then washed twice with 50 mM Na_2PO_4 buffer (pH 7.2) at room temperature. Washed seedlings were immersed in GUS staining solution consisting of 50 mM Na_2PO_4 buffer (pH 7.2), 1 mM EDTA, 0.1% (v/v) Triton X-100 and 0.5 mg mL^{-1} X-Gluc. When specified, the solution was supplemented with 1 mM potassium ferrocyanide/ferricyanide. Samples were incubated in the dark at 37 °C until staining was clearly visible (incubation times for each experiment are specified in figure legends).

After staining, the buffer was discarded, and the seedlings were sequentially washed with solutions with different levels of ethanol (70%, 100% and 50% (v/v), consecutively). Finally, samples were transferred to 50% (v/v) glycerol and mounted on microscope slides for visualization and image acquisition.

M.10 Carotenoid analysis

Leaf carotenoids were extracted from 4 mg of freeze-dried tissue, placed in 2 mL microcentrifuge tubes. Extractions were carried out by adding 375

µL methanol as extraction solvent and 25 µL of 10% (w/v) canthaxanthin solution in chloroform (Sigma-Aldrich) as internal standard. Three 4-mm glass beads were added to each tube, and samples were homogenized in a TissueLyser II (QIAGEN) for 30 s after each solvent addition step.

Subsequently, 400 µL Tris–NaCl buffer (pH 7.5) and 800 µL chloroform were added sequentially. As calibration controls, two tubes containing only 25 µL of the canthaxanthin solution were processed in parallel but left untreated until the end of the extraction procedure.

Samples were centrifuged at 13,000 rpm for 5 min at 4 °C, and the lower organic phase was transferred to new 1.5 mL tubes. Extracts were concentrated in a SpeedVac system for at least 1 h. The dried residue was resuspended in 200 µL acetone, and samples were sonicated for 15 s to recover any carotenoids adhering to tube walls. Finally, extracts were filtered through 0.2 µm cellulose-acetate syringe filters into amber 2 mL glass vials, which were used as receptacles for HPLC analysis.

A 33 µL aliquot of each extract was injected onto an Agilent 1200 Series HPLC system (Agilent Technologies). Eluting carotenoids were monitored with a photodiode array detector (PDA), and peak areas were determined at 470 nm for lycopene, lutein, β-carotene, violaxanthin, neoxanthin, and canthaxanthin, using Agilent ChemStation software. Quantification was performed by comparison with the internal standard (Canthaxanthin, Sigma-Aldrich), and normalized to the sample weight.

M.11 VOC production analysis

Fresh leaf tissue from tomato plants was sampled and frozen with liquid N_2. The tissue was ground while frozen using a TissueLyser II and 150mg of ground tissue was later transferred to 15mL GC-MS vials, keeping it frozen during the process. Vials were kept at -80ºC until GC-MS pre-processing.

Samples were taken in groups of 5 to pre-processing, 15 minutes prior to the start of GC-MS analysis. 1 mL of CaCl 6M and 150 µL of EDTA 0.5M were added to the vial, and once closed again, the vial underwent sonication for 5 minutes. After this process, vials were placed in the GC-MS to be processed.

Volatile compound analysis was performed by head-space solid-phase microextraction (HS-SPME) (López-Gresa *et al.*, 2017). Enhanced ChemStation software (Agilent) was the program used to obtain and analyze the chromatograms and mass spectra. Identification of the compounds was achieved by running compound standards and/or comparing their mass spectra with the one of NIST (NIH). Quantification of compounds was either relativized and/or estimated with standard solutions (M.12). For VOC quantification, the following m/z quantifier ions GC areas and retention times were used: β-cyclocitral (β-cc): 137/152 and 31.43 min. / β-ionone (β-ion): 177 and 38.7 min.

M.12 System for airborne apocarotenoids treatment

To apply apocarotenoids strictly as volatiles, we developed a simple system based on standard 9-cm round Petri dishes (Fig. 3.S1). Depending on the experimental design (Plant growth described in M.1.2), at the required time point the micropore tape covering the dish edge was removed, and under a laminar flow hood a sterilized cap cleaved from 100-µL qPCR tubes was placed upright in the center of the Petri dish, where the seeds or seedlings were growing. Into this cap, 10 µL of a solution at a known concentration of either β-cyclocitral (500 mM) or β-ionone (100 mM) was pipetted, unless otherwise specified. The dish was then sealed with two rounds of Parafilm, and four equidistant holes were punctured with a sterile pipette tip (Fig. 3.S2) to allow air exchange while minimizing apocarotenoid leakage. Once completed, the system was transferred back to the growth chamber and placed under the corresponding light conditions.

M.13 Estimation of airborne apocarotenoid HS concentration

M.13.1 Standard curve for volatile apocarotenoids

To establish a calibration curve correlating airborne apocarotenoid concentrations with their corresponding extracted ion chromatogram (EIC) peak areas, standard solutions of β-cc (Sigma-Aldrich, >90%) and β-ion (Sigma-Aldrich, 96%) were prepared in DMSO (LabKem, >99.9%) at concentrations ranging from 100 nM to 10 mM in tenfold dilution series. Aliquots of 10 µL from each solution were transferred into 15 mL GC-MS

vials, which were subsequently analyzed under the same SPME-GC-MS conditions described in M.11 (López-Gresa *et al.*, 2017). During the initial heating step, it was assumed that the entire content of the 10 µL aliquot volatilized, allowing the calculation of the specific headspace (HS) concentration in each vial. Peak areas of the characteristic m/z quantifier ions were recorded, and the correlation between HS concentration and peak area was log-transformed to yield a linear relationship between the two variables.

M.13.2 Estimation of atmospheric concentration in the Petri dish experimental setup

SPME fibers for GC-MS analysis were positioned above 0.5× MS medium in 12 × 12 cm square plates, which were used instead of standard 9 cm Petri dishes to allow proper fiber placement within the system. To maintain proportionality with the standard setup (M.12), the amount of apocarotenoid solution applied to the tube caps was increased threefold (0.5 M for β-cc and 0.1 M for β-ion, respectively). After placing the apocarotenoid solution on the tube cap, plates were sealed with Parafilm, which was then pierced four times (one on each side of the square plate). From that point, apocarotenoids volatilized and accumulated in the headspace (HS), enabling fiber adsorption of the atmospheric fraction. The system was kept closed for 1, 4, 24, 48, 72, 96, or 120 hours, after which fibers were collected and the adsorbed content of β-cc and β-ion was analyzed by SPME-GC-MS (M.11). Headspace concentrations of both compounds were determined based on calibration curves described in M.13.1.

M.14 Germination studies

A. thaliana seeds were sterilized and stratified as described in M.1.2. Following stratification, seeds were transferred either to white light (W) or to darkness (D) after a 2 h germination-inducing light pulse. Under these conditions, germination rates were scored every 24 h, up to 7 days or to stable germination rates in each population. Radicle emergence was used as the criterion for germination. For seedlings kept in darkness,

observations and counting were performed under green-filtered light to avoid light-induced responses.

M.15 Glucosinolates extraction and analysis

Glucosinolate measurements were performed at the Max Planck Institute for Chemical Ecology (Jena, Germany). For each sample, 10 mg of freeze-dried and finely ground tissue from A. thaliana or C. hirsuta seedlings were weighed into 2 mL Eppendorf tubes. Intact glucosinolates were extracted with 1.5 mL of 80% (v/v) methanol under continuous shaking for 5 min in a TissueLyser. Insoluble debris was pelleted by centrifugation (2500 × g, 10 min), and the supernatants were applied to columns preloaded with 0.4 mL of a 10% (w/v) suspension of DEAE Sephadex A25 in water. Columns were sequentially washed with 1 mL 80% (v/v) methanol, 1 mL water, and 1 mL 0.02 M MES buffer (pH 5.2), after which 50 µL of sulfatase solution were added. Following overnight incubation at room temperature, desulphated glucosinolates were eluted with 2 × 0.8 mL of 60% (v/v) methanol, dried at 50 °C under a nitrogen stream, and resuspended in 0.4 mL water. Identification and quantification of glucosinolates were carried out by HPLC as described in Burow *et al.*, 2006.

M.16 Phytohormone extraction and analysis

Phytohormone measurements were carried out at the Max Planck Institute for Chemical Ecology (Jena, Germany). For each sample, 10 mg of freeze-dried and finely ground tissue from A. thaliana or C. hirsuta seedlings were weighed into 96-well plates. Extraction was performed by adding 1 mL of methanol containing internal standards (D_2-JA, D_4-SA, and D_6-ABA at 10 ng/mL) using a micropipette. Plates were hermetically sealed, shaken for 15 min using an adapted vortexer, and centrifuged. Subsequently, 400 µL of the supernatant were collected. Quantification of targeted compounds was performed by HPLC–MS/MS (HPLC 1260 Infinity II, Agilent Technologies, Santa Clara, CA, USA – QTrap® 6500+, AB Sciex, Waltham, MA, USA) in multiple reaction monitoring mode, following Medina-van Berkum *et al.*, 2024 with few modifications. with minor modifications. Phytohormone levels were determined relative to their corresponding authentic standards (D_2-JA, D_4-SA, and D_6-ABA).

M.17 Confocal Imaging

M.17.1 Calcofluor White staining – Cell Length Quantification

To measure cell length along the hypocotyl axis, seedlings were excised from the growth medium, and the roots and cotyledons were removed with a razor blade. Hypocotyls were immediately transferred to 4% (w/v) paraformaldehyde (PFA) in 1× phosphate-buffered saline (PBS) for fixation. Samples were subjected to vacuum infiltration for 1 h, followed by two washes of 1 min each in 1× PBS.

Fixed tissues were then cleared in ClearSee solution (10% w/v xylitol, 15% w/v sodium deoxycholate, 25% w/v urea, dissolved in distilled water) (Kurihara *et al.*, 2015) for at least one week. After clearing, samples were incubated for 1 h in 0.1% (w/v) Calcofluor White (Fluorescent Brightener 28; Sigma-Aldrich) prepared in ClearSee. Tissues were subsequently washed in ClearSee for ≥30 min prior to mounting on slides.

Imaging was performed with a Zeiss confocal laser scanning microscope (Zeiss® 780 Axio-Observer) equipped with a 405 nm (1.5%) fluorescence source and a 415-510 nm detection threshold. Images were processed using Fiji (v1.54p), and cell lengths were measured using the calibrated scale bar provided by the microscope.

M.17.2 35S:PHYB-GFP line – Photobody quantification and analysis

For visualization of PHYB-GFP photobodies, seedlings expressing the 35S:PHYB-GFP construct were excised from the growth medium and mounted directly in distilled water on microscope slides. No fixation or clearing was applied to preserve GFP fluorescence.

Imaging was performed using the same Zeiss confocal laser scanning microscope equipped with a GFP-compatible excitation/emission setup (excitation: 488 nm laser line, 2%; detection window: 490–530 nm). Seedlings were imaged under identical acquisition settings across treatments to ensure comparability.

Imaging analysis was carried out using Fiji (v1.54p). Per every image, nuclei within the image range were counted. For each nucleus, the number of photobodies was manually counted.

M.18 Docking in-silico analysis

In silico docking analyses were performed to evaluate potential binding pockets for β-ionone on the *A. thaliana* RACK1A protein. The 3D structure of RACK1A was obtained from Protein Data Bank (PDB, ID: 3DM0), and prepared by removing water molecules and adding hydrogen atoms. β-ionone 3D structure was retrieved from PubChem (CID: 638014). Docking simulations were performed with AutoDock Vina v.1.1.2, using a blind docking approach with a search grid covering the entire protein surface. β-ionone structure was energy-minimized and converted to a PDBQT format. The top-ranked pose was selected based on binding energy (kcal/mol) and cluster consistency, and further analyzed using PyMOL to visualize predicted interactions.

M.19 Data Visualization

All graphical representations were generated either in GraphPad Prism (v8.0.1) for basic statistical plots (boxplots, bar charts with error bars, scatterplots) or in R (v4.4.1; R Core Team, 2024) for custom transcriptomic and metabolomic visualizations. In R, we employed *DESeq2* (Love *et al.*, 2014) for variance-stabilizing transformation (VST) of RNA-seq count data, followed by *pheatmap* (Kolde, 2019) for clustered heatmaps with significance annotation. *clusterProfiler* (Wu *et al.*, 2021) together with *org.At.tair.db* (Carlson *et al.*, 2019) was used for GO Biological Process and KEGG pathway enrichment, visualized with dotplots using *enrichplot* (Yu, 2023). Exploratory analysis of transcriptome-wide structure relied on PCA computed with *DESeq2* VST values and visualized in both 2D using *ggplot2* (Wickham, 2016). Complementary GO-BP barplots were produced by direct gene-to-term mapping via *GO.db* (The Gene Ontology Consortium, 2021), summarizing enriched terms by associated gene counts. Targeted metabolite data (glucosinolates) were represented as faceted barplots using *tidyverse* packages (Wickham *et al.*, 2019), where mean ± SD values were overlaid with jittered raw points to highlight within-group dispersion. Together, these tools provided a reproducible, flexible framework to tailor visualizations to each dataset.

Specifications for all data visualizations created with R are given in the subsections below. All R scripts used for data visualization are publicly

available at GitHub: https://github.com/mikatxu-thesis/Thesis-R-Scripts/tree/main, ensuring transparency and reproducibility.

M.19.1 PCA Analysis

Principal component analysis (PCA) was performed on variance-stabilized counts obtained with *DESeq2* in R. Raw read count matrices and associated sample metadata were used to build a *DESeq2* dataset, which was then filtered to remove genes with consistently low expression (≥10 reads in at least 4 samples). Variance stabilizing transformation (VST) was applied prior to PCA to reduce mean–variance dependency across genes. The first three principal components were extracted, and the variance explained by each was reported. Two-dimensional (PC1 vs PC2) visualizations were generated with *ggplot2*, including replicate labels and custom color coding by treatment group.

M.19.2 KEGG pathway enrichment dotplots

For KEGG pathway enrichment, we performed pathway enrichment on predefined gene sets (ATG identifiers) using *clusterProfiler*. TAIR IDs were mapped to Entrez IDs (org.At.tair.db), and enrichment was tested against a whole-genome background (all TAIRs mappable to Entrez). Results were visualized with dot plots (top categories by adjusted p-value), and full enrichment tables were exported for reproducibility.

M.19.3 GO-BP enrichment dotplots

Gene Ontology (GO) enrichment analysis for Biological Process (BP) categories was performed in R using the *clusterProfiler* package. Input gene lists (TAIR IDs) were obtained from differential expression overlaps, and enrichment was calculated against a custom RNA-seq–derived universe. Results were visualized as dotplots, displaying the top enriched categories ranked by adjusted p-value.

M.19.4 GO-BP Distribution Barplots

Gene Ontology annotations were retrieved by mapping TAIR IDs to GO terms with *org.At.tair.db* and *GO.db* in R. For each input gene list (CSV column), GO records were filtered to Biological Process (BP) and collapsed to unique (gene, term) pairs to avoid double counting. Terms were then tallied as the number of associated genes per BP term, filtered by a minimum gene threshold (default ≥5), and the top N terms (default 25) were visualized as horizontal bar plots using *ggplot2*. Term labels were wrapped to improve readability. Outputs included the bar plot (PNG) and a CSV table reporting counts per BP term; an auxiliary table preserving GO IDs was also generated, together with helper queries to list the TAIR genes contributing to any selected term.

M.19.5 Heatmaps

Heatmaps were generated from raw RNA-seq counts of A. thaliana using variance-stabilizing transformation (VST) implemented in DESeq2. Replicates were collapsed into treatment–time groups, and predefined gene sets (provided as lists of ATG identifiers) were extracted for visualization. For each set, a matrix was plotted representing row Z-scores (Each row–gene–is scaled independently: the mean expression of the gene across all conditions is set to 0, and values are expressed in units of standard deviations from this mean). Columns were ordered according to experimental design, and samples were annotated by treatment and time. Gene identifiers were mapped to symbols where available, ensuring consistent labeling across heatmaps. Plots were generated with the *pheatmap* package in R, using a blue–white–red palette to reflect relative expression levels.

M.19.6 Glucosinolates barplots

Glucosinolate data (μmol g^{-1} FW) were processed in R (*tidyverse*). Wide tables were minimally curated (column renaming) and reshaped to long format (compound-wise) prior to summarization. For each species × treatment × compound combination, we computed the mean and standard deviation. Visualization used *ggplot2* as dodged bar charts (mean ± SD) with jittered raw points overlaid to display within-group dispersion. Plots

were faceted by compound with free y-scales, employed custom color palettes for treatments (bars and points), and included axis/panel styling facets.

M.20 Language editing and use of AI-assisted tools

The preparation of this thesis was supported using AI-based tools (OpenAI, ChatGPT). These tools were employed in two ways: (i) to improve grammar, clarity, and style of sections already drafted by the author, and (ii) to assist in generating and troubleshooting R scripts. All scripts obtained through AI assistance were reviewed, validated, and adapted by the author before being applied to data analysis. No data, analyses, or scientific interpretations were generated by AI. All conceptual content, experimental design, data analysis, and interpretation of results remain the sole responsibility of the author.

Bibliography

Bibliography

Alder, A., Jamil, M., Marzorati, M., Bruno, M., Vermathen, M., Bigler, P., Ghisla, S., Bouwmeester, H., Beyer, P., & Al-Babili, S. (2012). The path from β-carotene to carlactone, a strigolactone-like plant hormone. *Science*, *335*(6074), 1348–1351.

Alonso, J. M., Hirayama, T., Roman, G., Nourizadeh, S., & Ecker, J. R. (1999). EIN2, a Bifunctional Transducer of Ethylene and Stress Responses in *Arabidopsis*. *Science*, *284*(5423), 2148–2152. https://doi.org/10.1126/science.284.5423.2148

Amtmann, A., Hammond, J. P., Armengaud, P., & White, P. J. (2005). Nutrient Sensing and Signalling in Plants: Potassium and Phosphorus. In *Advances in Botanical Research* (Vol. 43, pp. 209–257). Elsevier. https://doi.org/10.1016/S0065-2296(05)43005-0

Argueso, C. T., Hansen, M., & Kieber, J. J. (2007). Regulation of ethylene biosynthesis. *Journal of Plant Growth Regulation*, *26*(2), 92–105.

Attridge, T. H. (1990). *Light and plant responses: A study of plant photophysiology and the natural environment*. Cambridge University Press.

Auldridge, M. E., McCarty, D. R., & Klee, H. J. (2006). Plant carotenoid cleavage oxygenases and their apocarotenoid products. *Current Opinion in Plant Biology*, *9*(3), 315–321. https://doi.org/10.1016/j.pbi.2006.03.005

Baba, S. A., Jain, D., Abbas, N., & Ashraf, N. (2015). Overexpression of *Crocus* carotenoid cleavage dioxygenase, *CsCCD4b*, in *Arabidopsis* imparts tolerance to dehydration, salt and oxidative stresses by modulating ROS machinery. *Journal of Plant Physiology*, *189*, 114–125. https://doi.org/10.1016/j.jplph.2015.11.001

Bae, G., & Choi, G. (2008). Decoding of light signals by plant phytochromes and their interacting proteins. *Annu. Rev. Plant Biol.*, *59*, 281–311.

Baldwin, I. T., Halitschke, R., Paschold, A., Von Dahl, C. C., & Preston, C. A. (2006). Volatile Signaling in Plant-Plant Interactions: “Talking Trees” in the Genomics Era. *Science*, *311*(5762), 812–815. https://doi.org/10.1126/science.1118446

Baldwin, I. T., & Schultz, J. C. (1983). Rapid changes in tree leaf chemistry induced by damage: Evidence for communication between plants. *Science*, *221*(4607), 277–279. https://doi.org/10.1126/science.221.4607.277

Ballaré, C. L. (1999). Keeping up with the neighbours: Phytochrome sensing and other signalling mechanisms. *Trends in Plant Science*, *4*(3), 97–102.

Ballaré, C. L., & Pierik, R. (2017). The shade-avoidance syndrome: Multiple signals and ecological consequences. *Plant, Cell & Environment*, *40*(11), 2530–2543. https://doi.org/10.1111/pce.12914

Ballaré, C. L., Scopel, A. L., & Sanchez, R. A. (1990). Far-red radiation reflected from adjacent leaves: An early signal of competition in plant canopies. *Science*, *247*(4940), 329–332.

Banerjee, S., Siemianowski, O., Liu, M., Lind, K. R., Tian, X., Nettleton, D., & Cademartiri, L. (2019). Stress response to CO2 deprivation by Arabidopsis thaliana in plant cultures. *PLOS ONE*, *14*(3), e0212462. https://doi.org/10.1371/journal.pone.0212462

Basu, S., Ramegowda, V., Kumar, A., & Pereira, A. (2016). Plant adaptation to drought stress. *F1000Research*, *5*, 1554. https://doi.org/10.12688/f1000research.7678.1

Batschauer, A. (1999). Light perception in higher plants. *Cellular and Molecular Life Sciences CMLS*, *55*(2), 153–166.

Bedini, A., Mercy, L., Schneider, C., Franken, P., & Lucic-Mercy, E. (2018). Unraveling the Initial Plant Hormone Signaling, Metabolic Mechanisms and Plant Defense Triggering the Endomycorrhizal Symbiosis Behavior. *Frontiers in Plant Science*, *9*. https://doi.org/10.3389/fpls.2018.01800

Beisel, K. G., Schurr, U., & Matsubara, S. (2011). Altered turnover of β-carotene and Chl a in Arabidopsis leaves treated with lincomycin or norflurazon. *Plant and Cell Physiology*, *52*(7), 1193–1203.

Bengtsson, J., Fagerström, T., & Rydin, H. (1994). Competition and coexistence in plant communities. *Trends in Ecology & Evolution*, *9*(7), 246–250.

Binder, B. M., O'Malley, R. C., Rodriguez, F. I., Esch, J. J., O'Donnell, P., Klee, H. J., & Bleecker, A. B. (2005). *Ethylene-Binding Activity, Gene-Expression Levels, and Receptor-System Output for Ethylene-Receptor Family Members from Arabidopsis and Tomato*.

Björkman, T. (1988). *Perception of Gravity by Plants*. Academic Press.

Bleecker, A. B. (1999). Ethylene perception and signaling: An evolutionary perspective. *Trends in Plant Science*, *4*(7), 269–274.

Bleeker, P. M., Diergaarde, P. J., Ament, K., Guerra, J., Weidner, M., Schütz, S., De Both, M. T. J., Haring, M. A., & Schuurink, R. C. (2009). The Role of Specific Tomato Volatiles in Tomato-Whitefly Interaction. *Plant Physiology*, *151*(2), 925–935. https://doi.org/10.1104/pp.109.142661

Blom, C. W. P. M., & Voesenek, L. A. C. J. (1996). Flooding: The survival strategies of plants. *Trends in Ecology & Evolution*, *11*(7), 290–295. https://doi.org/10.1016/0169-5347(96)10034-3

Böhning, R. H., & Burnside, C. A. (1956). The effect of light intensity on rate of apparent photosynthesis in leaves of sun and shade plants. *American Journal of Botany*, 557–561.

Bolton, M. D. (2009, April 6). *Primary Metabolism and Plant Defense—Fuel for the Fire* (world) [Research-article]. Https://Doi.Org/10.1094/MPMI-22-5-0487; The American Phytopathological Society. https://doi.org/10.1094/MPMI-22-5-0487

Boncan, D. A. T., Tsang, S. S. K., Li, C., Lee, I. H. T., Lam, H.-M., Chan, T.-F., & Hui, J. H. L. (2020). Terpenes and Terpenoids in Plants: Interactions with Environment and Insects. *International Journal of Molecular Sciences*, *21*(19), 7382. https://doi.org/10.3390/ijms21197382

Booker, M. A., & DeLong, A. (2015). Producing the Ethylene Signal: Regulation and Diversification of Ethylene Biosynthetic Enzymes1. *Plant Physiology*, *169*(1), 42–50. https://doi.org/10.1104/pp.15.00672

Bou-Torrent, J., Toledo-Ortiz, G., Ortiz-Alcaide, M., Cifuentes-Esquivel, N., Halliday, K. J., Martinez-García, J. F., & Rodriguez-Concepcion, M. (2015).

Regulation of carotenoid biosynthesis by shade relies on specific subsets of antagonistic transcription factors and cofactors. *Plant Physiology*, *169*(3), 1584–1594.

Braam, J. (2005). In touch: Plant responses to mechanical stimuli. *New Phytologist*, *165*(2), 373–389. https://doi.org/10.1111/j.1469-8137.2004.01263.x

Braasch, J., & Kaplan, I. (2012). Over what distance are plant volatiles bioactive? Estimating the spatial dimensions of attraction in an arthropod assemblage. *Entomologia Experimentalis et Applicata*, *145*(2), 115–123. https://doi.org/10.1111/j.1570-7458.2012.01317.x

Broeckling, C. D., Broz, A. K., Bergelson, J., Manter, D. K., & Vivanco, J. M. (2008). Root Exudates Regulate Soil Fungal Community Composition and Diversity. *Applied and Environmental Microbiology*, *74*(3), 738–744. https://doi.org/10.1128/aem.02188-07

Brooker, R. W., Maestre, F. T., Callaway, R. M., Lortie, C. L., Cavieres, L. A., Kunstler, G., Liancourt, P., Tielbörger, K., Travis, J. M., & Anthelme, F. (2008). Facilitation in plant communities: The past, the present, and the future. *Journal of Ecology*, 18–34.

Büchel, K., Malskies, S., Mayer, M., Fenning, T. M., Gershenzon, J., Hilker, M., & Meiners, T. (2011). How plants give early herbivore alert: Volatile terpenoids attract parasitoids to egg-infested elms. *Basic and Applied Ecology*, *12*(5), 403–412. https://doi.org/10.1016/j.baae.2011.06.002

Burbano-Erazo, E., Francesca, S., Palau-Rodriguez, J., Berdonces, A., Valverde-Carbajal, L., Perez-Beser, J., Addonizio, M., Martinez-Garcia, J. F., Rigano, M. M., & Rodriguez-Concepcion, M. (2025). *A tomato line hyposensitive to simulated proximity shade shows altered auxin-related gene expression and improved fruit yield under high-density field conditions*. Plant Biology. https://doi.org/10.1101/2025.03.18.643865

Burgie, E. S., Bussell, A. N., Walker, J. M., Dubiel, K., & Vierstra, R. D. (2014). Crystal structure of the photosensing module from a red/far-red light-absorbing plant phytochrome. *Proceedings of the National Academy of Sciences*, *111*(28), 10179–10184.

Burow, M., Müller, R., Gershenzon, J., & Wittstock, U. (2006). Altered Glucosinolate Hydrolysis in Genetically Engineered Arabidopsis thaliana

and its Influence on the Larval Development of Spodoptera littoralis. *Journal of Chemical Ecology*, *32*(11), 2333–2349. https://doi.org/10.1007/s10886-006-9149-1

Canarini, A., Kaiser, C., Merchant, A., Richter, A., & Wanek, W. (2019). Root Exudation of Primary Metabolites: Mechanisms and Their Roles in Plant Responses to Environmental Stimuli. *Frontiers in Plant Science*, *10*. https://doi.org/10.3389/fpls.2019.00157

Cargnel, M. D., Demkura, P. V., & Ballaré, C. L. (2014). Linking phytochrome to plant immunity: Low red: Far-red ratios increase A rabidopsis susceptibility to B otrytis cinerea by reducing the biosynthesis of indolic glucosinolates and camalexin. *New Phytologist*, *204*(2), 342–354.

Carlson, M., Falcon, S., Pages, H., & Li, N. (2019). Org. At. Tair. Db: Genome wide annotation for Arabidopsis. *Bioconductor Version*, 3.

Casal, J. J. (2013). Photoreceptor signaling networks in plant responses to shade. *Annual Review of Plant Biology*, *64*(1), 403–427.

Catola, S., Centritto, M., Cascone, P., Ranieri, A., Loreto, F., Calamai, L., Balestrini, R., & Guerrieri, E. (2018). Effects of single or combined water deficit and aphid attack on tomato volatile organic compound (VOC) emission and plant-plant communication. *Environmental and Experimental Botany*, *153*, 54–62.

Cerrudo, I., Keller, M. M., Cargnel, M. D., Demkura, P. V., de Wit, M., Patitucci, M. S., Pierik, R., Pieterse, C. M. J., & Ballaré, C. L. (2012). Low Red/Far-Red Ratios Reduce Arabidopsis Resistance to Botrytis cinerea and Jasmonate Responses via a COI1-JAZ10-Dependent, Salicylic Acid-Independent Mechanism. *Plant Physiology*, *158*(4), 2042–2052. https://doi.org/10.1104/pp.112.193359

Chen, I.-J., Lo, W.-S., Chuang, J.-Y., Cheuh, C.-M., Fan, Y.-S., Lin, L.-C., Wu, S.-J., & Wang, L.-C. (2013). A chemical genetics approach reveals a role of brassinolide and cellulose synthase in hypocotyl elongation of etiolated Arabidopsis seedlings. *Plant Science*, *209*, 46–57. https://doi.org/10.1016/j.plantsci.2013.04.005

Chen, J.-G. (2006). RACK1 mediates multiple hormone responsiveness and developmental processes in Arabidopsis. *Journal of Experimental Botany*, *57*(11), 2697–2708. https://doi.org/10.1093/jxb/erl035

Chen, M., Chory, J., & Fankhauser, C. (2004). Light signal transduction in higher plants. *Annu. Rev. Genet.*, *38*(1), 87–117.

Chen, M., Tao, Y., Lim, J., Shaw, A., & Chory, J. (2005). Regulation of Phytochrome B Nuclear Localization through Light-Dependent Unmasking of Nuclear-Localization Signals. *Current Biology*, *15*(7), 637–642. https://doi.org/10.1016/j.cub.2005.02.028

Chen, Y., Chen, Y., Shi, C., Huang, Z., Zhang, Y., Li, S., Li, Y., Ye, J., Yu, C., & Li, Z. (2018). SOAPnuke: A MapReduce acceleration-supported software for integrated quality control and preprocessing of high-throughput sequencing data. *Gigascience*, *7*(1), gix120.

Cheng, Z., Li, J.-F., Niu, Y., Zhang, X.-C., Woody, O. Z., Xiong, Y., Djonović, S., Millet, Y., Bush, J., McConkey, B. J., Sheen, J., & Ausubel, F. M. (2015). Pathogen-secreted proteases activate a novel plant immune pathway. *Nature*, *521*(7551), 213–216. https://doi.org/10.1038/nature14243

Chory, J., & Li, J. (1997). Gibberellins, brassinosteroids and light-regulated development. *Plant, Cell & Environment*, *20*(6), 801–806.

Chou, C.-H. (1999). Roles of allelopathy in plant biodiversity and sustainable agriculture. *Critical Reviews in Plant Sciences*, *18*(5), 609–636.

Christaki, E., Bonos, E., Giannenas, I., & Florou-Paneri, P. (2012). Aromatic Plants as a Source of Bioactive Compounds. *Agriculture*, *2*(3), 228–243. https://doi.org/10.3390/agriculture2030228

Clouse, S. D. (2001). Integration of light and brassinosteroid signals in etiolated seedling growth. *Trends in Plant Science*, *6*(10), 443–445.

Coppola, M., Cascone, P., Madonna, V., Di Lelio, I., Esposito, F., Avitabile, C., Romanelli, A., Guerrieri, E., Vitiello, A., Pennacchio, F., Rao, R., & Corrado, G. (2017). Plant-to-plant communication triggered by systemin primes anti-herbivore resistance in tomato. *Scientific Reports*, *7*(1). https://doi.org/10.1038/s41598-017-15481-8

Cortés, L. E., Weldegergis, B. T., Boccalandro, H. E., Dicke, M., & Ballaré, C. L. (2016). Trading direct for indirect defense? Phytochrome B inactivation in tomato attenuates direct anti-herbivore defenses whilst enhancing volatile-mediated attraction of predators. *New Phytologist*, *212*(4), 1057–1071. https://doi.org/10.1111/nph.14210

Courbier, S., Snoek, B. L., Kajala, K., Li, L., Van Wees, S. C., & Pierik, R. (2021). Mechanisms of far-red light-mediated dampening of defense against Botrytis cinerea in tomato leaves. *Plant Physiology*, *187*(3), 1250–1266.

D'Alessandro, S., Ksas, B., & Havaux, M. (2018). Decoding β-Cyclocitral-Mediated Retrograde Signaling Reveals the Role of a Detoxification Response in Plant Tolerance to Photooxidative Stress. *The Plant Cell*, *30*(10), 2495–2511. https://doi.org/10.1105/tpc.18.00578

Das, D., St. Onge, K. R., Voesenek, L. A., Pierik, R., & Sasidharan, R. (2016). Ethylene-and shade-induced hypocotyl elongation share transcriptome patterns and functional regulators. *Plant Physiology*, *172*(2), 718–733.

De Wit, M., Spoel, S. H., Sanchez-Perez, G. F., Gommers, C. M. M., Pieterse, C. M. J., Voesenek, L. A. C. J., & Pierik, R. (2013). Perception of low red:far-red ratio compromises both salicylic acid- and jasmonic acid-dependent pathogen defences in A rabidopsis. *The Plant Journal*, *75*(1), 90–103. https://doi.org/10.1111/tpj.12203

Delory, B. M., Delaplace, P., Fauconnier, M.-L., & Du Jardin, P. (2016). Root-emitted volatile organic compounds: Can they mediate belowground plant-plant interactions? *Plant and Soil*, *402*(1–2), 1–26. https://doi.org/10.1007/s11104-016-2823-3

Deshpande, S., Manoharan, R., & Mitra, S. (2021). Exogenous β-cyclocitral treatment primes tomato plants against drought by inducing tolerance traits, independent of abscisic acid. *Plant Biology (Stuttgart, Germany)*, *23 Suppl 1*, 170–180. https://doi.org/10.1111/plb.13210

Deshpande, S., & Mitra, S. (2023). β-Cyclocitral-Mediated Metabolic Changes Optimize Growth and Defense Responses in Solanum lycopersicum L. *Metabolites*, *13*(3), 329. https://doi.org/10.3390/metabo13030329

Deshpande, S., Purkar, V., & Mitra, S. (2021). β-Cyclocitral, a Master Regulator of Multiple Stress-Responsive Genes in Solanum lycopersicum L. Plants. *Plants*, *10*(11), 2465. https://doi.org/10.3390/plants10112465

Devlin, P. F., Patel, S. R., & Whitelam, G. C. (1998). Phytochrome E Influences Internode Elongation and Flowering Time in Arabidopsis. *The Plant Cell*, *10*(9), 1479–1487. https://doi.org/10.1105/tpc.10.9.1479

Devlin, P. F., Robson, P. R. H., Patel, S. R., Goosey, L., Sharrock, R. A., & Whitelam, G. C. (1999). Phytochrome D Acts in the Shade-Avoidance Syndrome in Arabidopsis by Controlling Elongation Growth and Flowering Time1. *Plant Physiology*, *119*(3), 909–916. https://doi.org/10.1104/pp.119.3.909

Dickinson, A. J., Lehner, K., Mi, J., Jia, K.-P., Mijar, M., Dinneny, J., Al-Babili, S., & Benfey, P. N. (2019). β-Cyclocitral is a conserved root growth regulator. *Proceedings of the National Academy of Sciences*, *116*(21), 10563–10567. https://doi.org/10.1073/pnas.1821445116

Djakovic-Petrovic, T., Wit, M. de, Voesenek, L. A. C. J., & Pierik, R. (2007). DELLA protein function in growth responses to canopy signals. *The Plant Journal*, *51*(1), 117–126. https://doi.org/10.1111/j.1365-313X.2007.03122.x

Durand, M., Murchie, E. H., Lindfors, A. V., Urban, O., Aphalo, P. J., & Robson, T. M. (2021). Diffuse solar radiation and canopy photosynthesis in a changing environment. *Agricultural and Forest Meteorology*, *311*, 108684. https://doi.org/10.1016/j.agrformet.2021.108684

Elhakeem, A., Markovic, D., Broberg, A., Anten, N. P. R., & Ninkovic, V. (2018). Aboveground mechanical stimuli affect belowground plant-plant communication. *PLOS ONE*, *13*(5), e0195646. https://doi.org/10.1371/journal.pone.0195646

Engelberth, J., Alborn, H. T., Schmelz, E. A., & Tumlinson, J. H. (2004). Airborne signals prime plants against insect herbivore attack. *Proceedings of the National Academy of Sciences*, *101*(6), 1781–1785. https://doi.org/10.1073/pnas.0308037100

Escobar-Bravo, R., Schimmel, B. C. J., Zhang, Y., Wang, L., Robert, C. A. M., Glauser, G., Ballaré, C. L., & Erb, M. (2024). Far-red light increases maize volatile emissions in response to volatile cues from neighbouring

plants. *Plant, Cell & Environment*, *47*(10), 3979–3998. https://doi.org/10.1111/pce.14995

Fawzy, S., Osman, A. I., Doran, J., & Rooney, D. W. (2020). Strategies for mitigation of climate change: A review. *Environmental Chemistry Letters*, *18*(6), 2069–2094. https://doi.org/10.1007/s10311-020-01059-w

Felemban, A., Moreno, J. C., Mi, J., Ali, S., Sham, A., AbuQamar, S. F., & Al-Babili, S. (2024). The apocarotenoid β-ionone regulates the transcriptome of *Arabidopsis thaliana* and increases its resistance against *Botrytis cinerea*. *The Plant Journal*, *117*(2), 541–560. https://doi.org/10.1111/tpj.16510

Fennell, H., Olawin, A., Mizanur, R. M., Izumori, K., Chen, J.-G., & Ullah, H. (2012). Arabidopsis scaffold protein RACK1A modulates rare sugar D-allose regulated gibberellin signaling. *Plant Signaling & Behavior*, *7*(11), 1407–1410. https://doi.org/10.4161/psb.21995

Finlayson, S. A., Lee, I.-J., & Morgan, P. W. (1998). *Phytochrome B and the Regulation of Circadian Ethylene Production in Sorghum*.

Finlayson, S. A., Lee, I.-J., Mullet, J. E., & Morgan, P. W. (1999). The Mechanism of Rhythmic Ethylene Production in Sorghum. The Role of Phytochrome B and Simulated Shading1. *Plant Physiology*, *119*(3), 1083–1090. https://doi.org/10.1104/pp.119.3.1083

Fluhr, R., Mattoo, A. K., & Dilley, D. R. (1996). Ethylene—Biosynthesis and perception. *Critical Reviews in Plant Sciences*, *15*(5–6), 479–523.

Frank, H. A., & Cogdell, R. J. (1996). Carotenoids in Photosynthesis. *Photochemistry and Photobiology*, *63*(3), 257–264. https://doi.org/10.1111/j.1751-1097.1996.tb03022.x

Franklin, K. A., & Quail, P. H. (2010). Phytochrome functions in Arabidopsis development. *Journal of Experimental Botany*, *61*(1), 11–24.

Franklin, K. A., & Whitelam, G. C. (2007). Light-quality regulation of freezing tolerance in Arabidopsis thaliana. *Nature Genetics*, *39*(11), 1410–1413.

Fu, Y., Zhu, W., Zhou, Y., Su, Y., Li, Z., Zhang, D., Zhang, D., Shen, J., & Liang, J. (2024). RACK1A promotes hypocotyl elongation by scaffolding

light signaling components in *Arabidopsis*. *Journal of Integrative Plant Biology*, *66*(5), 956–972. https://doi.org/10.1111/jipb.13651

Galstyan, A., Cifuentes-Esquivel, N., Bou-Torrent, J., & Martinez-Garcia, J. F. (2011). The shade avoidance syndrome in Arabidopsis: A fundamental role for atypical basic helix–loop–helix proteins as transcriptional cofactors. *The Plant Journal*, *66*(2), 258–267. https://doi.org/10.1111/j.1365-313X.2011.04485.x

Galvão, V. C., & Fankhauser, C. (2015). Sensing the light environment in plants: Photoreceptors and early signaling steps. *Current Opinion in Neurobiology*, *34*, 46–53.

Gamble, R. L., Coonfield, M. L., & Schaller, G. E. (1998). Histidine kinase activity of the ETR1 ethylene receptor from Arabidopsis. *Proceedings of the National Academy of Sciences*, *95*(13), 7825–7829.

Gangappa, S. N., & Botto, J. F. (2016). The Multifaceted Roles of HY5 in Plant Growth and Development. *Molecular Plant*, *9*(10), 1353–1365. https://doi.org/10.1016/j.molp.2016.07.002

García-Gómez, P., Almagro, G., Sánchez-López, Á. M., Bahaji, A., Ameztoy, K., Ricarte-Bermejo, A., Baslam, M., Antolín, M. C., Urdiain, A., López-Belchi, M. D., López-Gómez, P., Morán, J. F., Garrido, J., Muñoz, F. J., Baroja-Fernández, E., & Pozueta-Romero, J. (2019). Volatile compounds other than CO_2 emitted by different microorganisms promote distinct posttranscriptionally regulated responses in plants. *Plant, Cell & Environment*, *42*(5), 1729–1746. https://doi.org/10.1111/pce.13490

Gershenzon, J. (2007). Plant volatiles carry both public and private messages. *Proceedings of the National Academy of Sciences*, *104*(13), 5257–5258. https://doi.org/10.1073/pnas.0700906104

González-Grandío, E., Poza-Carrión, C., Sorzano, C. O. S., & Cubas, P. (2013). BRANCHED1 Promotes Axillary Bud Dormancy in Response to Shade in Arabidopsis. *The Plant Cell*, *25*(3), 834–850. https://doi.org/10.1105/tpc.112.108480

Gonzalez-Guzman, M., Pizzio, G. A., Antoni, R., Vera-Sirera, F., Merilo, E., Bassel, G. W., Fernández, M. A., Holdsworth, M. J., Perez-Amador, M. A., Kollist, H., & Rodriguez, P. L. (2012). Arabidopsis PYR/PYL/RCAR Receptors Play a Major Role in Quantitative Regulation of Stomatal

Aperture and Transcriptional Response to Abscisic Acid. *The Plant Cell*, *24*(6), 2483–2496. https://doi.org/10.1105/tpc.112.098574

Gruber, M. Y., Xu, N., Grenkow, L., Li, X., Onyilagha, J., Soroka, J. J., Westcott, N. D., & Hegedus, D. D. (2009). Responses of the Crucifer Flea Beetle to Brassica Volatiles in an Olfactometer. *Environmental Entomology*, *38*(5), 1467–1479. https://doi.org/10.1603/022.038.0515

Guo, D., Liu, Z., Raaijmakers, J. M., Xu, Y., Yang, J., Erb, M., Zhang, J., Zhu, Y.-G., Xu, J., & Hu, L. (2025). Linalool-triggered plant-soil feedback drives defense adaptation in dense maize plantings. *Science*, *389*(6761), eadv6675. https://doi.org/10.1126/science.adv6675

Guo, H., & Ecker, J. R. (2004). The ethylene signaling pathway: New insights. *Current Opinion in Plant Biology*, *7*(1), 40–49. https://doi.org/10.1016/j.pbi.2003.11.011

Guo, J., & Chen, J.-G. (2008). RACK1 genes regulate plant development with unequal genetic redundancy in Arabidopsis. *BMC Plant Biology*, *8*(1), 108. https://doi.org/10.1186/1471-2229-8-108

Gyula, P., Schäfer, E., & Nagy, F. (2003). Light perception and signalling in higher plants. *Current Opinion in Plant Biology*, *6*(5), 446–452. https://doi.org/10.1016/S1369-5266(03)00082-7

Halkier, B. A., & Gershenzon, J. (2006). Biology and biochemistry of glucosinolates. *Annu. Rev. Plant Biol.*, *57*(1), 303–333.

Halliday, K. J., Koornneef, M., & Whitelam, G. C. (1994). Phytochrome B and at Least One Other Phytochrome Mediate the Accelerated Flowering Response of Arabidopsis thaliana L. to Low Red/Far-Red Ratio. *Plant Physiology*, *104*(4), 1311–1315. https://doi.org/10.1104/pp.104.4.1311

Hay, A. S., Pieper, B., Cooke, E., Mandáková, T., Cartolano, M., Tattersall, A. D., Ioio, R. D., McGowan, S. J., Barkoulas, M., Galinha, C., Rast, M. I., Hofhuis, H., Then, C., Plieske, J., Ganal, M., Mott, R., Martinez-Garcia, J. F., Carine, M. A., Scotland, R. W., … Tsiantis, M. (2014). Cardamine hirsuta: A versatile genetic system for comparative studies. *The Plant Journal*, *78*(1), 1–15. https://doi.org/10.1111/tpj.12447

Heil, M., & Karban, R. (2010). Explaining evolution of plant communication by airborne signals. *Trends in Ecology & Evolution*, *25*(3), 137–144.

Heilman, M. D., Meredith, F. I., & Gonzalez, C. L. (n.d.). *Ethylene Production in the Cotton Plant (Gossypium hirsutum L.) Canopy and Its Effect on Fruit Abscission*. *11*(1). https://doi.org/10.2135/cropsci1971.0011183X001100010008x

Herrmann, K. M. (1995). The Shikimate Pathway: Early Steps in the Biosynthesis of Aromatic Compounds. *The Plant Cell*, *7*, 907–919.

Holopainen, J. K., & Gershenzon, J. (2010). Multiple stress factors and the emission of plant VOCs. *Trends in Plant Science*, *15*(3), 176–184. https://doi.org/10.1016/j.tplants.2010.01.006

Ho-Plágaro, T., & García-Garrido, J. M. (2022). Molecular Regulation of Arbuscular Mycorrhizal Symbiosis. *International Journal of Molecular Sciences*, *23*(11), 5960. https://doi.org/10.3390/ijms23115960

Hornitschek, P., Lorrain, S., & Fankhauser, C. (2009, October 22). *Inhibition of the shade avoidance response by formation of non-DNA binding bHLH heterodimers | The EMBO Journal*. https://www.embopress.org/doi/full/10.1038/emboj.2009.306

Hu, L., Robert, C. A. M., Cadot, S., Zhang, X., Ye, M., Li, B., Manzo, D., Chervet, N., Steinger, T., Van Der Heijden, M. G. A., Schlaeppi, K., & Erb, M. (2018). Root exudate metabolites drive plant-soil feedbacks on growth and defense by shaping the rhizosphere microbiota. *Nature Communications*, *9*(1). https://doi.org/10.1038/s41467-018-05122-7

Huang, X.-Q., & Dudareva, N. (2023). Plant specialized metabolism. *Current Biology*, *33*(11), R473–R478. https://doi.org/10.1016/j.cub.2023.01.057

Huber, M., Nieuwendijk, N. M., Pantazopoulou, C. K., & Pierik, R. (2021). Light signalling shapes plant-plant interactions in dense canopies. *PLANT CELL AND ENVIRONMENT*, *44*(4), 1014–1029. https://doi.org/10.1111/pce.13912

Hughes, J. E., Morgan, D. C., Lambton, P. A., Black, C. R., & Smith, H. (1984). Photoperiodic time signals during twilight. *Plant, Cell & Environment*, *7*(4), 269–277.

Ibdah, M., Azulay, Y., Portnoy, V., Wasserman, B., Bar, E., Meir, A., Burger, Y., Hirschberg, J., Schaffer, A. A., Katzir, N., Tadmor, Y., & Lewinsohn, E.

(2006). Functional characterization of CmCCD1, a carotenoid cleavage dioxygenase from melon. *Phytochemistry*, *67*(15), 1579–1589. https://doi.org/10.1016/j.phytochem.2006.02.009

Ilg, A., Beyer, P., & Al-Babili, S. (2009). Characterization of the rice carotenoid cleavage dioxygenase 1 reveals a novel route for geranial biosynthesis. *The FEBS Journal*, *276*(3), 736–747. https://doi.org/10.1111/j.1742-4658.2008.06820.x

Islas-Flores, T., Rahman, A., Ullah, H., & Villanueva, M. A. (2015). The Receptor for Activated C Kinase in Plant Signaling: Tale of a Promiscuous Little Molecule. *Frontiers in Plant Science*, *6*. https://doi.org/10.3389/fpls.2015.01090

Jamil, F., Mukhtar, H., Fouillaud, M., & Dufossé, L. (2022). Rhizosphere Signaling: Insights into Plant–Rhizomicrobiome Interactions for Sustainable Agronomy. *Microorganisms*, *10*(5), 899. https://doi.org/10.3390/microorganisms10050899

Ji, Y., Ouzounis, T., Schouten, H. J., Visser, R. G. F., Marcelis, L. F. M., & Heuvelink, E. (2021). Dissecting the Genotypic Variation of Growth Responses to Far-Red Radiation in Tomato. *Frontiers in Plant Science*, *11*, 614714. https://doi.org/10.3389/fpls.2020.614714

Jiroutová, P., Mikulík, J., Novák, O., Strnad, M., & Oklestkova, J. (2019). Brassinosteroids Induce Strong, Dose-Dependent Inhibition of Etiolated Pea Seedling Growth Correlated with Ethylene Production. *Biomolecules*, *9*(12), 849. https://doi.org/10.3390/biom9120849

Ju, C., Yoon, G. M., Shemansky, J. M., Lin, D. Y., Ying, Z. I., Chang, J., Garrett, W. M., Kessenbrock, M., Groth, G., & Tucker, M. L. (2012). CTR1 phosphorylates the central regulator EIN2 to control ethylene hormone signaling from the ER membrane to the nucleus in Arabidopsis. *Proceedings of the National Academy of Sciences*, *109*(47), 19486–19491.

Junker, R. R., & Tholl, D. (2013). Volatile Organic Compound Mediated Interactions at the Plant-Microbe Interface. *Journal of Chemical Ecology*, *39*(7), 810–825. https://doi.org/10.1007/s10886-013-0325-9

Kegge, W., Ninkovic, V., Glinwood, R., Welschen, R. A. M., Voesenek, L. A. C. J., & Pierik, R. (2015). Red:far-red light conditions affect the emission

of volatile organic compounds from barley (*Hordeum vulgare*), leading to altered biomass allocation in neighbouring plants. *Annals of Botany*, *115*(6), 961–970. https://doi.org/10.1093/aob/mcv036

Kegge, W., Weldegergis, B. T., Soler, R., Eijk, M. V., Dicke, M., Voesenek, L. A. C. J., & Pierik, R. (2013). Canopy light cues affect emission of constitutive and methyl jasmonate-induced volatile organic compounds in *A rabidopsis thaliana* . *New Phytologist*, *200*(3), 861–874. https://doi.org/10.1111/nph.12407

Kessler, A., Mueller, M. B., Kalske, A., & Chautá, A. (2023). Volatile-mediated plant–plant communication and higher-level ecological dynamics. *Current Biology*, *33*(11), R519–R529. https://doi.org/10.1016/j.cub.2023.04.025

Khait, I., Obolski, U., Yovel, Y., & Hadany, L. (2019). Sound perception in plants. *Seminars in Cell & Developmental Biology*, *92*, 134–138. https://doi.org/10.1016/j.semcdb.2019.03.006

Khashi U Rahman, M., Zhou, X., & Wu, F. (2019). The role of root exudates, CMNs, and VOCs in plant–plant interaction. *Journal of Plant Interactions*, *14*(1), 630–636. https://doi.org/10.1080/17429145.2019.1689581

Kigathi, R. N., Unsicker, S. B., Reichelt, M., Kesselmeier, J., Gershenzon, J., & Weisser, W. W. (2009). Emission of Volatile Organic Compounds After Herbivory from Trifolium pratense (L.) Under Laboratory and Field Conditions. *Journal of Chemical Ecology*, *35*(11), 1335–1348. https://doi.org/10.1007/s10886-009-9716-3

Kigathi, R. N., Weisser, W. W., Reichelt, M., Gershenzon, J., & Unsicker, S. B. (2019). Plant volatile emission depends on the species composition of the neighboring plant community. *BMC Plant Biology*, *19*(1), 58. https://doi.org/10.1186/s12870-018-1541-9

Kim, J. I., Dolan, W. L., Anderson, N. A., & Chapple, C. (2015). Indole Glucosinolate Biosynthesis Limits Phenylpropanoid Accumulation in *Arabidopsis thaliana*. *The Plant Cell*, *27*(5), 1529–1546. https://doi.org/10.1105/tpc.15.00127

Kim, J. I., Zhang, X., Pascuzzi, P. E., Liu, C., & Chapple, C. (2020). Glucosinolate and phenylpropanoid biosynthesis are linked by

proteasome-dependent degradation of PAL. *New Phytologist*, *225*(1), 154–168. https://doi.org/10.1111/nph.16108

Kolde, R. (2019). Pheatmap: Pretty heatmaps. *R Package Version*, *1*(2), 726.

Kong, C.-H., Zhang, S.-Z., Li, Y.-H., Xia, Z.-C., Yang, X.-F., Meiners, S. J., & Wang, P. (2018). Plant neighbor detection and allelochemical response are driven by root-secreted signaling chemicals. *Nature Communications*, *9*(1). https://doi.org/10.1038/s41467-018-06429-1

Kono, A., & Yin, Y. (2020). Updates on BES1/BZR1 regulatory networks coordinating plant growth and stress responses. *Frontiers in Plant Science*, *11*, 617162.

Korbei, B., Moulinier-Anzola, J., De-Araujo, L., Lucyshyn, D., Retzer, K., Khan, M. A., & Luschnig, C. (2013). Arabidopsis TOL Proteins Act as Gatekeepers for Vacuolar Sorting of PIN2 Plasma Membrane Protein. *Current Biology*, *23*(24), 2500–2505. https://doi.org/10.1016/j.cub.2013.10.036

Kos, M., Houshyani, B., Overeem, A., Bouwmeester, H. J., Weldegergis, B. T., Van Loon, J. J., Dicke, M., & Vet, L. E. (2013). Genetic engineering of plant volatile terpenoids: Effects on a herbivore, a predator and a parasitoid. *Pest Management Science*, *69*(2), 302–311. https://doi.org/10.1002/ps.3391

Kost, C., & Heil, M. (2006). Herbivore-induced plant volatiles induce an indirect defence in neighbouring plants. *Journal of Ecology*, *94*(3), 619–628. https://doi.org/10.1111/j.1365-2745.2006.01120.x

Kreslavski, V. D., Los, D. A., Schmitt, F.-J., Zharmukhamedov, S. K., Kuznetsov, V. V., & Allakhverdiev, S. I. (2018). The impact of the phytochromes on photosynthetic processes. *Biochimica et Biophysica Acta (BBA) - Bioenergetics*, *1859*(5), 400–408. https://doi.org/10.1016/j.bbabio.2018.03.003

Kundu, N., Dozier, U., Deslandes, L., Somssich, I. E., & Ullah, H. (2013). *Arabidopsis* scaffold protein RACK1A interacts with diverse environmental stress and photosynthesis related proteins. *Plant Signaling & Behavior*, *8*(5), e24012. https://doi.org/10.4161/psb.24012

Kurihara, D., Mizuta, Y., Sato, Y., & Higashiyama, T. (2015). ClearSee: A rapid optical clearing reagent for whole-plant fluorescence imaging. *Development*, *142*(23), 4168–4179.

Lambers, H., & Oliveira, R. S. (2019). Responses to Availability of Water. In *Plant Physiological Ecology* (pp. 59–64). Springer International Publishing. https://doi.org/10.1007/978-3-030-29639-1

Le, J., Vandenbussche, F., De Cnodder, T., Van Der Straeten, D., & Verbelen, J.-P. (2005). Cell elongation and microtubule behavior in the Arabidopsis hypocotyl: Responses to ethylene and auxin. *Journal of Plant Growth Regulation*, *24*(3), 166–178.

Leivar, P., & Monte, E. (2014). PIFs: Systems integrators in plant development. *The Plant Cell*, *26*(1), 56–78.

Leivar, P., & Quail, P. H. (2011). PIFs: Pivotal components in a cellular signaling hub. *Trends in Plant Science*, *16*(1), 19–28. https://doi.org/10.1016/j.tplants.2010.08.003

Leschevin, M., Ksas, B., Baltenweck, R., Hugueney, P., Caffarri, S., & Havaux, M. (2024). Photosystem rearrangements, photosynthetic efficiency, and plant growth in far red-enriched light. *The Plant Journal*, *120*(6), 2536–2552. https://doi.org/10.1111/tpj.17127

Li, L., Rodríguez-Concepción, M., & Al-Babili, S. (2025). Advances in carotenoid and apocarotenoid metabolisms and functions in plants. *Plant Physiology*, *198*(4), kiaf304. https://doi.org/10.1093/plphys/kiaf304

Li, Z., Fu, Y., Wang, Y., & Liang, J. (2023). Scaffold protein RACK1 regulates BR signaling by modulating the nuclear localization of BZR1. *New Phytologist*, *239*(5), 1804–1818. https://doi.org/10.1111/nph.19049

Lihová, J., Marhold, K., Kudoh, H., & Koch, M. A. (2006). Worldwide phylogeny and biogeography of Cardamine flexuosa (Brassicaceae) and its relatives. *American Journal of Botany*, *93*(8), 1206–1221. https://doi.org/10.3732/ajb.93.8.1206

Liu, L., Shao, Z., Zhang, M., & Wang, Q. (2015). Regulation of Carotenoid Metabolism in Tomato. *Molecular Plant*, *8*(1), 28–39. https://doi.org/10.1016/j.molp.2014.11.006

Liu, Z., Wang, M., Wu, M., Li, X., Liu, H., Niu, N., Li, S., & Chen, L. (2023). Volatile organic compounds (VOCs) from plants: From release to detection. *TrAC Trends in Analytical Chemistry*, *158*, 116872. https://doi.org/10.1016/j.trac.2022.116872

Llorente, B., D'Andrea, L., Ruiz-Sola, M. A., Botterweg, E., Pulido, P., Andilla, J., Loza-Alvarez, P., & Rodriguez-Concepcion, M. (2016). Tomato fruit carotenoid biosynthesis is adjusted to actual ripening progression by a light-dependent mechanism. *The Plant Journal*, *85*(1), 107–119. https://doi.org/10.1111/tpj.13094

Lo, M.-M., Benfodda, Z., Bénimélis, D., Fontaine, J.-X., Molinié, R., & Meffre, P. (2021). Extraction and Identification of Volatile Organic Compounds Emitted by Fragrant Flowers of Three Tillandsia Species by HS-SPME/GC-MS. *Metabolites*, *11*(9), 594. https://doi.org/10.3390/metabo11090594

Lo, M.-M., Benfodda, Z., Molinié, R., & Meffre, P. (2024). Volatile Organic Compounds Emitted by Flowers: Ecological Roles, Production by Plants, Extraction, and Identification. *Plants*, *13*(3), 417. https://doi.org/10.3390/plants13030417

López-Gresa, M. P., Lisón, P., Campos, L., Rodrigo, I., Rambla, J. L., Granell, A., Conejero, V., & Bellés, J. M. (2017). A Non-targeted Metabolomics Approach Unravels the VOCs Associated with the Tomato Immune Response against Pseudomonas syringae. *Frontiers in Plant Science*, *8*. https://doi.org/10.3389/fpls.2017.01188

Loreto, F., & D'Auria, S. (2022). How do plants sense volatiles sent by other plants? *Trends in Plant Science*, *27*(1), 29–38. https://doi.org/10.1016/j.tplants.2021.08.009

Loreto, F., Dicke, M., SCHNITZLER, J.-P., & Turlings, T. C. (2014). Plant volatiles and the environment. *Plant, Cell & Environment*, *37*(8), 1905–1908.

Lorrain, S., Allen, T., Duek, P. D., Whitelam, G. C., & Fankhauser, C. (2008). Phytochrome-mediated inhibition of shade avoidance involves degradation of growth-promoting bHLH transcription factors. *The Plant Journal*, *53*(2), 312–323.

Love, M., Anders, S., & Huber, W. (2014). Differential analysis of count data–the DESeq2 package. *Genome Biol*, *15*(550), 10–1186.

Lukić, I., Išić, N., Ban, D., Salopek Sondi, B., & Goreta Ban, S. (2023). Comprehensive Volatilome Signature of Various Brassicaceae Species. *Plants*, *12*(1), 177. https://doi.org/10.3390/plants12010177

Ma, Q., Liu, S., Raggi, S., Doyle, S. M., Pařízková, B., Barange, D. K., Wilkinson, E. G., Garcia, I. C., Bygdell, J., Wingsle, G., Boer, D. R., Strader, L. C., Almqvist, F., Novák, O., & Robert, S. (2024). *Identification of RACK1A as a component of the auxin-ethylene crosstalk regulating apical hook development in* Arabidopsis thaliana. Plant Biology. https://doi.org/10.1101/2024.03.04.582885

Maffei, M. E., Gertsch, J., & Appendino, G. (2011). Plant volatiles: Production, function and pharmacology. *Natural Product Reports*, *28*(8), 1359–1380.

Mancinelli, A. L. (1994). The physiology of phytochrome action. In *Photomorphogenesis in plants* (pp. 211–269). Springer.

Mao, J., & Li, J. (2020). Regulation of Three Key Kinases of Brassinosteroid Signaling Pathway. *International Journal of Molecular Sciences*, *21*(12), 4340. https://doi.org/10.3390/ijms21124340

Martin, F. M., Uroz, S., & Barker, D. G. (2017). Ancestral alliances: Plant mutualistic symbioses with fungi and bacteria. *Science*, *356*(6340), eaad4501.

Martínez-García, J. F., Gallemí, M., Molina-Contreras, M. J., Llorente, B., Bevilaqua, M. R. R., & Quail, P. H. (2014). The Shade Avoidance Syndrome in Arabidopsis: The Antagonistic Role of Phytochrome A and B Differentiates Vegetation Proximity and Canopy Shade. *PLOS ONE*, *9*(10), e109275. https://doi.org/10.1371/journal.pone.0109275

Martínez-García, J. F., Galstyan, A., Salla-Martret, M., Cifuentes-Esquivel, N., Gallemí, M., & Bou-Torrent, J. (2010). Regulatory components of shade avoidance syndrome. In *Advances in botanical research* (Vol. 53, pp. 65–116). Elsevier.

Martinez-Garcia, J. F., & Rodriguez-Concepcion, M. (2023). Molecular mechanisms of shade tolerance in plants. *New Phytologist*, *239*(4), 1190–1202. https://doi.org/10.1111/nph.19047

Matsui, K., & Engelberth, J. (2022). Green Leaf Volatiles—The Forefront of Plant Responses Against Biotic Attack. *Plant and Cell Physiology*, *63*(10), 1378–1390. https://doi.org/10.1093/pcp/pcac117

Medina-van Berkum, P., Albracht, C., Bröcher, M., Gershenzon, J., & Unsicker, S. B. (2024). *Plant diversity shapes plant volatile emission differently at the species and community level*.

Meng, N., Yan, G.-L., Zhang, D., Li, X.-Y., Duan, C.-Q., & Pan, Q.-H. (2019). Characterization of two Vitis vinifera carotenoid cleavage dioxygenases by heterologous expression in Saccharomyces cerevisiae. *Molecular Biology Reports*, *46*(6), 6311–6323. https://doi.org/10.1007/s11033-019-05072-3

Merelo, P., Agustí, J., Arbona, V., Costa, M. L., Estornell, L. H., Gómez-Cadenas, A., Coimbra, S., Gómez, M. D., Pérez-Amador, M. A., & Domingo, C. (2017). Cell wall remodeling in abscission zone cells during ethylene-promoted fruit abscission in citrus. *Frontiers in Plant Science*, *8*, 126.

Michaud, O., Krahmer, J., Galbier, F., Lagier, M., Galvão, V. C., Ince, Y. Ç., Trevisan, M., Knerova, J., Dickinson, P., Hibberd, J. M., Zeeman, S. C., & Fankhauser, C. (2023). Abscisic acid modulates neighbor proximity-induced leaf hyponasty in Arabidopsis. *Plant Physiology*, *191*(1), 542–557. https://doi.org/10.1093/plphys/kiac447

Midzi, J., Jeffery, D. W., Baumann, U., Rogiers, S., Tyerman, S. D., & Pagay, V. (2022). Stress-Induced Volatile Emissions and Signalling in Inter-Plant Communication. *Plants*, *11*(19), 2566. https://doi.org/10.3390/plants11192566

Mitchell, C. E., Agrawal, A. A., Bever, J. D., Gilbert, G. S., Hufbauer, R. A., Klironomos, J. N., Maron, J. L., Morris, W. F., Parker, I. M., Power, A. G., Seabloom, E. W., Torchin, M. E., & Vázquez, D. P. (2006). Biotic interactions and plant invasions. *Ecology Letters*, *9*(6), 726–740. https://doi.org/10.1111/j.1461-0248.2006.00908.x

Molina-Contreras, M. J., Paulišić, S., Then, C., Moreno-Romero, J., Pastor-Andreu, P., Morelli, L., Roig-Villanova, I., Jenkins, H., Hallab, A., & Gan, X. (2019). Photoreceptor activity contributes to contrasting responses to shade in Cardamine and Arabidopsis seedlings. *The Plant Cell*, *31*(11), 2649–2663.

Moon, J., Zhu, L., Shen, H., & Huq, E. (2008). PIF1 directly and indirectly regulates chlorophyll biosynthesis to optimize the greening process in Arabidopsis. *Proceedings of the National Academy of Sciences*, *105*(27), 9433–9438. https://doi.org/10.1073/pnas.0803611105

Morelli, L., Paulišić, S., Qin, W., Iglesias-Sanchez, A., Roig-Villanova, I., Florez-Sarasa, I., Rodriguez-Concepcion, M., & Martinez-Garcia, J. F. (2021). Light signals generated by vegetation shade facilitate acclimation to low light in shade-avoider plants. *Plant Physiology*, *186*(4), 2137–2151. https://doi.org/10.1093/plphys/kiab206

Moreno, J. C., Mi, J., Alagoz, Y., & Al-Babili, S. (2021). Plant apocarotenoids: From retrograde signaling to interspecific communication. *The Plant Journal: For Cell and Molecular Biology*, *105*(2), 351–375. https://doi.org/10.1111/tpj.15102

Morrell, K., & Kessler, A. (2014). The scent of danger: Volatile-mediated information transfer and defence priming in plants. *The Biochemist*, *36*(5), 26–31.

Nagesh, K. M., & Piovene, C. (2011). Emission and function of volatile organic compounds in response to abiotic stress. *Abiotic Stress in Plants: Mechanisms and Adaptations*, 367.

Nielsen, M. H., Flygaard, R. K., & Jenner, L. B. (2017). Structural analysis of ribosomal RACK1 and its role in translational control. *Cellular Signalling*, *35*, 272–281. https://doi.org/10.1016/j.cellsig.2017.01.026

Niinemets, Ü., Kännaste, A., & Copolovici, L. (2013). Quantitative patterns between plant volatile emissions induced by biotic stresses and the degree of damage. *Frontiers in Plant Science*, *4*. https://doi.org/10.3389/fpls.2013.00262

Ninkovic, V., Rensing, M., Dahlin, I., & Markovic, D. (2019). Who is my neighbor? Volatile cues in plant interactions. *Plant Signaling & Behavior*, *14*(9), 1634993.

Nugroho, A. B. D., Lee, S. W., Pervitasari, A. N., Moon, H., Choi, D., Kim, J., & Kim, D.-H. (2021). Transcriptomic and metabolic analyses revealed the modulatory effect of vernalization on glucosinolate metabolism in radish (Raphanus sativus L.). *Scientific Reports*, *11*(1), 24023. https://doi.org/10.1038/s41598-021-03557-5

Nunes-Nesi, A., Fernie, A. R., & Stitt, M. (2010). Metabolic and Signaling Aspects Underpinning the Regulation of Plant Carbon Nitrogen Interactions. *Molecular Plant*, *3*(6), 973–996. https://doi.org/10.1093/mp/ssq049

Okushima, Y., Mitina, I., Quach, H. L., & Theologis, A. (2005). AUXIN RESPONSE FACTOR 2 (ARF2): A pleiotropic developmental regulator. *The Plant Journal*, *43*(1), 29–46.

Ômura, H., Honda, K., & Hayashi, N. (2000). Floral Scent of Osmanthus fragrans Discourages Foraging Behavior of Cabbage Butterfly, Pieris rapae. *Journal of Chemical Ecology*, *26*(3), 655–666. https://doi.org/10.1023/A:1005424121044

Ortiz-Alcaide, M., Llamas, E., Gomez-Cadenas, A., Nagatani, A., Martínez-García, J. F., & Rodríguez-Concepción, M. (2019). Chloroplasts Modulate Elongation Responses to Canopy Shade by Retrograde Pathways Involving HY5 and Abscisic Acid. *The Plant Cell*, *31*(2), 384–398. https://doi.org/10.1105/tpc.18.00617

Park, H. L., Seo, D. H., Lee, H. Y., Bakshi, A., Park, C., Chien, Y.-C., Kieber, J. J., Binder, B. M., & Yoon, G. M. (2023). Ethylene-triggered subcellular trafficking of CTR1 enhances the response to ethylene gas. *Nature Communications*, *14*(1), 365. https://doi.org/10.1038/s41467-023-35975-6

Pashkovskiy, P., Vereshchagin, M., Kartashov, A., Ivanov, Y., Ivanova, A., Zlobin, I., Abramova, A., Ashikhmina, D., Glushko, G., Kreslavski, V. D., & Kuznetsov, V. V. (2024). Influence of Additional White, Red and Far-Red Light on Growth, Secondary Metabolites and Expression of Hormone Signaling Genes in Scots Pine under Sunlight. *Cells*, *13*(2), 194. https://doi.org/10.3390/cells13020194

Pastor-Andreu, P., Moreno-Romero, J., & Urdin-Bravo, M. (2024). *Temporal and spatial frameworks supporting plant responses to vegetation proximity*.

Pattyn, J., Vaughan-Hirsch, J., & Van de Poel, B. (2021). The regulation of ethylene biosynthesis: A complex multilevel control circuitry. *New Phytologist*, *229*(2), 770–782.

Paudel Timilsena, B., Seidl-Adams, I., & Tumlinson, J. H. (2020). Herbivore-specific plant volatiles prime neighboring plants for nonspecific defense responses. *Plant, Cell & Environment*, *43*(3), 787–800.

Paulišić, S., Qin, W., Arora Verasztó, H., Then, C., Alary, B., Nogue, F., Tsiantis, M., Hothorn, M., & Martínez-García, J. F. (2021). Adjustment of the PIF7-HFR1 transcriptional module activity controls plant shade adaptation. *The EMBO Journal*, *40*(1), e104273.

Pierik, R., Cuppens, M. L. C., Voesenek, L. A. C. J., & Visser, E. J. W. (2004). Interactions between Ethylene and Gibberellins in Phytochrome-Mediated Shade Avoidance Responses in Tobacco. *Plant Physiology*, *136*(2), 2928–2936. https://doi.org/10.1104/pp.104.045120

Pierik, R., Whitelam, G. C., Voesenek, L. A. C. J., De Kroon, H., & Visser, E. J. W. (2004). Canopy studies on ethylene-insensitive tobacco identify ethylene as a novel element in blue light and plant–plant signalling. *The Plant Journal*, *38*(2), 310–319. https://doi.org/10.1111/j.1365-313X.2004.02044.x

Ponzio, C., Gols, R., Pieterse, C. M., & Dicke, M. (2013). Ecological and phytohormonal aspects of plant volatile emission in response to single and dual infestations with herbivores and phytopathogens. *Functional Ecology*, *27*(3), 587–598.

Rambla, J. L., Tikunov, Y. M., Monforte, A. J., Bovy, A. G., & Granell, A. (2013). The expanded tomato fruit volatile landscape. *Journal of Experimental Botany*, *65*(16), 4613–4623. https://doi.org/10.1093/jxb/eru128

Ramel, F., Birtic, S., Ginies, C., Soubigou-Taconnat, L., Triantaphylidès, C., & Havaux, M. (2012). Carotenoid oxidation products are stress signals that mediate gene responses to singlet oxygen in plants. *Proceedings of the National Academy of Sciences*, *109*(14), 5535–5540. https://doi.org/10.1073/pnas.1115982109

Ramel, F., Mialoundama, A. S., & Havaux, M. (2013). Nonenzymic carotenoid oxidation and photooxidative stress signalling in plants. *Journal*

of Experimental Botany, *64*(3), 799–805. https://doi.org/10.1093/jxb/ers223

Ramírez-Rodríguez, V., López-Bucio, J., & Herrera-Estrella, L. (2005). Adaptive responses in plants to nonoptimal soil pH. *Plant Abiotic Stress*, 145–170.

Reed, J. W., Wu, M.-F., Reeves, P. H., Hodgens, C., Yadav, V., Hayes, S., & Pierik, R. (2018). Three Auxin Response Factors Promote Hypocotyl Elongation. *Plant Physiology*, *178*(2), 864–875. https://doi.org/10.1104/pp.18.00718

Reichel, P., Munz, S., Hartung, J., Kotiranta, S., & Graeff-Hönninger, S. (2022). Impacts of Different Light Spectra on CBD, CBDA and Terpene Concentrations in Relation to the Flower Positions of Different Cannabis Sativa L. Strains. *Plants*, *11*(20), 2695. https://doi.org/10.3390/plants11202695

Ren, H., & Gray, W. M. (2015). SAUR Proteins as Effectors of Hormonal and Environmental Signals in Plant Growth. *Molecular Plant*, *8*(8), 1153–1164. https://doi.org/10.1016/j.molp.2015.05.003

Rhoades, D. (1983). Responses of Alder and Willow to Attack by Tent Caterpillars and Webworms: Evidence for Pheromonal Sensitivity of Willows. In *Plant Resistance to Insects: Vol. Chapter 4* (pp. 55–68).

Rice, E. L. (2012). *Allelopathy*.

Rockwell, N. C., Su, Y.-S., & Lagarias, J. C. (2006). Phytochrome structure and signaling mechanisms. *Annu. Rev. Plant Biol.*, *57*(1), 837–858.

Rodrigues, M. A., Bianchetti, R. E., & Freschi, L. (2014). Shedding light on ethylene metabolism in higher plants. *Frontiers in Plant Science*, *5*, 665.

Roig-Villanova, I., Bou-Torrent, J., Galstyan, A., Carretero-Paulet, L., Portolés, S., Rodríguez-Concepción, M., & Martínez-García, J. F. (2007). Interaction of shade avoidance and auxin responses: A role for two novel atypical bHLH proteins. *The EMBO Journal*, *26*(22), 4756–4767. https://doi.org/10.1038/sj.emboj.7601890

Roig-Villanova, I., & Martínez-García, J. F. (2016). Plant responses to vegetation proximity: A whole life avoiding shade. *Frontiers in Plant Science*, *7*, 236.

Roig-Villanova, I., Torres-Montilla, S., López-Ortiz, E., Di Marzo, M., Sánchez-García, Á., Esteve-Codina, A., Gómez-Cadenas, A., & Martínez-García, J. F. (2025). Plant proximity reduces seed yield in Arabidopsis plants by decreasing the number of ovule primordia. *Physiologia Plantarum*, *177*(2), e70220.

Rose, J. K. C., Braam, J., Fry, S. C., & Nishitani, K. (2002). The XTH Family of Enzymes Involved in Xyloglucan Endotransglucosylation and Endohydrolysis: Current Perspectives and a New Unifying Nomenclature. *Plant and Cell Physiology*, *43*(12), 1421–1435. https://doi.org/10.1093/pcp/pcf171

Rosenkranz, M., Chen, Y., Zhu, P., & Vlot, A. C. (2021). Volatile terpenes – mediators of plant-to-plant communication. *The Plant Journal*, *108*(3), 617–631. https://doi.org/10.1111/tpj.15453

Rozpądek, P., Domka, A. M., Nosek, M., Ważny, R., Jędrzejczyk, R. J., Wiciarz, M., & Turnau, K. (2018). The Role of Strigolactone in the Cross-Talk Between Arabidopsis thaliana and the Endophytic Fungus Mucor sp. *Frontiers in Microbiology*, *9*. https://doi.org/10.3389/fmicb.2018.00441

Schaller, G. E., & Kieber, J. J. (2002). Ethylene. *The Arabidopsis Book*, *1*, e0071. https://doi.org/10.1199/tab.0071

Schikora, A., Schenk, S. T., & Hartmann, A. (2016). Beneficial effects of bacteria-plant communication based on quorum sensing molecules of the N -acyl homoserine lactone group. *Plant Molecular Biology*, *90*(6), 605–612. https://doi.org/10.1007/s11103-016-0457-8

Schmitt, J., & Wulff, R. D. (1993). Light spectral quality, phytochrome and plant competition. *Trends in Ecology & Evolution*, *8*(2), 47–51. https://doi.org/10.1016/0169-5347(93)90157-K

Schwartz, S. H., Qin, X., & Loewen, M. C. (2004). The Biochemical Characterization of Two Carotenoid Cleavage Enzymes from *Arabidopsis* Indicates That a Carotenoid-derived Compound Inhibits Lateral Branching*. *Journal of Biological Chemistry*, *279*(45), 46940–46945. https://doi.org/10.1074/jbc.M409004200

Schwartz, S. H., Qin, X., & Zeevaart, J. A. (2003). Elucidation of the indirect pathway of abscisic acid biosynthesis by mutants, genes, and enzymes. *Plant Physiology*, *131*(4), 1591–1601.

Semchenko, M., Saar, S., & Lepik, A. (2014). Plant root exudates mediate neighbour recognition and trigger complex behavioural changes. *New Phytologist*, *204*(3), 631–637.

Seo, H. S., Watanabe, E., Tokutomi, S., Nagatani, A., & Chua, N.-H. (2004). Photoreceptor ubiquitination by COP1 E3 ligase desensitizes phytochrome A signaling. *Genes & Development*, *18*(6), 617–622. https://doi.org/10.1101/gad.1187804

Shakeel, S. N., Gao, Z., Amir, M., Chen, Y.-F., Rai, M. I., Haq, N. U., & Schaller, G. E. (2015). Ethylene regulates levels of ethylene receptor/CTR1 signaling complexes in Arabidopsis thaliana. *Journal of Biological Chemistry*, *290*(19), 12415–12424.

Sheerin, D. J., & Hiltbrunner, A. (2017). Molecular mechanisms and ecological function of far-red light signalling. *Plant, Cell & Environment*, *40*(11), 2509–2529.

Shin, D., Perez, V. C., Dickinson, G. K., Zhao, H., Dai, R., Tomiczek, B., Cho, K. H., Zhu, N., Koh, J., Grenning, A., & Kim, J. (2023). Altered methionine metabolism impacts phenylpropanoid production and plant development in *Arabidopsis thaliana*. *The Plant Journal*, *116*(1), 187–200. https://doi.org/10.1111/tpj.16370

Shinomura, T., Nagatani, A., Hanzawa, H., Kubota, M., Watanabe, M., & Furuya, M. (1996). Action spectra for phytochrome A- and B-specific photoinduction of seed germination in Arabidopsis thaliana. *Proceedings of the National Academy of Sciences*, *93*(15), 8129–8133. https://doi.org/10.1073/pnas.93.15.8129

Shiojiri, K., Kishimoto, K., Ozawa, R., Kugimiya, S., Urashimo, S., Arimura, G., Horiuchi, J., Nishioka, T., Matsui, K., & Takabayashi, J. (2006). Changing green leaf volatile biosynthesis in plants: An approach for improving plant resistance against both herbivores and pathogens. *Proceedings of the National Academy of Sciences*, *103*(45), 16672–16676. https://doi.org/10.1073/pnas.0607780103

Simkin, A. J., Schwartz, S. H., Auldridge, M., Taylor, M. G., & Klee, H. J. (2004). The tomato carotenoid cleavage dioxygenase 1 genes contribute to the formation of the flavor volatiles β-ionone, pseudoionone, and

geranylacetone. *The Plant Journal*, *40*(6), 882–892. https://doi.org/10.1111/j.1365-313X.2004.02263.x

Simkin, A. J., Underwood, B. A., Auldridge, M., Loucas, H. M., Shibuya, K., Schmelz, E., Clark, D. G., & Klee, H. J. (2004). Circadian regulation of the PhCCD1 carotenoid cleavage dioxygenase controls emission of beta-ionone, a fragrance volatile of petunia flowers. *Plant Physiology*, *136*(3), 3504–3514. https://doi.org/10.1104/pp.104.049718

Smalle, J., Haegman, M., Kurepa, J., Van Montagu, M., & Straeten, D. V. D. (1997). Ethylene can stimulate *Arabidopsis* hypocotyl elongation in the light. *Proceedings of the National Academy of Sciences*, *94*(6), 2756–2761. https://doi.org/10.1073/pnas.94.6.2756

Smith, D. L., Subramanian, S., Lamont, J. R., & Bywater-Ekegärd, M. (2015). Signaling in the phytomicrobiome: Breadth and potential. *Frontiers in Plant Science*, *6*. https://doi.org/10.3389/fpls.2015.00709

Smith, H., & Whitelam, G. C. (1997). The shade avoidance syndrome: Multiple responses mediated by multiple phytochromes. *Plant, Cell & Environment*, *20*(6), 840–844. https://doi.org/10.1046/j.1365-3040.1997.d01-104.x

Soria, A. C., García-Sarrió, M. J., & Sanz, M. L. (2015). Volatile sampling by headspace techniques. *TrAC Trends in Analytical Chemistry*, *71*, 85–99. https://doi.org/10.1016/j.trac.2015.04.015

Stamm, P., & Kumar, P. P. (2013). Auxin and gibberellin responsive Arabidopsis SMALL AUXIN UP RNA36 regulates hypocotyl elongation in the light. *Plant Cell Reports*, *32*(6), 759–769.

Stirling, S. A., Guercio, A. M., Patrick, R. M., Huang, X.-Q., Bergman, M. E., Dwivedi, V., Kortbeek, R. W. J., Liu, Y.-K., Sun, F., Tao, W. A., Li, Y., Boachon, B., Shabek, N., & Dudareva, N. (2024). Volatile communication in plants relies on a KAI2-mediated signaling pathway. *Science*, *383*(6689), 1318–1325. https://doi.org/10.1126/science.adl4685

Stortenbeker, N., & Bemer, M. (2019). The SAUR gene family: The plant's toolbox for adaptation of growth and development. *Journal of Experimental Botany*, *70*(1), 17–27.

Su, J., Xu, J., & Zhang, S. (2015). RACK1, scaffolding a heterotrimeric G protein and a MAPK cascade. *Trends in Plant Science*, *20*(7), 405–407. https://doi.org/10.1016/j.tplants.2015.05.002

Tadrosova, M., Uhlik, O., & Suman, J. (2025). What goes underground comes around: The molecular basis of crosstalk between plants and soil microorganisms. *Phytochemistry Reviews*, *24*(2), 1971–1987. https://doi.org/10.1007/s11101-024-09989-x

Tanaka, K., Nakamura, Y., Asami, T., Yoshida, S., Matsuo, T., & Okamoto, S. (2003). Physiological roles of brassinosteroids in early growth of Arabidopsis: Brassinosteroids have a synergistic relationship with gibberellin as well as auxin in light-grown hypocotyl elongation. *Journal of Plant Growth Regulation*, *22*(3), 259–271.

Taniguchi, S., Takeda, A., Kiryu, M., & Gomi, K. (2023). Jasmonic Acid-Induced β-Cyclocitral Confers Resistance to Bacterial Blight and Negatively Affects Abscisic Acid Biosynthesis in Rice. *International Journal of Molecular Sciences*, *24*(2), 1704. https://doi.org/10.3390/ijms24021704

Thain, S. C., Vandenbussche, F., Laarhoven, L. J., Dowson-Day, M. J., Wang, Z.-Y., Tobin, E. M., Harren, F. J., Millar, A. J., & Van Der Straeten, D. (2004). Circadian rhythms of ethylene emission in Arabidopsis. *Plant Physiology*, *136*(3), 3751–3761.

Toledo-Ortiz, G., Huq, E., & Rodríguez-Concepción, M. (2010). Direct regulation of phytoene synthase gene expression and carotenoid biosynthesis by phytochrome-interacting factors. *Proceedings of the National Academy of Sciences*, *107*(25), 11626–11631. https://doi.org/10.1073/pnas.0914428107

Torres-Montilla, S., & Rodriguez-Concepcion, M. (2021). Making extra room for carotenoids in plant cells: New opportunities for biofortification. *Progress in Lipid Research*, *84*, 101128. https://doi.org/10.1016/j.plipres.2021.101128

Ullah, H., Hou, W., Dakshanamurthy, S., & Tang, Q. (2019). Host targeted antiviral (HTA): Functional inhibitor compounds of scaffold protein RACK1 inhibit herpes simplex virus proliferation. *Oncotarget*, *10*(35), 3209–3226. https://doi.org/10.18632/oncotarget.26907

Urdin-Bravo, M., Sanchez-Garcia, A., Rodriguez-Concepcion, M., & Martinez-Garcia, J. F. (2024). Effect of Higher Ethylene Levels Emitted by Shade-Avoider Plants on Neighboring Seedlings. *Plants*, *13*(22), 3212. https://doi.org/10.3390/plants13223212

Van Buskirk, E. K., Decker, P. V., & Chen, M. (2012). Photobodies in Light Signaling. *Plant Physiology*, *158*(1), 52–60. https://doi.org/10.1104/pp.111.186411

Van Dam, N. M. (2009). How plants cope with biotic interactions. *Plant Biology*, *11*(1), 1–5. https://doi.org/10.1111/j.1438-8677.2008.00179.x

Van de Poel, B., Smet, D., & Van Der Straeten, D. (2015). Ethylene and hormonal cross talk in vegetative growth and development. *Plant Physiology*, *169*(1), 61–72.

Vandenbussche, F., Vaseva, I., Vissenberg, K., & Van Der Straeten, D. (2012). Ethylene in vegetative development: A tale with a riddle. *New Phytologist*, *194*(4), 895–909.

Vicherová, E., Glinwood, R., Hájek, T., Šmilauer, P., & Ninkovic, V. (2020). Bryophytes can recognize their neighbours through volatile organic compounds. *Scientific Reports*, *10*(1), 7405. https://doi.org/10.1038/s41598-020-64108-y

Vives-Peris, V., De Ollas, C., Gómez-Cadenas, A., & Pérez-Clemente, R. M. (2020). Root exudates: From plant to rhizosphere and beyond. *Plant Cell Reports*, *39*(1), 3–17. https://doi.org/10.1007/s00299-019-02447-5

Vogel, J. T., Tieman, D. M., Sims, C. A., Odabasi, A. Z., Clark, D. G., & Klee, H. J. (2010). Carotenoid content impacts flavor acceptability in tomato (*Solanum lycopersicum*). *Journal of the Science of Food and Agriculture*, *90*(13), 2233–2240. https://doi.org/10.1002/jsfa.4076

Wang, E., Schornack, S., Marsh, J. F., Gobbato, E., Schwessinger, B., Eastmond, P., Schultze, M., Kamoun, S., & Oldroyd, G. E. D. (2012). A Common Signaling Process that Promotes Mycorrhizal and Oomycete Colonization of Plants. *Current Biology*, *22*(23), 2242–2246. https://doi.org/10.1016/j.cub.2012.09.043

Wang, J. Y., Haider, I., Jamil, M., Fiorilli, V., Saito, Y., Mi, J., Baz, L., Kountche, B. A., Jia, K.-P., & Guo, X. (2019). The apocarotenoid metabolite

zaxinone regulates growth and strigolactone biosynthesis in rice. *Nature Communications*, *10*(1), 810.

Wang, K. L.-C., Li, H., & Ecker, J. R. (2002). Ethylene biosynthesis and signaling networks. *The Plant Cell*, *14*(suppl_1), S131–S151.

Wang, S., Ghisalberti, E. L., & Ridsdill-Smith, J. (1999). Volatiles from *Trifolium* as feeding deterrents of redlegged earth mites. *Phytochemistry*, *52*(4), 601–605. https://doi.org/10.1016/S0031-9422(99)00254-X

Wang, Y., Xu, J., & Liu, A. (2022). Identification of the carotenoid cleavage dioxygenase genes and functional analysis reveal DoCCD1 is potentially involved in beta-ionone formation in Dendrobium officinale. *Frontiers in Plant Science*, *13*, 967819. https://doi.org/10.3389/fpls.2022.967819

Wen, X., Zhang, C., Ji, Y., Zhao, Q., He, W., An, F., Jiang, L., & Guo, H. (2012). Activation of ethylene signaling is mediated by nuclear translocation of the cleaved EIN2 carboxyl terminus. *Cell Research*, *22*(11), 1613–1616.

Wickham, H. (2016). Data analysis. In *Ggplot2: Elegant graphics for data analysis* (pp. 189–201). Springer.

Wickham, H., Averick, M., Bryan, J., Chang, W., McGowan, L. D., François, R., Grolemund, G., Hayes, A., Henry, L., & Hester, J. (2019). Welcome to the Tidyverse. *Journal of Open Source Software*, *4*(43), 1686.

Willige, B. C., Yoo, C. Y., & Saldierna Guzmán, J. P. (2024). What is going on inside of phytochrome B photobodies? *The Plant Cell*, *36*(6), 2065–2085. https://doi.org/10.1093/plcell/koae084

Wimalasekera, R. (2019). Effect of light intensity on photosynthesis. *Photosynthesis, Productivity and Environmental Stress*, 65–73.

Wu, T., Hu, E., Xu, S., Chen, M., Guo, P., Dai, Z., Feng, T., Zhou, L., Tang, W., & Zhan, L. I. (2021). clusterProfiler 4.0: A universal enrichment tool for interpreting omics data. *The Innovation*, *2*(3).

Yang, C., & Li, L. (2017). Hormonal Regulation in Shade Avoidance. *Frontiers in Plant Science*, *8*. https://doi.org/10.3389/fpls.2017.01527

Yin, Y., Wang, Z.-Y., Mora-Garcia, S., Li, J., Yoshida, S., Asami, T., & Chory, J. (2002). BES1 Accumulates in the Nucleus in Response to

Brassinosteroids to Regulate Gene Expression and Promote Stem Elongation. *Cell*, *109*(2), 181–191. https://doi.org/10.1016/S0092-8674(02)00721-3

Yoneya, K., & Takabayashi, J. (2014). Plant–plant communication mediated by airborne signals: Ecological and plant physiological perspectives. *Plant Biotechnology*, *31*(5), 409–416.

Yoo, H. J., Chung, M.-Y., Lee, H.-A., Lee, S.-B., Grandillo, S., Giovannoni, J. J., & Lee, J. M. (2023). Natural overexpression of CAROTENOID CLEAVAGE DIOXYGENASE 4 in tomato alters carotenoid flux. *Plant Physiology*, *192*(2), 1289–1306. https://doi.org/10.1093/plphys/kiad049

Yoshida, H., Nagata, M., Saito, K., Wang, K. L., & Ecker, J. R. (2005). Arabidopsis ETO1 specifically interacts with and negatively regulates type 2 1-aminocyclopropane-1-carboxylate synthases. *BMC Plant Biology*, *5*, 14. https://doi.org/10.1186/1471-2229-5-14

Yu, G. (2023). Enrichplot: Visualization of Functional Enrichment Result. R package version 1.20. 3. *Mol Ther Nucleic Acids.[Google Scholar]*.

Zhang, H., Wang, J.-Y., Chen, Y.-J., Siemann, E., Ji, X.-Y., Jiang, J.-X., & Wan, N.-F. (2022). Beta-ionone is a functional plant volatile that attracts the parasitic wasp, Microplitis pallidipes. *BioControl*, *67*(1), 1–13. https://doi.org/10.1007/s10526-021-10117-3

Zhang, S., Guo, Y., Zhang, Y., Guo, J., Li, K., Fu, W., Jia, Z., Li, W., Tran, L.-S. P., Jia, K.-P., & Miao, Y. (2021). Genome-wide identification, characterization and expression profiles of the CCD gene family in Gossypium species. *3 Biotech*, *11*(5), 249. https://doi.org/10.1007/s13205-021-02805-9

Zhao, C., Zhang, H., Song, C., Zhu, J.-K., & Shabala, S. (2020). Mechanisms of Plant Responses and Adaptation to Soil Salinity. *The Innovation*, *1*(1), 100017. https://doi.org/10.1016/j.xinn.2020.100017

Zheng, G., Tian, B., Zhang, F., Tao, F., & Li, W. (2011). Plant adaptation to frequent alterations between high and low temperatures: Remodelling of membrane lipids and maintenance of unsaturation levels. *Plant, Cell & Environment*, *34*(9), 1431–1442. https://doi.org/10.1111/j.1365-3040.2011.02341.x

Zhu, A., Ibrahim, J. G., & Love, M. I. (2019). Heavy-tailed prior distributions for sequence count data: Removing the noise and preserving large differences. *Bioinformatics*, *35*(12), 2084–2092.

Zhu, W., Fu, Y., Zhou, H., Zhou, Y., Zhang, D., Wang, Y., Su, Y., Li, Z., & Liang, J. (2024). RACK1 links PHYB and BES1 to coordinate brassinosteroid-dependent root meristem development. *New Phytologist*, *244*(3), 883–899. https://doi.org/10.1111/nph.20055